RECEIVED
LAWRENCE
RADIATION LABORATORY

DEC 1 1972

LIBRARY AND
DOCUMENTS SECTION

LBL-1255

LARGE SEPARATIONS VIA CYCLING ZONE ADSORPTION

Ross Dale Rieke* and Robert L. Pigford

September 1972

AEC Contract No. W-7405-eng-48

*Filed as a Ph.D. Thesis

For Reference

Not to be taken from this room

LBL-1255

DISCLAIMER

This document was prepared as an account of work sponsored by the United States Government. While this document is believed to contain correct information, neither the United States Government nor any agency thereof, nor the Regents of the University of California, nor any of their employees, makes any warranty, express or implied, or assumes any legal responsibility for the accuracy, completeness, or usefulness of any information, apparatus, product, or process disclosed, or represents that its use would not infringe privately owned rights. Reference herein to any specific commercial product, process, or service by its trade name, trademark, manufacturer, or otherwise, does not necessarily constitute or imply its endorsement, recommendation, or favoring by the United States Government or any agency thereof, or the Regents of the University of California. The views and opinions of authors expressed herein do not necessarily state or reflect those of the United States Government or any agency thereof or the Regents of the University of California.

0 0 0 0 3 8 0 0 4 3 4

Acknowledgement

In the six years of study with you I have been constantly reminded, through my friends within the department and by the faculty, that it would be extremely difficult to find a better teacher. But I feel that I have truly gained more from you then just a potential ability to become a chemical engineer. You have provided for me the means to look objectively at problems, whether technical or not, and this gift I feel to be the most important of all. I shall try to use it, Dr. Pigford, to the best of my ability.

LARGE SEPARATIONS VIA CYCLING ZONE ADSORPTION

Ross Dale Rieke and Robert L. Pigford

Department of Chemical Engineering and
Lawrence Berkeley Laboratory
University of California
Berkeley, California 94720

September 1972

Abstract

A theoretical and experimental study is presented of "Cycling Zone Adsorption," a wave-propagating adsorption process which produces alternating high- and low-concentration product streams from a packed bed, the temperature of which is cycled. Although the separations are small for a single zone of such a process, large changes in composition can be obtained by adding stages in series, by feed-back of product streams to the feed, and by arranging groups of stages into cascades.

Liquid mixtures of n-heptane and toluene were separated using silica gel adsorbent particles. Optimum operating conditions of a single-cycling zone adsorber were investigated with the main emphasis upon optimum bed temperature switching frequency as a function of liquid concentration and bed length. Failure to achieve square-wave changes in solid-particle temperatures, owing to resistance to heat transfer, caused a reduction in performance which was minimized by correct allowance for mass transfer. Use of a square-wave feed concentration, either from product feed-back or from recycling output portions of a previous cycling stage in a cascade, led to increased separations but was limited by longitudinal diffusion in the interstitial fluid as it passed through the packing.

A theoretical development allowed calculation of effluent stream concentration profiles for a single stage experiencing a square-wave temperature response, with either a square-wave feed concentration input or a constant feed concentration input. The theoretical calculations have accounted for the limiting effect of longitudinal diffusion.

Study of several variations in the arrangement of stages in a cascade led to the conclusion that large separations can be obtained in a well-designed plant. The energy requirements of such a system are estimated to be attractive in comparison with a conventional separation process.

Table of Contents

Page

Abstract iv

List of Figures x

List of Tables xv

INTRODUCTION 1

CHAPTER 1. QUALITATIVE DESCRIPTION OF CYCLING ZONE ADSORPTION 4

Single-Zone Operation 8

Multi-Zone Operation 14

CHAPTER 2. EXPERIMENTAL SYSTEM CHARACTERISTICS AND APPARATUS 25

Introduction 26

Solid-Liquid Characteristics 26

Solids Capacity 30

Void Fractions and Particle Densities 31

Experimental Apparatus 35

Columns 35

Temperature Control 41

Feed Degassing Units 42

Liquid Composition Analysis System 44

CHAPTER 3. A SIMPLIFIED MATHEMATICAL STATEMENT OF CYCLING ZONE ADSORPTION (EXCLUSION OF DIFFUSION TERM) 47

The General Equation 48

Solution of Equation (3-2) 50

Calculation of Concentration Change Due to Temperature Change 53

Calculation of Concentration Shock-Wave Velocity 57

Determination of Simple Concentration Wave Generation 64

Table of Contents (Continued)

Page

Example Calculation of Single-Zone Performance... 65
Example of Dual-Zone Performance..... 72

CHAPTER 4. EXPERIMENTAL: SINGLE-ZONE, CONTINUOUS-FLOW SEPARATION OF n-HEPTANE AND TOLUENE ON SILICA GEL..... 78

Optimum Temperature Switching Time..... 84
Effect of Solid Particle Size..... 96
Improvement of Zone Temperature Response..... 103
Variable-Feed Operation of a Single Zone..... 115

CHAPTER 5. EXPERIMENTAL: VARIABLE-FEED OPERATION OF A SINGLE ZONE..... 121

Variable-Feed Recycle Scheme..... 122
Effect of Feed Amplitude Upon Breakthrough During Hot-Phase Operation..... 126
Effect of Feed Amplitude Upon Breakthrough During Cold-Phase Operation..... 133
Overall Diffusion Coefficient for Breakthrough in Cold- and Hot-Phase Operations With Variable-Feed Amplitudes..... 144
Effect of Feed Flow Rate Upon Breakthrough During Hot-Phase Operation..... 148
Effect of Average Feed Concentration Upon Breakthrough Time During Hot-Phase Operation... 158
Derivation of Breakthrough Curve for a Fixed Bed With Longitudinal Diffusion and Local Mass Transfer Equilibrium..... 161

CHAPTER 6. MATHEMATICAL STATEMENT OF CYCLING ZONE ADSORPTION ALLOWING FOR LONGITUDINAL DIFFUSION..... 170

Continuous-Flow, Constant Feed Concentration Single-Zone Operation (Analytic Solution)..... 171

Table of Contents (Continued)

Page

Continuous-Flow, Constant-Feed Concentration Single-Zone Operation (Analytic Solution, Zero Diffusion) 179
Continuous-Flow, Constant-Feed Concentration, Single-Zone Operation (Analytic Solution, Infinite Diffusion) 180
Continuous-Flow, Variable-Feed Input, Single-Zone Operation (Analytic Solution) 188
Computer Programs for Effluent Concentration Profiles 200

CHAPTER 7. SINGLE-ZONE STAGING IN THE DEVELOPMENT OF A CYCLING ZONE ADSORPTION CASCADE 207

Introduction 208
Continuous-Flow Operation With Constant-Feed Concentration into Each Zone 208
Effect of Recycle Stream Mixing Location 221
Zone-to-Zone Calculations in the Development of a Cascade 229
Use of Finite-Difference Equations 234
Graphical Solution Technique 239
Continuous-Flow Operation With Square-Wave Feed Concentration Input to Each Zone (Variable-Feed Operation) 243
Use of Finite-Difference Equations 252
Graphical Solution Technique 255
Noncontinuous-Flow Operation of a Single Variable-Feed Zone 255

CHAPTER 8. HEAT LOAD REQUIREMENTS FOR DISTILLATION VERSUS CYCLING ZONE ADSORPTION 263

Introduction 264

Table of Contents (Continued)

Page

Heat Load Requirements for Cycling Zone Adsorption..... 265
Heat Load Requirements for Distillation..... 267

CHAPTER 9. SUMMARY AND CONCLUSIONS..... 270

Chapter 3. A Simplified Mathematical Statement of Cycling Zone Adsorption (Exclusion of Diffusion Term)..... 271
Chapter 4. Experimental: Single-Zone, Continuous-Flow Separation of n-Heptane and Toluene on Silica Gel..... 273
Chapter 5. Experimental: Variable-Feed Operation of a Single Zone..... 275
Chapter 6. Mathematical Statement of Cycling Zone Adsorption Allowing for Longitudinal Diffusion..... 276
Chapter 7. Single-Zone Staging in the Development of a Cycling Zone Adsorption Cascade..... 279
Chapter 8. Heat Load Requirements for Distillation Versus Cycling Zone Adsorption.... 280

Nomenclature..... 281

Bibliography..... 284

0 0 0 0 3 8 0 7 4 5 7

List of Figures

No.		Page
1-1	Solid-Liquid Equilibrium Isotherm Relationship	6
1-2	Simplified Explanation of a Cycling Zone Adsorption Process	9
1-3	Idealized Single-Zone Temperature and Effluent Concentration Profile	12
1-4	Parallel Zone Arrangement	15
1-5	Series Zone Arrangement	17
1-6	Two-Zone Product Recycle Scheme	20
1-7	Variable-Feed, Recycle Operation of a Cycling Zone Adsorber	23
2-1	Solid-Liquid Equilibrium Isotherms (Eq. 2-1)	28
2-2	Experimental Apparatus	37
2-3	Experimental Adsorption Columns	39
2-4	Refractive Index Versus Volume % Toluene in n-Heptane-Toluene Mixtures (23.5°C)	45
3-1	Characteristic Slope Versus Volume % Fraction Toluene in Fluid	55
3-2	Theoretical Equilibrium Product Concentrations Versus Feed Concentration	58
3-3	Concentration Shock-Wave	61
3-4	Simple Concentration Wave	65
3-5	Example Calculation: Single-Zone Effluent Concentration Profile	70
3-6	Qualitative Use of Method of Characteristics for Two-Zone Series Operation	73

List of Figures (Continued)

No.		Page
4-1	Temperature and Effluent Concentration Profiles for the Experimental Operation of a Single Zone	80
4-2	Experimental Product Concentrations Versus Feed Concentrations	82
4-3	Qualitative Feed Breakthrough Profile	86
4-4	Experimental Feed Breakthrough Analysis	89
4-5	Effect of Temperature Switching Frequency Upon Effluent Profile	92
4-6	Effect of Particle Size Upon Effluent Concentration Profile	98
4-7	Effect of 200-Mesh Silica Gel Upon Effluent Concentration Profile	101
4-8	A Stop-Go Mode of Operation to Produce a Square-Wave Temperature Response	105
4-9	A Qualitative Solids-Liquid Concentration Response to Establish Validity of Local Equilibrium Assumption	110
4-10	Experimental Verification of Local Equilibrium Assumption	113
4-11	Idealized Variable-Feed Effluent Concentration Profile	116
4-12	Experimental Variable-Feed Effluent Concentration Profile	118
5-1	Operation of a Variable-Feed, Recycle Cycling Zone Adsorber	123
5-2	Qualitative Determination of Maximum Feed Amplitude	127

List of Figures (Continued)

No.		Page
5-3	Experimental Low-Concentration Feed Breakthrough Data	130
5-4	Simple-Wave: Qualitative Comparison of Effluent Concentration Profile With That Predicted by the Simplified Mathematical Analysis of Chapter 3	134
5-5	Experimental High-Concentration Feed Breakthrough Data	137
5-6	Shock-Wave: Qualitative Comparison of Effluent Concentration Profile With That Predicted by the Simplified Mathematical Analysis of Chapter 3	140
5-7	Diffusion Coefficient Versus Feed Amplitude for Hot- and Cold-Phase Operation	145
5-8	Effect of Volumetric Flow Rate Upon Effluent Concentration Profile	150
5-9	Effect of Feed Flow Rate Upon Diffusion Coefficient	152
5-10	Peclet Number Versus Reynolds Number	155
5-11	Effect of Flow Rate Upon High Product and Simple Wave Flow Duration	159
5-12	Variable-Feed Operation: Effect of Average Feed Concentration Upon Feed Concentration Breakthrough Time	162
5-13	Qualitative Description of Transformation of Experimental Breakthrough Data to Allow Calculation of Diffusion Coefficients	167
6-1	Dimensionless Plot of Eq. (6-9) for Five Values of the Peclet Number	184

List of Figures (Continued)

No.		Page
6-2	Dimensionless Plot of Eq. (6-20) for Variations in the Phase Shift Factor F.....	192
6-3	Dimensionless Plot of Eq. (6-9): Temperature Switch Effect Upon Effluent Concentration Profile.....	195
6-4	Dimensionless Plot of Eq. (6-21): Effect of Feed Amplitude Upon Effluent Concentration Profile for Variation of Phase Shift Factor F.....	197
7-1	Dimensionless Plot of Eq. (6-9) Used in Cascade Design.....	209
7-2	The Factors $P = m_T \Delta T/(1+m)$ and m Versus Volume Fraction Toluene in Feed, X_{LF}.....	212
7-3	Repetitive Combination of Two Single Zones in Series With Recycle.....	215
7-4	Continuously Operating Cycling Zone Adsorption Cascade.....	218
7-5	Comparison of a Two-Zone Recycle Leg and a Three-Zone Recycle Leg Producing the Same Separation.....	224
7-6	A Generalized Two-Zone Recycle Leg of a Cascade.....	230
7-7	P_N Versus $X_{L,N}$, $X_{H,N}$, and $X_{F,N}$ (Constant-Feed Operation).....	236
7-8	Generalized Graphical Solution for Design of a Two-Zone Recycle Cascade.....	240

List of Figures (Continued)

No.		Page
7-9	Dimensionless Effluent Concentration Profile for Variable-Feed Operation in the Design of a Cascade (Eq. 6-20)	244
7-10	Q_N Versus X_{FAVG}, $X_{H,avgN}$, $X_{L,avgN}$ (Variable-Feed Operation)	247
7-11	Variable-Feed, Single-Zone Recycle Core of Cascade	250
7-12	Generalized Variable-Feed Cycling Zone Adsorption Cascade With Recycle	253
7-13	Generalized Graphical Solution of a Variable-Feed Recycle Cascade	256
7-14	Noncontinuous-Flow Operation of a Single Cycling Zone Adsorber	260

List of Tables

No.		Page
2-1	Solid-Liquid Isotherm Data	32
2-2	Liquid and Solid Properties	34
2-3	Range of Variables Studied	43
3-1	Characteristic Properties of Two-Zone System	76
4-1	Temperature Switching Time Versus Peak Concentration Differences	91
4-2	Particle Size Versus Peak Concentration Difference and Product Flow Duration	97
5-1	Variable-Feed Breakthrough Data (Hot-Phase)	132
5-2	Variable-Feed Breakthrough Data (Cold-Phase)	139
5-3	Feed Amplitude Versus Diffusion Coefficient for Hot- and Cold-Phase Operation	147
5-4	Hot-Phase, Variable-Feed Operation: Feed Flow Rate Versus Diffusivity	154
7-1	Concentration and Flow Rate Data: Continuous-Flow, Two-Zone Recycle Cascade	220
7-2	Feed Concentration, Flow Rate, and Cross-Sectional Area Data: Continuous-Flow, Two-Zone Recycle Cascade	222
7-3	Low-Product Leg Characteristics of Continuous-Flow, Two-Zone Recycle Cascade	226
7-4	Low-Product Leg Characteristics of Continuous-Flow, Three-Zone Recycle Cascade	228

INTRODUCTION

The field of chemical engineering, through advances in refinery research, has over the last half century developed numerous separation techniques. Processes such as distillation, absorption, adsorption, extraction, and ion exchange take advantage of certain system characteristics in order to effect a separation of components. The mechanisms governing such separation techniques are well understood; consequently, there are few new major separation innovations. However, what remains are basic, if not novel, improvements upon the well-known separation techniques themselves. In distillation, for example, there have been considerable advances in tray design to improve vapor-liquid contact. Nevertheless, the well-known process of adsorption is still hindered by the required regeneration period which is needed after feed concentration breakthrough.

Cycling Zone Adsorption, as conceived by Pigford, Baker, and Blum (36), is a fundamental improvement upon the process of adsorption. Through the periodic change of a thermodynamic potential, it is possible to operate a packed adsorption column in a cyclic fashion. For example, in a binary liquid system of toluene and n-heptane flowing over solid silica gel packing, there occurs a preferential adsorption or desorption of toluene with a periodic change of a thermodynamic potential. Inherent in such an operation

is the ability to produce periodically both a high- and a low-concentration product stream, accompanied by the column's ability to self-regenerate. The ability of a single column, or zone, to produce both high- and low-concentration product streams may be extended into the design of a cascade, incorporating a number of single-zone, linked stages. Such a cascade then allows very large separations to be made.

The main objective of this dissertation is to overcome the limitations of previous works which have only used a single-cycling zone adsorption column to effect small component separations. This is done through an experimental and theoretical investigation of product stream feed back, or recycle, to increase the separation factor for a series of zones incorporated into a multi-zone cascade designed to increase recovery of both components of a binary feed stream. The binary liquid used is n-heptane and toluene, the solid packing being silica gel.

Chapter 1 is a qualitative description of Cycling Zone Adsorption, with a brief disucssion of simple recycling and cascade design. Chapter 2 provides the experimental system characteristics and a description of the apparatus. Chapter 3 contains a simplified mathematical analysis of Cycling Zone Adsorption. Chapters 4 and 5 present a discussion of experimental operations of an absorber, while Chapter 6 further develops the mathematics describing

0 0 0 0 3 8 0 7 . 7 1

Cycling Zone Adsorption. Chapter 7 concerns the design of a Cycling Zone Adsorption Cascade, a heat-load comparison with distillation being presented in Chapter 8. Chapter 9 provides a final summary of Chapters 3 through 8, with conclusions developed by the analysis in each of these chapters. The bibliography contains a number of recent papers on the subject, including separations of gas streams.

CHAPTER 1

QUALITATIVE DESCRIPTION OF CYCLING ZONE ADSORPTION

Single-Zone Operation..... 8

Multi-Zone Operation..... 14

CHAPTER 1

QUALITATIVE DESCRIPTION OF CYCLING ZONE ADSORPTION

Consider a solid adsorbate, such as silica gel, surrounded by a binary fluid mixture, such as n-heptane and toluene. Under an environment of constant thermodynamic conditions, the solid will have an equilibrium concentration X_S, while the fluid will have an equilibrium concentration X_L. These two concentrations may be related by an equilibrium distribution coefficient K. The distribution coefficient is then a function of the thermodynamic conditions and possibly the fluid concentrations. Such a relationship establishes a solid-fluid equilibrium curve.

The distribution coefficient may be altered by a simple change in some thermodynamic potential. These may be magnetic field, electric field, pressure, concentration, temperature, or any combination thereof. Such a shift causes a change in the solid and fluid equilibrium concentrations. Cycling zone adsorption takes advantage of this change in the equilibrium distribution coefficient between solid and fluid.

In this study, the thermodynamic potential that is changed is the temperature of a packed bed of solid adsorbate. The temperature change occurs as a step-change alternately in both directions between a high and a low temperature. Figure 1-1 shows the solid-liquid relationship

Figure 1-1

Solid-Liquid Equilibrium Isotherm Relationship

This figure explains the relationship of solid-liquid equilibrium compositions for a binary liquid experiencing two equilibrium temperature changes.

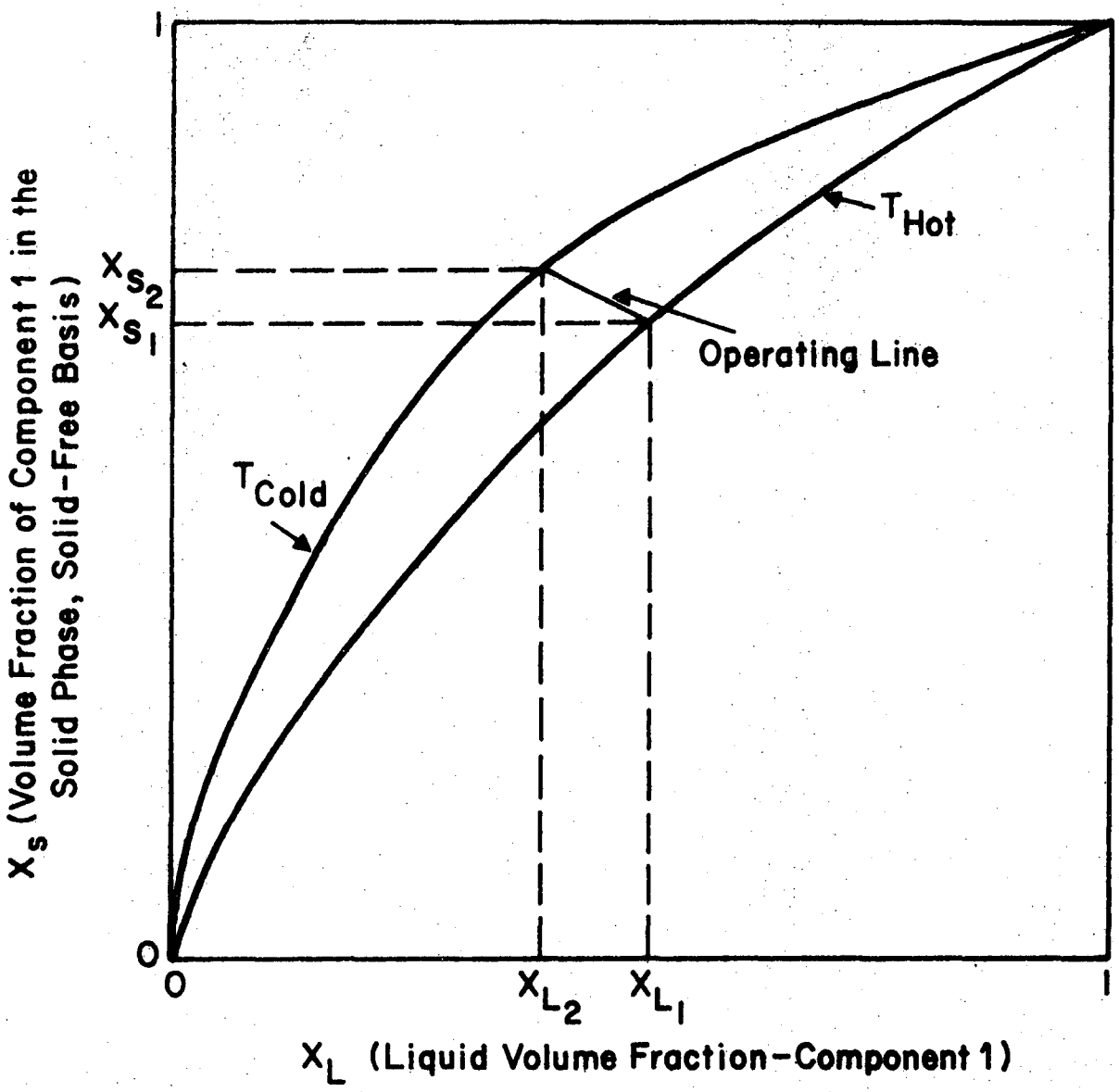
1
0
0
1
X_{S_2}
X_{S_1}
X_{L_2}
X_{L_1}
T_{Hot}
T_{Cold}
Operating Line
X_S (Volume Fraction of Component 1 in the Solid Phase, Solid-Free Basis)
X_L (Liquid Volume Fraction-Component 1)

(solid-liquid isotherms) for such a system at two different temperatures. Consider the point (X_{s1}, X_{L1}) on the isotherm for temperature T_H. For a sudden change in the temperature to T_c, there is a following change in the solid and fluid equilibrium concentrations. These new equilibrium concentrations are now established at (X_{s2}, X_{L2}). A simple material balance establishes the operating line connecting the two points (X_{s1}, X_{L1}) and (X_{s2}, X_{L2}). This change occurs because of preferential adsorption or desorption of the two components due to the thermodynamically induced change in the equilibrium distribution coefficient.

Single-Zone Operation

Consider a packed column that may either be heated or cooled through its walls such that a step-change in temperature may occur. Such a scheme is shown in Figure 1-2. At time zero, the column is filled with feed concentration liquid X_{Feed}, at a temperature T_{cold}. At time zero the column temperature is now changed to T_{hot}. At this moment the solid particles preferentially desorb component 1 of the binary liquid mixture into the liquid phase. Under equilibrium conditions the column is now filled with a liquid enriched in component 1. Its concentration is now X_{high}, while the solids concentration is X_{s-low}. At time zero the flow into the column begins at the feed concentration X_{Feed}. During the following time period the high-

Figure 1-2

Simplified Explanation of a Cycling Zone Adsorption Process

This figure qualitatively explains how a single cycling-zone adsorber produces a periodic high- and low-concentration product stream through a square-wave cycling of bed temperature.

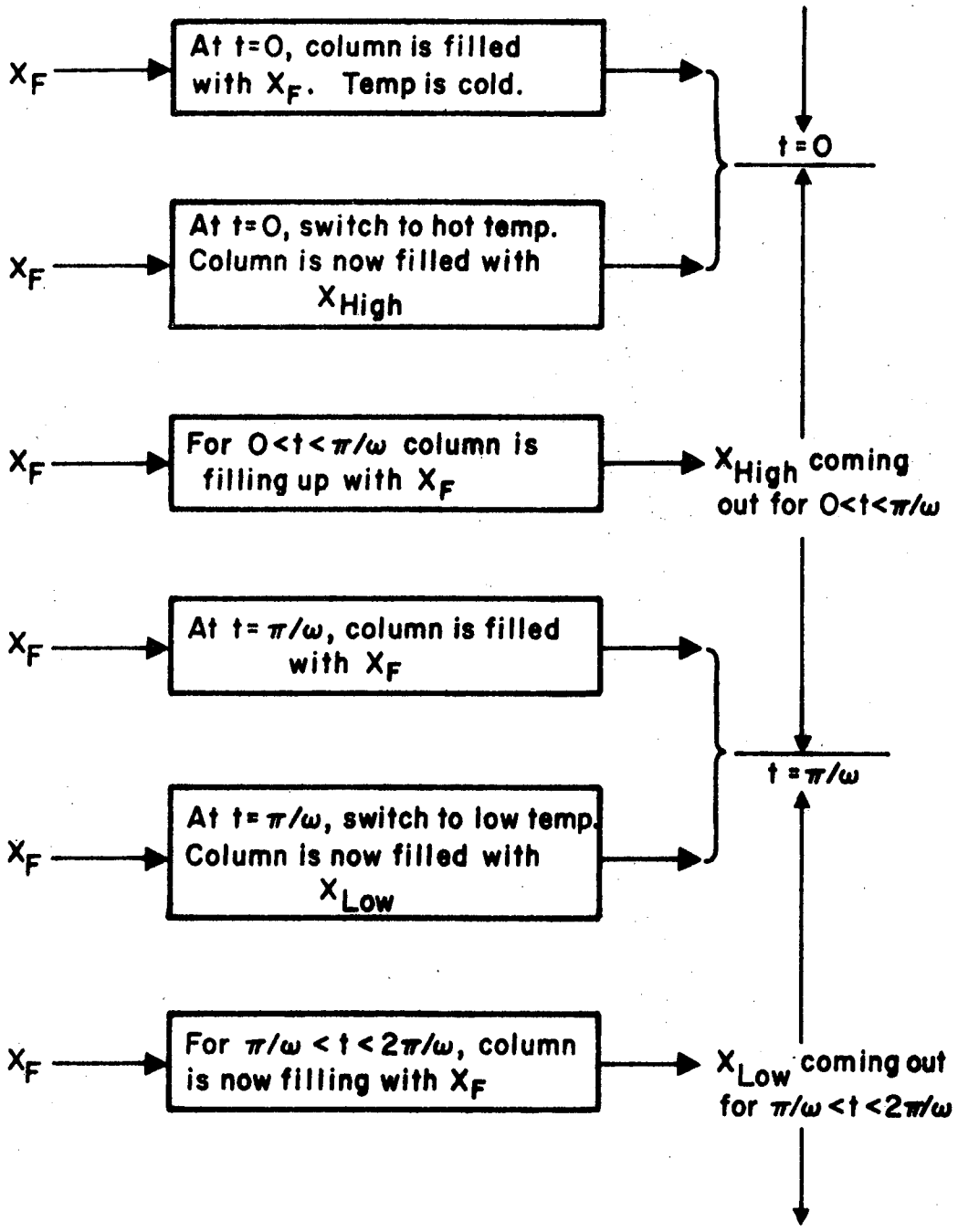
X_F
At t=0, column is filled with X_F. Temp is cold.
X_F
At t=0, switch to hot temp. Column is now filled with X_{High}
t=0
X_F
For $0<t<\pi/\omega$ column is filling up with X_F
X_{High} coming out for $0<t<\pi/\omega$
X_F
At $t=\pi/\omega$, column is filled with X_F
X_F
At $t=\pi/\omega$, switch to low temp. Column is now filled with X_{Low}
$t=\pi/\omega$
X_F
For $\pi/\omega<t<2\pi/\omega$, column is now filling with X_F
X_{Low} coming out for $\pi/\omega<t<2\pi/\omega$

concentration liquid is displaced until the column is completely filled with the feed liquid again. The displaced liquid is collected as the high-concentration product.

The column is now filled with the feed-concentration liquid and the temperature is switched to T_{cold}. Component 1 is now preferentially adsorbed by the solid particles. The liquid equilibrium concentration in the column now becomes X_{L-low}, while the solids concentration becomes X_{s-high}. The low-concentration liquid is now displaced by the feed liquid. The displaced liquid is collected as the low-concentration product. The column is now again filled with feed-concentration liquid and the process is repeated.

In this fashion high-and low-concentration products are produced cyclically by a periodic step-change in the column temperature. Figure 1-3 is a plot of the temperature and concentration changes of such an idealized packed-bed operation. Such a continuous flow operation is the heart of Cycling Zone Adsorption. As described, the process is idealized in that it was assumed that a perfect step-change in the column temperature can be induced and that the fluid and solid compositions respond immediately to the temperature change. As would be expected, the main disability of such an operation is the development of a step-change in the column temperature. Any deviation from such a column temperature response causes either a reduction in the maximum

Figure 1-3

Idealized Single-Zone Temperature and Effluent Concentration Profile

This figure explains the ideal periodic variation of bed temperature and the resulting idealized effluent concentration profile.

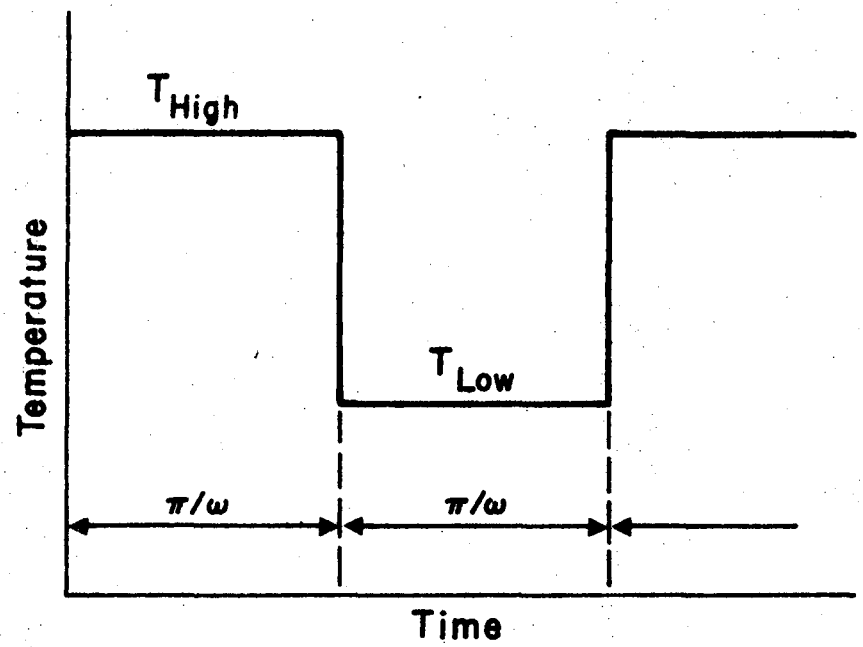
T High
T Low
Temperature
π/ω
π/ω
Time

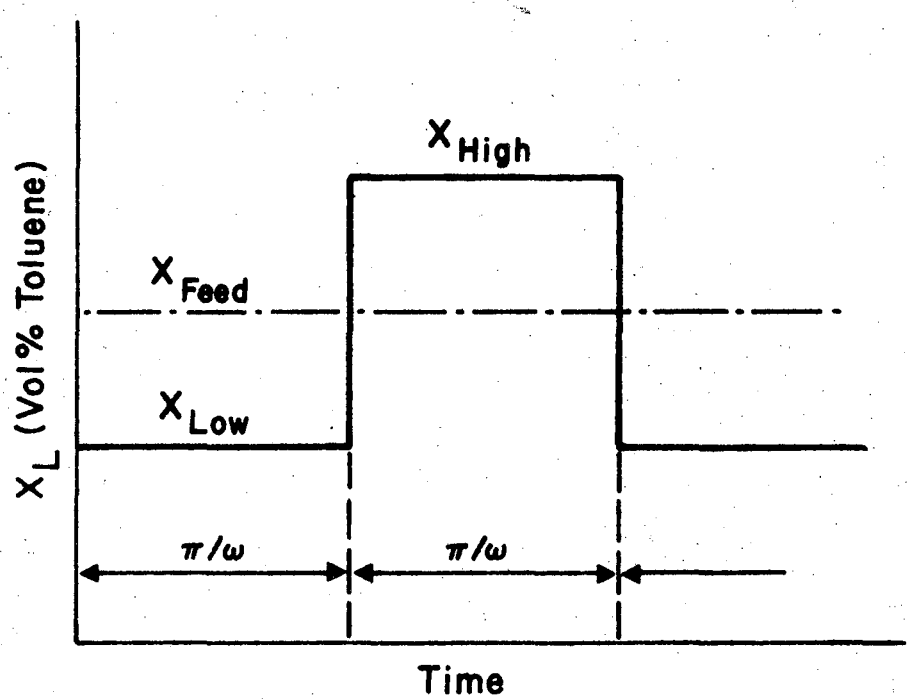
X High
X Feed
X Low
X L (Vol % Toluene)
π/ω
π/ω
Time

concentration changes or the duration of concentration peak flows. Chapter 4 is devoted to techniques that optimally improve the operation of a single-packed bed, or single "zone."

Multi-Zone Operation

One may take advantage of the separations resulting from a single zone by the addition of zones in an appropriately designed cascade. Figure 1-4 depicts a simple arrangement that replaces the periodic changes in the production rate with a continuous, constant production rate by running two zones in parallel. Such an arrangement requires that the temperature responses of each zone be 180° out of phase with the other, that is, while one zone is hot, the other is cold. In this manner, both high- and low-concentration products are produced simultaneously.

Figure 1-5 is a simple diagram of a series of zones which amplify the separation of a single zone by a factor roughly equal to the number of zones in the series. The ability of a series to increase the separation is explained as follows: The first zone in the series produces two product streams, one of concentration higher than the feed and one of concentration lower than the feed. For example, since the product streams are produced periodically, the high-concentration product stream may be passed as a new feed stream to a following zone in the series. During the other half-period of operation the low-concentration product

0 0 0 0 0 8 0 7 4 7 7

Figure 1-4

Parallel Zone Arrangement

This figure presents an idealized parallel zone arrangement used to continuously produce a high- and a low-concentration product from a constant concentration feed. The idealized bed temperature and effluent concentration profiles are given.

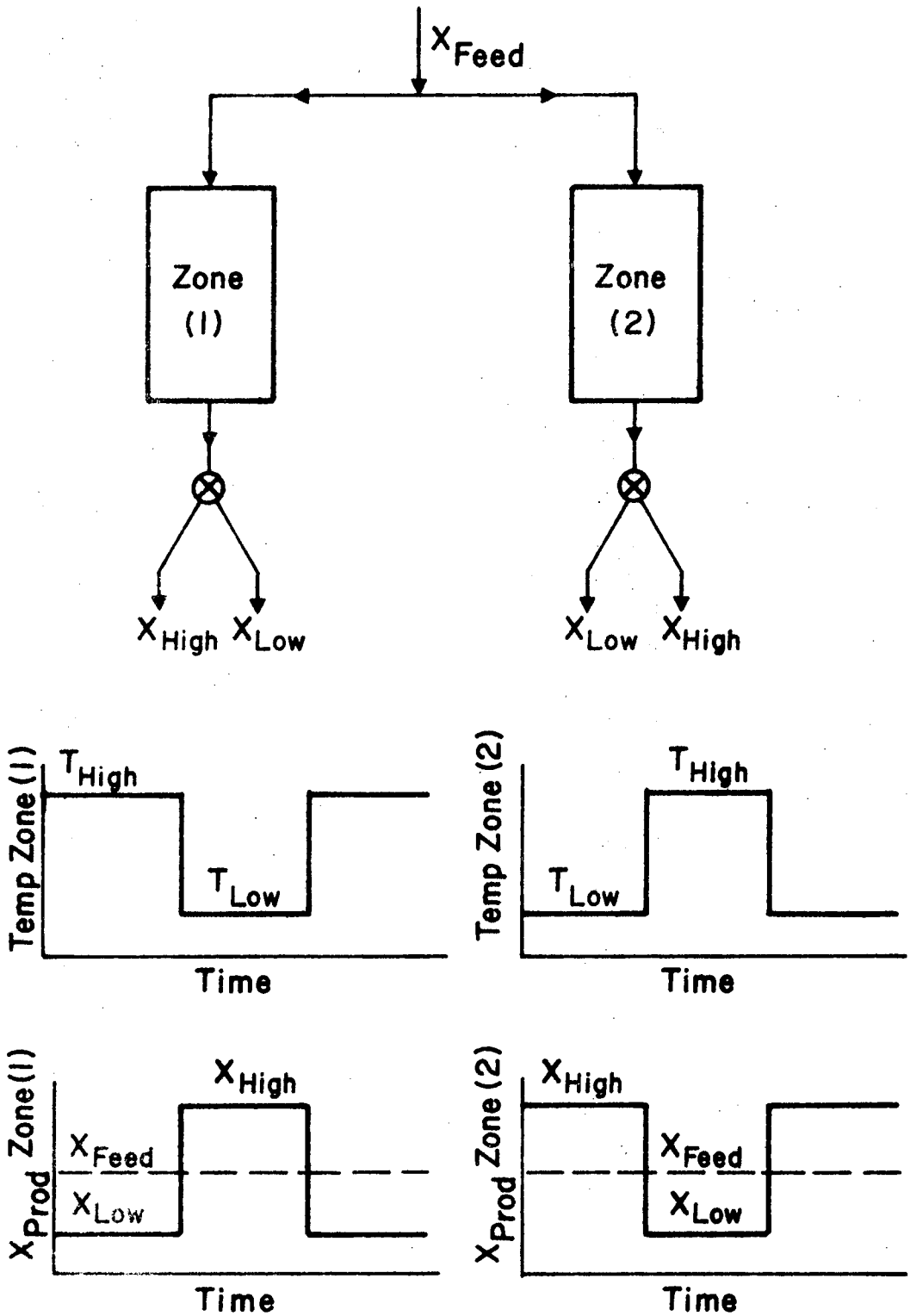
X Feed
Zone (1)
Zone (2)
X High
X Low
X Low
X High
Temp Zone (1)
T High
T Low
Time
Temp Zone (2)
T High
T Low
Time
X Prod Zone (1)
X High
X Feed
X Low
Time
X Prod Zone (2)
X High
X Feed
X Low
Time

Figure 1-5

Series Zone Arrangement

This figure presents the arrangement of single zones into a series of zones. The idealized bed temperature and effluent concentration profiles for each zone are given.

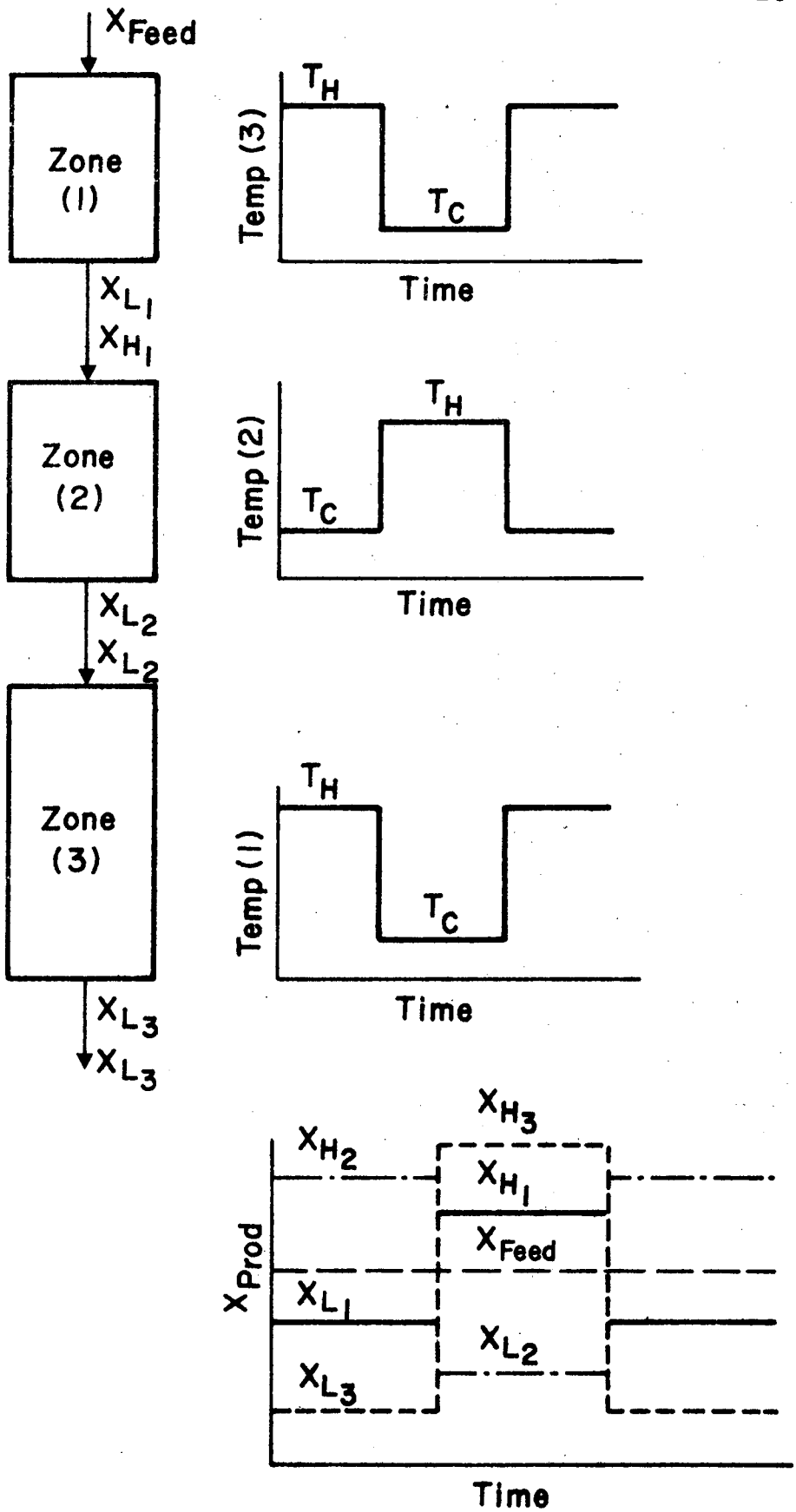
X_{Feed}
Zone (1)
X_{L_1}
X_{H_1}
Zone (2)
X_{L_2}
X_{L_2}
Zone (3)
X_{L_3}
X_{L_3}
T_H
T_C
Temp (3)
Time
T_H
T_C
Temp (2)
Time
T_H
T_C
Temp (1)
Time
X_{H_3}
X_{H_2}
X_{H_1}
X_{Feed}
X_{Prod}
X_{L_1}
X_{L_2}
X_{L_3}
Time

stream from the first zone is passed to the second zone in the series as a new feed. The second zone therefore experiences periodically a high- and then a low-concentration feed. By cycling the temperature of the second zone, it is then possible to produce an even higher high-concentration product stream from the high-concentration feed to the second zone, and an even lower low-concentration product stream from the low-concentration feed to the second zone. The temperature response of each zone in the series is 180° out of phase with the preceding zone in the series. Such a simplified series of zones should then be capable of producing very large separations of a binary liquid feed from small single-zone separations. The effluent concentration profiles for such an operation of three zones in a series is also shown in Figure 1-5.

These simplified zone arrangements can be further improved by using recycle streams. Such a recycle scheme is pictured in Figure 1-6 for the operation of two zones in a series of zones. In this case the high-concentration product stream from each zone is passed to the following zone as feed, with the low-concentration product stream being recycled to a preceding zone. Such a recycle arrangement then minimizes the reduction of throughput from zone to zone. To produce a low-concentration product, the same procedure is used with the high-concentration product streams being recycled.

Figure 1-6

Two-Zone Product Recycle Scheme

This figure explains how partial recycle of product streams may be used in the legs of a cycling zone adsorption cascade. The recycle schemes are depicted for both the high-concentration product led and the low-concentation product led of a cascade.

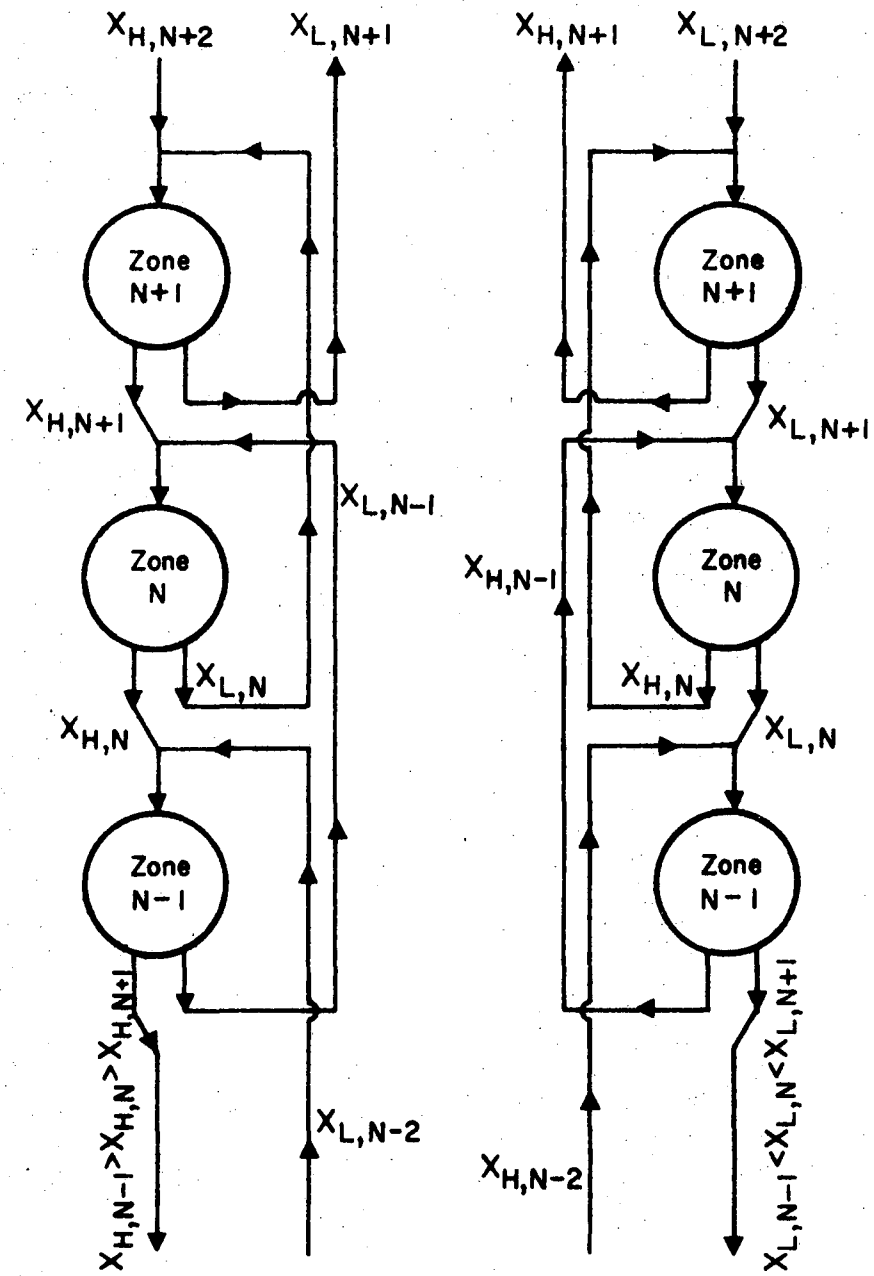
$X_{H,N+2}$
$X_{L,N+1}$
Zone N+1
$X_{H,N+1}$
$X_{L,N-1}$
Zone N
$X_{L,N}$
$X_{H,N}$
Zone N-1
$X_{H,N+1} > X_{H,N} > X_{H,N-1}$
$X_{L,N-2}$
High-Conc Product to Next Zone
$X_{H,N+1}$
$X_{L,N+2}$
Zone N+1
$X_{L,N+1}$
$X_{H,N-1}$
Zone N
$X_{H,N}$
$X_{L,N}$
Zone N-1
$X_{L,N+1} < X_{L,N} < X_{L,N-1}$
$X_{H,N-2}$
Low-Conc Product to Next Zone

It is also possible to have recycle around a single zone. Such recycle introduces variable feed to the zone. This is shown in Figure 1-7. Here a portion of the high-concentration product stream is recycled back to mix with a feed of constant concentration, being less than that of the high-concentration recycle stream. This produces a high-concentration feed stream into the zone, which, through the temperature change, is enriched to become the high-concentration product stream. The low-concentration product stream may be partially recycled to mix with the feed of constant concentration to produce a low-concentration feed into the zone. Upon changing the temperature of the zone, a low-concentration product stream may be produced. Such an operation considerably complicates the flow diagram, but offers the possibility of obtaining greater differences in product stream concentration through the introduction of a feed concentration difference. The introduction of a variable-feed into a single zone will be considered in Chapter 5.

It is apparent that as concentration differences increase within a zone, as in the case of variable-feed operation or zone-series operation, factors arise that effect the idealized square-wave effluent concentration profiles. It will be shown that longitudinal diffusion is the major problem in the cyclic operation of an absorber. The following chapters investigate, both theoretically and experimentally, the major factors limiting the operation of a cycling-zone adsorber.

Figure 1-7

Variable-Feed, Recycle Operation of a Cycling Zone Adsorber

This figure explains how partial product recycle may be used to maintain a variable-feed concentration input to a single zone.

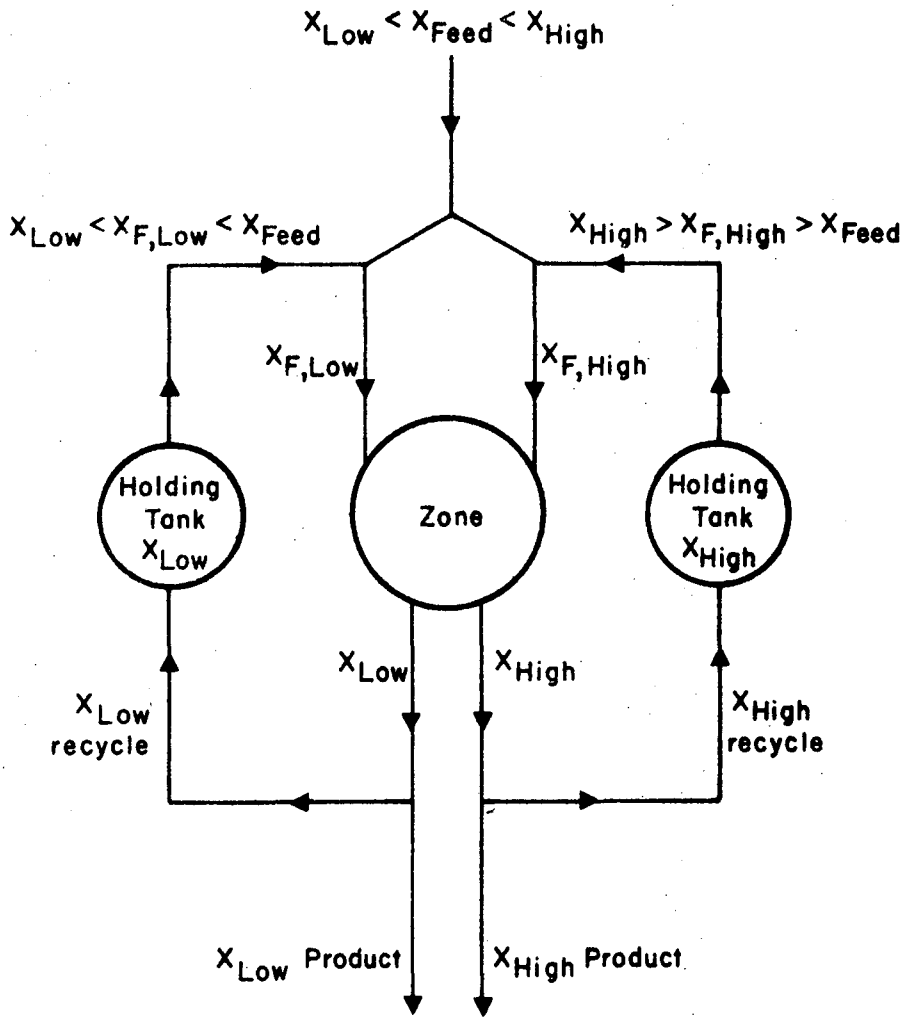
$X_{Low} < X_{Feed} < X_{High}$
$X_{Low} < X_{F,Low} < X_{Feed}$
$X_{High} > X_{F,High} > X_{Feed}$
$X_{F,Low}$
$X_{F,High}$
Holding Tank X_{Low}
Zone
Holding Tank X_{High}
X_{Low}
X_{High}
X_{Low} recycle
X_{High} recycle
X_{Low} Product
X_{High} Product

0 0 0 0 0 8 0 . . 8 2

CHAPTER 2

EXPERIMENTAL SYSTEM CHARACTERISTICS AND APPARATUS

Introduction..... 26

Solid-Liquid Characteristics..... 26

Solids Capacity..... 30

Void Fractions and Particle Densities.... 31

Experimental Apparatus..... 35

Columns..... 35

Temperature Control..... 41

Feed Degassing Units..... 42

Liquid Composition Analysis System.. 44

CHAPTER 2

EXPERIMENTAL SYSTEM CHARACTERISTICS AND APPARATUS

Introduction

Silica gel was used as a solid adsorbent with which the separation of the liquid binary mixture n-heptane-toluene was carried out. This system was chosen since these chemicals are relatively inexpensive and because previous studies in adsorption have been carried out using this binary liquid-solid system (57,58). Vapor-liquid composition data are also readily available, allowing comparison calculations of C.Z.A. to distillation to be made. Whereas separations by C.Z.A. have been previously limited to very low concentration ranges, use of this system permits separations to be observed over the total range of the binary liquid compositions.

Solid-Liquid Characteristics

Solid-liquid isotherm data were obtained experimentally at temperatures of 2°C and 59°C. A continuously stirred bath was constructed in which small amounts of the solid-liquid mixtures could be immersed. The mixtures were sealed in 125-ml flasks and continuously agitated by means of a motor-driven cam shaft. Samples were allowed to reside within the bath for two hours. Each sample contained 9 g of silica gel and 20 ml of the binary liquid mixture. Refractive index readings on the liquid were taken before

and after introduction of the silica gel. The later reading gave the composition of the liquid in equilibrium with the solid at the prescribed temperature. The solids composition was determined by removing the drained solids from the liquid mixture, and then by displacing the liquid from the solids by adding water. Since the silica gel is a desiccant, its affinity to water is almost infinite in comparison with the hydrocarbon. When the solids come in contact with the water, they split and upon rupturing release of all the adsorbed and entrapped hydrocarbons, which then floated on top of the water. The hydrocarbon could then be removed and these samples could be tested with an Abbé refractometer, giving the solid's equilibrium composition. This composition was an average of the liquid in the pores of the solid and of the liquid adsorbed upon the surface of the pores of the solid silica gel. It is important to remember that this composition is the average of the surface composition and the pore liquid composition. All compositions are given as volume percent toluene.

Equilibrium data obtained in the previous fashion were then plotted as solids composition (X_S) versus the liquid composition (X_L) for the two temperatures of interest. The plot of the experimental isotherm data appear in Figure 2-1. These data were then fit to a two-constant curve of the following form:

Figure 2-1

Solid-Liquid Equilibrium Isotherms (Eq. 2-1)

Binary liquid system: n-heptane and toluene (analytic reagent grade). Solid particles: silica gel, 4-16 mesh (Davison Chemical). Isotherm temperatures: 2.0°C and 59°C.

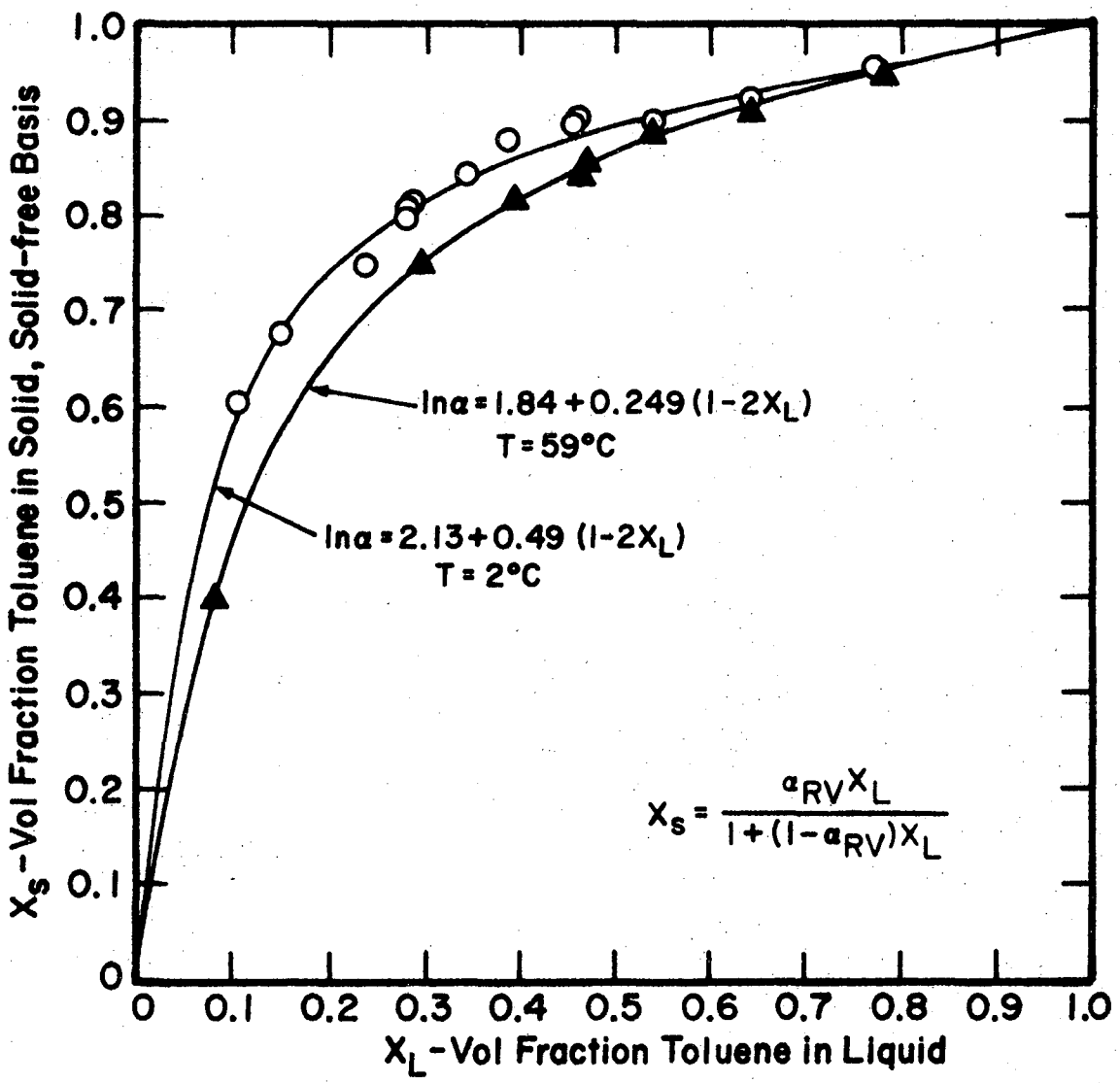
1.0
0.9
0.8
0.7
0.6
0.5
0.4
0.3
0.2
0.1
0
0 0.1 0.2 0.3 0.4 0.5 0.6 0.7 0.8 0.9 1.0
X_S-Vol Fraction Toluene in Solid, Solid-free Basis
X_L-Vol Fraction Toluene in Liquid
$\ln\alpha = 1.84 + 0.249(1-2X_L)$
T = 59°C
$\ln\alpha = 2.13 + 0.49(1-2X_L)$
T = 2°C
$X_S = \frac{\alpha_{RV} X_L}{1+(1-\alpha_{RV})X_L}$

$$X_s = \frac{\alpha_{R_V} X_L}{1 + (\alpha_{R_V} - 1)X_L} \qquad (2\text{-}1)$$

where $\ln \alpha_{R_V} = a + b(1 - 2X_L)$. A least-squares computer program fit of the data in Figure 2-1 gave the following values of the two constants at the two different temperatures:

$2°C$, $\ln \alpha_{R_V} = 2.1348 + 0.4948\ (1 - 2X_L)$, and

$59°C$, $\ln \alpha_{R_V} = 1.8433 + 0.2495\ (1 - 2X_L)$.

These curves are also plotted in Fig. 2-1.

Solids Capacity

A simple displacement procedure was used to determine the liquid capacity of the solid silica gel. Ten grams of silica gel were placed in a 25-ml graduated burette, which was then filled with the liquid hydrocarbon. The solid-liquid mixture was then allowed to stand for three days, with periodic agitation to remove entrapped gases. The solid-liquid mixture was also placed under vacuum to help remove gases. The liquid was then rapidly drained off of the solid silica gel and distilled water was then placed in the burette. The solid-water mixture was now allowed to stand for a day. The hydrocarbon saturating the solid was displaced by the water and floated to the top of the water in the burette, allowing its volume measurement. Such experiments, using different concentrations of the n-heptane-toluene mixture, gave a solids capacity of 0.300 cc/g of dry silica gel.

Void Fractions and Particle Densities

Knowing the liquid capacity of the solid, the intraparticle and interparticle void fractions were determined by using a known volume of liquid hydrocarbon. The following is a list of data used to calculate the void fractions for an approximately 60-mesh solid (measurements taken in a 25-ml graduated cylinder):

Weight of dry silica gel = 14.50 g
Total volume of liquid = 17.00 ml
Volume of liquid above the solids = 5.0 ml
Volume to top of solids = 19.0 ml
Volume of liquid in and between the solid particles = 17.00-5.0 = 12.0 ml
Volume of liquid in solid particles
= (capacity)(weight of solids)
= (0.3 cc/g)(14.5 g) = 4.35 ml
Volume of liquid between solid particles
= 12.00 - 4.35 = 7.65 ml
Interparticle void fraction, α = 7.65/19.0
= 0.40
Dry-packed density = ρ_{sb} = 14.5 g/19.0 cc
= 0.763 g/cc
ρ_s = Density of dry solids = $\rho_{sb}/(1-\alpha)$
= 0.763 g/cc/0.597 = 1.28 g/cc
Intraparticle void fraction ϵ =
= (ρ_s')(capacity) = (1.28 g/cc)(0.300 cc/g)
= 0.383
True density of solid $\rho_s = \rho_s'/(1-\epsilon)$
= 1.278 g/cc/0.616 = 2.07 g/cc

Table 2-1

Solid-Liquid Isotherm Data

The following values are calculated from the solid-liquid equilibrium isotherm equation, Eq. (2-1). The temperatures are 2°C and 59°C (compositions in vol % toluene).

X_L	X_s (2°C)	X_s (59°C)	X_L	X_s (2°C)	X_s (59°C)	X_L	X_s (2°C)	X_s (59°C)
0.00	0.0000	0.0000	0.34	0.8362	0.7790	0.67	0.9355	0.9218
0.01	0.1218	0.0753	0.35	0.8408	0.7857	0.68	0.9376	0.9247
0.02	0.2172	0.1408	0.36	0.8453	0.7921	0.69	0.9397	0.9275
0.03	0.2940	0.1981	0.37	0.8496	0.7983	0.70	0.9418	0.9303
0.04	0.3571	0.2488	0.38	0.8537	0.8043	0.71	0.9439	0.9330
0.05	0.4099	0.2939	0.39	0.8577	0.8101	0.72	0.9459	0.99357
0.06	0.4548	0.3343	0.40	0.8616	0.8157	0.73	0.9479	0.9384
0.07	0.4934	0.3708	0.41	0.8653	0.8212	0.74	0.9499	0.9410
0.08	0.5270	0.4039	0.42	0.8689	0.8264	0.75	0.9519	0.99436
0.09	0.5565	0.4340	0.43	0.8724	0.8315	0.76	0.9539	0.9462
0.10	0.5826	0.4615	0.44	0.8758	0.8365	0.77	0.9559	0.9487
0.11	0.6059	0.4868	0.45	0.8791	0.8413	0.78	0.9578	0.9512
0.12	0.6268	0.5101	0.46	0.8823	0.8459	0.79	0.9598	0.9536
0.13	0.6457	0.5317	0.47	0.8854	0.8505	0.80	0.9617	0.9561
0.14	0.6628	0.5517	0.48	0.8884	0.8549	0.81	0.9637	0.9585
0.15	0.6784	0.5704	0.49	0.8914	0.8592	0.82	0.9656	0.9608
0.16	0.6928	0.5878	0.50	0.8942	0.8633	0.83	0.9675	0.9632
0.17	0.7060	0.6040	0.51	0.8971	0.8674	0.84	0.9694	0.9655
0.18	0.7181	0.6193	0.52	0.8998	0.8714	0.85	0.9713	0.9678
0.19	0.7294	0.6337	0.53	0.9025	0.8753	0.86	0.9732	0.9701
0.20	0.7399	0.6472	0.54	0.9051	0.8791	0.87	0.9751	0.9723
0.21	0.7497	0.6600	0.55	0.9077	0.8828	0.88	0.9770	0.9746
0.22	0.7588	0.6720	0.56	0.9102	0.8864	0.89	0.9790	0.9768
0.23	0.7674	0.6835	0.57	0.9127	0.8900	0.90	0.9809	0.9790
0.24	0.7755	0.6943	0.58	0.9152	0.8934	0.91	0.9828	0.9812
0.25	0.7831	0.7046	0.59	0.9176	0.8968	0.92	0.9847	0.9833
0.26	0.7902	0.7145	0.60	0.9199	0.9002	0.93	0.9866	0.9854
0.27	0.7970	0.7238	0.61	0.9222	0.9034	0.94	0.9885	0.9876
0.28	0.8035	0.7328	0.62	0.9245	0.9066	0.95	0.9904	0.9897
0.29	0.8096	0.7413	0.63	0.9268	0.9098	0.96	0.9923	0.9918
0.30	0.8154	0.7495	0.64	0.9290	0.9128	0.97	0.9942	0.9938
0.31	0.8209	0.7573	0.65	0.9312	0.9159	0.98	0.9961	0.9959
0.32	0.8262	0.7648	0.66	0.9334	0.9188	0.99	0.9981	0.9980
0.33	0.8313	0.7721				1.00	1.0000	1.0000

Table 2-1 (Continued)

The following lists the experimentally determined solid-liquid equilibrium isotherm data points at a temperature of 2°C.

X_L	X_s
0.1096	0.6049
0.1096	0.6049
0.1539	0.6753
0.2369	0.7479
0.2369	0.7479
0.2820	0.7996
0.2820	0.8054
0.2866	0.8142
0.3446	0.8407
0.3446	0.8407
0.3874	0.8795
0.4533	0.8946
0.4582	0.9037
0.5419	0.8946
0.6479	0.9220
0.7679	0.9529

The following lists the experimentally determined solid-liquid equilibrium isotherm data points at a temperature of 59°C.

X_L	X_s
0.0826	0.3994
0.2958	0.7479
0.3922	0.8172
0.4632	0.8437
0.4707	0.8526
0.5419	0.8946
0.6479	0.9068
0.7794	0.9498

Table 2-2 summarizes the necessary physical constants which characterize the properties of the liquid hydrocarbons and silica gel used in this study.

Table 2-2

Liquid and Solid Properties

Binary Liquid Properties (n-heptane and toluene)[a]

Mallinckrodt Chemical Works, analytical reagent grade n-heptane and toluene
M.W. n-heptane: 100.2 g/mole
M.W. toluene: 92.13 g/mole
$\rho_{heptane}$: 0.68376 g/cc at 20°C
$\rho_{toluene}$: 0.86694 g/cc at 20°C
B.P. n-heptane: 98.4°C
B.P. toluene: 110.6°C
Latent Heat Vap. $\lambda_{heptane}$: 7,341.51 cal/g-mole at 98.4°C
Latent Heat Vap. $\lambda_{toluene}$: 8,028.72 cal/g-mole at 110.6°C
$C_{p,heptane}$: 0.507 cal/g-°C
$C_{p,toluene}$: 0.400 cal/g-°C
Thermal conductivity of 50 vol % mixture: 3.281×10^{-4} cal/cm-sec-°C

Solid Silica Gel Properties

Activated silica gel desiccant (Tel-Tale), Davison Chemical Co., grade 42, code No. 42-08-08-237, specification MIL-D-3716
Dry-packed density ρ_{sb}: 0.763 g/cc
Dry density ρ_s': 1.278 g/cc
True density ρ_s: 2.07 g/cc
$C_{p,solid}$: 0.122 cal/g-°C
Thermal conductivity k: 2.388×10^{-4} cal/cm-sec-°C
Shape: irregular particles
Size: 4-16 mesh, 20 mesh, and 60-mesh size
Color: dark blue in hydrocarbon liquid, pink in water
Solid capacity: 0.300 ± 0.01 cc of liquid/g of dry solid

a. Reference: "Handbook of Chem. & Phys.," Rubber Publishing Co., 42nd Edition, 1960.

0 0 0 0 3 8 0 7 4 8 7

Experimental Apparatus

The experimental equipment is shown in the photograph on page 36 and in the schematic drawing (Figure 2-2). Two different adsorption columns, the vital part of the system, are shown in Figure 2-3. The design of the experimental equipment is centered around the ability to generate a square-wave temperature response in the packed column. The central portions of the apparatus will be described below.

Columns

Two radically different columns, schematic Figure 2-3, were used. The column in Figure 2-3a is made of a Pyrex glass tube, 64 cm in length and 65-mm inside diameter. The column was jacketed for radial heat transfer. Centrally placed inside the column was a four-finned copper tube which transfered heat radially. Both water jacket and finned-tube heat exchanger then allowed a rapid transfer of heat to and from the solid-liquid phase in the column. Entrance and exit column caps were made of machined brass, 65-mm inside diameter and 6-cm long. One-quarter-inch I.D. Swage-Lok fittings were attached to both. Active silica gel filled the region between the top and bottom of the finned-tube heat exchanger. Inert glass beads, 1-mm diameter, filled the entrance and exit regions of the column. Four copper-constantan thermocouples were placed inside the column. Two were attached directly to

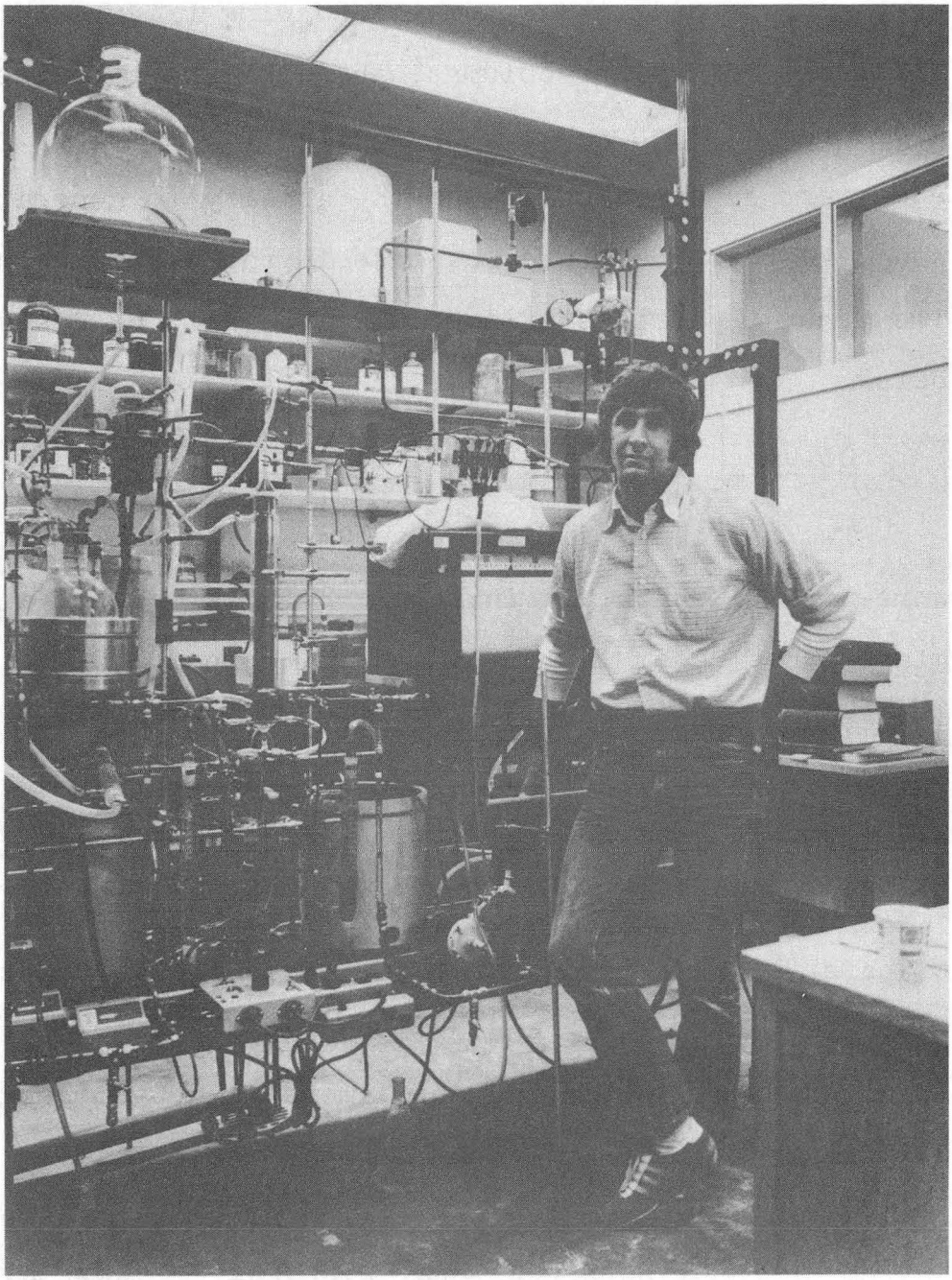

0 0 0 0 0 8 0 / 1 0 8

Figure 2-2

Experimental Apparatus

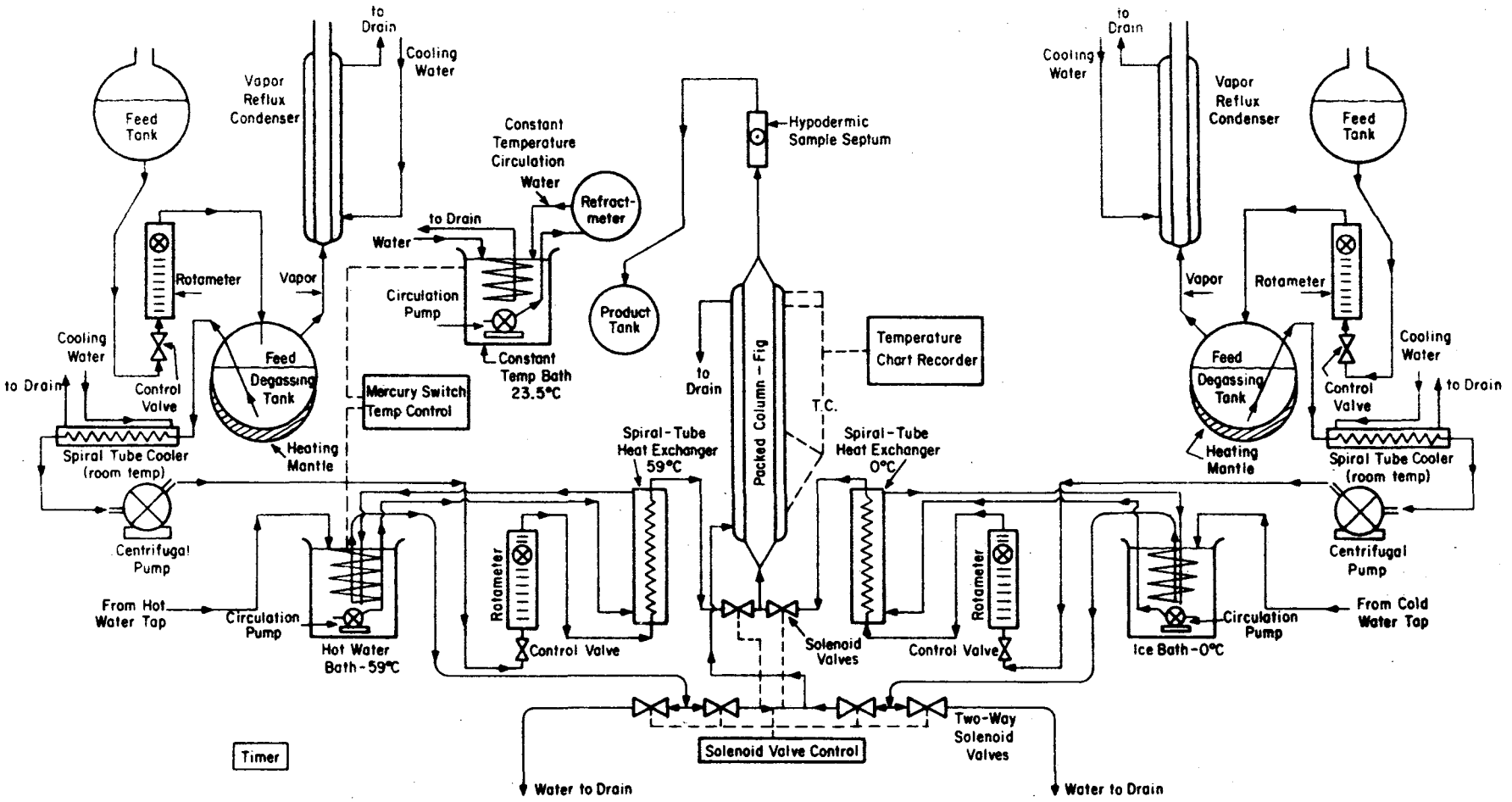
Feed Tank
Vapor Reflux Condenser
to Drain
Cooling Water
Constant Temperature Circulation Water
Refract-meter
Hypodermic Sample Septum
Rotameter
Vapor
Circulation Pump
Constant Temp Bath 23.5°C
Product Tank
Cooling Water
to Drain
Control Valve
Feed Degassing Tank
Mercury Switch Temp Control
Heating Mantle
Spiral Tube Cooler (room temp)
Centrifugal Pump
Temperature Chart Recorder
T.C.
Packed Column - Fig
Spiral-Tube Heat Exchanger 59°C
Spiral-Tube Heat Exchanger 0°C
From Hot Water Tap
Hot Water Bath - 59°C
Control Valve
Solenoid Valves
Ice Bath - 0°C
From Cold Water Tap
Timer
Solenoid Valve Control
Two-Way Solenoid Valves
Water to Drain

0 0 0 0 3 8 0 . 4 3 9

Figure 2-3

Experimental Adsorption Columns

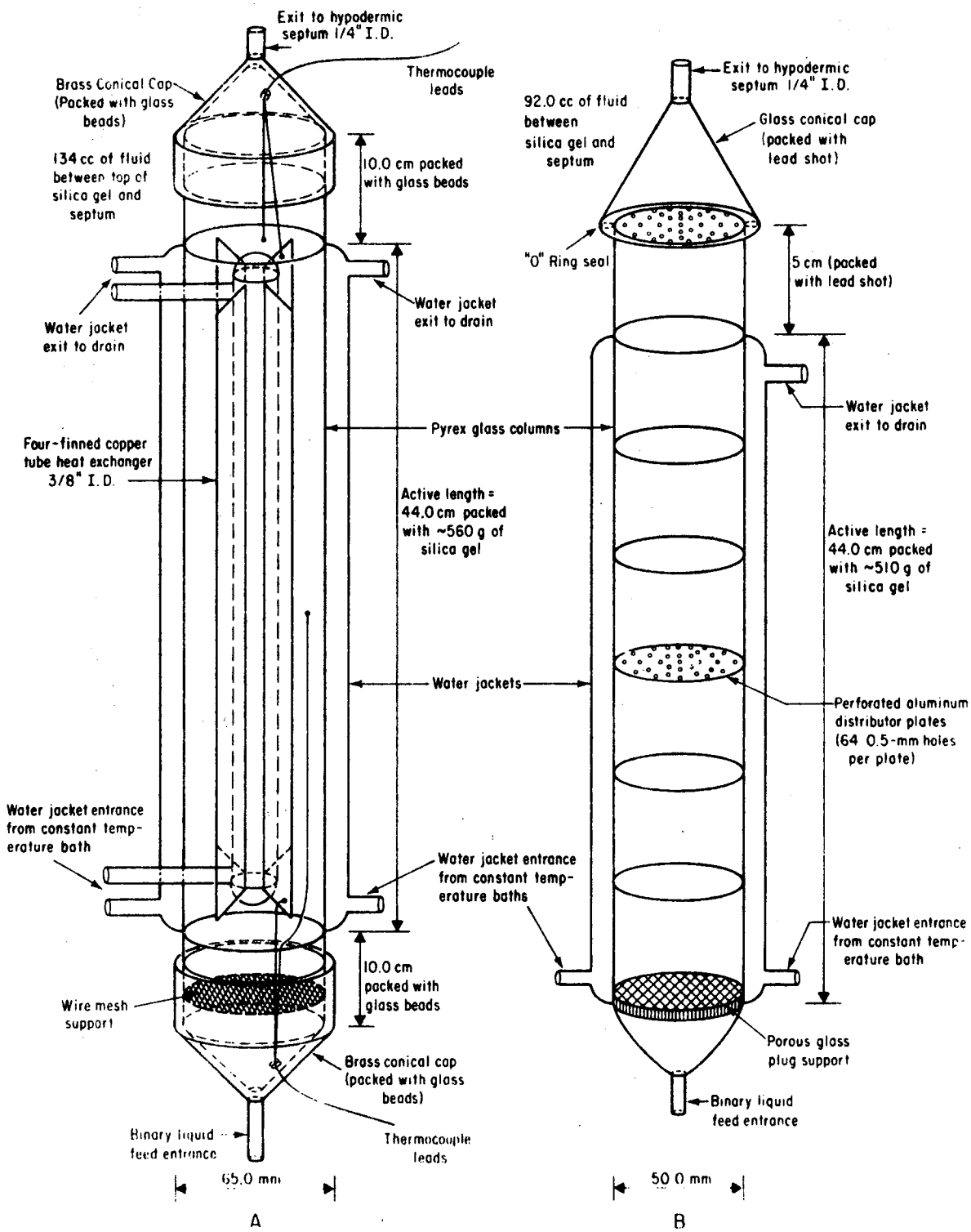
Exit to hypodermic septum 1/4" I.D.
Thermocouple leads
Brass Conical Cap (Packed with glass beads)
134 cc of fluid between top of silica gel and septum
10.0 cm packed with glass beads
Water jacket exit to drain
Water jacket exit to drain
Pyrex glass columns
Four-finned copper tube heat exchanger 3/8" I.D.
Active length = 44.0 cm packed with ~560 g of silica gel
Water jackets
Water jacket entrance from constant temperature bath
Water jacket entrance from constant temperature baths
10.0 cm packed with glass beads
Wire mesh support
Brass conical cap (packed with glass beads)
Binary liquid feed entrance
Thermocouple leads
65.0 mm
A
Exit to hypodermic septum 1/4" I.D.
92.0 cc of fluid between silica gel and septum
Glass conical cap (packed with lead shot)
"O" Ring seal
5 cm (packed with lead shot)
Water jacket exit to drain
Active length = 44.0 cm packed with ~510 g of silica gel
Perforated aluminum distributor plates (64 0.5-mm holes per plate)
Water jacket entrance from constant temperature bath
Porous glass plug support
Binary liquid feed entrance
50.0 mm
B

the copper heat exchanger, at the top and the bottom, while two were freely placed within the column packing, one at the midpoint of the column and the other at the exit. This allowed a constant monitoring of the column temperature. This column was used primarily for continuous flow experiments.

A smaller column, Figure 2-3b, was designed for non-continuous flow experimentation. The column was constructed of Pyrex glass, 50-mm inside diameter and 49-cm long. The column was also jacketed for radial heat transfer. A 80-micron mean pore diameter fritted glass disc was fit in the column at the entrance, minimizing the volume of the entrance. Equally spaced within the column were seven perforated aluminum discs, used for flow distribution and to minimized the effects of longitudinal diffusion and mixing. The void space at the top of the column was filled with 3-mm lead spheres. Flow was in the upward direction for both columns. The smaller column had no thermocouples for temperature monitoring.

Temperature Control

Column temperature was controlled by water flow through two constant temperature baths (Figure 2-2). The baths were constructed from five-gallon ceramic tanks. Within each bath was fifty feet of 1/4-in. I.D. coiled copper tubing through which tap water flowed to the column. Surrounding water in the hot bath was heated by a heating knife blade,

controlled by a mercury switch thermometer. The cold bath was maintained by the continual addition of ice to the bath. Through the appropriate switching of the solenoid valves, shown in Figure 2-2, the column could be periodically heated or cooled to the desired temperatures. Submersible pumps in each bath pumped hot and cold water to glass spiral condensers, through which the hydrocarbon feed could be preheated or precooled before entrance into the column.

This particular column-heating design allowed the column to generate three different temperature responses: (1) A standing wave response by heating only the bed without feed preheat; (2) a travelling wave response by using only the feed preheat units; and (3) a combination of 1 and 2 by using both feed preheat and column heating.

Table 2-3 lists the range of variable studied that could be tolerated by the experimental apparatus.

Feed Degassing Units

Because of the temperature swing experienced by the column, gas contained by the feed continually nucleated upon the small silica gel particles in the column. Consequently the solid particles were partially coated by air, reducing their effective capacity. This phenomenon was quite apparent when using small mesh particles, approximately 60-mesh size. To alleviate this problem, the feeds to the column were boiled, then preheated to the desired temperature before entrance into the column. The feed

Table 2-3

Range of Variables Studied

Bed temperature: cold-cycle at 2°C, hot-cycle at 59°C
Solid packing: silica gel, 4- to 60-mesh particle size
Feed preheat temperature: 2°C and 59°C
Column length: 38 cm and 44 cm of active silica gel
Feed composition: 10 vol % toluene to 80 vol % toluene
Superficial fluid velocity: 0.242 cc/sec to 5.00 cc/sec
Interstitial fluid velocity (time of passage of fluid through silica gel packing): 0.0466 cm/sec to 1.000 cm/sec
Feed input: constant-feed composition or variable-feed composition input
Feed input amplitudes: 0.00 vol % toluene (constant feed) to 40 vol % toluene
Temperature switching frequency: (sec^{-1})
Period (Total time for hot and cold operation)
Column temperature response: square-wave (noncontinuous operation termed Stop-Go), sine wave, and rounded square wave.

degassing units are shown in Figure 2-2. They consisted of 3000-cc flasks mounted in Glas-Co Heating Mantles. Feeds were metered into the boiling units, cooled by glass spiral condensers, then preheated before entrance into the column.

Liquid Composition Analysis System

Liquid analysis system is shown in Figure 2-2. One-cc samples of liquid were hypodermically drawn off the column through a small septum at the outlet of the column. The hypodermic samples were then analysed by use of a Spenser 2082 Refractometer. Refractive indices could be read to an accuracy of 0.18 vol % toluene. Figure 2-4 is a calibration chart for refractive index versus volume percent toluene at 23.5°C.

0 0 0 0 0 8 0 7 4 9 2

Figure 2-4

Refractive Index Versus Volume % Toluene in n-Heptane-Toluene Mixtures (23.5°C)

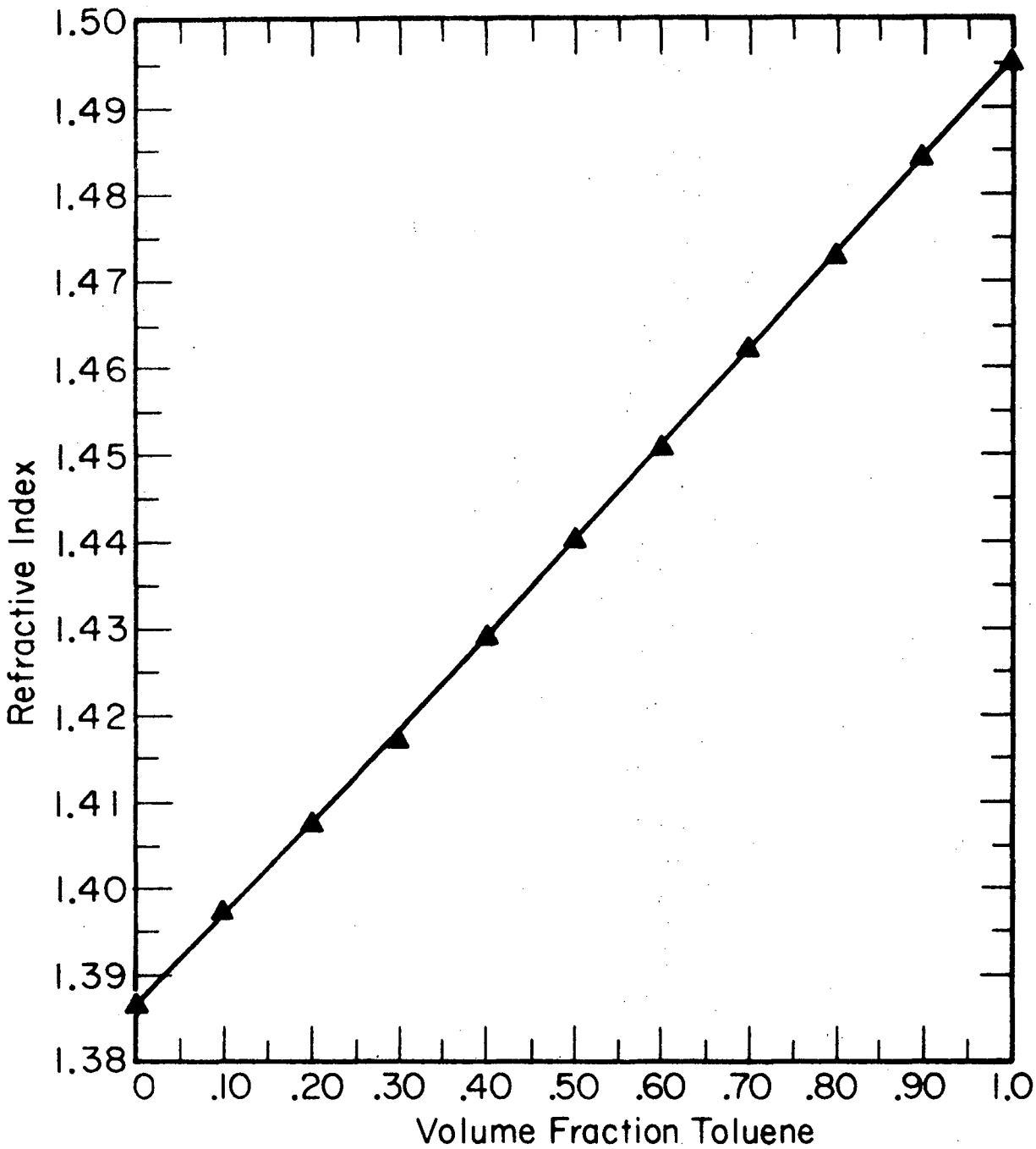
1.50
1.49
1.48
1.47
1.46
1.45
1.44
1.43
1.42
1.41
1.40
1.39
1.38
Refractive Index
0
.10
.20
.30
.40
.50
.60
.70
.80
.90
1.0
Volume Fraction Toluene

CHAPTER 3

A SIMPLIFIED MATHEMATICAL STATEMENT OF CYCLING ZONE ADSORPTION (EXCLUSION OF DIFFUSION TERM)

The General Equation..... 48

Solution of Equation (3-2)..... 50

Calculation of Concentration Change due to Temperature Change..... 53

Calculation of Concentration of Shock-Wave Velocity..... 57

Determination of Simple Concentration Wave Generation..... 64

Example Calculation of Single-Zone Performance..... 65

Example of Dual-Zone Performance..... 72

CHAPTER 3

A SIMPLIFIED MATHEMATICAL STATEMENT OF CYCLING ZONE ADSORPTION (EXCLUSION OF DIFFUSION TERM)

A general equation governing mass transfer in a nonisothermal packed bed shall be given. Assumptions allowing its solutions are discussed along with the resulting operational characteristics of such a packed bed.

General Equation

A material balance over the solid and liquid phase results in the following differential equation:

$$\frac{\partial X_L}{\partial t} + A \frac{\partial X_s}{\partial t} + V \frac{\partial X_L}{\partial z} - \mathfrak{D} \frac{\partial^2 X_L}{\partial z^2} = 0 \qquad (3\text{-}1)$$

where: t = time; z = axial direction along the column; $\mathfrak{D}$ = overall diffusion coefficient in axial direction; V = interstitial fluid velocity; $A = [(1-\alpha)/\alpha]\epsilon$; where α = interparticle void fraction; ϵ = intraparticle void fraction; X_L = volume percent component 1 of binary liquid in liquid phase; X_s = volume percent of component 1 within the solid, solid-free basis.

Note that in the mass balance, the solid is treated in only one part, whereas in previous work (55) it has been treated in two parts. The volume percent X_s accounts for both the

liquid adsorbed on the solid surfaces and the liquid residing within the pores. Although there may be a difference between the composition of the liquid in the pores and that actually adsorbed, there is no need to distinguish between these compositions when the two are assumed to be in equilibrium, as in the work discussed here. If there were a need to account for a finite rate of adsorption inside the particles or for diffusion through the pores the two kinds of internal liquid could not be treated as one. In Eq. (3-1), however, the only diffusional process is that in the interstitial fluid in its direction of flow.

The first term of Eq. (3-1) accounts for the accumulation of component 1 in the liquid phase, the second for the accumulation of component 1 in the solid phase, the third for bulk transport of component 1, and the fourth for transport by diffusional processes.

It is apparent that a number of assumptions are inherent in Eq. (3-1). The fluid velocity is constant over the whole cross section. The primary assumption is that mass transfer in the radial direction can be neglected. It is also assumed that the densities of both solid and liquid remain constant with composition and temperature. The capacity of the solid is assumed to be constant. The last assumption is invariably true because a solid particle in a liquid environment is always completely loaded. For a

solid-gas phase adsorbing system, as investigated by Blum (55), this assumption is not valid in that solid adsorbing sites are not always filled completely.

If the diffusional term of Eq. (3-1), which accounts for longitudinal mixing in the direction of flow of the liquid, is neglected, then Eq. (3-1) takes on the following form:

$$\frac{\partial X_L}{\partial t} + A \frac{\partial X_s}{\partial t} + V \frac{\partial X_L}{\partial z} = 0 \qquad (3\text{-}2)$$

Solution of Equation (3-2)

Frequently, as will be shown elsewhere, a valid assumption in cycling-zone adsorption is local equilibrium. That is, at any point and time in the packed bed, the liquid phase is in equilibrium with the solid phase. Such an assumption requires a relationship between the solid and liquid concentrations. Such a relationship is the solid-liquid equilibrium isotherm, developed in Chapter 2. Let the relationship take the form

$$X_s = F(X_L, T)$$

where F is some function of the liquid composition and packed-bed temperature. Differentiation of X_s with respect to time and substitution into Eq. (3-2) gives the following differential equation:

$$\frac{\partial X_L}{\partial t} + \left[A\left(\frac{\partial F}{\partial T}\right)\left(\frac{dT}{dt}\right) + \left(\frac{\partial F}{\partial X_L}\right)\left(\frac{\partial X_L}{\partial t}\right)\right] + V\frac{\partial X_L}{\partial z} = 0$$

rearranging gives:

$$\left(1 + A\frac{\partial F}{\partial X_L}\right)\frac{\partial X_L}{\partial t} + V\frac{\partial X_L}{\partial z} = -A\left(\frac{\partial F}{\partial T}\right)\frac{dT}{dt} \qquad (3\text{-}3)$$

Information may be obtained from Eq. (3-3) by using the method of characteristics as a method of solution. Equation (3-3) is equivalent to the following set of ordinary differential equations:

$$\frac{dt}{1 + A\left(\frac{\partial F}{\partial X_L}\right)} = \frac{dz}{V} = -\frac{dX_L}{A\left(\frac{\partial F}{\partial T}\right)\left(\frac{dT}{dt}\right)} \qquad (3\text{-}4)$$

Solving for X_L as a function of time along the t-z characteristics satisfying the first equality in Eq. (3-4) gives:

$$A\left(\frac{\partial F}{\partial T}\right)\left(\frac{dT}{dt}\right)dt = -\left[1 + A\left(\frac{\partial F}{\partial X_L}\right)\right]dX_L \qquad (3\text{-}5)$$

Since the temperature varies as a step function of time, dT/dt is zero for all time except at the instant of the temperature switch in the packed bed, when it is infinity. Considering only the time between switching, it is seen that X_L is a constant value along its concentration characteristic since dT/dt is zero. For any step change in the temperature, however, the liquid concentration X_L will then take on a new value for the new temperature, satisfying Eq. (3-5).

The slope of a concentration characteristic, dz/dt, reveals the velocity at which a concentration wave travels through the packed bed. Using Eq. (3-4), the following differential equation may be solved to determine the characteristic slope for a given liquid concentration:

$$\frac{dz}{dt} = \frac{V}{1 + A\left(\frac{\partial F}{\partial X_L}\right)} \tag{3-6}$$

At this point the derivative of the isotherm function, $\partial F/\partial X_L$ must be evaluated. Experimental data have been fitted empirically to give the following form of the solid-liquid equilibrium isotherm:

$$X_s = F(X_L,T) = \frac{\alpha_{RV} X_L}{1 + (\alpha_{RV}-1)X_L} \tag{3-7}$$

where

$$\ln \alpha_{RV} = B(T) + C(T)(1-2X_L)$$

$$\alpha_{RV} = \exp[B + C(1-2X_L)] = e^{B+C} e^{-2CX_L}$$

$$\therefore \quad \alpha_{RV} = He^{-2CX_L}$$

where the constants B, C, and H are dependent upon temperature, either the high temperature or the low temperature in the step change being the only values of interest. Evaluation of the differential $\partial F/\partial X_L$ gives:

$$\left(\frac{\partial F}{\partial X_L}\right) = \frac{He^{-2CX_L}(1 - 2CX_L + 2CX_L^2)}{\left[1 + (He^{-2CX_L} - 1)X_L\right]^2} \tag{3-8}$$

Substitution of Eq. (3-8) into Eq. (3-6) gives the following form of the slope of the concentration characteristics:

$$V_c = \frac{dz}{dt} = \frac{V}{1 + A\left\{\dfrac{He^{-2CX_L}(1-2CX_L+2CX_L^2)}{[1 + (He^{-2CX_L}-1)X_L]^2}\right\}} \tag{3-9}$$

From the characteristic slope, equal to the concentration velocity, the length of a cycling-zone adsorption packed bed may be calculated for any temperature switching time.

<u>Calculation of Concentration Change Due To Temperature Change</u>

Equation (3-7), the solid-liquid equilibrium isotherm equation, may be used to determine the liquid and solid concentration changes that occur upon a step temperature change within the packed bed. From Eq. (3-5),

$$dX_L = -A\left[\left(\frac{\partial F}{\partial X_L}\right) dX_L + \left(\frac{\partial F}{\partial T}\right) dT\right]$$

since

$$dF = \left(\frac{\partial F}{\partial X_L}\right) dX_L + \left(\frac{\partial F}{\partial T}\right) dT$$

$$dX_L = -AdF \tag{3-10}$$

and integration gives

$$\left(X_{L_2}-X_{L_1}\right) = A\left[F\left(X_{L_1},T_1\right)-F\left(X_{L_2},T_2\right)\right]$$

or

$$\left(X_{L_2}-X_{L_1}\right) = A\left(X_{s_1}-X_{s_2}\right) \qquad (3\text{-}11)$$

Equation (3-11) may be evaluated by trial and error with a knowledge of the constant A and through use of the equilibrium isotherms at the high and low temperatures, given by Eq. (3-7).

From the above development, it has been shown that the method of characteristics applied to the simplified equilibrium theory allows the calculations of concentration wave velocities and concentration changes that occur upon a step temperature change within the packed bed.

For a n-heptane-toluene-silica gel system operating at temperatures of 2°C and 59°C with void fractions of $\alpha = 0.403$ and $\epsilon = 0.383$, the plot in Figure 3-1 is developed for the concentration characteristic slope versus the volume percent toluene in the feed to a packed bed. Equation (3-9) is used with constants evaluated at the two different temperatures: At temperature = 2°C:

$$\ln \alpha_{RV} = 2.1348 + 0.4948(1-2X_L)$$

$$\alpha_{RV} = H \exp(-2CX_L) = 13.858 \exp(-0.9896\ X_L) \qquad (3\text{-}12)$$

where the constants H = 13.858 and C = -0.9896.

Figure 3-1

Characteristic Slope Versus Vol %

Fraction Toluene in Fluid

This figure may be used to determine the concentration velocity at the two temperatures of zone operation. Curves are developed from Eq. (3-9).

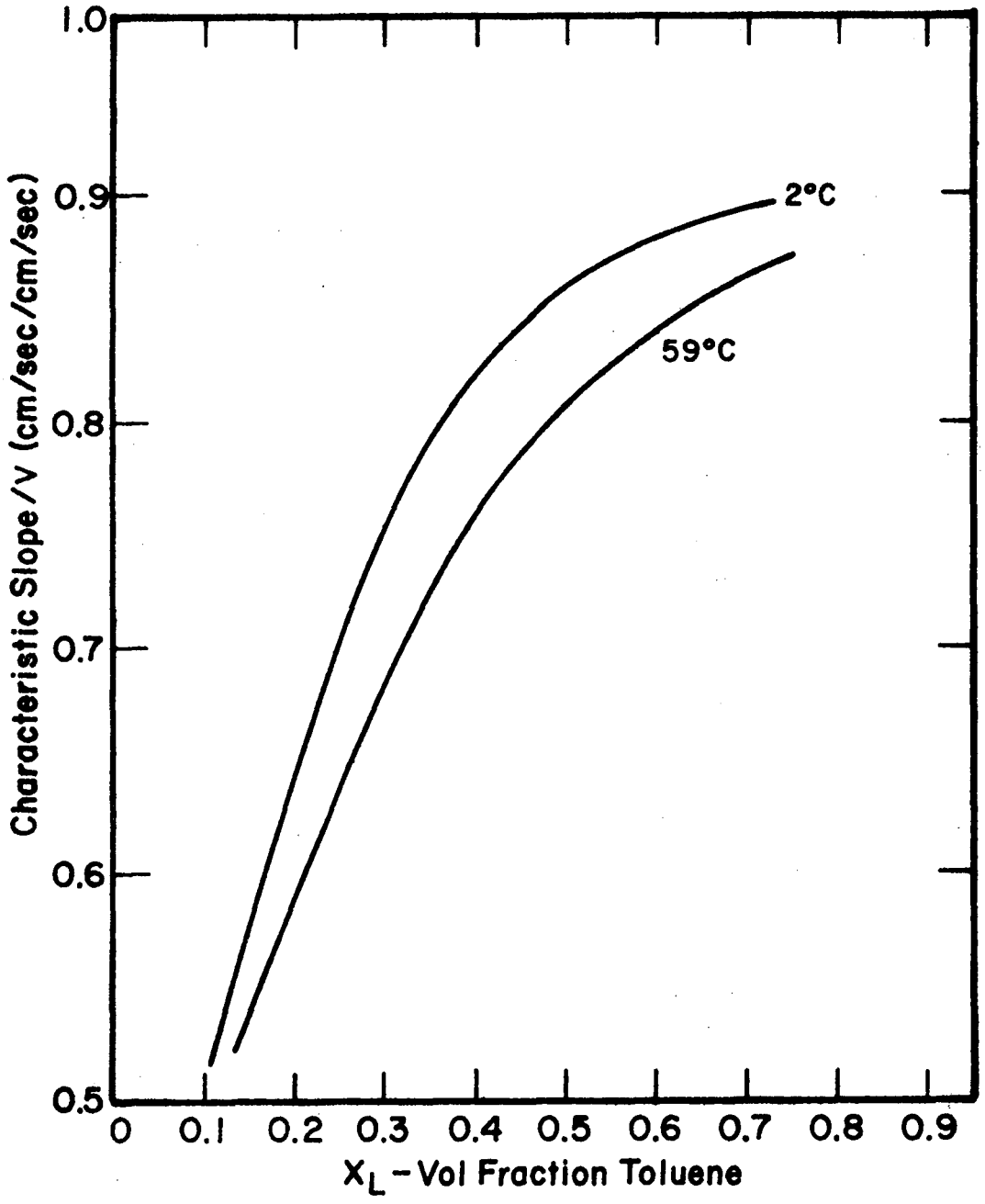
1.0
0.9
0.8
0.7
0.6
0.5
Characteristic Slope /V (cm/sec/cm/sec)
2°C
59°C
0
0.1
0.2
0.3
0.4
0.5
0.6
0.7
0.8
0.9
X_L – Vol Fraction Toluene

The values of H and C at temperature = 2°C, used in Eq. (3-9) give the higher curve in Figure 3-1. At temperature = 59°C:

$$\ln \alpha_{RV} = 1.8433 + 0.249478(1-2X_L)$$

$$\alpha_{RV} = H \exp(-2CX_L) = 8.102 \exp(-0.5X_L) \quad (3\text{-}13)$$

where the constants H = 8.102 and C = 0.500. The values of H and C at the temperature = 59°C used in Eq. (3-9) then give the lower curve in Figure 3-1.

Using Eq. (3-11), with the values of α_{RV} given by Eqs. (3-12) and (3-13), a plot of high and low product concentrations versus feed concentration into a packed bed can be developed. Figure 3-2 is such a plot. The curve above the forty-five degree line represents the concentration of product displaced from a zone, previously at equilibrium with the feed composition, when the temperature has been switched from the low value to the high value. The lower curve represents the concentration of displaced product from a zone that has just undergone a temperature change from the high value to the low value.

Calculation of Concentration Shock-Wave Velocity

Equation (3-9) and Figure 3-1 point out that different concentrations of liquid travel at different velocities through a packed bed of silica gel. Two special phenomena may develop in a zone because of this difference in concentration velocities.

Figure 3-2

Theoretical Equilibrium Product Concentrations Versus Feed Concentration

This figure may be used to determine the concentration change that occurs upon a switch of the bed temperature. The curve is developed from Eq. (3-11).

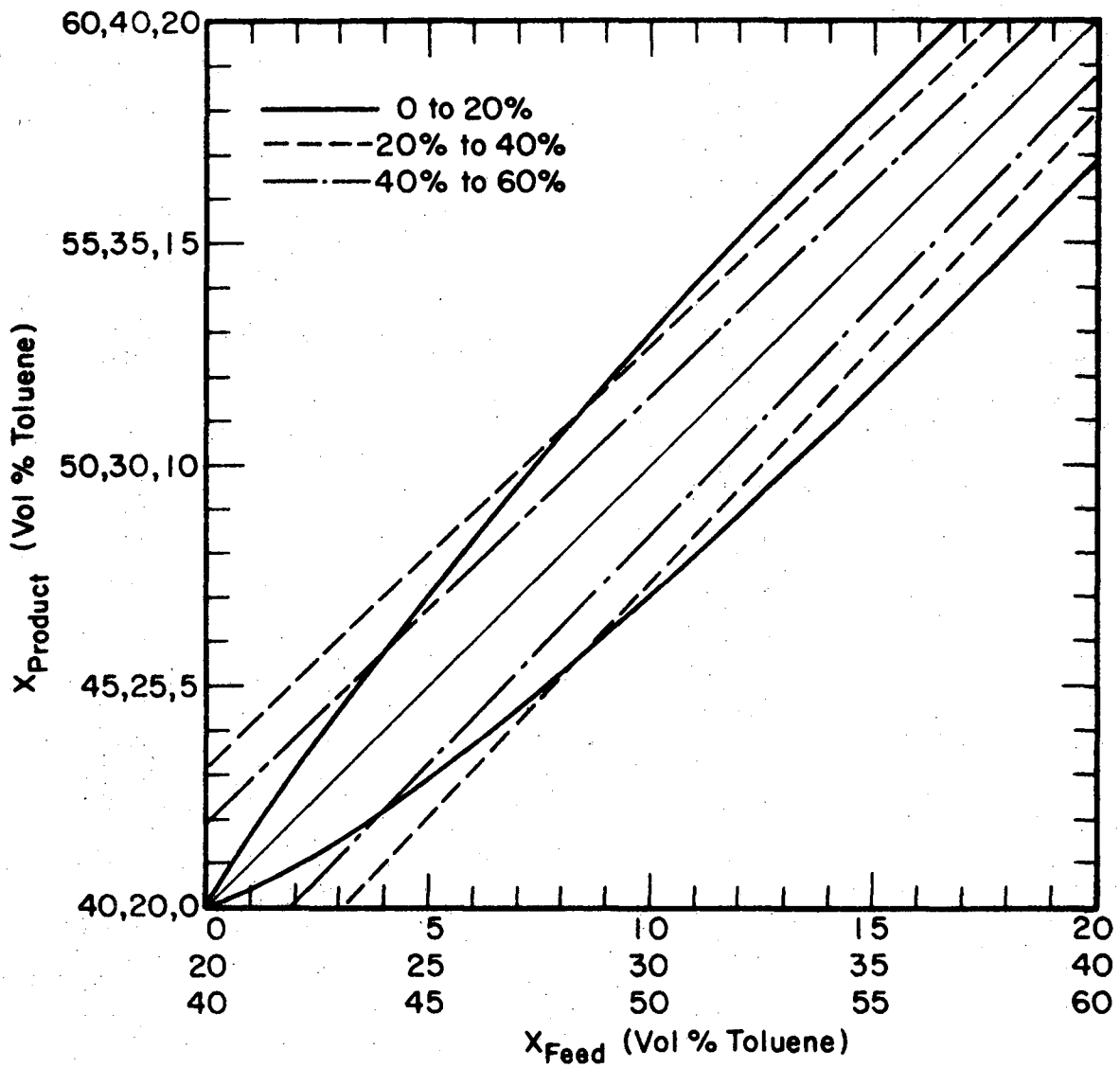
60,40,20
55,35,15
50,30,10
45,25,5
40,20,0
0 to 20%
20% to 40%
40% to 60%
$X_{Product}$ (Vol % Toluene)
0 5 10 15 20
20 25 30 35 40
40 45 50 55 60
X_{Feed} (Vol % Toluene)

Consider the case of a low-concentration product being displaced by feed of a higher concentration. According to Eq. (3-9), the feed concentration travelling into the zone will move at a higher velocity than the low-concentration product being displaced. If one plots concentration characteristics on a graph of distance versus time as in Figure 3-3, it is seen that there is a convergence of the two sets of characterics representing the high-concentration feed and the low-concentration product. Such an intersection of concentration characteristics implies a "concentration shock-wave." This phenomenon is comparable to an acoustical shock-wave, where more rapidly traveling sound waves overtake slower sound waves, forming a shock front which moves at some particular velocity between those of the two converging waves.

An expression will now be developed for the velocity of such a concentration shock-wave. Consider the following material balance:

U_{sh} = velocity of the shock

Temp = T_{cold}

A' = cross sectional area (C.S.A.)

X_L = volume percent of component 1 in liquid ahead of shock front (the low concentration)

X_F = volume percent of component 1 in liquid in feed behind the shock front (the high concentration)

0 0 0 0 3 8 0 4 1 9 5

Figure 3-3

Concentration Shock-Wave

This figure explains how the method of characteristics may be used to analyze concentration shock. The effluent concentration profile resulting from the concentration shock-wave is also presented.

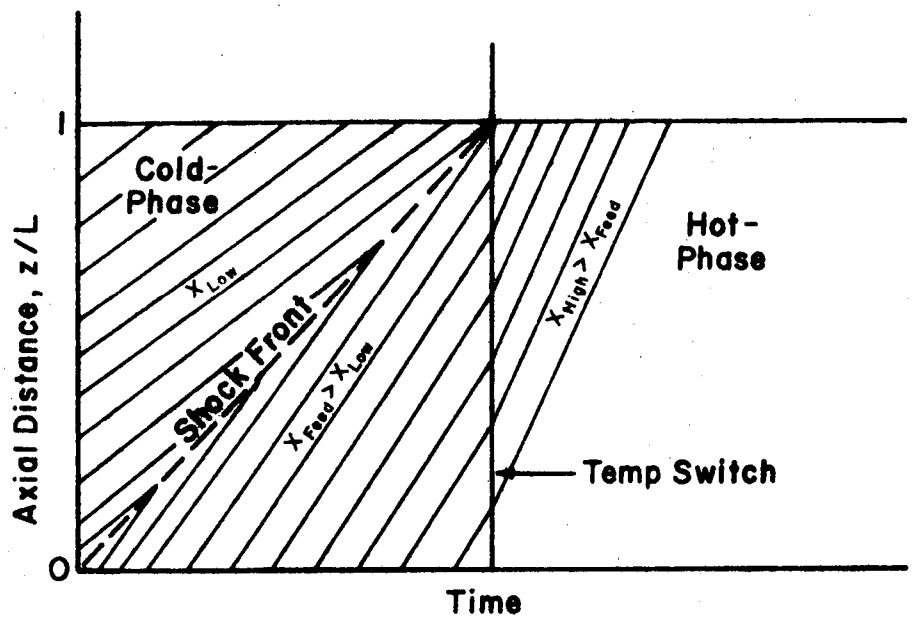
1
0
Axial Distance, z/L
Cold-Phase
Hot-Phase
X_{Low}
Shock Front
$X_{Feed} > X_{Low}$
$X_{High} > X_{Feed}$
Temp Switch
Time

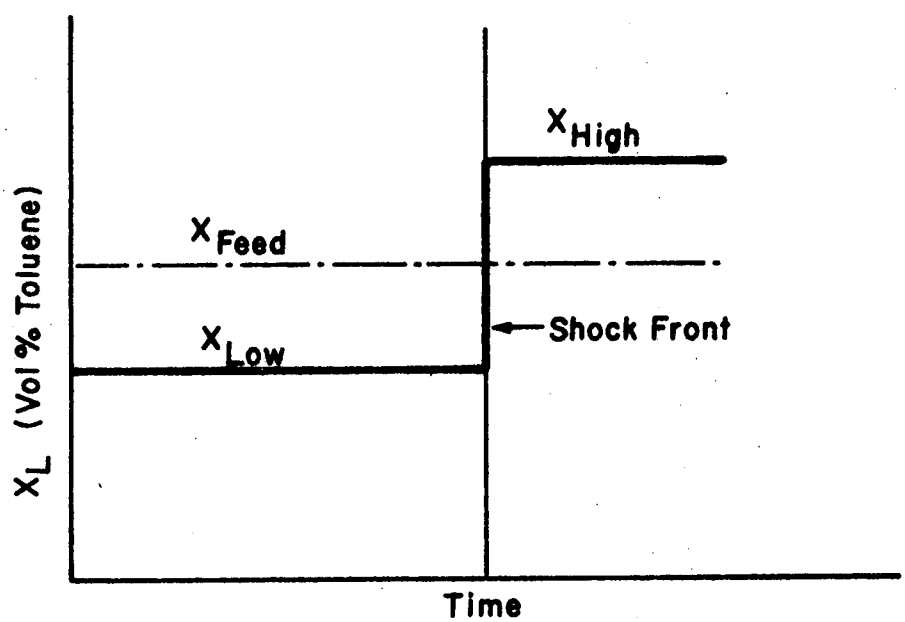
X_L (Vol % Toluene)
X_{High}
X_{Feed}
X_{Low}
Shock Front
Time

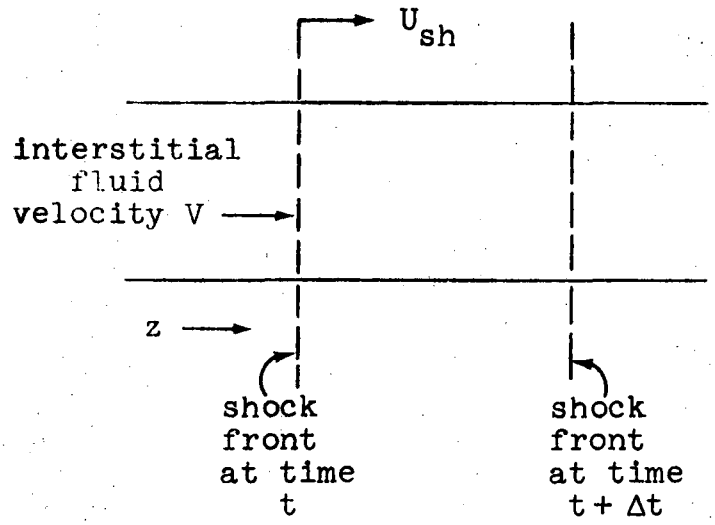

Material transported into front by stream at the left in time Δt:

$$= \alpha A' \Delta z (V - U_{sh}) X_F \Delta t$$

Material transported from shock front by stream to the right in time Δt:

$$= \alpha A' \Delta z (V - U_{sh}) X_L \Delta t$$

Material stored in solids between successive positions of shock front during time Δt:

$$= (1-\alpha)\epsilon A' \Delta z \{F(X_F, T_c) - F(X_L, T_c)\} U_{sh} \Delta t$$

Equating gives:

$$(V - U_{sh}) X_F - (V - U_{sh}) X_L = (1-\alpha)\epsilon U_{sh} \{F(X_F, T_c) - F(X_L, T_c)\}$$

Solving for the shock velocity U_{sh}:

$$U_{sh} = \frac{V}{1 + \frac{(1-\alpha)\epsilon}{a} \left\{ \frac{F(X_F, T_c) - F(X_L, T_c)}{(X_F - X_L)} \right\}} \qquad (3\text{-}14)$$

Note the similarity to Eq. (3-6), which gave the velocity of propagation of a concentration wave of differentially small magnitude. With the use of Eq. (3-7), evaluated at the cold temperature, Eq. (3-14) may be used to determine the concentration shock velocity resulting from the displacement of a low-concentration product by a high-concentration feed.

It is interesting to note that the emergence of a concentration shock front from an adsorbing zone results in a discontinuity of concentration at that point, that is, a step change in concentration emerges.

Determination of Simple Concentration Wave Generation

Consider the case of a high-concentration product being displaced by a low-concentration feed, as is the case when the column is run at the high temperature. As indicated by Eq. (3-9) and Figure 3-1, the high-concentration product has a concentration wave velocity that is greater than that of the feed. In this case there is a divergence of the concentration characteristics, as shown in Figure 3-4. From the time zero to the time t_a it is seen that the concentration characteristics are of constant slope a. From time t_b and greater, the concentration characteristics are of constant slope b for the low-concentration product. In the region between t_a and t_b, there is a region of variable characteristic slopes, lying between the high slope a and the low slope b. What emerges from

0 0 0 0 3 8 0 2 4 9 7

Figure 3-4

Simple Concentration Wave

This figure explains how the method of characteristics may be used to analyse a simple concentration wave in a cycling zone adsorber. The effluent concentration profile resulting from the simple wave is also provided.

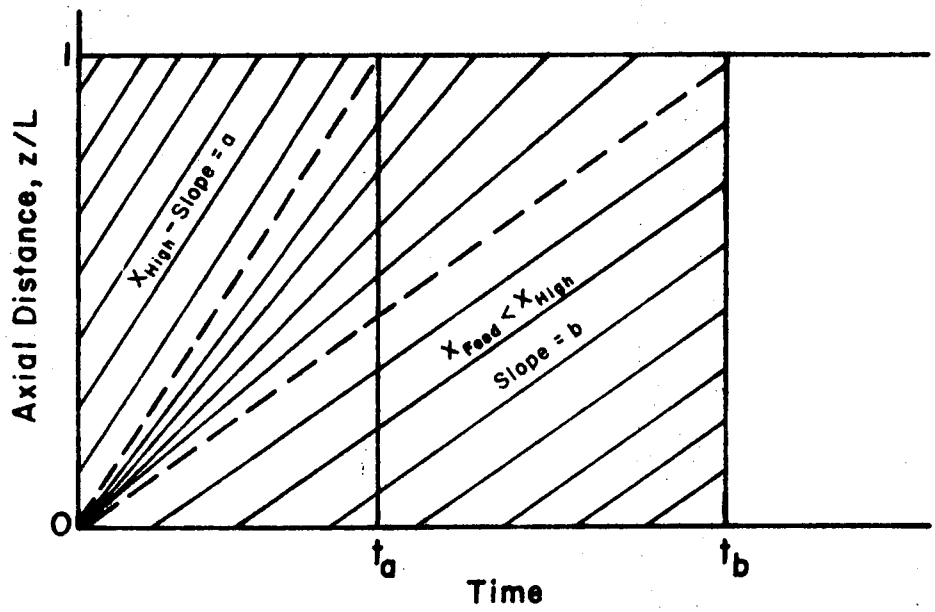
1
0
Axial Distance, z/L
X_{High} - Slope = a
$X_{Feed} < X_{High}$
Slope = b
t_a
t_b
Time

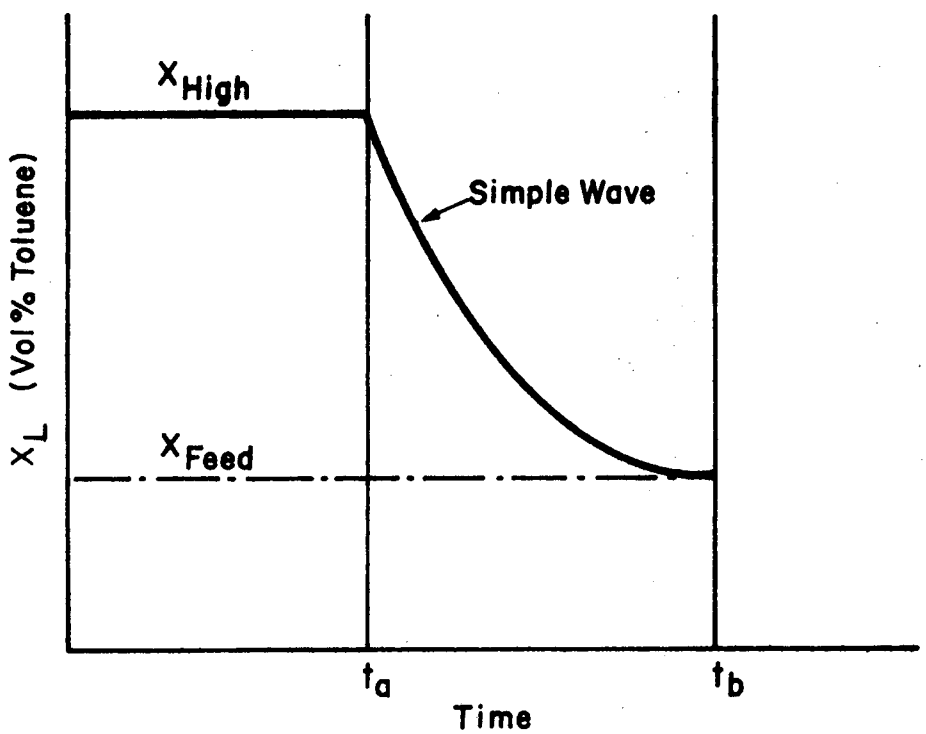
X_{High}
Simple Wave
X_L (Vol % Toluene)
X_{Feed}
t_a
t_b
Time

the packed bed is a time duration $(t_b - t_a)$ of product of concentration varying between the high-concentration product and the low-concentration feed. The region between t_a and t_b is termed a "simple wave." The concentrations in the simple wave region may be solved by using Eq. (3-9) by substitution of the range of slopes and solving for X_L.

The simplified mathematical analysis allows the following calculations to be made for the operation of a single cycling zone adsorption packed bed:

1. Liquid and solid concentration changes for a a packed bed subjected to step changes in temperature in both directions.
2. Concentration wave velocities as functions of concentration, for the two different temperatures of operation.
3. The velocity of shock-waves generated in a cold bed by displacement of low-concentration product by high-concentration feed.
4. The duration and concentrations of the simple wave generated by the displacement of high-concentration product by low-concentration feed.
5. The length of a packed bed for a given temperature switching time.
6. The duration of high- and low-concentration product flows.

Example Calculation of Single-Zone Performance

Using the above information the following example calculation details the design and operation of a single packed bed operating as a cycling-zone adsorber.

Operating Conditions:

X_{feed} = 5.0 Volume % Toluene

Step changes in temperature = 2°C to 59°C; 59°C to 2°C.

Temperature switching: every 1000 seconds.

Interstitial liquid feed velocity = 0.05 cm/sec.

Column packing = 60 mesh silica gel. α = 0.402, ϵ = 0.383, A = 0.568

The unknown factors need to be calculated are the high and low product concentrations, the concentration shock-wave velocity, the duration of the simple-wave, and the column length.

High and Low Product Concentrations:

These concentrations may be calculated from Eqs. (3-7) and (3-11) at the high and low temperatures, or read from Figure 3-2.

X_{high} = 51.5 Vol %

X_{low} = 48.5 Vol %

Concentration Shock-Wave Velocity:

The shock velocity is calculated from Eq. (3-14), using the constants given in the equation at the low temperature

and the values of X_{feed} and X_{low}:

$$U_{sh} = 0.043 \text{ cm/sec}$$

The slope of the characteristics are determined by Eq. (3-9):

for X_{feed} = 50.0% at 2°C; slope = 0.043 cm/sec

for X_{feed} = 50.0% at 59°C; slope = 0.0404 cm/sec

for X_{low} = 48.5% at 2°C; slope = 0.0428 cm/sec

for X_{high} = 51.5% at 59°C; slope = 0.0407 cm/sec.

Since the slopes involved in the calculation vary by less than 6%, the visual value of a plot of concentration characteristics is useless here. Such a plot would have to be many times larger than the page size, therefore it is excluded. However, from an enlarged characteristic plot, it is possible to develop the effluent concentration profile. Figure 3-5 is a plot of the effluent profile for a single zone operating under the prescribed conditions. It is seen from Fig. 3-5 that a zone length of 43 cm gives product durations of 1000 seconds for X_{high} = 51.5% and 920 seconds for X_{low} = 48.5%.

As will be shown in the following chapters, the simplified mathematical statement of Cycling Zone Adsorption has one major deficiency: The theory does not account for longitudinal diffusion in the interstitial fluid. Such diffusion leads to considerable round off of the square-

Figure 3-5

Example Calculation: Single-Zone

Effluent Concentration Profile

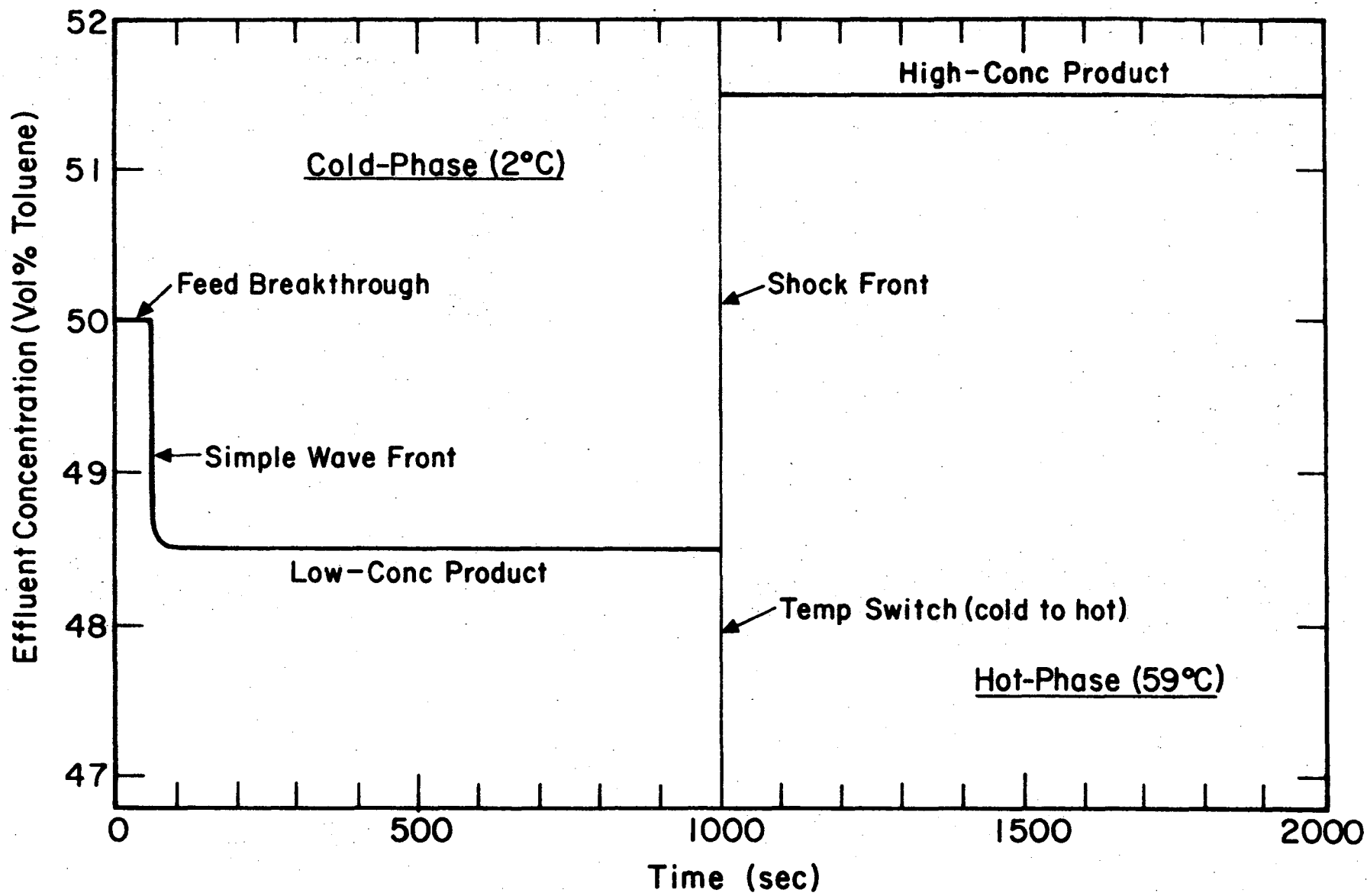
52
51
50
49
48
47
Effluent Concentration (Vol% Toluene)
0
500
1000
1500
2000
Time (sec)
High-Conc Product
Cold-Phase (2°C)
Feed Breakthrough
Shock Front
Simple Wave Front
Low-Conc Product
Temp Switch (cold to hot)
Hot-Phase (59°C)

wave effluent concentration profiles predicted by the simple theory. The rounding off of the sharp wave fronts has the undesired effect of reducing the length of time during which product streams have the maximum or minimum concentrations. Chapter 6 investigates the problem of longitudinal diffusion through the development of a more refined mathematical theory.

Example of Dual-Zone Performance

As briefly discussed in Chapter 1, single zones may be staged in a series. This arrangement allows the effluent product from a preceding zone to become the feed into the following zone. This feed, because of the enrichment or depletion in the first zone, is now either higher or lower in concentration than the average feed into the original zone. The final product concentrations emerging from the second zone are now even more greatly separated. This is elucidated in the following qualitative example, shown in Figure 3-6, which is a plot of the concentration characteristics for two zones. Notice that the temperature of the second zone for this arrangement is 180° out of phase with that of the first zone, that is, when zone one is hot, zone two is cold and when zone one is cold, zone two is hot.

Notice also that the shock-wave velocity of the second zone during the cold cycle is greater than that in

0 0 0 0 0 8 0 0 0 1

Figure 3-6

Qualitative Use of Method of Characteristics for Two-Zone Series Operation

This figure explains, through the method of characteristics, how successive zones in a series may distort the effluent concentration profile.

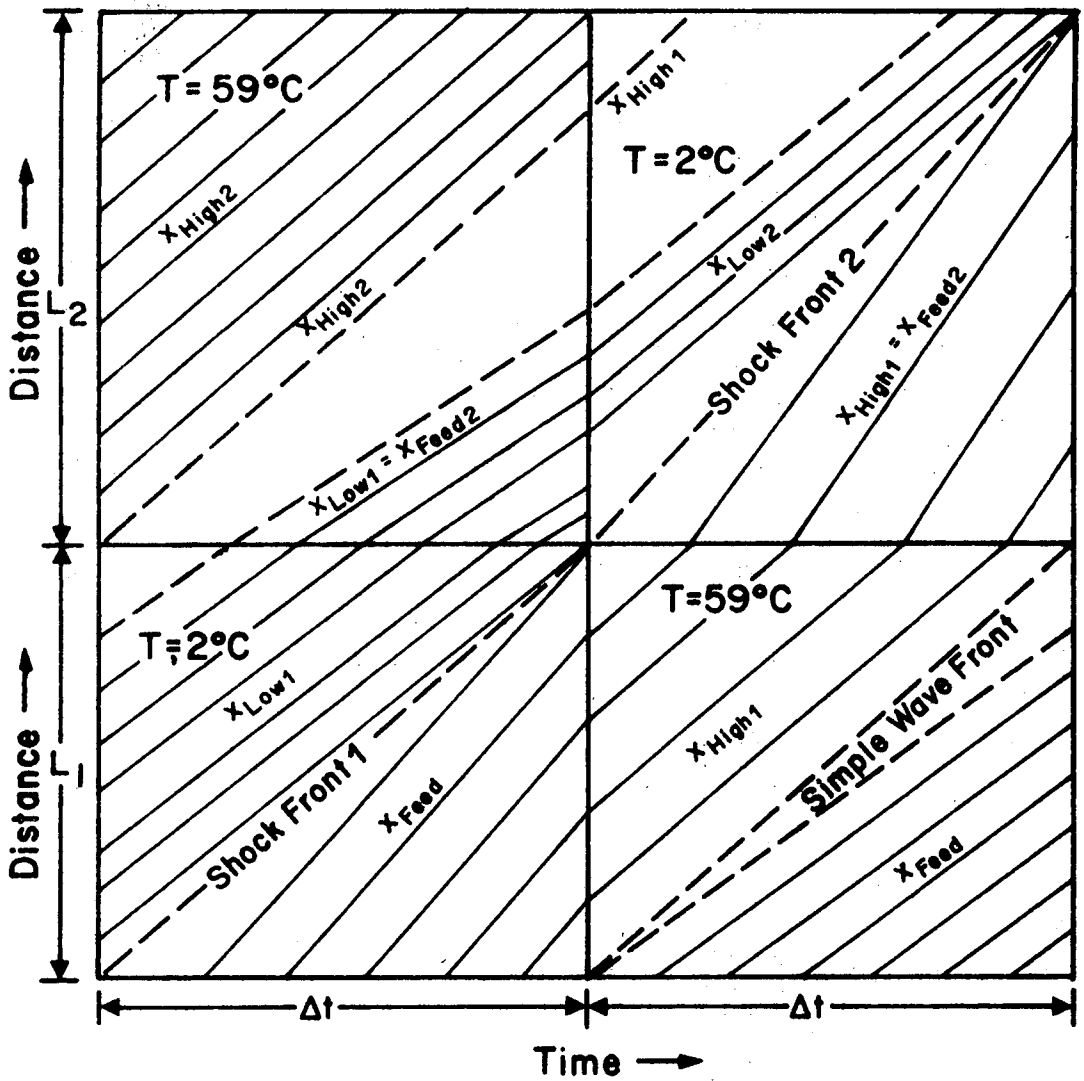
T = 59°C
x_{High2}
x_{High2}
x_{High1}
T = 2°C
x_{Low2}
Shock Front 2
$x_{High1} = x_{Feed2}$
$x_{Low1} = x_{Feed2}$
Distance
L_2
T = 2°C
x_{Low1}
Shock Front 1
x_{Feed}
T = 59°C
x_{High1}
Simple Wave Front
x_{Feed}
Distance
L_1
Δt
Δt
Time

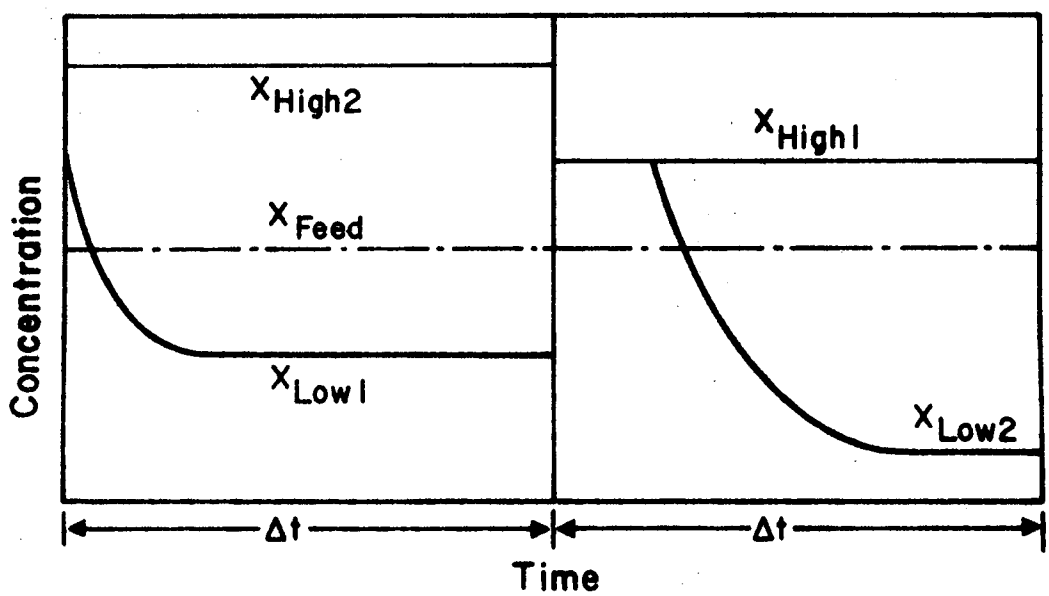
x_{High2}
x_{High1}
x_{Feed}
x_{Low1}
x_{Low2}
Concentration
Δt
Δt
Time

the first zone and also that the spread of the simple-wave is also greater during the hot cycle of the second zone. This is due to the greater concentration differences occurring in the second zone. It is evident because of this that the length of the second zone will have to be different from that of the first zone, if maximum flow durations of high and low products are to be obtained. It is also apparent that with an increasing number of successive zones that the flow duration of the product decreases because of the increasing duration of the simple-wave that is generated within a zone experiencing the hot cycle. Stated in another fashion, the greater the number of zones in a simple series cascade, the more the concentration profile deviates from a square-wave response. This result is inherent in cycling zone adsorption because of the difference in concentration wave velocities. Table 3-1 lists the characteristic properties of the two-zone series system for cycling zone adsorption.

The following chapters of this study compare the predictions of the simplified mathematical analysis with experimental results. It will be seen that the main value of the simplified theory is its ability to predict the maximum concentration changes which follow step changes in temperature. On the other hand, the omission of the longitudinal diffusion from in the simplified wave analysis causes the calculated wave shapes to be somewhat different from those observed. (Although not explored here, the

Table 3-1

Characteristic Properties of Two-Zone System

Zone 2 length (L_2)
Zone 1 length (L_1)
Shock front velocity 2
Shock front velocity 1
Spread of simple wave in zone 2
Spread of simple wave in zone 1
$X_{low2} < X_{low1} < X_{feed} < X_{high1} < X_{high2}$
During Cold Phase Operation
slope X_{low1} < slope X_{feed}
slope X_{low2} < slope X_{high1}
slope X_{low2} < slope X_{low1} [may be developed from Eq. (3-9)]
During Hot Phase Operation
slope X_{high1} > slope X_{feed}
slope X_{low1} < slope X_{high1}

0 0 0 0 0 8 0 0 0 0 3

above theory is not restricted to a step change in column temperature. As in the case of Baker (55) and Blum (56), it may be equally applied to sinusoidal changes of column temperature.)

CHAPTER 4

EXPERIMENTAL: SINGLE-ZONE, CONTINUOUS-FLOW SEPARATION OF n-HEPTANE AND TOLUENE ON SILICA GEL

Optimum Temperature Switching Time..... 84

Effect of Solid Particle Size..... 96

Improvement of Zone Temperature Response.....103

Variable-Feed Operation of a Single Zone.....115

CHAPTER 4

EXPERIMENTAL: SINGLE-ZONE, CONTINUOUS-FLOW SEPARATION OF n-HEPTANE AND TOLUENE ON SILICA GEL

The experimental apparatus has been fully described in Chapter 2. Consider the packed bed operating under the following conditions:

Interstitial velocity, V = 0.109 cm/sec
Step change in temperature = 2°C to 59°C; 59°C to 2°C
Length of column = 44 cm active length
Period = 1000 seconds
Temperature switching time = every 500 seconds
Column feed, X_{feed} = 24.7 vol % toluene, constant

The experimentally-found effluent concentration profile is plotted in Figure 4-1, along with the observed column temperature response. The highest and lowest product concentrations are, respectively, 26.15 vol % toluene and 22.85 vol % toluene. If the column is run at the optimum temperature switching time, as discussed below, a plot of peak product concentrations versus various feed concentrations may be developed by running experiments at each of several different feed concentrations. Figure 4-2 is such a plot for the continuous operation of a single experimental zone. The lines on the figure show the concentrations predicted by the simplified mathematical analysis of Chapter 3.

Of importance in the operation of a single zone is the ability to develop not only a maximum difference in peak product compositions but also a maximum duration of

Figure 4-1

Temperature and Effluent Concentration Profiles for the Experimental Operation of a Single Zone

Period: 1000 seconds
Temperature switch: every 500 seconds
Interstitial fluid velocity: 0.06 cm/sec
Temperatures: 2°C and 59°C
Feed concentration: 24.7 vol % toluene
Product concentrations: 22.85 and 26.1 vol % toluene

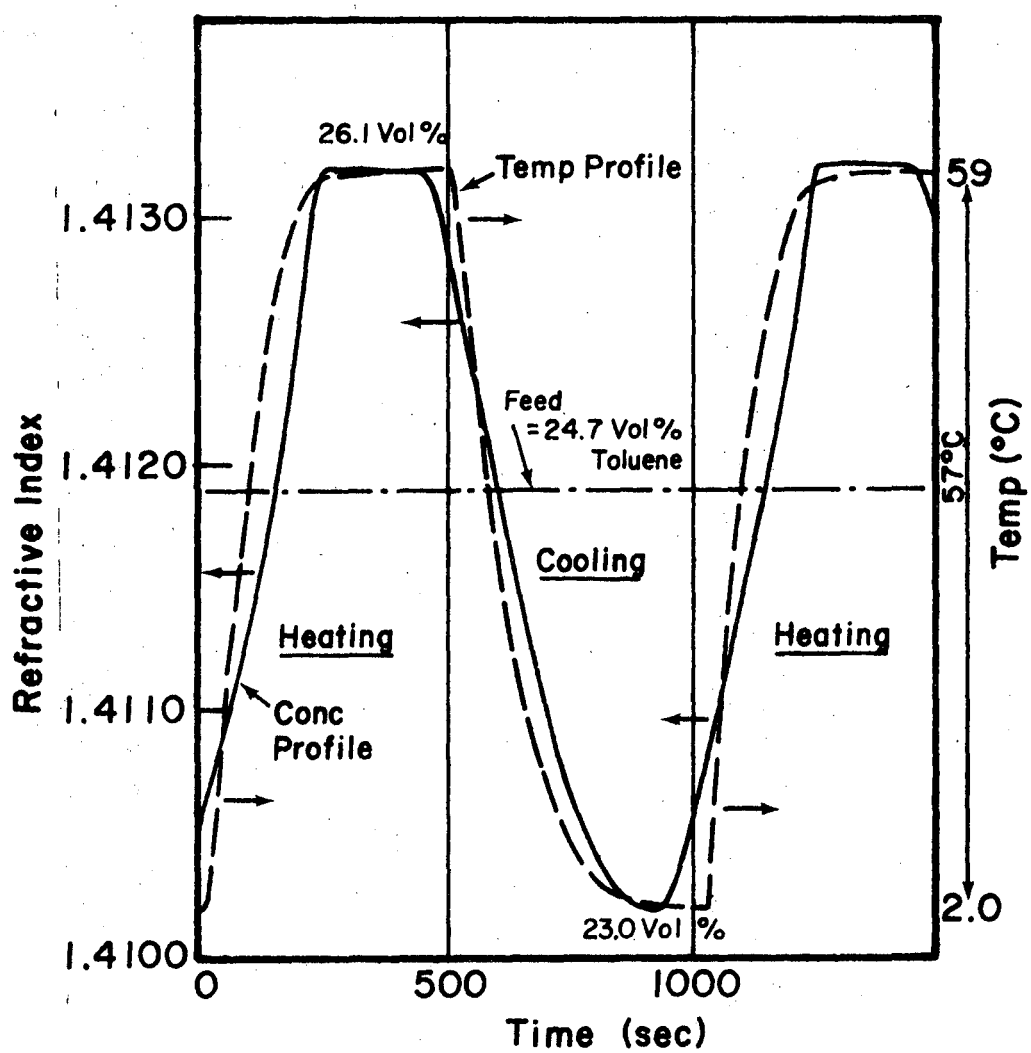
26.1 Vol %
Temp Profile
59
1.4130
Feed
=24.7 Vol %
Toluene
1.4120
57°C
Temp (°C)
Cooling
Heating
Heating
Refractive Index
1.4110
Conc
Profile
2.0
23.0 Vol %
1.4100
0
500
1000
Time (sec)

Figure 4-2

Experimental Product Concentrations

versus Feed Concentrations

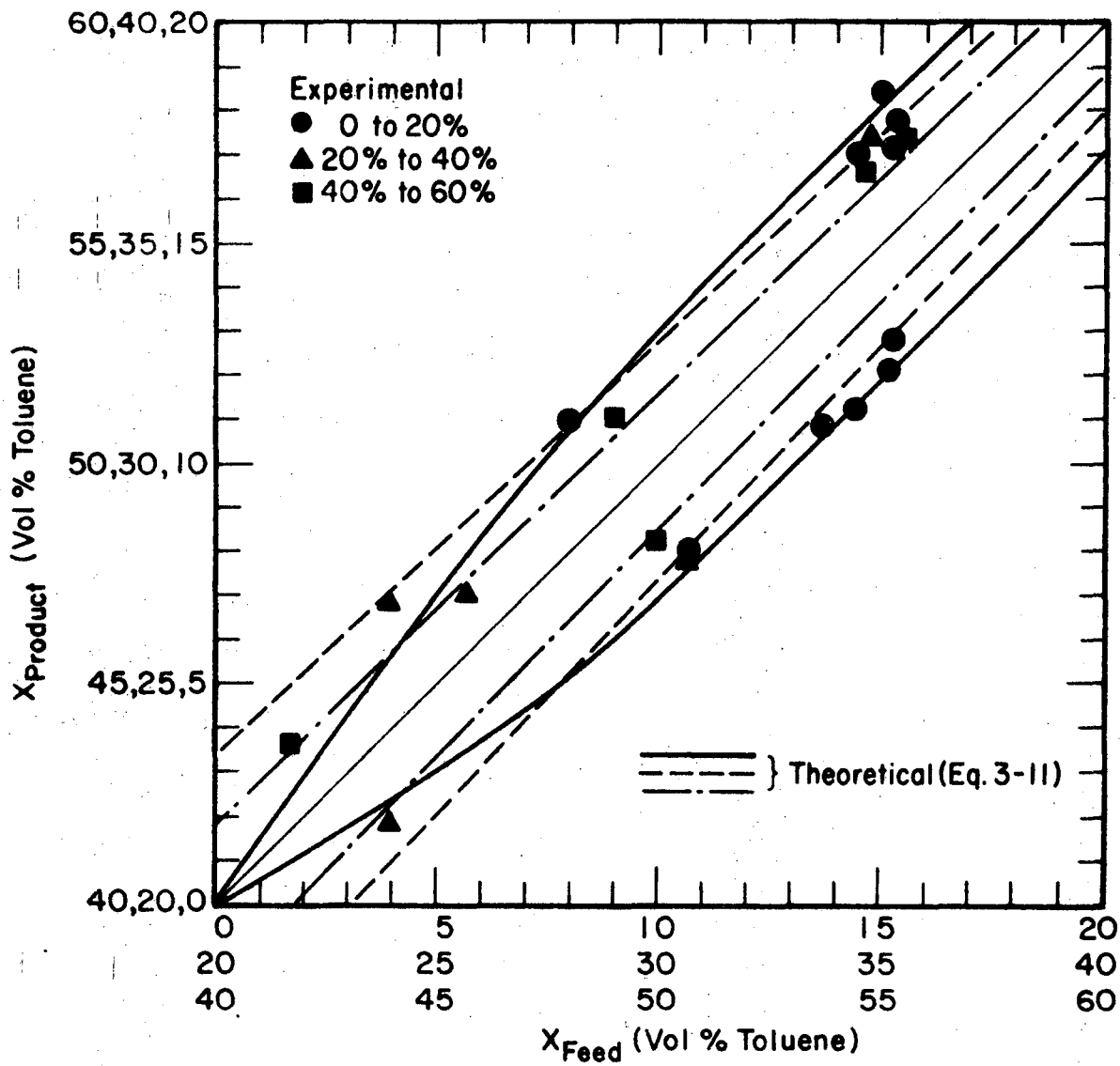
Experimental
0 to 20%
20% to 40%
40% to 60%
} Theoretical (Eq. 3-11)
60,40,20
55,35,15
50,30,10
45,25,5
40,20,0
0
20
40
5
25
45
10
30
50
15
35
55
20
40
60
$X_{Product}$ (Vol % Toluene)
X_{Feed} (Vol % Toluene)

the peak product flows. The following is a discussion of the methods used to improve the performance of a single-zone concentration response such that maximum separation occurs and that its shape approaches a square-wave.

Optimum Temperature Switching Time

Because of the previously discussed difference in concentration wave velocities, it is obvious that for a column of fixed active length, there will be different temperature switching time for a column that experiences different feed concentrations. Stated in a different manner, for columns in a series cascade, as in the Dual-Zone example of Chapter 1, each zone must be of a different length if the switching time is the same for all zones. The optimum switching time for a single zone of fixed length experiencing different feeds or the optimum length for different zones in a series experiencing the same switching time may be established by the following relationship:

$$\text{Length} = (\text{switching time})(\text{concentration wave velocity}) \tag{4-1}$$

Consider a column of fixed length, 44 cm. One may experimentally establish a curve of column feed concentration versus the optimum temperature switching time by running a series of feed-concentration breakthrough experiments. Such experiments are run in the following manner: The column is first brought to thermal equilibrium

0 0 0 0 3 8 0 0 0 3 7

at the high temperature of 59°C. Feed liquid, X_{feed}, is run through the column for a length of time such that there is a breakthrough of feed-concentration liquid at the exit of the column. This is established by successive refractive index readings of effluent liquid. At this time the column is filled with liquid at the feed concentration. Flow into the column is now stopped and the temperature is changed to 2°C. Because of the temperature change, the silica gel packing preferentially adsorbs toluene and the liquid in the column becomes lean in toluene at a concentration called X_{low}. The liquid in the column is now displaced by feed at prescribed interstitial velocity. Flow continues until all low-concentration product has been removed by feed-concentration product, at which time there is once again a breakthrough of feed in the effluent liquid. This establishes the switching time for a column of fixed length and fluid velocity.

Such a concentration breakthrough profile is shown in Figure 4-3. This also establishes the feed concentration wave velocity. From such data, it is then possible to determine either the switching time or the column length of a zone experiencing a feed of concentration X_{feed}. From Eq. (3-9) or Figure 3-1 of Chapter 3 it is seen that concentration waves travel more rapidly during the cold phase of a zone. Therefore, column lengths determined from breakthrough are the minimum lengths at which the

Figure 4-3

Qualitative Feed Breakthrough Profile

This figure explains how the optimum temperature switching time may be determined from experimental feed breakthrough analysis. Low-concentration product is displaced by feed at 2°C.

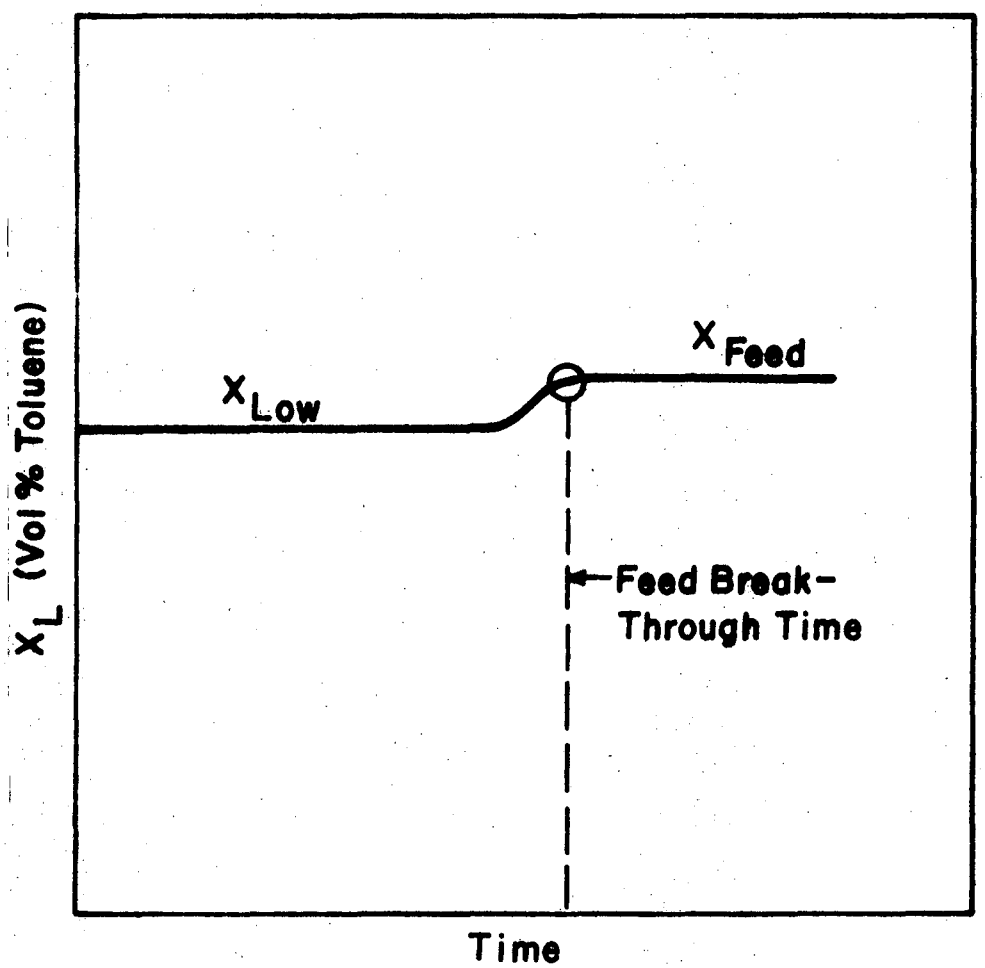
X_{Feed}
X_{Low}
X_L (Vol % Toluene)
Feed Break-
Through Time
Time

column can optimally operate. If the zone were of shorter length, there would be an undesired breakthrough of feed in the effluent product stream; if the length were greater there would be a portion of liquid within the column that would experience two temperature changes, resulting in its reversion back to the feed concentration before it emerges from the zone.

Experimental breakthrough data have been obtained in the manner described above for a range of feed concentrations expressed as refractive index. Breakthrough times were observed for a column of 44 cm active length and an interstitial displacement velocity of 0.0466 cm/sec. The column is pictured in Figure 2-3a of Chapter 2. Figure 4-4 is a plot of such experimental data. From this plot, it is possible to determine the lengths of the successive columns in a series cascade for a given temperature switching frequency and interstitial displacement velocity. Such a plot establishes the optimum length or switching frequency of a zone in cycling zone adsorption.

It is of interest to determine experimentally what effect premature or late temperature switching has upon the effluent concentration profile of a column of fixed length and interstitial fluid velocity. Moreover, the optimum switching time shown in Figure 4-4 was based on a single thermal cycle of the adsorbent, rather than repeated cycles in both directions. To determine whether

Figure 4-4

Experimental Feed Breakthrough Analysis

This figure may be used to determine the optimum temperature switching time from feed breakthrough experiments. Experiments are run under the following conditions:

Temperature: 2°C
Feed concentrations: variable
Interstitial fluid velocity: 0.0466 cm/sec
Column length: 44 cm
Low product displaced by feed

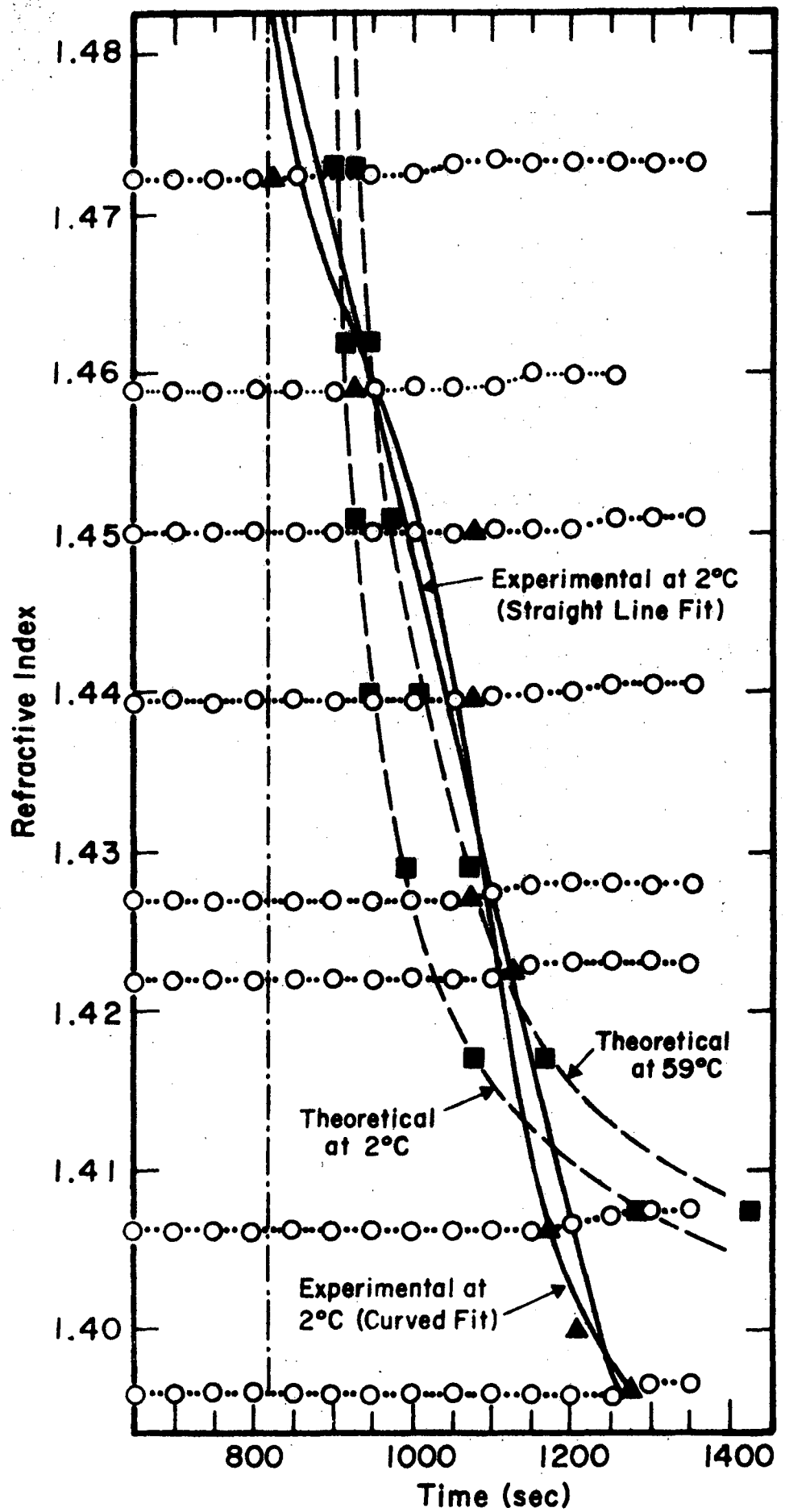
1.48
1.47
1.46
1.45
1.44
1.43
1.42
1.41
1.40
Refractive Index
800
1000
1200
1400
Time (sec)
Experimental at 2°C
(Straight Line Fit)
Theoretical
at 59°C
Theoretical
at 2°C
Experimental at
2°C (Curved Fit)

Figure 4-4 applies generally one must see if the maximum composition differences are observed in the output when repeating thermal cycles are used at the frequencies indicated by the breakthrough data.

A number of experiments have been run with temperature switching times varying about the optimum time determined from the data in Figure 4-4. Consider the experimental column experiencing a feed of X_{feed} = 15.0 vol % toluene. From the data in Figure 4-4, the optimum switching time should be 1225 seconds. With an interstitial velocity of 0.0466 cm/sec, a series of experiments were run with switching times of 900 sec, 1100 sec, 1225 sec, 1500 sec, and 2000 sec. (The third is the optimum time from Figure 4-4.) Figure 4-5 is a comparison plot of concentration profiles for these five experiments. Table 4-1 lists the observed difference in peak product volume percentages for the five different temperature switching times.

Table 4-1
Temperature Switching Time Versus
Peak Concentration Differences

Switching Time	Peak Concentration Difference
900 seconds	16.6% - 12.8% = 3.8%
1100 seconds	16.9% - 11.9% = 4.0%
1225 seconds	17.6% - 11.8% = 5.8% (optimum switching time)
1500 seconds	16.8% - 12.8% = 4.0%
2000 seconds	17.7% - 13.0% = 4.7%

Figure 4-5

Effect of Temperature Switching Frequency

Upon Effluent Profile

Interstitial fluid velocity:	0.0466 cm/sec
Temperature switching times:	900 sec
	1100 sec
	1225 sec (optimum)
	1500 sec
	2000 sec
Temperature:	2°C and 59°C

(BLANK PAGE)

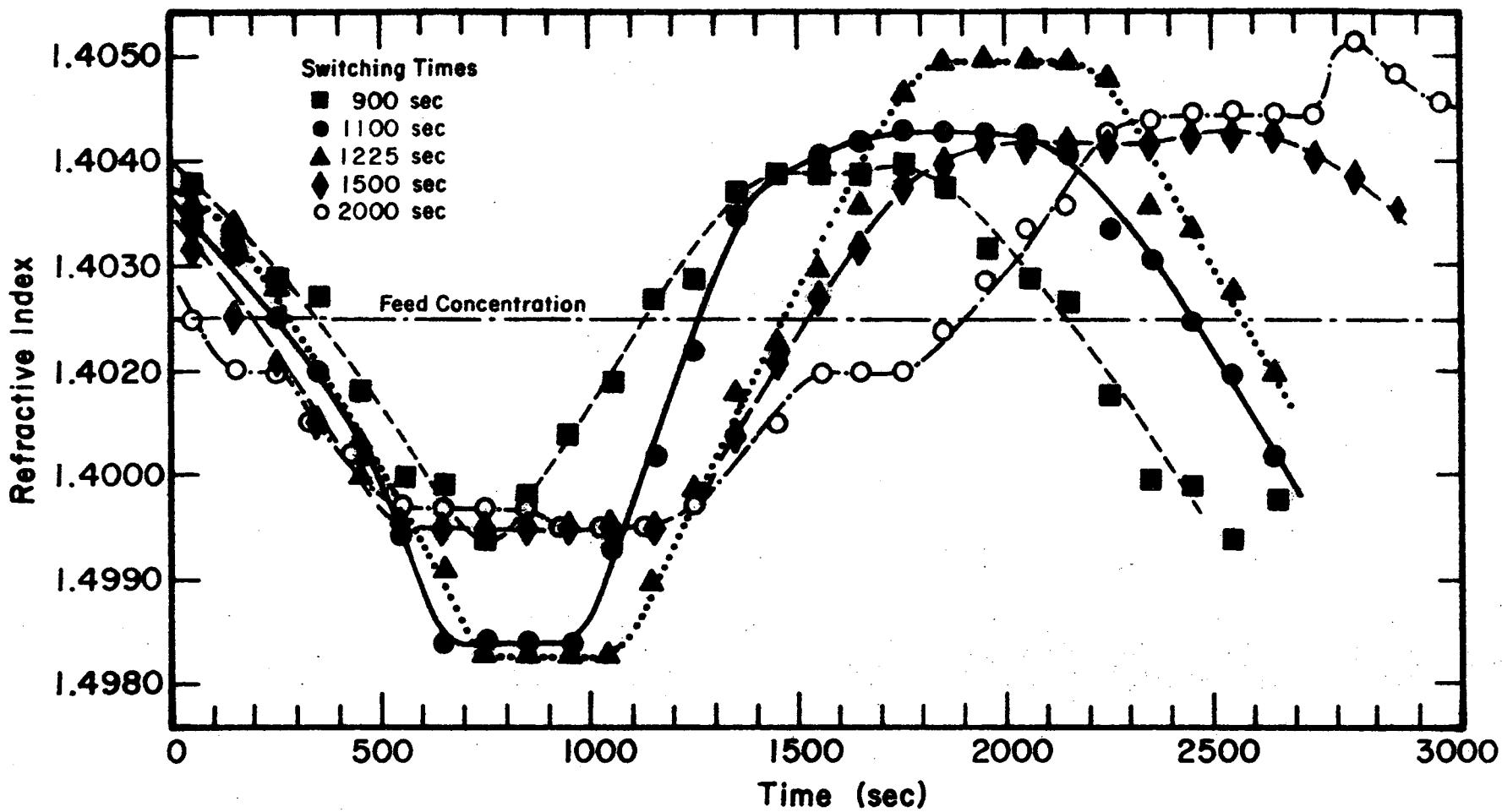
Switching Times
900 sec
1100 sec
1225 sec
1500 sec
2000 sec
Feed Concentration
Refractive Index
1.4050
1.4040
1.4030
1.4020
1.4000
1.4990
1.4980
0
500
1000
1500
2000
2500
3000
Time (sec)

It is apparent that switching the temperature at the time determined from Figure 4-4 gives the maximum product peak separation. That is, maximum separation of a given feed in a single zone occurs when using the optimum temperature switching time. The data in Table 4-1 indicate a decrease in separation of the feed as temperature switching times deviate from the optimum. The following evaluates the behavior at the two extremes, a switching time of 900 seconds and 2000 seconds.

A premature switch in temperature occurs when a zone is too long for a given switching frequency and interstitial fluid velocity, as indicated by Eq. (4-1). This means that liquid near the end of the zone will experience two changes in the temperature. The increase or decrease in the feed composition liquid due to the first temperature change at its entrance into the column is then destroyed by the second temperature change before the fluid can completely emerge from the column. As the number of cycles increases this effect becomes cumulatively larger. The final effect of a premature switch in temperature is that after a large number of cycles most of the fluid in the column will undergo two temperature changes before emerging and the separation will be completely destroyed.

Use of a temperature switching time that is greater than the optimum is equivalent to use of a column that is too short for a prescribed switching time and interstitial

velocity. The predominant result is that there is a breakthrough of feed liquid in the effluent of the column. This may be seen in the experimental run shown in Figure 4-5. After a large number of cycles this factor is compounded and again the separation is destroyed.

It is apparent that a detailed knowledge of the optimum temperature switching time must be available if a single zone is to be operated such that maximum separations occur. Simple breakthrough data, as shown in Figure 4-4 are sufficient to determine the optimum temperature switching time.

Effect of Solid Particle Size

Efficient cycling performance of an adsorber depends, among other things, on rapid mass transfer between the fluid and the porous solid particles. When the particles are too large diffusion inside the pores may be too slow for the adsorbent in their centers to reach equilibrium with the main fluid stream. Then, only the outer surface of the particles exchanges appreciable mass with the fluid and the effective capacity of the adsorbent bed is much smaller than its true capacity. To determine whether the separations observed with the silica gel-hydrocarbon system were affected by intraparticle diffusion, experiments were carried out to determine the effect of particle size.

Three experiments were run with a feed of X_{feed} = 24.7 vol % toluene, at an optimum switching time of 1000 seconds

0 0 0 0 3 8 0 7 0 1 3

and an interstitial fluid velocity of 0.0466 cm/sec. Three different lots of silica gel were used: 4- to 16-mesh size, 20-mesh size, and approximately 60-mesh size. The experimental effluent concentration profiles are shown in Figure 4-6. Table 4-2 lists comparative results for these three experiments.

Table 4-2

Particle Size Versus Peak Concentration Difference and Product Flow Duration

Particle Size	Peak Concentration Difference	Low-Product Duration	High-Product Duration
4 to 16 mesh	27.0%-22.9%=4.1%	300 seconds	250 seconds
20 mesh	27.0%-22.9%=4.1%	400 seconds	400 seconds
60 mesh	27.5%-22.6%=4.9%	400 seconds	500 seconds
60 to 200 mesh	-	700 seconds	700 seconds

The peak difference in product concentrations increases with a decrease in the solid particle size. The product flow durations also increase with a decrease in size. The concentration profiles increasingly become more like a square-wave as diffusion becomes easier.

These results can be accounted for by looking at the effect of particle size upon the particle capacity. For large mesh size silica gel it is very difficult for liquid to be exchanged deep within the interior of the solid particle when there is a temperature change. The result

Figure 4-6

Effect of Particle Size Upon Effluent Concentration Profile

Interstitial Fluid Velocity: 0.0466 cm/sec
Period: 2000 seconds
Temperature Switch: every 1000 seconds
Feed: 23.9 vol % toluene
Particle Size: 4-16 mesh
20 mesh
60 mesh
Temperature: 2°C and 59°C

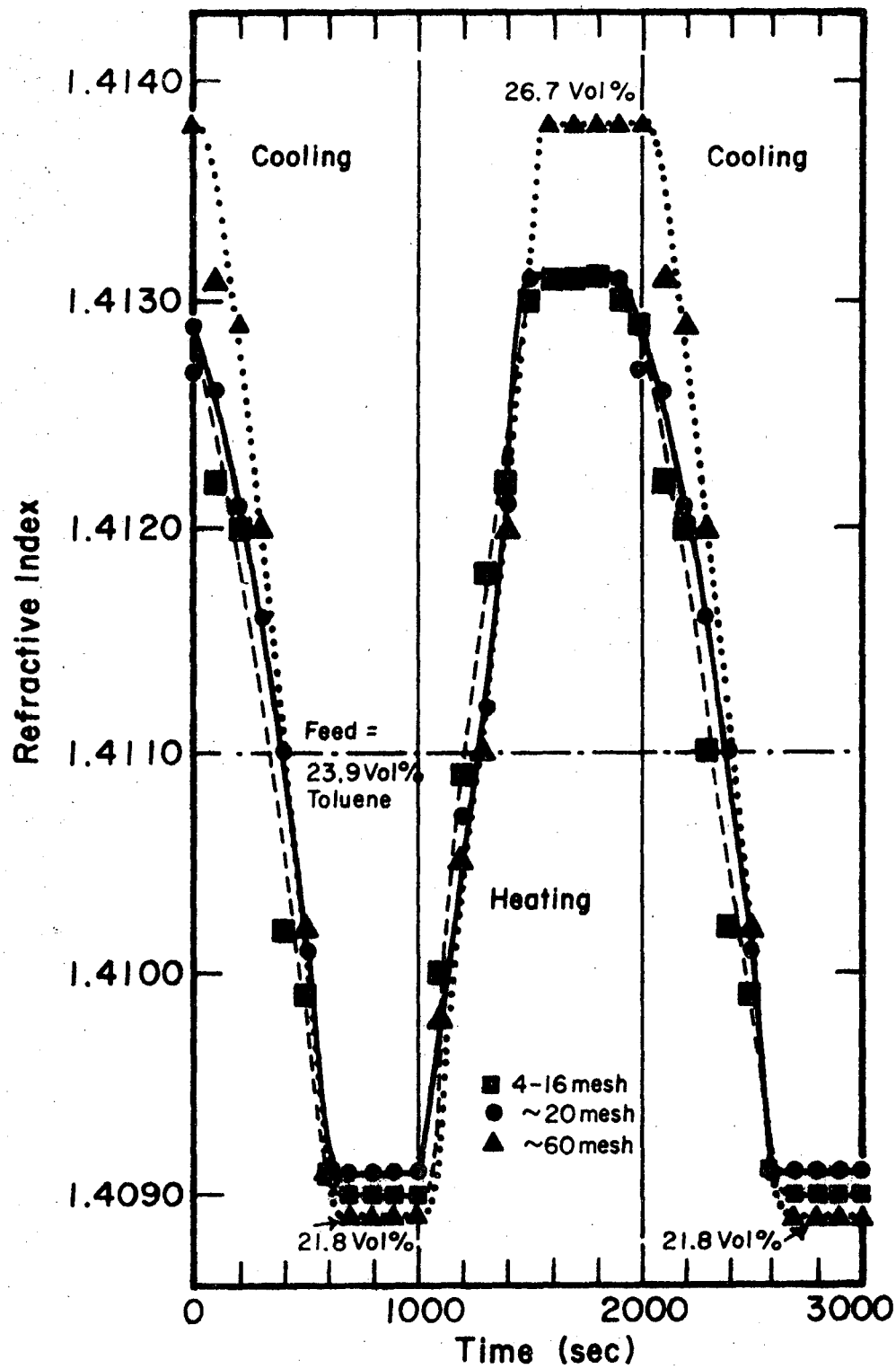
1.4140
1.4130
1.4120
1.4110
1.4100
1.4090
Refractive Index
Cooling
26.7 Vol%
Cooling
Feed =
23.9 Vol%
Toluene
Heating
4-16 mesh
~20 mesh
~60 mesh
21.8 Vol%
21.8 Vol%
0
1000
2000
3000
Time (sec)

is that the effective capacity of the particle is somewhat less than its total capacity. The amount of toluene that the particle can adsorb or desorb is then less, and consequently, the difference in product peaks is also smaller then would be calculated theoretically. Moreover, when diffusion inside the particles is impaired the interior of the particles cannot respond quickly to the sudden change in fluid composition when a wave front passes by. The result is a considerable distortion of the effluent concentration wave shape and a reduction in the duration of either maximum or minimum concentrations in the effluent. As the particle size decreases, the effective capacity of the silica gel approaches that of its true capacity. This results in a greater and more rapid exchange of toluene, causing larger product peak differences and product peak durations. If pumping cost can be disregarded, it would be best to operate a cycling zone adsorption column with the smallest possible packing.

Figure 4-7 is a plot of the concentration response of the experimental column packed with a 60- to 200-mesh powdered chromatographic silica gel made by the Baker Chemical Company. Since this silica gel is manufactured by a different company than that used in all previous experiments, one does not expect to find the same difference in product peak concentrations. This is due to the fact that the two silica gels are of a different grade. However, it is possible to compare the effect of small

Figure 4-7

Effect of 200-Mesh Silica Gel Upon Effluent Concentration Profile

Interstitial Fluid Velocity: 0.0466 cm/sec
Period: 2000 seconds
Half-Cycle: 1000 seconds
Temperature Switch: every 1000 seconds
Feed: 25.3 vol % toluene
Particle Size: 200 Mesh
Product Flow Durations: 700 seconds each
Temperature: 2°C and 59°C

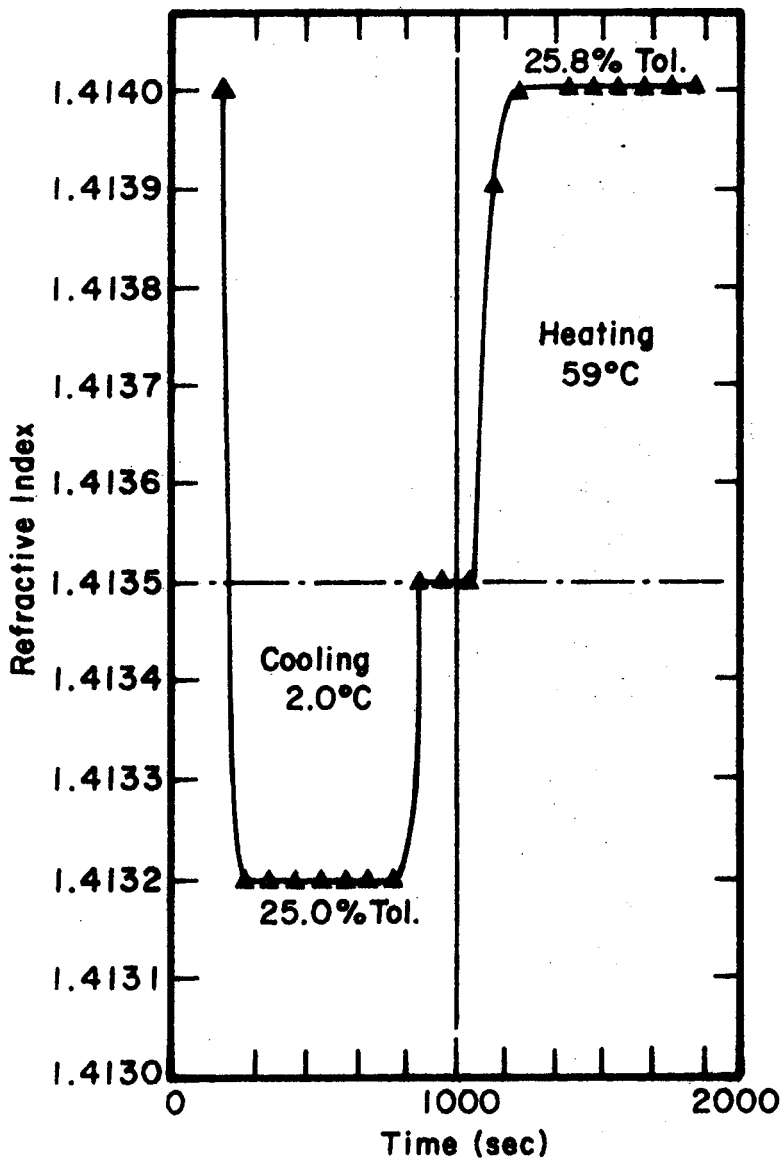
25.8% Tol.
Heating
59°C
Cooling
2.0°C
25.0% Tol.
Refractive Index
1.4140
1.4139
1.4138
1.4137
1.4136
1.4135
1.4134
1.4133
1.4132
1.4131
1.4130
0
1000
2000
Time (sec)

particle size upon the product peak durations. Notice that in Figure 4-7 the product peak durations are both 700 seconds out of a half-cycle time of 1000 seconds. This further confirms the fact that the smaller the particle size, the greater will be the peak durations of the product flow.

Improvement of Column Temperature Response

As indicated in Figure 4-1, the column temperature response for a continuous flow system is not a true square-wave response, although it does approach one. It is seen that approximately 30% of the half-cycle time is required for the column to reach either the high or low temperatures of the desired step change. Only if the solid particles responded instantaneously to a temperature change could the concentration profile be superimposed upon the temperature profile. Because of the design of the experimental apparatus, it was impossible to obtain a perfect step change in column temperature for a continuously flowing system. However, it was possible to operate the apparatus in a noncontinuous manner such that a perfect step change in column temperature did result.

Consider the following operation of the experimental column: Fill the column with feed at the cold temperature. The flow of feed is now stopped and the column temperature is switched to the high value. The flow remains stopped until thermal equilibrium is completely established at the

high temperature. Flow now begins into the column, displacing the high product residing within the column. Flow continues until there is a breakthrough of feed-concentration liquid in the effluent stream. At this point the flow is stopped, and the column temperature is changed to the low value. The flow is stopped until the column completely reaches the low temperature value. At this point the flow of feed begins and the low-concentration product is displaced until there is a breakthrough of feed-concentration liquid in the effluent stream. Flow stops and the process begins over again. If the column temperature is plotted against the time during which flow occurs, the result is a square-wave temperature response. This method of operation is termed the SGM, "Stop-Go Mode."

Figure 4-8 is a plot of the concentration profile for such an operation. The feed into the zone is X_{feed} = 15.3 vol % toluene, interstitial velocity = 0.0466 cm/sec, and the column displacement time is 1225 seconds. As expected, there is a very large increase in the duration of product peak flows, 1000 seconds and 1100 seconds for low and high products, respectively, the difference is due to the more rapidly traveling concentration wave in the cold phase of operation. The concentration profile is not completely square due to mixing at both ends of the column and inside the column itself, and because of gradual breakthrough to the feed concentration. The SGM of operation completely removes

Figure 4-8

A Stop-Go Mode of Operation to Produce a Square-Wave Temperature Response

Interstitial Fluid Velocity: 0.0466 cm/sec
Feed: 15.3 vol % toluene
High-Concentration Product: 17.7 vol % toluene
Low-Concentration Product: 12.9 vol % toluene
Half-Cycle Flow Duration: 1200 seconds
Flow Stoppage: 9 minutes
Temperature: 2°C and 59°C

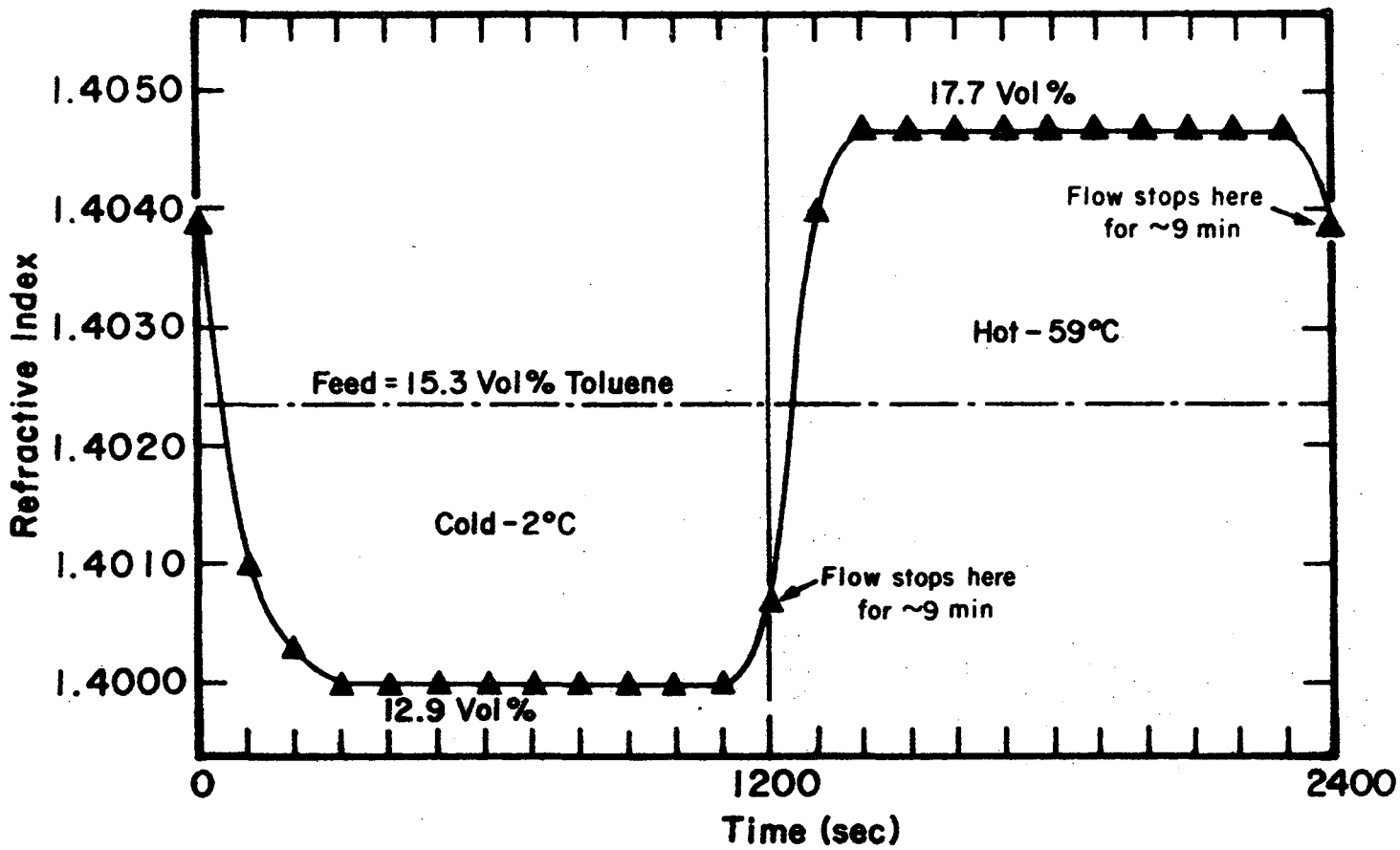
1.4050
1.4040
1.4030
1.4020
1.4010
1.4000
Refractive Index
17.7 Vol %
Flow stops here
for ~9 min
Hot - 59°C
Feed = 15.3 Vol % Toluene
Cold - 2°C
Flow stops here
for ~9 min
12.9 Vol %
0
1200
2400
Time (sec)

the effects of mass and heat transfer resistances that occur in the adsorption process, resulting in the nearly square-wave concentration response of Figure 4-8. The only diffusional process that remains in effect is longitudinal diffusion in the packing during the displacement of fluid from the column. Its effect is minor if the flow is fast enough.

Considering the results of the above operation, the following question must be answered: If an apparatus were designed that would develop a square-wave temperature response in the column, would the concentration response of the effluent stream also be a square wave? There are several reasons why perfectly square-concentration-waves are not expected. First, the variations of the concentration wave velocity with concentration and temperature discussed in Chapter 3 will cause sharpening of the concentration changes when concentrated fluid follows lean fluid through the packing and broadening when lean follows concentrated fluid, even if all diffusion effects are absent. Secondly, two kinds of diffusion phenomena have their effects. Longitudinal diffusion in the fluid itself occurs during the waiting period when flow is stopped, causing wave fronts to become diffuse, and diffusion between fluid and particles must be very rapid if a wave front is to remain sharp during fluid displacement. Thus, the effluent concentration wave will not be square unless the concentration differences are small, the longitudinal effect is small

during the full time of thermal equilibration and flow, and the fluid-particle mass transfer is rapid during flow.

Consider the particle heat transfer resistance. How rapidly does the particle reach the temperature of the surrounding liquid? The following simplified analysis determines the time lag between solid and liquid temperature: Assume that the silica gel particle is a sphere containing a 50 vol % mixture of n-heptane-toluene. Also assume that the heat transfer resistance between the surface of the particle and the surrounding liquid is negligible. This is the same as assuming that all heat transfer resistance is within the particle. If one applies the transient heat conduction equations to such a sphere, it is found that if the dimensionless group $E = (k\Delta t/R^2 C_p \rho)$ is large, then the time lag between the temperatures surrounding liquid and sphere is very small. Let $\Delta = (T_s - T_{\not{c}})/(T_s - T_i)$ where T_s is the temperature of the solid surface just after the column temperature change, $T_{\not{c}}$ is the temperature at the center of the sphere, and T_i is the initial temperature of the sphere before the column temperature change. The average properties of the sphere are: $R^2 = 6.25 \times 10^{-4}$ cm^2, $k = 2.8345 \times 10^{-4}$ cal/cm sec °C, $C_p = 0.124$ cal/g °C, and $\rho = 1.573$ g/cc. If $\Delta = 0.70 \times 10^{-2}$, establishing the temperature at the center of the particle to be within 0.70% of the surface temperature, then the dimensionless group $E = 0.800$. The value of

$\Delta t = 6.825 \times 10^{-3}$ seconds. This calculation indicates that the response of the saturated silica gel particle to a step-change of 57°C in temperature is virtually instantaneous.

It has just been established that the solids temperature closely follows the liquid temperature of a packed bed. It must now be determined if the concentration changes of the solid rapidly follow any concentration changes in the surrounding liquid, that is, if the local equilibrium assumption is valid. Consider the following experiment: A column packed with 60-mesh size silica gel is completely filled with liquid of a high concentration at the high temperature. The column liquid is now displaced with a very low-concentration feed liquid. At the point of feed concentration breakthrough in the effluent stream the flow is stopped and the temperature of the column is changed to the low value. The switch in the column temperature now causes the feed liquid in the column to take on the concentration of the low product. Flow of feed is resumed and now displaces the low-concentration product. If the solid particles were not constantly in equilibrium with the liquid phase, then the final low concentration product would be of a value somewhat higher than that predicted by the equilibrium theory. This is evident when considering Figure 4-9, which is a plot of the effluent concentration profile and the solids concentration profile. The solid lines indicate the equilibrium values while the dashed lines indicate the profiles obtained if there is a concentration lag in the

Figure 4-9

A Qualitative Solids-Liquid Concentration Response to Establish Validity of Local Equilibrium Assumption

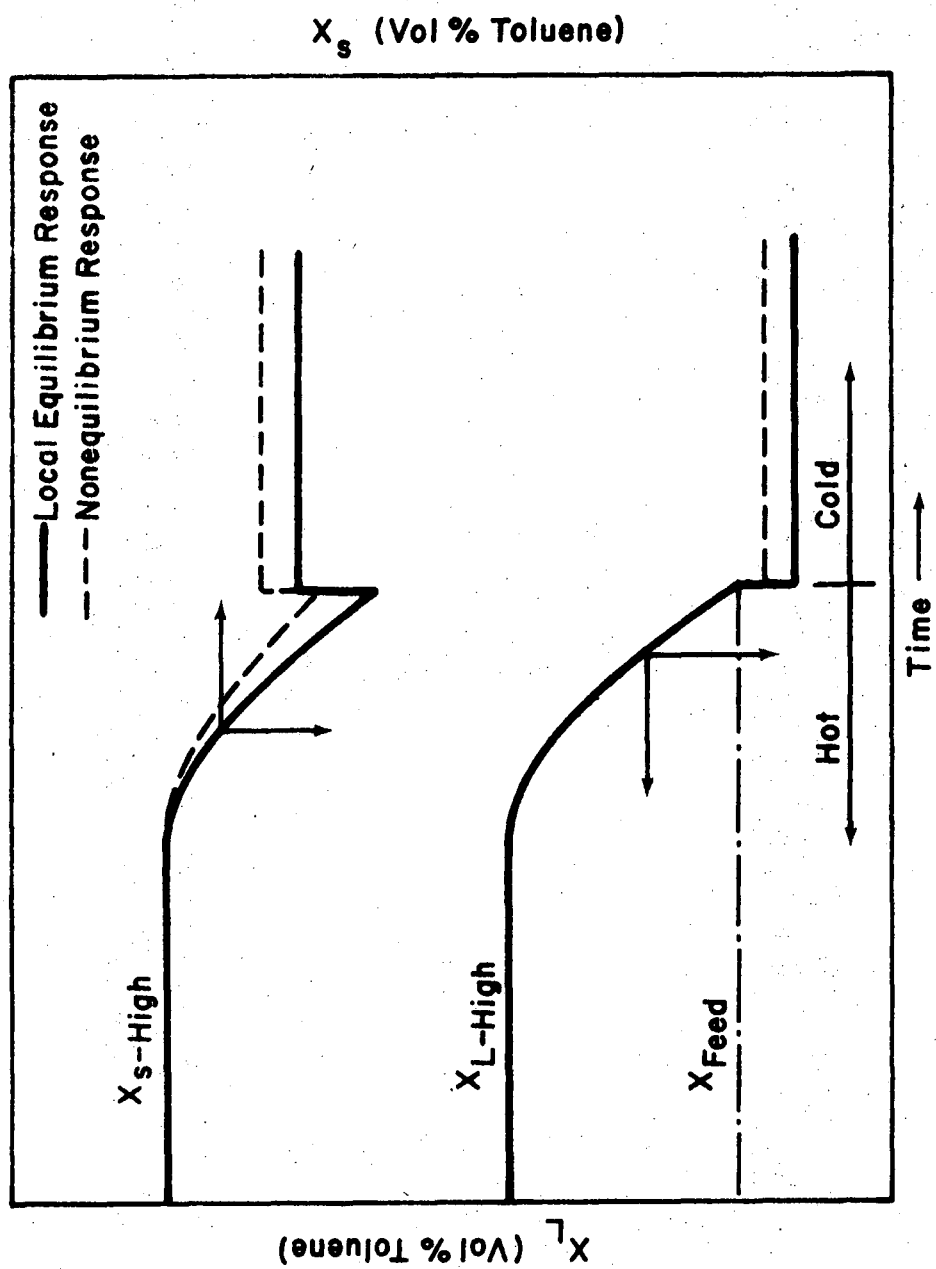
Local Equilibrium Response
Nonequilibrium Response
X_s (Vol % Toluene)
X_{s-High}
X_{L-High}
X_{Feed}
Hot
Cold
Time
X_L (Vol % Toluene)

solid silica gel particles. Figure 4-10 is a plot of the experimental effluent concentration profile for such a run. The final low product concentration is 29.8 vol % toluene. The value predicted by the equilibrium theory is 29.7 vol % toluene. Experimentally the concentration change is 2.4 vol %; that predicted by the equilibrium theory is 2.5 vol %. The experimental case therefore approaches the theoretical case within 96%. The refractive index analysis of effluent concentration has an accuracy of 0.18 vol % toluene, therefore, within experimental accuracy, it may be concluded that the solid silica gel is virtually in equilibrium with its surrounding liquid at all times.

The SGM of operation to establish a square-wave temperature response in the experimental column of this study can then be used to obtain data that would be characteristic of a thermally perfect column operating with a continuous feed stream.

The previous analysis of particle heat transfer and mass transfer therefore validates the assumption that if a column could be designed that would experience a square-wave temperature response, then the concentration response of the effluent stream would also be an approximate square wave. Such a design would then contribute considerably to the performance of a continuously flowing cycling zone adsorption column.

There is one remaining method of operation that greatly improves the separation in a single cycling zone adsorption column.

0 0 0 0 3 8 0 7 0 2 1

Figure 4-10

Experimental Verification of Local Equilibrium Assumption

Interstitial Fluid Velocity: 0.0466 cm/sec
Feed: 32.2 vol % toluene
Displaced High-Concentration Product:
51.7 vol % toluene
Low-Concentration Product: 29.8 vol % toluene
Temperature: 59°C and 2°C
Flow Stoppage: 4 minutes

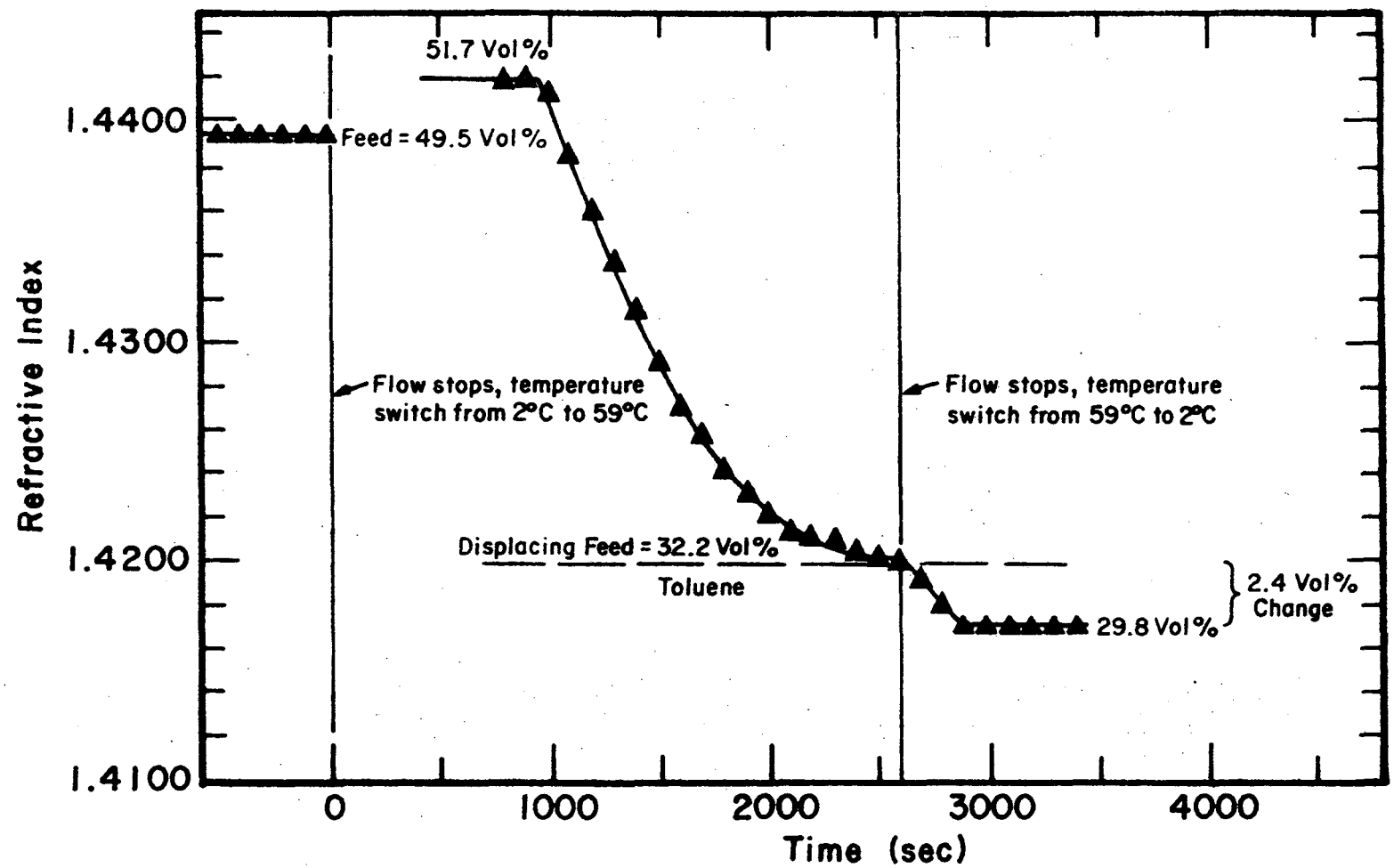
51.7 Vol%
Feed = 49.5 Vol%
Flow stops, temperature switch from 2°C to 59°C
Flow stops, temperature switch from 59°C to 2°C
Displacing Feed = 32.2 Vol%
Toluene
2.4 Vol% Change
29.8 Vol%
Refractive Index
1.4400
1.4300
1.4200
1.4100
0
1000
2000
3000
4000
Time (sec)

0 0 0 0 3 8 0 7 0 2 2

Variable-Feed Operation of a Single Zone

Since the separations occurring in cycling zone adsorption are dependent upon the concentration of liquid in the zone at the time of the temperature change, large product concentration differences may be obtained by a periodic introduction of two different feed concentrations rather then operating with a constant feed concentration. Consider the following operation of a single zone: High-concentration feed, $X_{F,high}$, fills a column which is at the low temperature. When the temperature is switched to the high value, the liquid in the column becomes high-concentration product, $X_{high} > X_{F,high}$. The high-concentration product is now displaced with a feed of low concentration, $X_{F,low} < X_{F,high}$. The temperature is now switched to the low value and the liquid in the column now becomes the low-concentration product, $X_{low} < X_{F,low}$. The low-concentration product, X_{low}, is now displaced with high-concentration feed, $X_{F,high}$, and the process repeats itself again. The idealized concentration profile for such an operation is shown in Figure 4-11. Figure 4-12 is a plot of the experimental effluent concentration profile for a variable-feed system operating in the SGM. It is apparent that the introduction of a step-change in feed at the entrance of a zone will be the cause of numerous operational problems. Such problems are fully discussed in Chapter 5 on Variable-Feed Operation of a Single Zone.

Figure 4-11

Idealized Variable-Feed Effluent Concentration Profile

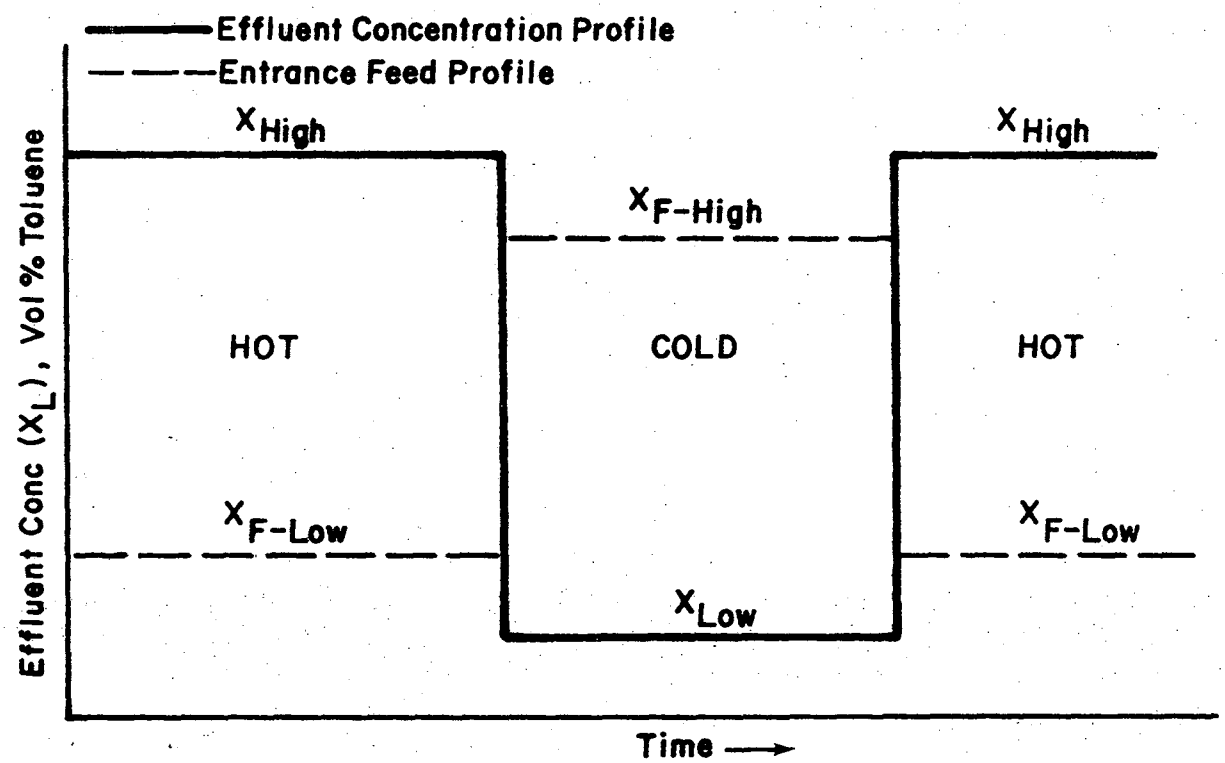
Effluent Concentration Profile
Entrance Feed Profile
Effluent Conc (X_L), Vol % Toluene
X_{High}
X_{F-High}
X_{High}
HOT
COLD
HOT
X_{F-Low}
X_{F-Low}
X_{Low}
Time

Figure 4-12

Experimental Variable-Feed Effluent Concentration Profile

Interstitial Fluid Velocity: 0.0466 cm/sec
High Feed Conc: 34.8 vol % toluene
Low Feed Conc: 30.7 vol % toluene
Period: 3000 seconds
Temperature Switching Frequency: every 1500 seconds
Temperatures: 2°C and 59°C
High-Conc Product: 37.4 vol % toluene
Low-Conc Product: 27.8 vol % toluene
Feed Amplitude: 5.0 vol % toluene
Product Amplitude: 9.6 vol % toluene

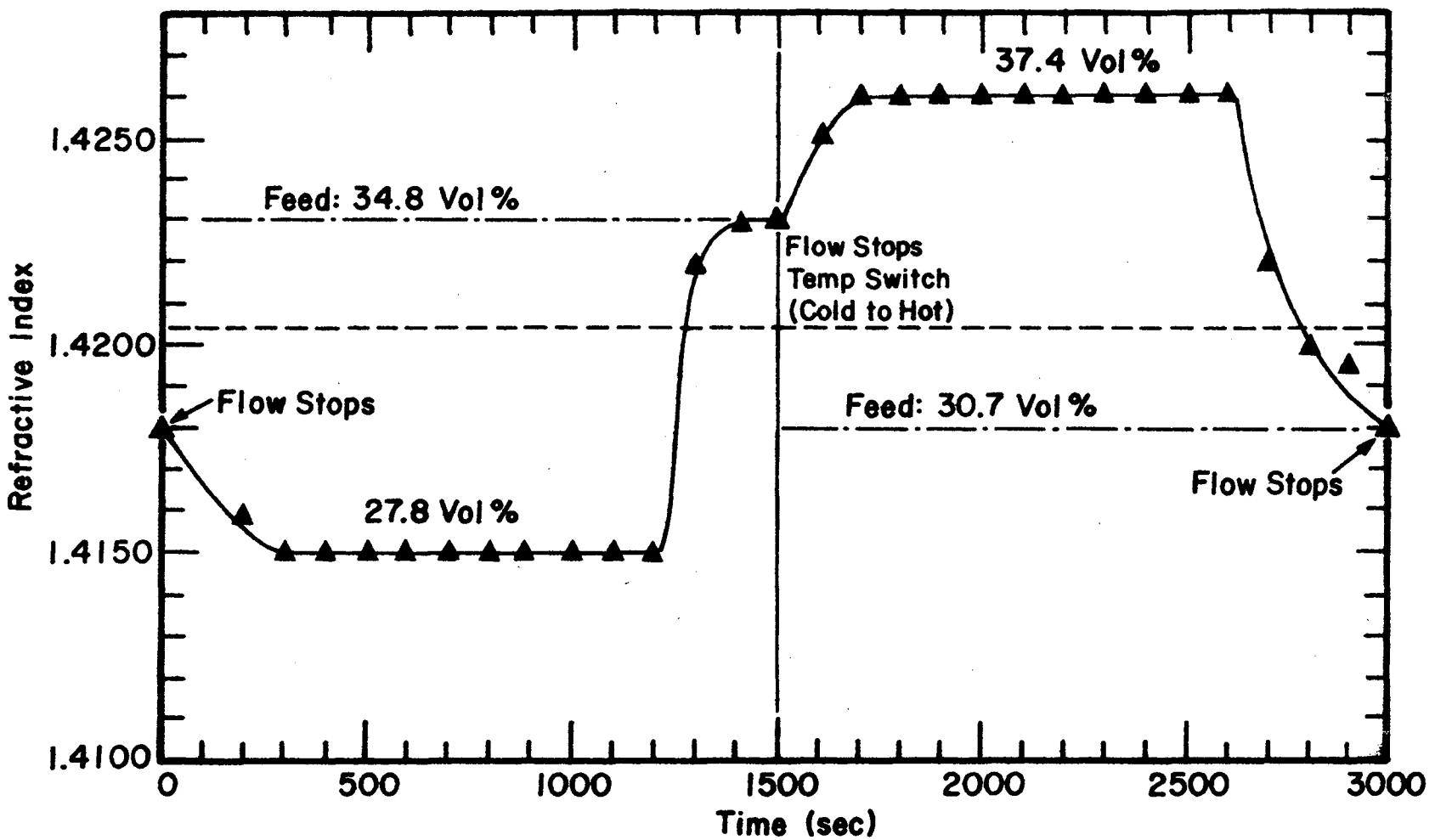
37.4 Vol %
Feed: 34.8 Vol %
Flow Stops
Temp Switch
(Cold to Hot)
Flow Stops
27.8 Vol %
Feed: 30.7 Vol %
Flow Stops
Refractive Index
1.4250
1.4200
1.4150
1.4100
0
500
1000
1500
2000
2500
3000
Time (sec)

In summary, it has been shown that the performance of a continuously operating single zone may be improved by consideration of (1) the optimum temperature switching frequency or optimum column length for a given switching time and interstitial velocity, (2) the size of silica gel particles in a packed column, (3) the production of a square-wave column temperature response, and (4) the optimal introduction of two different feed concentrations into the zone.

0 0 0 0 3 8 0 7 0 2 5

CHAPTER 5

EXPERIMENTAL: VARIABLE-FEED OPERATION OF A SINGLE ZONE

Variable-Feed Recycle Scheme..... 122

Effect of Feed Amplitude Upon Breakthrough During Hot-Phase Operation..... 126

Effect of Feed Amplitude Upon Breakthrough During Cold-Phase Operation..... 133

Overall Diffusion Coefficient for Breakthrough in Hot- and Cold-Phase Operation With Variable-Feed Amplitude..... 144

Effect of Feed Flow Rate Upon Breakthrough During Hot-Phase Operation..... 148

Effect of Average Feed Concentration Upon Breakthrough Time During Hot-Phase Operation..... 158

Derivation of Breakthrough Curve for a Fixed Bed With Longitudinal Diffusion and Local Mass Transfer Equilibrium..... 161

CHAPTER 5

EXPERIMENTAL: VARIABLE-FEED OPERATION OF A SINGLE ZONE

Variable-Feed Recycle Scheme

The logic of variable-feed operation of a single zone has been briefly discussed in the last section of Chapter 4. Bear in mind that the SGM of operation is used to simulate operation of a column in which the temperature is represented by a square wave. Figures 5-1a, 5-1b, and 5-1c are schematic recycle diagrams showing how a single zone would operate during the hot-cycle, the cold-cycle, and the total period of operation, respectively. It is obvious that the duration of product flows for a given variable-feed amplitude is of prime importance. Notice that at the end of each half-cycle there is a concentration approach from the product concentration to the feed concentration. This is pictured in Fig. 4-12. The breakthrough approach during the hot-phase of operation follows that of the "simple concentration wave" discussed in Chapter 3. The breakthrough approach during the cold phase corresponds to that of the concentration shock front discussed in Chapter 3. Notice that both these breakthrough curves are spread out considerably. This is due to longitudinal diffusion and mixing of the initial concentration front at the entrance to the column. If one plots R = This Ratio (product

0 0 0 0 3 8 0 7 0 2 6

Figure 5-1

Operation of a Variable-Feed, Recycle Cycling Zone Adsorber

Figure 1-a shows the operation during the hot-phase half-cycle. Figure 1-b shows the operation during the cold-phase half-cycle. Figure 1-c shows the operation over the whole period (sum of half-cycles).

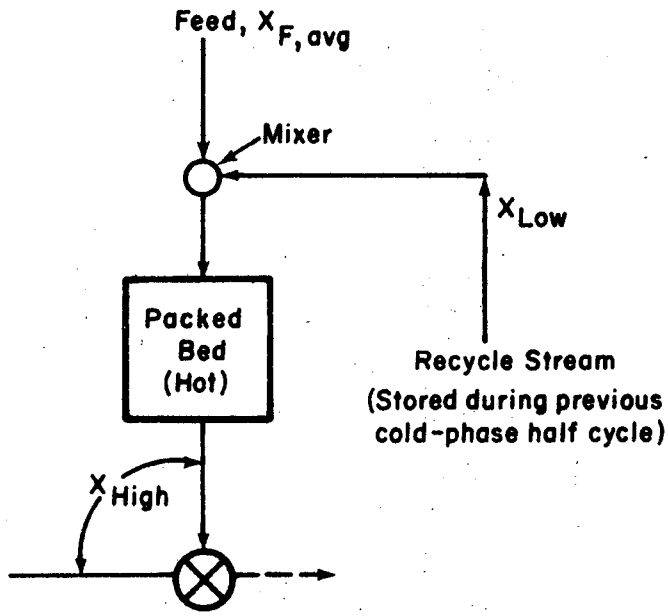

A. Hot-Phase Half Cycle

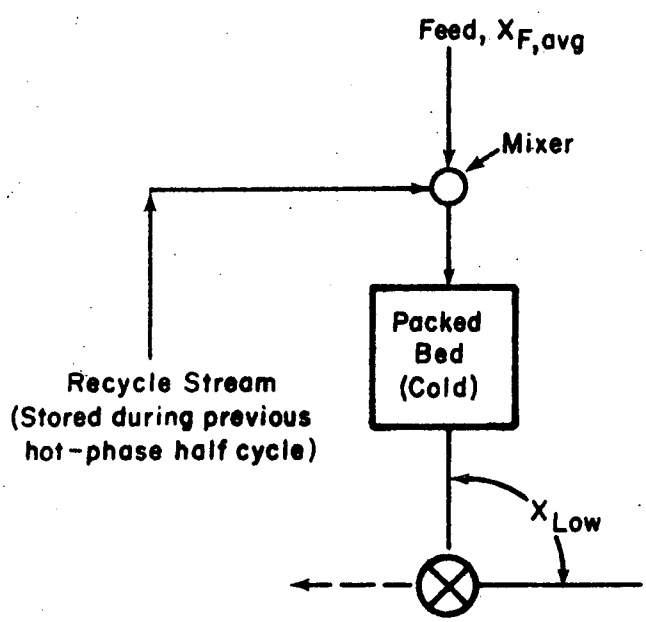

B. Cold-Phase Half Cycle

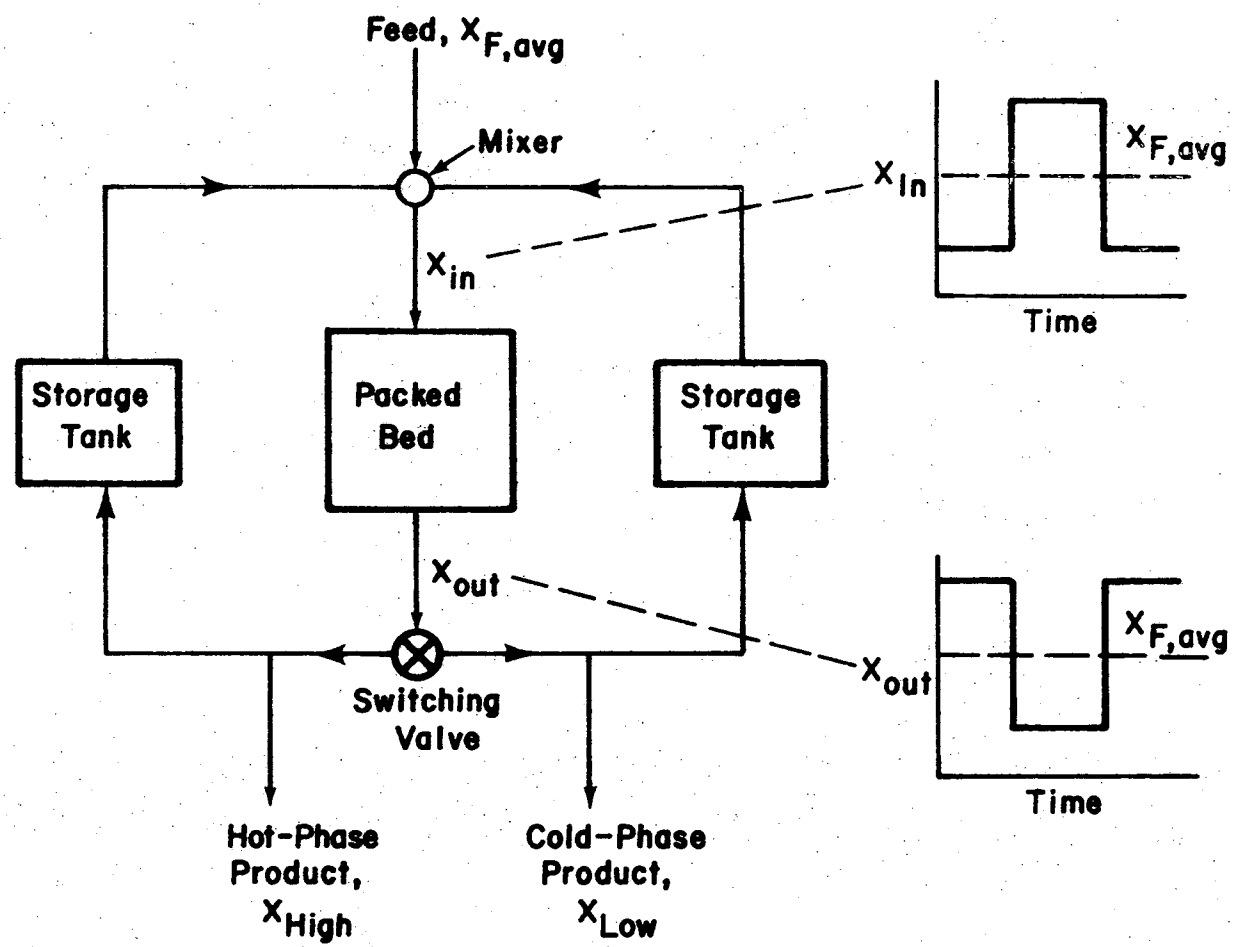

C. Total Period of Operation (Sum of A and B)

duration)/(temperature switching time) versus variable-feed amplitude (vol % toluene), it would be expected that there would be a general decrease in R as the feed amplitude increases. If one plots T = (percent of product stream required for recycle) versus variable-feed amplitude, it is seen that T increases with the feed amplitude. That is, for a single continuously operating zone with a very large feed concentration amplitude, a very large portion of the product streams must be recycled back to the feed point to maintain the large feed amplitude, as shown in Figure 5-2. It is obvious that there is some maximum feed amplitude that will allow recycle such that some fraction of the high and low product streams may be removed for further processing. It is therefore of great interest to investigate the effect of variable-feed amplitude upon breakthrough curves generated in the hot- and cold-phases of single-zone operation.

Effect of Feed Amplitude Upon Breakthrough During Hot-Phase Operation

When a zone has been filled with high-concentration feed and the bed temperature is changed to the hot temperature, the zone becomes filled with high-concentration product. This high product is then displaced from below with the low-concentration feed. In this case a high-density, high-viscosity liquid is being displaced by a low-density, low-viscosity liquid. As predicted by the

0 0 0 0 0 8 0 7 0 2 8

Figure 5-2

Qualitative Determination of Maximum Feed Amplitude

R = (product flow duration)/(temperature switching time)

T = percent of product stream recycled

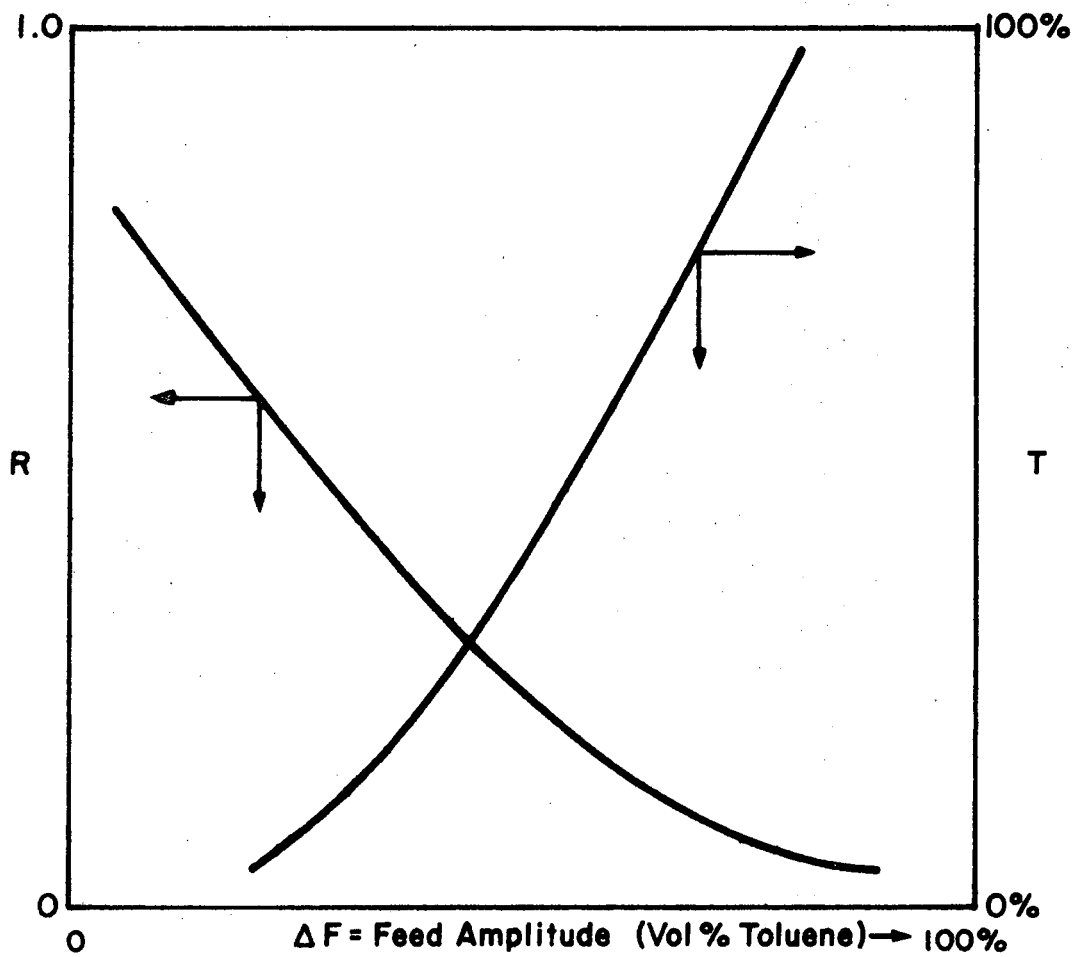
1.0
100%
R
T
0
0%
0
ΔF = Feed Amplitude (Vol % Toluene)→ 100%

simplified mathematical analysis, the higher concentration product travels at a concentration wave velocity that is greater than that of the trailing low-concentration liquid. A simple concentration wave is then expected in the column. It is seen from Eq. (3-9) or Figure 3-1 of Chapter 3 that the greater the difference in concentration, the greater will be the duration of the simple concentration wave in the effluent stream.

Consider experiments where high-concentration liquids are displaced by a low-concentration liquid at the high temperature. Figure 5-3 is a plot of effluent concentration profiles for such experiments. Table 5-1 lists the characteristics of these experiments, where the duration of product flow is the time for which the high-concentration product is displaced, and the duration of breakthrough is the time it takes the effluent stream concentration to change from the high product value to the displacing feed concentration.

The data in Table 5-1 reveal the following trends: (1) an increase in the duration of high-concentration product flow as the feed amplitude decreases, (2) a decrease in the duration of the breakthrough curve as the feed amplitude decreases, and (3) a decrease in the total displacement time as the feed amplitude decreases. The displacement time in seconds then approaches (column length)/(interstitial velocity) as the feed amplitude approaches zero.

Figure 5-3

Experimental Low-Concentration Feed Breakthrough Data

This figure shows the effect of various feed amplitudes upon the effluent concentration profile for high-concentration product being displaced by a low-concentration feed stream. The displacing feed is 30.8 vol % toluene, with five variable high-concentration products being displaced. The interstitial velocity is 0.0466 cm/sec, the column run at a temperature of 59°C.

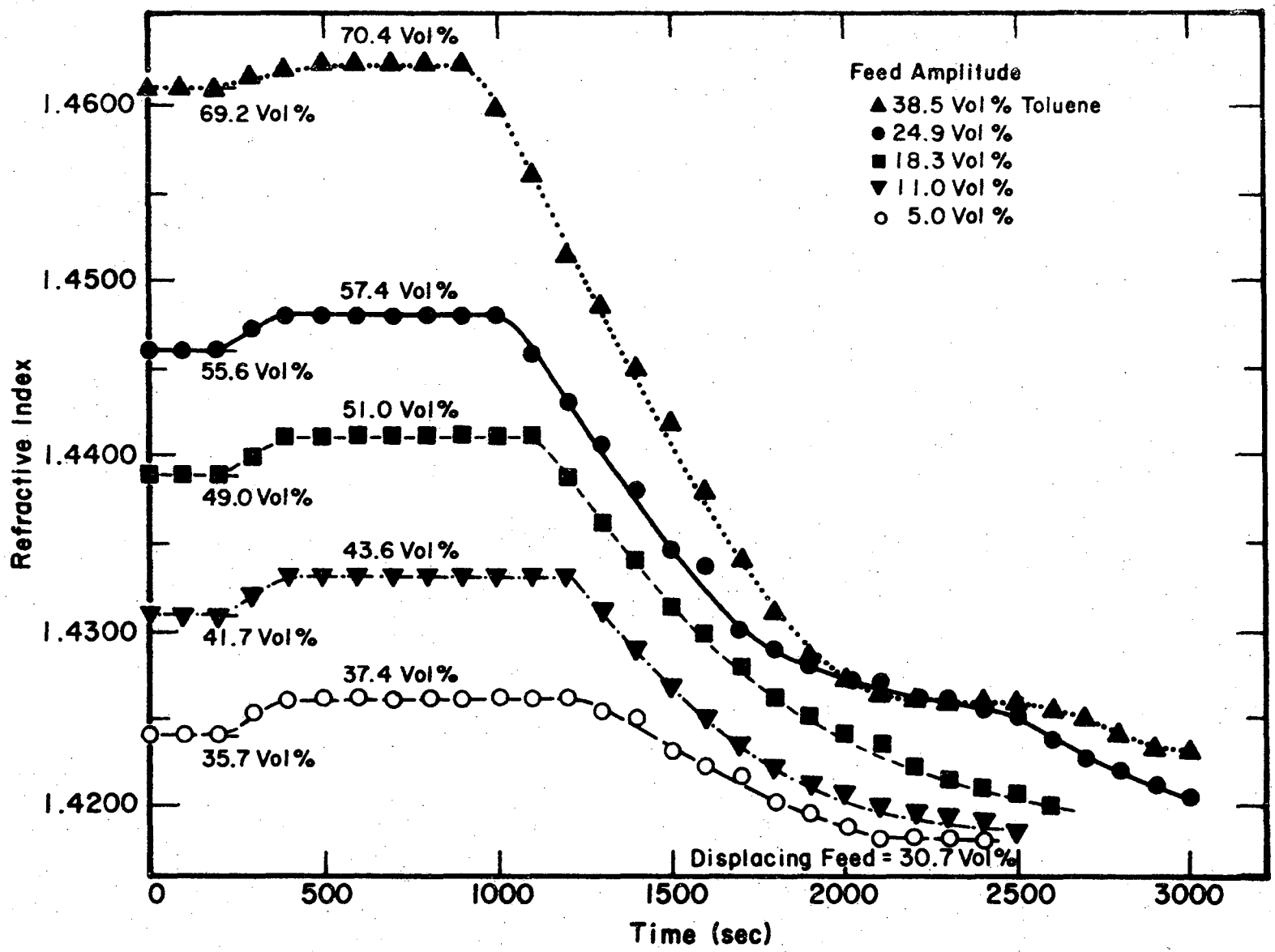
Feed Amplitude
▲ 38.5 Vol % Toluene
● 24.9 Vol %
■ 18.3 Vol %
▼ 11.0 Vol %
○ 5.0 Vol %
70.4 Vol %
69.2 Vol %
57.4 Vol %
55.6 Vol %
51.0 Vol %
49.0 Vol %
43.6 Vol %
41.7 Vol %
37.4 Vol %
35.7 Vol %
Displacing Feed = 30.7 Vol %
Refractive Index
1.4600
1.4500
1.4400
1.4300
1.4200
0
500
1000
1500
2000
2500
3000
Time (sec)

Table 5-1

Variable-Feed Breakthrough Data (Hot-Phase)

Feed Amplitude to Column (volume % toluene)	Duration of Product Flow (sec)	Total Time of Displacement (sec)	Duration of Breakthrough (sec)	Duration of Breakthrough / Total Displacement Time
70.4% - 30.7% = 39.7%	900	3900	3000	0.769
57.4% - 30.7% = 26.7%	1000	3100	2100	0.677
51.0% - 30.7% = 20.3%	1100	2600	1500	0.577
43.6% - 30.7% = 12.9%	1200	2300	1100	0.478
37.4% - 30.7% = 6.7%	1250	1750	500	0.286

Feed Amplitude to Column (volume % toluene)	$\rho_{prod.} - \rho_{feed}$ (unstable) (g/cc)	$\mu_{prod.} - \mu_{feed}$ (unstable) (cp)
70.4% - 30.7% = 39.7%	0.073	0.060
57.4% - 30.7% = 26.7%	0.049	0.040
51.0% - 30.7% = 20.3%	0.037	0.030
43.6% - 30.7% = 12.9%	0.024	0.020
37.4% - 30.7% = 6.7%	0.012	0.010

Consider the above experiment for a feed amplitude of 20.3 vol % toluene. Figure 5-4 is a comparison plot of the effluent concentration profile predicted by the simplified mathematical analysis and an experimental effluent concentration profile. There is a large spread of the breakthrough curve to the low-concentration feed. As discussed in Chapter 3, the simplified mathematical analysis does not predict such a long spread of the simple concentration wave. This is because the simple theory does not take into account any diffusional effects. It is apparent from Figure 5-4 that there is considerable longitudinal diffusion due to the large initial step change in concentration at the entrance of the zone. A qualitative explanation is given in a later portion of this chapter.

Effect of Feed Amplitude Upon Breakthrough During Cold-Phase Operation

When a zone is filled with low-concentration feed and the bed temperature is switched to the cold value, the zone becomes filled with lower concentration product. This product is then displaced with high-concentration feed. In this case a low-density, low-viscosity liquid is being displaced from below by a high-density, high-viscosity liquid. As predicted by the simplified mathematical analysis, the high-concentration feed travels at a wave velocity greater than the displaced low-concentration

Figure 5-4

Simple-Wave: Qualitative Comparison of Effluent Concentration Profile With That Predicted by the Simplified Mathematical Analysis of Chapter 3

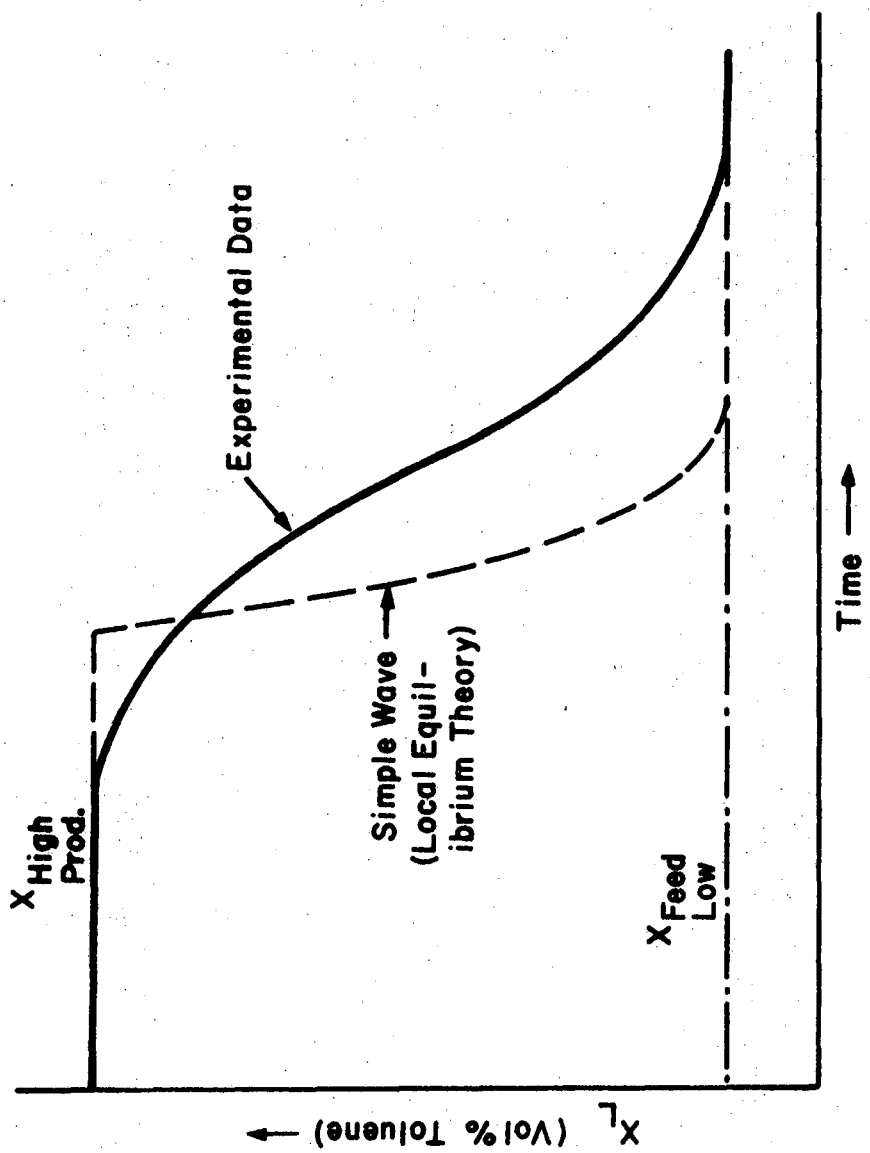
Experimental Data
Simple Wave
(Local Equil-
ibrium Theory)
$X_{High\ Prod.}$
$X_{Feed\ Low}$
X_L (Vol% Toluene)
Time

product. A concentration shock-wave is then predicted to be generated within the column.

Consider experiments where a low-concentration product is being displaced by various high-concentration feeds. Figure 5-5 is a plot of effluent concentration profiles for such experiments. Table 5-2 lists the characteristics of these experiments, where the duration of product flow is the time for which the low-concentration product is displaced and the duration of breakthrough is the time it takes for the effluent stream concentration to change from the low product value to the displacing feed concentration.

The data in Table 5-2 reveal the following trends: (1) an increase in the total displacement time with an increase with the feed amplitude, (2) a constant duration of low-concentration product, and (3) a decrease in the duration of the breakthrough curve as the feed amplitude decreases.

Consider the above experiment for a feed amplitude of 20.4 vol % toluene. Figure 5-6 is a comparison plot of the effluent concentration profile predicted by the simplified mathematical analysis and the experimental effluent concentration profile. Again the large deviation is due to diffusional and mixing mechanisms caused by the large step-change in concentration at the entrance of the column.

Figure 5-5

Experimental High-Concentration Feed Breakthrough Data

This figure shows the effect of various feed amplitudes upon the effluent concentration profile for a low-concentration product being displaced by various high-concentration feeds. The displaced product is 27.8 vol % toluene, with five variable high-concentration feeds displacing the product. The interstitial fluid velocity is 0.0466 cm/sec, the column run is at 2°C.

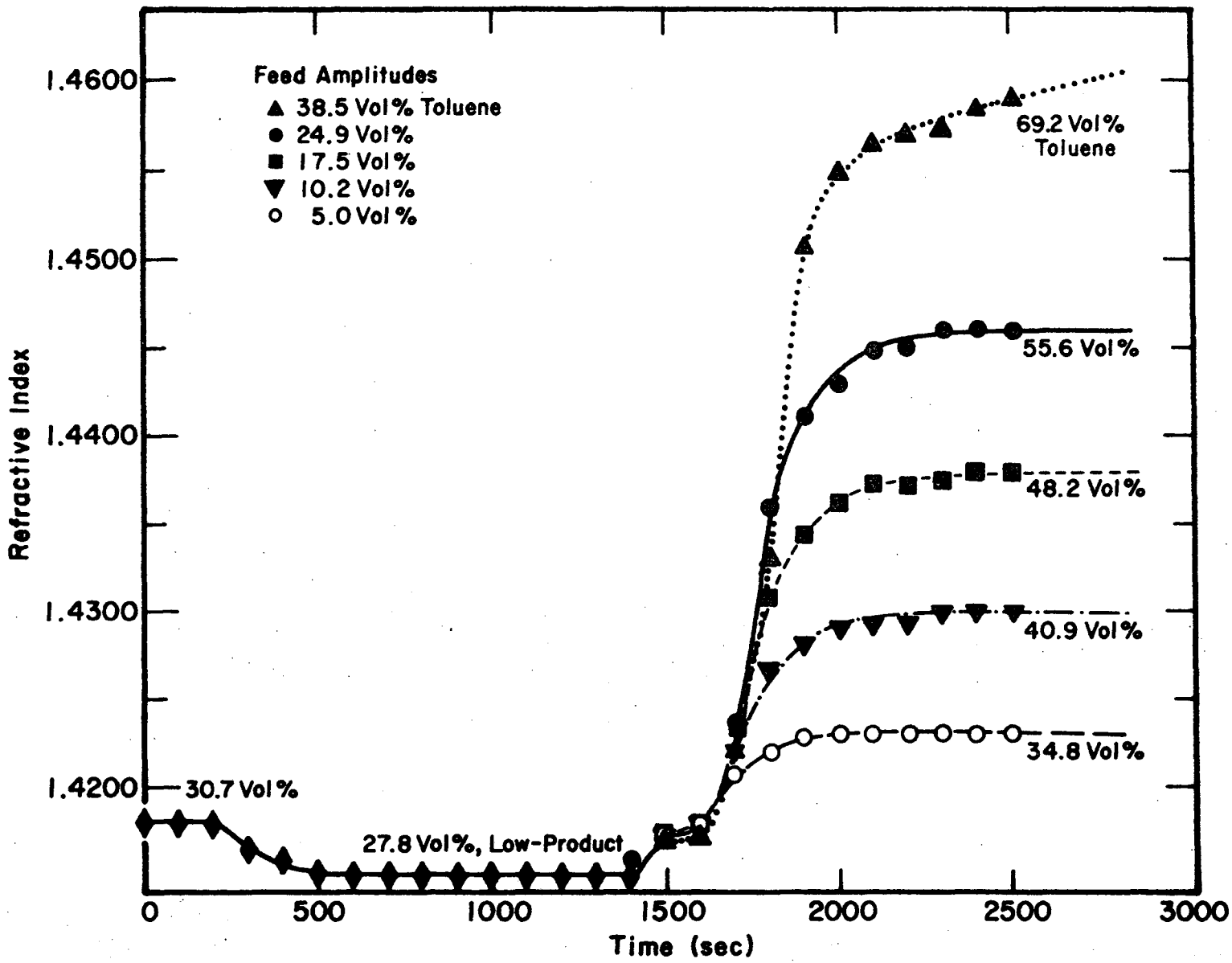
Feed Amplitudes
38.5 Vol% Toluene
24.9 Vol%
17.5 Vol%
10.2 Vol%
5.0 Vol%
69.2 Vol% Toluene
55.6 Vol%
48.2 Vol%
40.9 Vol%
34.8 Vol%
30.7 Vol%
27.8 Vol%, Low-Product
Refractive Index
1.4600
1.4500
1.4400
1.4300
1.4200
0
500
1000
1500
2000
2500
3000
Time (sec)

Table 5-2

Variable-Feed Breakthrough Data (Cold-Phase)

Feed Amplitude to Column (volume % toluene)	Duration of Product Flow (sec)	Total Time of Displacement (sec)	Duration of Breakthrough (sec)	Duration of Breakthrough / Total Displacement Time
69.2% - 27.8% = 41.4%	1400	2600	1200	0.461
48.2% - 27.8% = 20.4%	1400	2250	850	0.377
40.9% - 27.8% = 13.1%	1400	1950	550	0.282
34.8% - 27.8% = 7.0%	1400	1650	250	0.151

Feed Amplitude to Column (volume % toluene)	$\rho_{prod.} - \rho_{feed}$ (stable) (g/cc)	$\mu_{prod.} - \mu_{feed}$ (stable) (cp)
69.2% - 27.8% = 41.4%	-0.076	-0.052
48.2% - 27.8% = 20.4%	-0.038	-0.030
40.9% - 27.8% = 13.1%	-0.034	-0.020
34.8% - 27.8% = 7.0%	-0.013	-0.010

Figure 5-6

Shock-Wave: Qualitative Comparison of Effluent Concentration Profile With That Predicted by the Simplified Mathematical Analysis of Chapter 3

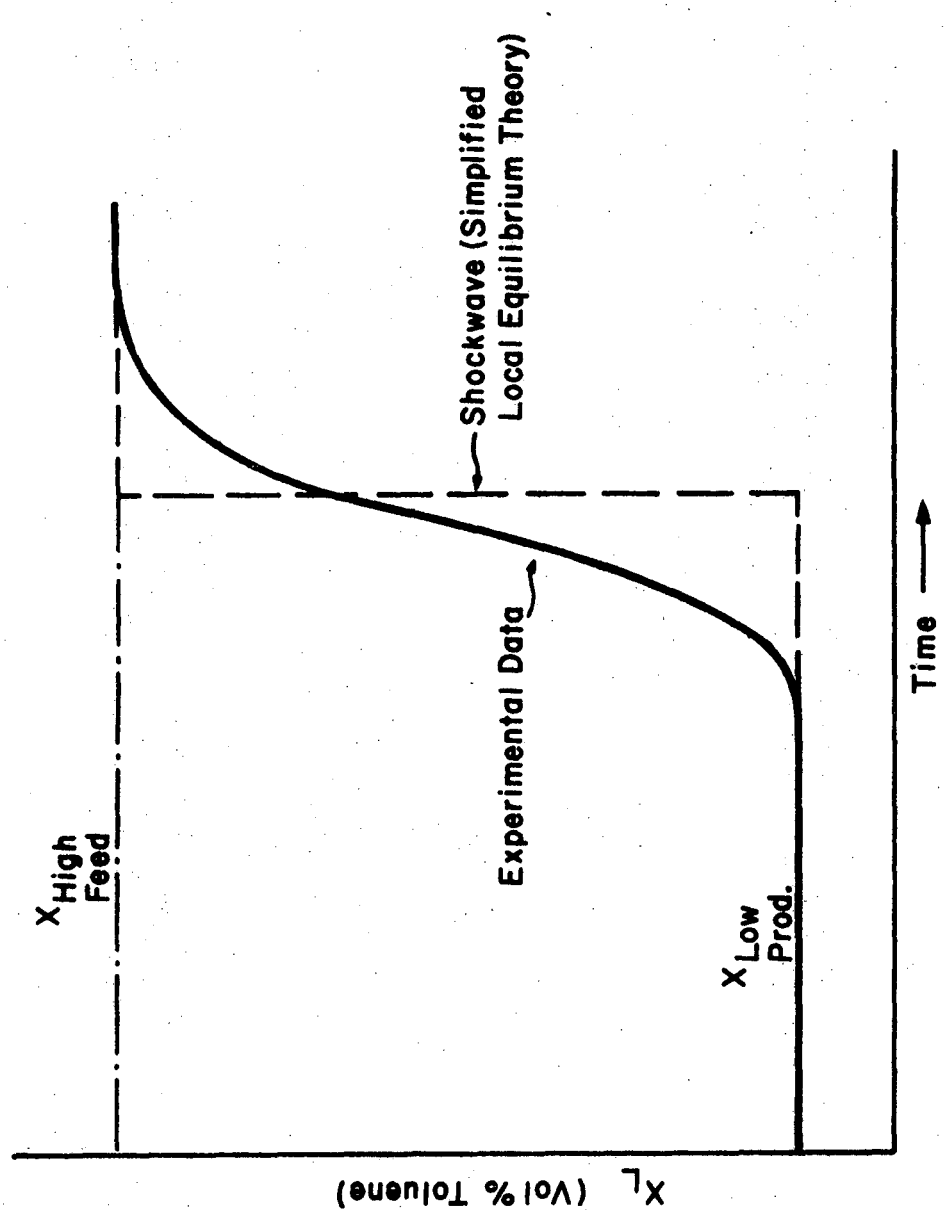
$X_{High\ Feed}$
Experimental Data
Shockwave (Simplified Local Equilibrium Theory)
$X_{Low\ Prod.}$
X_L (Vol % Toluene)
Time

A comparison of feed breakthrough data for the two different cases reveals that breakthrough times for the hot-phase operation of a zone are greater than those for the cold-phase operation of the column. The only differences for both cases are the densities and viscosities of the displaced product and the feeds. Considering the concentration interfaces, it is apparent that during the hot-phase operation that the interface has density instability, a more dense fluid resting on top of a less dense feed. During the cold-phase operation, a less dense fluid resides on top of a more dense feed resulting in a more stable concentration interface. The hot-phase then experiences a large density-driven instability, causing a large spread of the breakthrough curve as the density difference between product liquid and feed increases. Although there is a density difference for displacement in the cold-phase operation, the interface is more stable since a low-density fluid resides upon a high-density fluid. The result is a smaller spread of the breakthrough curve as the feed amplitude increases. In both cases there is diffusion due to the large step-change in concentration at the entrance of the zone. However, it appears that density-driven instability accounts in part for the large difference in breakthrough duration for the hot- and cold-phase operation of the zone.

A second point that bears consideration is the effect of viscosity upon the spread of the breakthrough curves. During the hot-phase operation (which has density-driven instability) a high-viscosity fluid is being displaced by a low-viscosity fluid. This arrangement of flowing liquids is considered unstable (63), and there should result mixing beyond that caused by the concentration and unstable density differences. Such a situation is analogous to the displacement of oil in a reservoir by water pumped from below. As with density-driven instability, it is found that there are fingers of fluid that penetrate through the interface. In this case there should result greater mixing than that caused by diffusion alone. During the cold-phase operation (which has density stability), a low-viscosity fluid is being displaced by a high-viscosity fluid. This arrangement of flowing liquids is considered stable (63).

It would be difficult to determine the separate contribution of each of the above phenomena to the spread of the breakthrough curves beyond that caused by diffusion along. However, the observed effects indicate that the unstable density and viscosity situation during the hot-phase operation seems to be the predominant cause of spreading of the breakthrough curve while diffusion effects seems to be the predominant cause of the short breakthrough curve during the cold-phase operation.

Overall Diffusion Coefficient For Breakthrough in Cold- and Hot-Phase Operations With Variable-Feed Amplitudes

The spreading of the breakthrough curves in both cases may be characterized by calculation of an apparent diffusion coefficient which represents the breakthrough phenomena. As shown in the calculations at the end of the chapter, the diffusion coefficient may be calculated from the breakthrough data of Figures 5-3 and 5-5 using the following relationship:

$$\langle d^2 \rangle = \left(\frac{4}{3}\right)\left(\frac{\mathcal{D} t_{1/2}}{1+m}\right) \tag{5-1}$$

For the hot-phase operation, Figure 5-7 is a plot of the diffusion coefficient versus the feed amplitude. Figure 5-7 also contains a plot of the diffusion coefficient versus the feed amplitude for the cold-phase operation of the column. In both cases, the spread of the breakthrough curves is characterized by an increase of the coefficient as the feed amplitude increases. Table 5-3 lists the diffusion coefficient versus the five feed amplitudes used in the hot- and cold-phase operations.

Figure 5-7

Diffusion Coefficient Versus Feed Amplitude for Hot- and Cold-Phase Operation

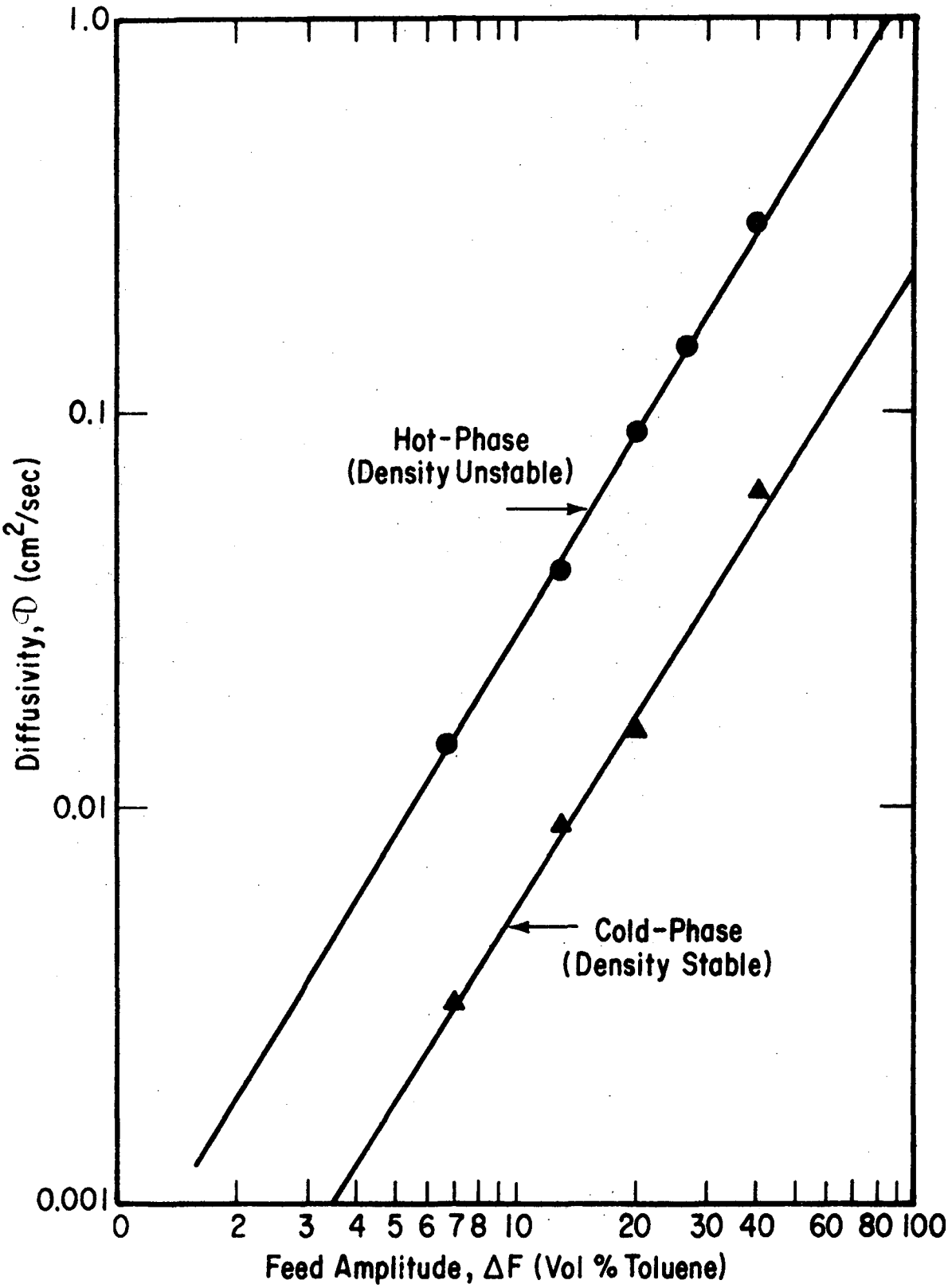
1.0
0.1
0.01
0.001
Diffusivity, $\mathcal{D}$ (cm^2/sec)
Hot-Phase
(Density Unstable)
Cold-Phase
(Density Stable)
0
2
3
4
5
6
7
8
10
20
30
40
60
80
100
Feed Amplitude, ΔF (Vol % Toluene)

Table 5-3

Feed Amplitude Versus Diffusion Coefficient for Hot- and Cold-Phase Operation

Feed Amplitude (vol % toluene)	Diffusion Coefficient (cm^2/sec)
Hot-Phase Operation (density-unstable, viscosity-unstable)	
6.7	0.014
12.9	0.040
20.3	0.087
26.7	0.145
39.5	0.299
(Molecular Diffusivity = 3.72×10^{-5} cm^2/sec)	
Cold-Phase Operation (density-stable, viscosity-stable)	
7.0	0.003
13.1	0.008
20.4	0.015
27.8	0.011
41.4	0.063

It is apparent that the unstable density and viscosity effects occurring in the hot-phase operation tend to be greater than the diffusional effect common to both the cold- and hot-phase operation. If the data are extrapolated to feed amplitudes of zero and 100%, the hot-phase operation diffusion coefficient varies from 0.000065 cm^2/sec to 1.270 cm^2/sec, an increase by a factor of 2.0×10^4, while the cold-phase operation diffusion coefficient varies from 0.000023 cm^2/sec to 0.225 cm^2/sec, an increase by a factor of 1.0×10^4.

The following summarizes the effects contributing to the spread of the breakthrough curves as the feed amplitude increases.

Hot-phase operation:

(1) Diffusion due to initial step-change in feed concentration.

(2) Mixing due to the initial unstable step-change in feed density and viscosity.

Cold-phase operation:

(1) Diffusion due to the initial step-change in feed concentration.

It has been just shown that diffusional and mixing effects all clearly limit the operation of a variable-feed cycling adsorption zone. It is apparent that the ability of a zone to accommodate a large feed amplitude is governed by the spread of the breakthrough curve occurring in the hot-phase operation. It would then be of interest to investigate operational procedures that would sharpen the breakthrough curve.

Effect of Feed Flow Rate Upon Breakthrough During Hot-Phase Operation

One such procedure would be to examine the effect of column flow rate upon the feed breakthrough curve. Consider the following experiments: the experimental column is filled with 50 vol % toluene feed at the low temperature. The temperature is switched to the high value, and the

column now becomes filled with high-concentration product, 52.4 vol % toluene. The high-concentration product is now displaced in each case at five different feed flow rates, the feed in each case being 31.5 vol % toluene. Flow is continued at the prescribed rate until there is a breakthrough of feed concentration liquid in the effluent stream.

For comparison, all effluent concentration profiles are standardized on the time axis to an interstitial fluid velocity of 0.0466 cm/sec. Figure 5-8 is a plot of effluent concentration profiles for five different interstitial feed velocities: 0.051 cm/sec (0.265 cc/sec); 0.1104 cm/sec (0.5733 cc/sec); 0.4170 cm/sec (2.167 cc/sec); 0.5670 cm/sec (2.95 cc/sec); and 0.7444 cm/sec (3.866 cc/sec). As indicated by Figure 5-8 there is a considerable sharpening of the breakthrough curve as the feed velocity is increased.

This phenomenon may be characterized again by calculation of an overall diffusion coefficient from Eq. (5-1). Table 5-4 lists the diffusion coefficient versus the flow rate. Figure 5-9 is a plot of the overall diffusion coefficient versus the volumetric flow rate. It is seen that there is a definite decrease in the coefficient as the flow rate increases, characterizing the sharper breakthrough of feed concentration liquid.

Figure 5-10 is a plot of the Peclet Number, using the above coefficients, versus the Reynolds Number. The

Figure 5-8

Effect of Volumetric Flow Rate Upon Effluent Concentration Profile

This figure summarizes five experiments where a high-concentration product of 52.4 vol % toluene was displaced by 31.5 vol % feed In each experiment the volumetric flow rate of the feed was different. The column with perforated distributor plates was used and run at a temperature of 59°C. The feed amplitude was 18.5 vol % toluene. Curves are all standardized on the time axis to an interstitial fluid velocity of 0.0466 cm/sec.

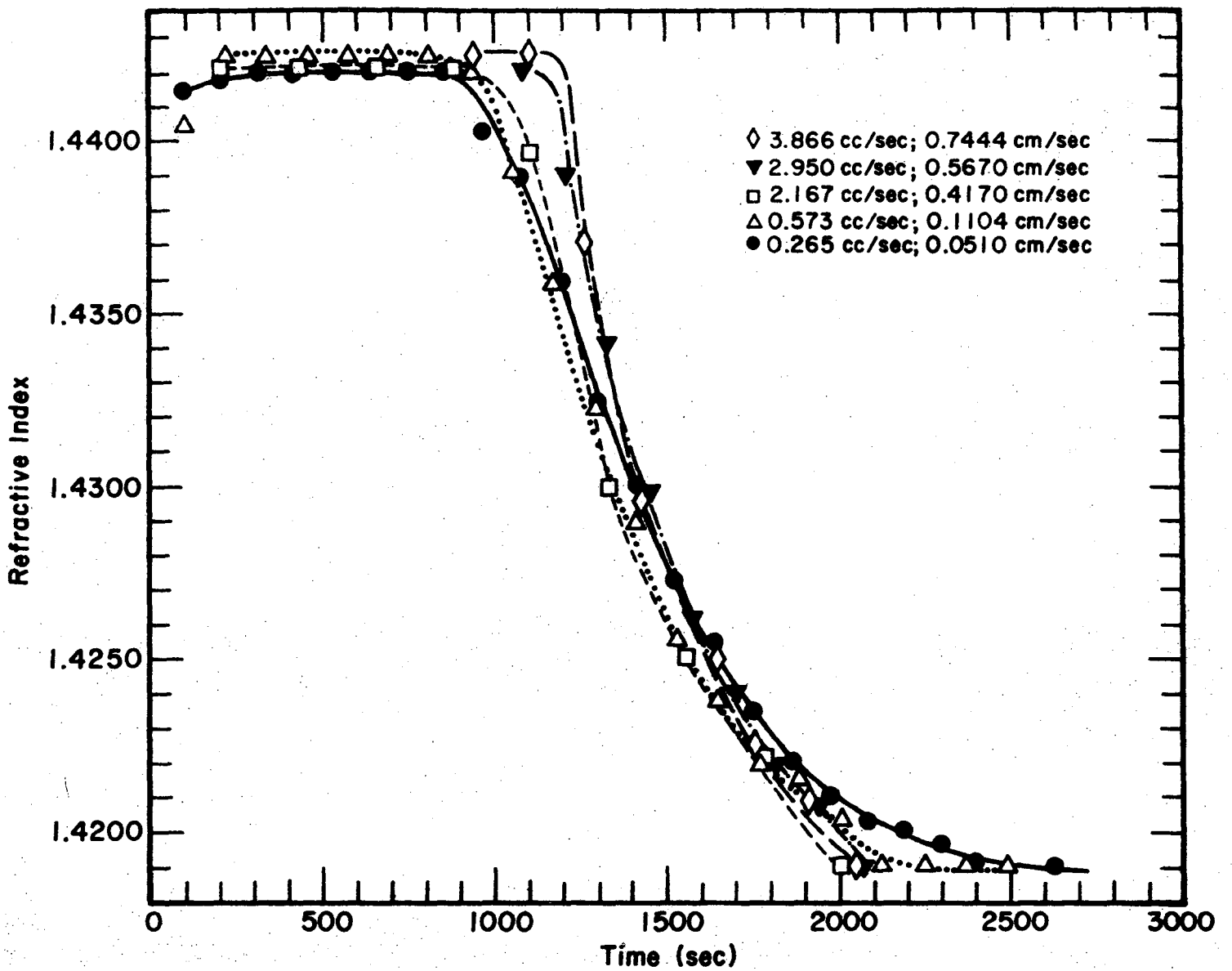
◊ 3.866 cc/sec; 0.7444 cm/sec
▼ 2.950 cc/sec; 0.5670 cm/sec
□ 2.167 cc/sec; 0.4170 cm/sec
△ 0.573 cc/sec; 0.1104 cm/sec
● 0.265 cc/sec; 0.0510 cm/sec
Refractive Index
1.4400
1.4350
1.4300
1.4250
1.4200
0
500
1000
1500
2000
2500
3000
Time (sec)

Figure 5-9

Effect of Feed Flow Rate Upon Diffusion Coefficient

Coefficients were calculated from the data in Figure 5-8, using the mathematical development in the last section of Chapter 5.

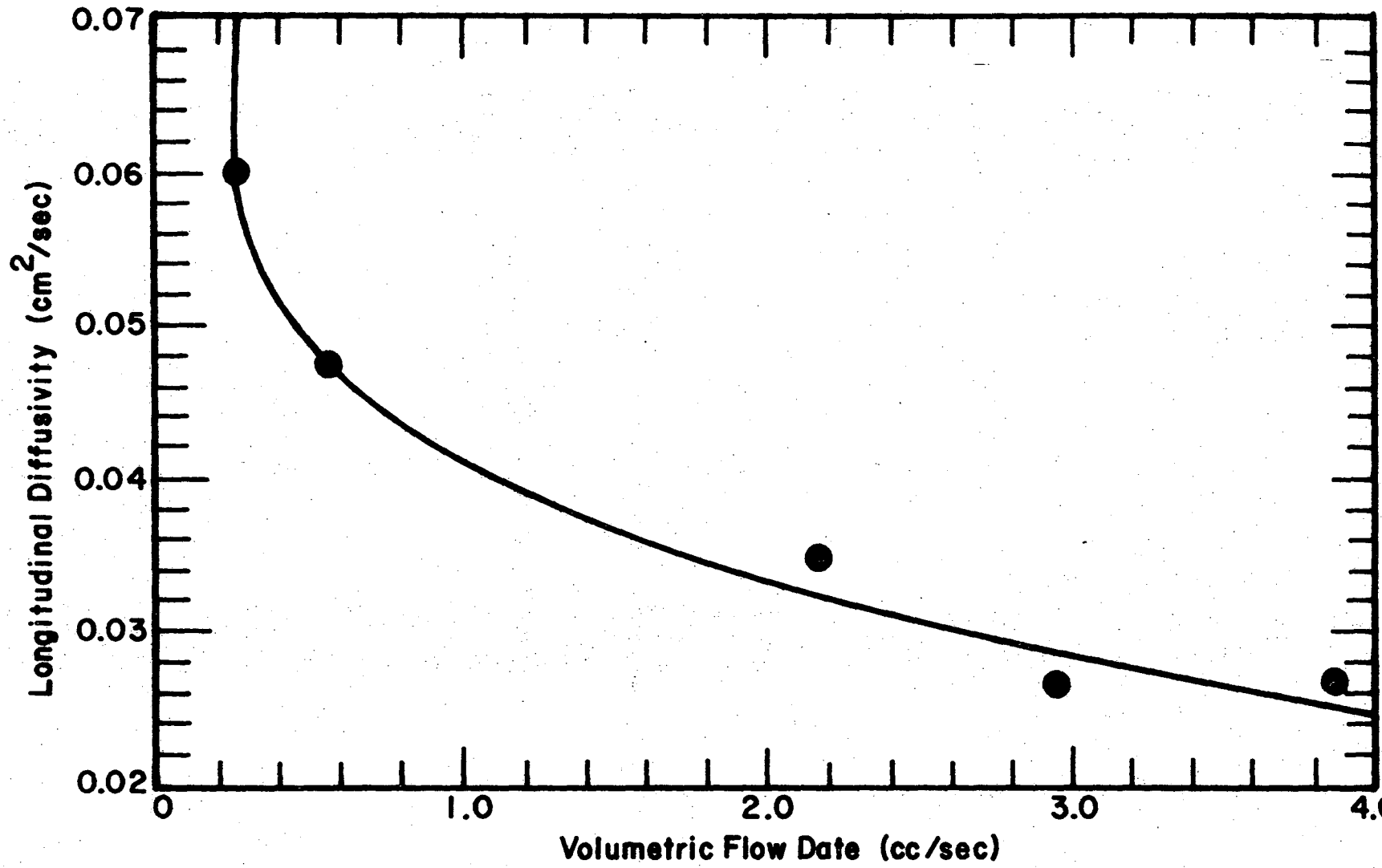
0.07
0.06
0.05
0.04
0.03
0.02
Longitudinal Diffusivity (cm²/sec)
0
1.0
2.0
3.0
4.0
Volumetric Flow Date (cc/sec)

Table 5-4

Hot-Phase, Variable-Feed Operation: Feed Flow Rate Versus Diffusivity

Volume Flow Rate (cc/sec)	Fluid Velocity (cm/sec)	Diffusion Coefficient (cm^2/sec)
0.265	0.0510	0.06012
0.573	0.1100	0.04765
2.167	0.4170	0.03495
2.950	0.5670	0.02662
3.866	0.7440	0.02708

Figure 5-10

Peclet Number Versus Reynolds Number (63)

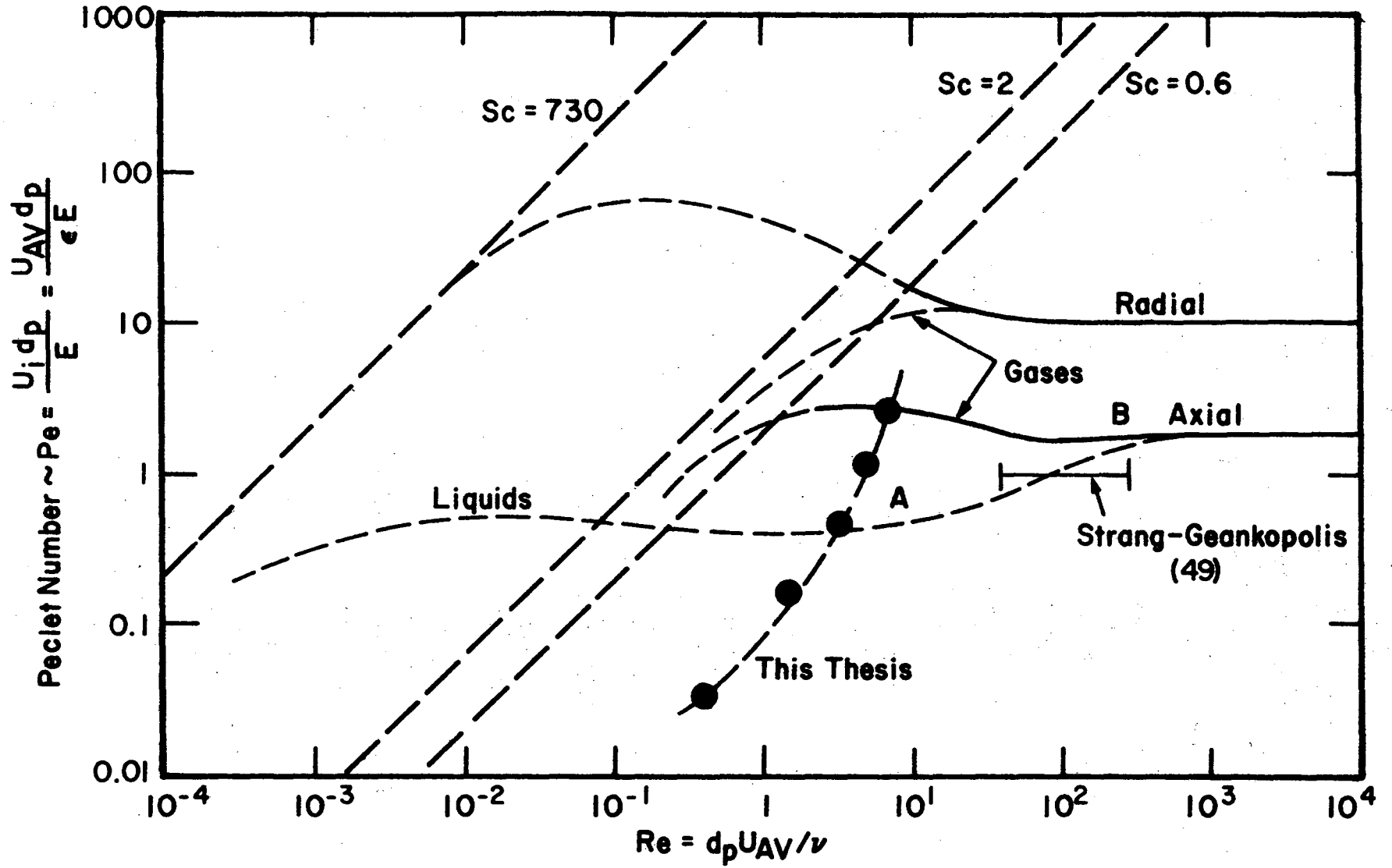
Peclet Number ~ Pe = $\frac{U_i d_p}{E} = \frac{U_{AV} d_p}{\epsilon E}$
1000
100
10
1
0.1
0.01
10^{-4}
10^{-3}
10^{-2}
10^{-1}
1
10^{1}
10^{2}
10^{3}
10^{4}
Re = $d_p U_{AV}/\nu$
Sc = 730
Sc = 2
Sc = 0.6
Radial
Gases
B
Axial
Liquids
A
Strang-Geankopolis
(49)
This Thesis

Peclet Number varies approximately between 0.03 and 7.0 as the Reynolds Number varies between 0.5 and 7.0. Although the diffusion coefficient decreases with an increase in the Reynolds Number, the interstitial velocity increases enough to cause an increase in the Peclet Number with an increase in the Reynolds Number. Such a phenomenon has been observed by various investigators (12,18,19). These authors base their explanation upon a cell model for dispersion in packed beds. Consider the void space between solid packings as a cell. For a Reynolds Number of approximately 0.1 or less, molecular diffusion may account for mixing within each cell, and from cell to cell. However, as the Reynolds Number increases, convective transport dominates and mixing between successive cells becomes incomplete. In this case, multiple streamers of fluid tend to pass through the column, resulting in very little backmixing owing to molecular diffusion. Consequently, the step change in concentration tends to maintain itself as the Reynolds Number is increased. The transition from a regime of molecular diffusion to one of convective transport apparently accounts for the increase in the Peclet Number and decrease in the diffusion coefficient as the Reynolds Number increases.

From the above discussion, it is now possible to determine the column flow rate for a given feed amplitude such that a variable-feed zone may function with product

recycle streams used to maintain the step changes in feed composition. From the breakthrough data in Figure 5-8, it is possible to plot the duration of high-product flow and the duration of the simple-wave flow (the breakthrough period) versus the volumetric flow rate. Figure 5-11 is such a plot for a feed amplitude of 20.9 vol % toluene. By extrapolation of the data, it is found that a flow rate of approximately 7.0 cc/sec is required to maintain the step change in feed by product recycle. The temperature switching time is found by adding the two times shown in Figure 5-11.

Effect of Average Feed Concentration Upon Breakthrough Time During Hot-Phase Operation

A last point of consideration needs to be investigated: Consider the case of a constant feed amplitude in a variable-feed operation; however, let the average feed concentration be either some high value or some relatively low value. For instance, let there be a feed amplitude of 6.0 vol % toluene, but in one case let the average feed concentration be 80 vol % (high feed = 83%, low feed = 77%), and in the other case 20 vol % (high feed = 23.0%, low feed = 17%). The question to be answered is: what will be the difference in the low-feed breakthrough time (hot-phase operation) for both cases? It is expected that the case with the higher average feed concentration (80%) will have a much more rapid breakthrough to its low feed (77%)

Figure 5-11

Effect of Flow Rate Upon High Product and Simple Wave Flow Duration

This figure is the result of experiments where a high-concentration product of 52.4 vol % toluene is displaced at various flow rates of 31.5 vol % toluene feed. The duration of high-concentration product flow and the duration of flow of the simple wave--the time required to change the effluent concentration from 52.4 vol % to 31.5 vol %--is plotted versus the volumetric flow rate of the feed.

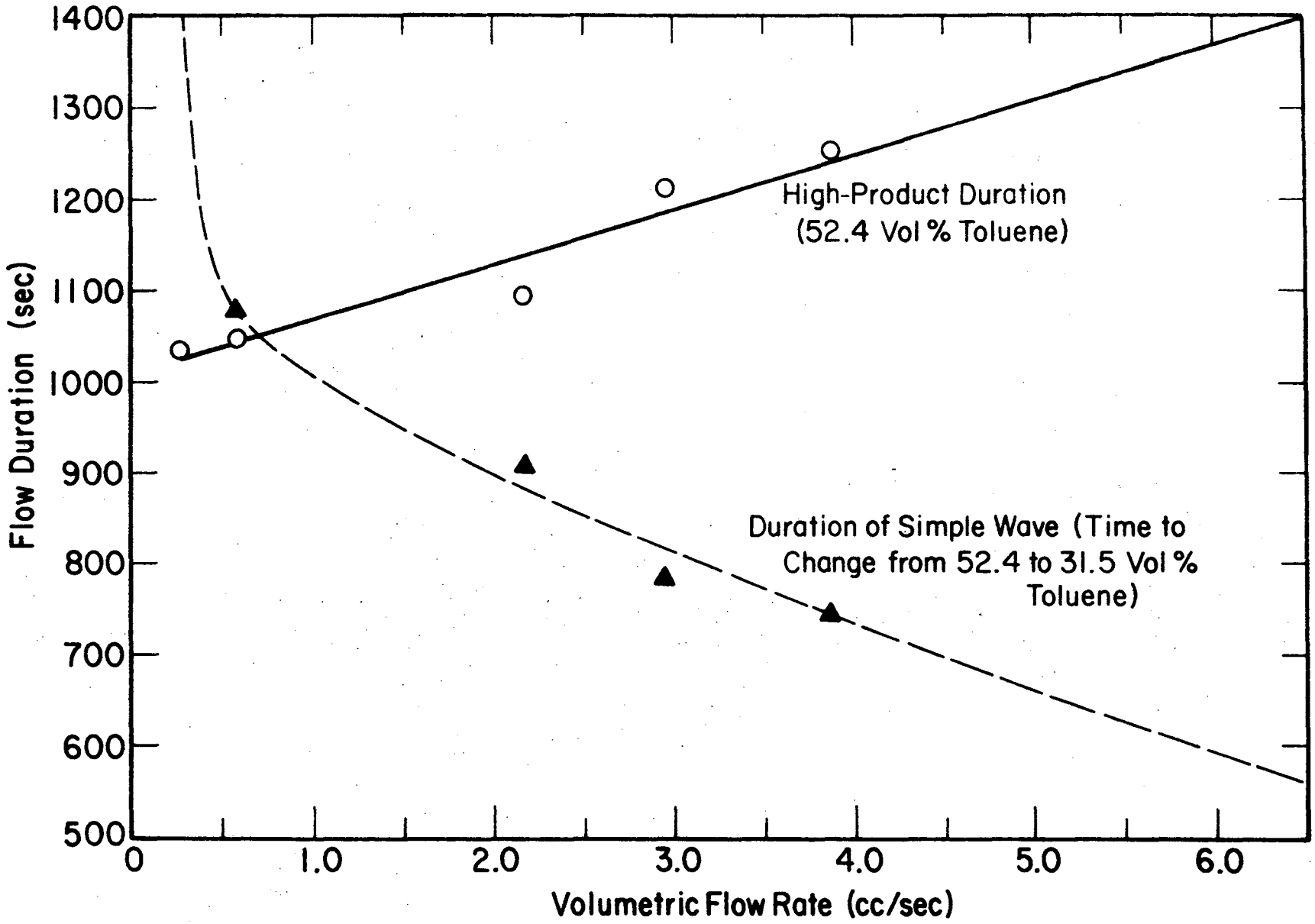
1400
1300
1200
1100
1000
900
800
700
600
500
Flow Duration (sec)
0
1.0
2.0
3.0
4.0
5.0
6.0
Volumetric Flow Rate (cc/sec)
High-Product Duration
(52.4 Vol % Toluene)
Duration of Simple Wave (Time to
Change from 52.4 to 31.5 Vol %
Toluene)

than the case with the lower average feed (20%). Although the feed amplitude is the same in both cases, there is a large difference in concentration wave velocities. It is then necessary to run experiments at constant feed amplitude, but with varying average feed concentration. Figure 5-13 is such a plot for feed amplitudes of 6.0 vol % and 12.0 vol %. Note that the slope for 12.0 vol % is less than that for 6.0 vol %. This is because of the increased spreading of the breakthrough as the feed amplitude increases, as previously discussed in this chapter. As the feed amplitude goes to zero, the curves of Figure 5-12 then approach the curve plotted in Figure 4-4. A complete plot of the form in Figure 5-12 would then allow the calculation of the optimum lengths of columns in a cascade whose zones experience the same feed amplitude, but different average feed compositions.

Derivation of Breakthrough Curve for a Fixed Bed With Longitudinal Diffusion and Local Mass Transfer Equilibrium

The following differential equation may be written to describe adsorption with longitudinal diffusion:

$$\frac{\partial X_L}{\partial t} + A\,\frac{\partial X_s}{\partial t} + V\,\frac{\partial X_L}{\partial z} = \mathcal{D}\,\frac{\partial^2 X_L}{\partial z^2} \qquad (5\text{-}1)$$

The following boundary conditions apply for a column of infinite length, experiencing a step change in feed concentration at the entrance to the column:

Figure 5-12

Variable-Feed Operation: Effect of Average Feed Concentration Upon Feed Concentration Breakthrough Time

This figure summarizes experiments where high-concentration product is displaced by low-concentration feed of a zone operating under a variable-feed input. The average feed concentration is the average of the two feeds, high and low, used to displace the high-concentration product. The breakthrough time is the time required for the low-concentration feed to appear in the effluent stream. The experiments were run with a feed amplitude of 6.0 vol % toluene and 12.0 vol % toluene. The column temperature was 59°C and the interstitial fluid velocity was 0.0466 cm/sec.

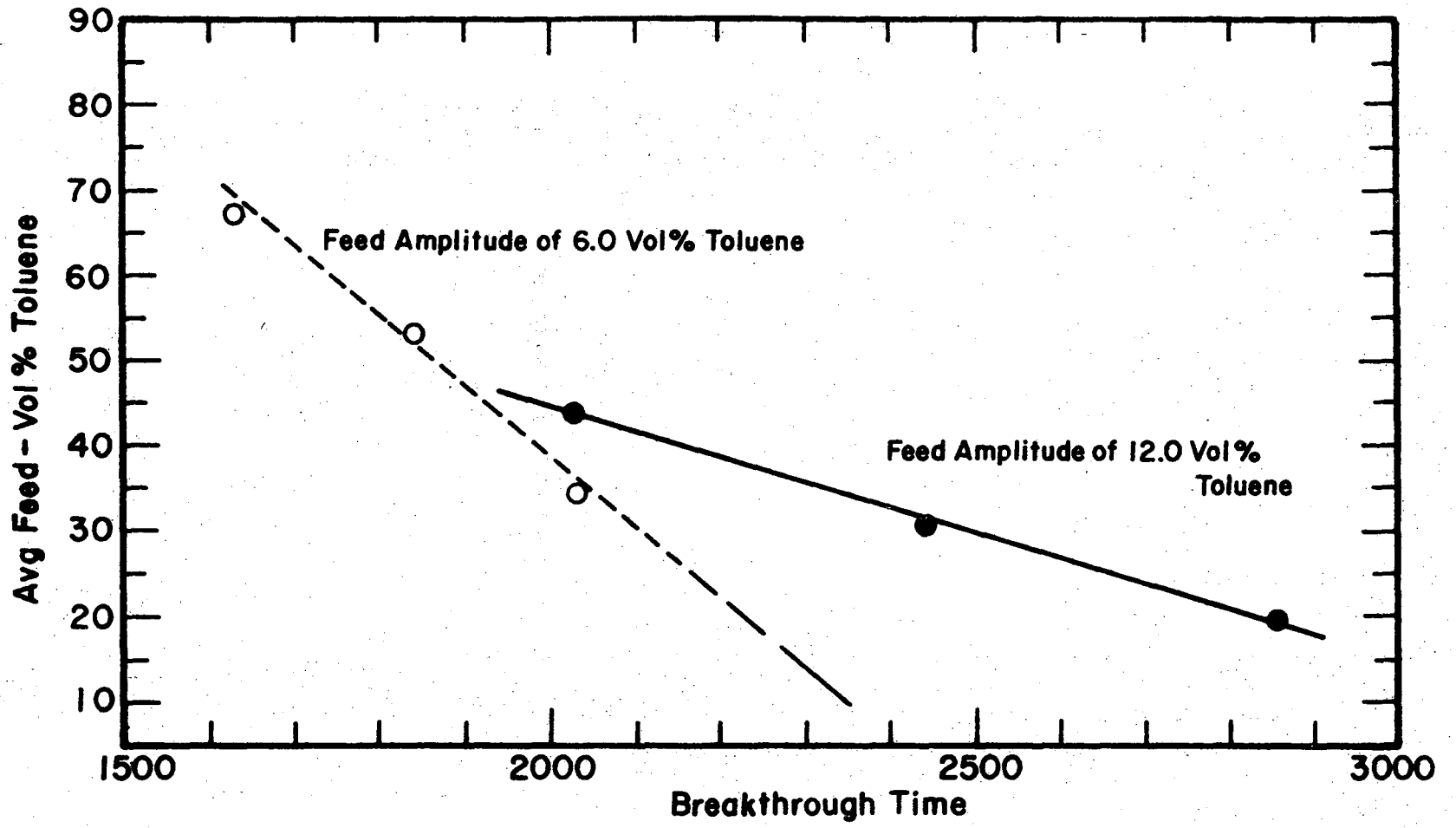
Avg Feed - Vol % Toluene
90
80
70
60
50
40
30
20
10
1500
2000
2500
3000
Breakthrough Time
Feed Amplitude of 6.0 Vol% Toluene
Feed Amplitude of 12.0 Vol% Toluene

(1) $X_L(-\infty,t) = \Delta X_L$

(2) $X_L(+\infty,t) = 0$

(3) $X_L(z,0) = 0$

The boundary conditions are written such that the influence of the bed entrance and exit are disregarded. Although an approximation, it should be more accurate the longer the bed in relation to its width, thus minimizing the effect of transitions at the entrance and exit of the column.

Using the local equilibrium assumption,

$$\frac{\partial X_s}{\partial t} = \left(\frac{\partial X_s}{\partial X_L}\right)\left(\frac{\partial X_L}{\partial t}\right)$$

which may be evaluated at the desired temperature using the isotherm relationship in Chapter 2. Let the following substitutions be made:

$$m = A(\partial X_s/\partial X_L)_{T_{avg}}$$

$$V_c = V/(1+m) = \text{velocity of concentration wave}$$

$$\mathfrak{D}_c = \mathfrak{D}/(1+m)$$

Substitution into Eq. (5-1) gives the following equation with the same boundary conditions:

$$\frac{\partial X_L}{\partial t} + V_c \frac{\partial X_L}{\partial z} = \mathfrak{D}_c \frac{\partial^2 X_s}{\partial z^2} \qquad (5\text{-}2)$$

The independent variables z and t are now changed as follows:

$$\xi = \frac{z - V_c t}{2\sqrt{\mathcal{D}_c t}}$$

$$\theta = t$$

Substitution of the new variables into Eq. (5-2) and multiplying both sides by 4θ gives:

$$-2\xi\left(\frac{\partial X_L}{\partial \xi}\right) + 4\theta\left(\frac{\partial X_L}{\partial \theta}\right) = \left(\frac{\partial^2 X_L}{\partial \xi^2}\right) \tag{5-3}$$

The new boundary conditions become

(1) $X_L(-\infty,\theta) = \Delta X_L$

(2) $X_L(+\infty,\theta) = 0$

(3) $X_L(\xi,0) = 0$

A solution as a function of ξ only then obeys the following equation:

$$\frac{d^2 X_L}{d\xi^2} + 2\xi\,\frac{dX_L}{d\xi} = 0 \tag{5-4}$$

with $X_L(-\infty) = X_L$ and $X_L(+\infty) = 0$. Let $U = dX_L/dz$, then $d^2X_L/dz^2 = dU/d\xi$, and Eq. (5-4) becomes

$$dU/d\xi = -2\xi U \tag{5-5}$$

The solution to Eq. (5-5) is

$$X_L = \left(\frac{\Delta X_L}{2}\right)[1 + \mathrm{erf}(-\xi)] \tag{5-6}$$

Equation (5-6) is a mathematical representation of the breakthrough curve obeying the boundary conditions given.

The diffusion coefficient may now be calculated by application to the breakthrough data given in Figures 5-3 and 5-5.

All breakthrough data may be replotted on the dimensionless concentration scale versus time as indicated in Figure 5-13. The value of $t_{1/2}$ is determined as shown in Figure 5-13. Now assume that the wave emerging from the exit of the column is not altered on its leading edge ($t < t_{1/2}$) by flow into additional packing which might be added to the column. Also assume that the wave that has not yet emerged by $t = t_{1/2}$ is the same as that observed for $t > t_{1/2}$. This is also shown in Figure 5-13. On this basis it is now possible to determine the mean-square displacement of a tracer in the leading and trailing edges of the concentration wave. For the leading edge mean-square displacement ($t < t_{1/2}$);

$$\langle d_+^2 \rangle = V_c^2 \frac{\int_0^{-\infty} (t_{1/2}-t)^2 (c)dt}{\int_0^{-\infty} (c)dt} \qquad (5\text{-}7)$$

where $c = \left(\frac{X_{High}-X_L}{\Delta X_L}\right)$ for hot-phase operation, and

$c = \left(\frac{X_L-X_{Low}}{\Delta X_L}\right)$ for cold-phase operation.

The right side of equation may be evaluated graphically from the experimental breakthrough data. The analytic evaluation of Eq. (5-7) reveals that

Figure 5-13

Qualitative Description of Transformation of Experimental Breakthrough Data to Allow Calculation of Diffusion Coefficients

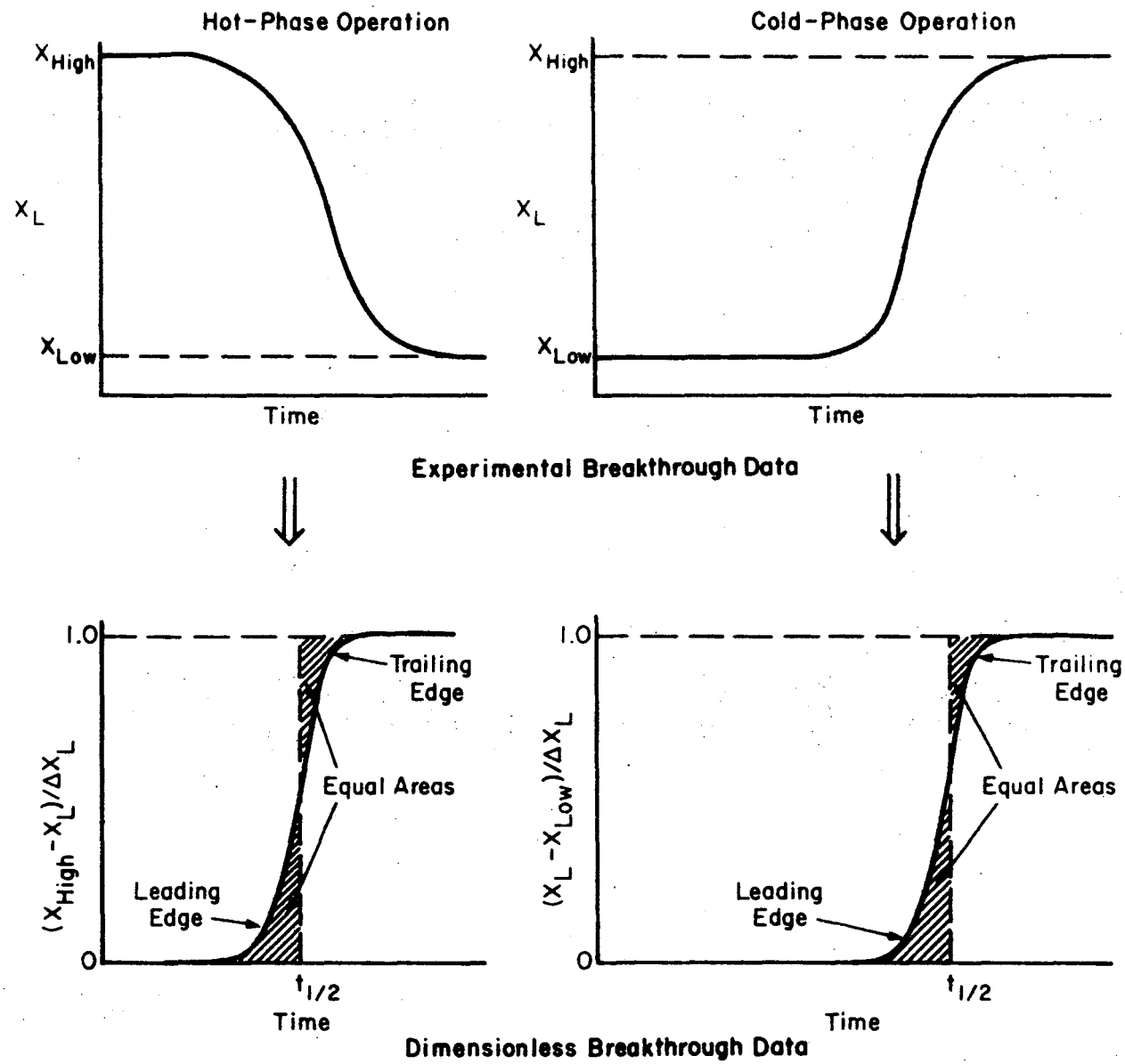
Hot-Phase Operation
Cold-Phase Operation
X_{High}
X_L
X_{Low}
Time
Experimental Breakthrough Data
1.0
0
$(X_{High}-X_L)/\Delta X_L$
$(X_L-X_{Low})/\Delta X_L$
Trailing Edge
Equal Areas
Leading Edge
$t_{1/2}$
Dimensionless Breakthrough Data

$$\langle d_+^2 \rangle = \left(\frac{4}{3}\right)\frac{\mathcal{D}_+ t_{1/2}}{1+m} \quad \text{or,} \quad \mathcal{D}_+ = \frac{0.75(1+m)\langle d_+^2 \rangle}{t_{1/2}} \tag{5-8}$$

For the trailing edge mean-square displacement ($t > t_{1/2}$):

$$\langle d_-^2 \rangle = V_c^2 \frac{\int_\infty^0 (t-t_{1/2})^2 [1-(c)]dt}{\int_\infty^0 [1-(c)]dt} \tag{5-9}$$

where c is defined as above.

The right side of Eq. (5-9) may be evaluated graphically from the experimental breakthrough data. The analytic evaluation of Eq. (5-9) reveals that

$$\mathcal{D}_- = \frac{0.75(1+m)\langle d_-^2 \rangle}{t_{1/2}} \tag{5-10}$$

The concentration wave velocity used in Eqs. (5-7) and (5-9) is determined at the mean value of the initial step change in concentration introduced into the entrance of the column. The final value of the diffusion coefficient is determined by the average value of the leading and trailing edge coefficients given by Eqs. (5-8) and (5-10).

CHAPTER 6

MATHEMATICAL STATEMENT OF CYCLING ZONE ADSORPTION ALLOWING FOR LONGITUDINAL DIFFUSION

Continuous-Flow, Constant-Feed Concentration, Single-Zone Operation (Analytic Solution)... 171

Continuous-Flow, Constant-Feed Concentration, Single-Zone Operation (Analytic Solution, Zero Diffusion)..... 179

Continuous-Flow, Constant-Feed Concentration, Single-Zone Operation (Analytic Solution, Infinite Diffusion)..... 180

Continuous-Flow, Variable-Feed Input, Single-Zone Operation (Analytic Solution)... 188

Computer Programs for Effluent Concentration Profiles..... 200

0 0 0 0 3 8 0 7 0 4 9

CHAPTER 6

MATHEMATICAL STATEMENT OF CYCLING ZONE ADSORPTION ALLOWING FOR LONGITUDINAL DIFFUSION

From the previous discussions, it is seen that diffusion plays an important role in altering the square-wave concentration response predicted by the simplified mathematical analysis of Chapter 3. It would then be of interest to develop an equation that would account for any diffusional affects occurring in cycling zone adsorption, and that would give the final effluent liquid concentration profile. Whereas in Chapter 3, the first-order equations and method of characteristics applied to the nonlinear equation and the results were valid for any concentration amplitude if diffusion was zero; however, the mathematical analysis of Chapter 6 presents a solution of the linearized problem. The results will be valid for only sufficiently small values of the concentration changes. However, improvement over Chapter 3 is gained by allowing for longitudinal diffusion.

Continuous-Flow, Constant Feed Concentration, Single-Zone Operation (Analytic Solution)

Consider a single zone, operating with a constant, continuous feed and experiencing a square-wave temperature change. The following differential equation may be written:

$$\alpha \frac{\partial X_L}{\partial t} + (1-\alpha)\epsilon \frac{\partial X_s}{\partial t} + \alpha V \frac{\partial X_L}{\partial z} = \alpha \mathfrak{D} \frac{\partial^2 X_L}{\partial z^2} \qquad (6\text{-}1)$$

with boundary conditions:

1. $X_{LF} = X_L(0,t) - \frac{\mathfrak{D}}{V} \frac{\partial X_L}{\partial t}(0,t)$

2. $0 = \frac{\partial X_L}{\partial z}(Z,t)$

3. $X_{LF} = X_L(z,0)$

At equilibrium between the two phases,

$X_s = F(X_L,T)$ (the equilibrium isotherm equation)

Differentiation gives:

$$\frac{\partial X_s}{\partial t} = \underbrace{\left.\frac{\partial X_s}{\partial X_L}\right)_T}_{= m\frac{\alpha}{(1-\alpha)\epsilon}} \frac{\partial X_L}{\partial t} + \underbrace{\left.\frac{\partial X_s}{\partial T}\right)_{X_L}}_{= m_T \frac{\alpha}{(1-\alpha)\epsilon}} \frac{\partial T}{\partial t} \qquad (6\text{-}2)$$

here m and m_T are evaluated at average temperature and the liquid feed concentration, respectively. Let $V_c = V/(1+m)$ and $\mathfrak{D}_c = \mathfrak{D}/(1+m)$. Equation (6-1) can then be rearranged into the following form:

$$\frac{\partial X_L}{\partial t} + V_c \frac{\partial X_L}{\partial z} - \mathfrak{D}_c \frac{\partial^2 X_L}{\partial z^2} = - \frac{m_T}{1+m} \frac{\partial T}{\partial t} \qquad (6\text{-}3)$$

The boundary conditions remain the same as above.

A Fourier series may be used to describe the square wave variation of the temperature of the zone. The partial derivative on the right-hand side of Eq. (6-3) may then be expressed as follows:

$$T(t) = T_o + \frac{\Delta T}{\pi} \sum_{n=1}^{\infty} \frac{1-(-1)^n}{n} \sin(n\pi \frac{t}{\Delta t}) \qquad (6\text{-}3a)$$

$$\frac{\partial T}{\partial t} = \frac{\Delta T}{\Delta t} \sum_{n=1}^{\infty} [1-(-1)^n] \cos(n\pi \frac{t}{\Delta t}) \qquad (6\text{-}3b)$$

where ΔT and Δt are the amplitude of the step change in temperature and the time duration of half the square wave, i.e., the temperature switching time. Substitution into Eq. (6-3) gives the final form of the equation to be solved:

$$\frac{\partial X_L}{\partial t} + V_c \frac{\partial X_L}{\partial z} - \mathcal{D}_c \frac{\partial^2 X_L}{\partial z^2}$$

$$= - \frac{m_T \Delta T}{(1+m)\Delta t} \sum_{n=1}^{\infty} [1-(-1)^n] \cos(n\pi \frac{t}{\Delta t}) \qquad (6\text{-}3c)$$

Now introduce the LaPlace transform:

$$\overline{X}_L(z,p) = \mathscr{L}\{X_L(z,t)\} = p \int_0^{\infty} e^{-pt} X_L(z,t)dt$$

Equation (6-3c) now takes the following form:

$$p(\overline{X}_L - X_{LF}) + V_c \frac{d\overline{X}_L}{dz} - \mathcal{D}_c \frac{d^2\overline{X}_L}{dz^2}$$

$$= - \left(\frac{m_T}{1+m}\right)\left(\frac{\Delta T}{\Delta t}\right) \sum_{n=1}^{\infty} \frac{[1-(-1)^n]p^2}{\left(\frac{n\pi}{\Delta t}\right)^2 + p^2} \qquad (6\text{-}4)$$

The boundary conditions are:

$$(1) \quad X_{LF} = \overline{X}_L(0) - \frac{\mathfrak{D}_c}{V_c}\frac{d\overline{X}_L}{dz}(0)$$

$$(2) \quad 0 = \frac{d\overline{X}_L(Z)}{dz}$$

Equation (6-4) is a second-order differential equation with a particular solution and a complementary solution. The particular solution takes is:

$$\overline{X}_L = X_{LF} - \frac{m_T}{(1+m)}\frac{\Delta T}{\pi}\sum_{n=1}^{\infty}\left\{\frac{[1-(-1)^n]}{n}\right\}\frac{(n\pi/\Delta t)p}{(n\pi/\Delta t)^2+p^2} \tag{6-5a}$$

The inverse of the transform gives the final form of the particular solution:

$$X_L = X_{LF} - \left(\frac{m_T}{1+m}\right)\left(\frac{\Delta T}{\pi}\right)\sum_{n=1}^{\infty}\frac{[1-(-1)^n]}{n}\sin\left(n\pi\frac{t}{\Delta t}\right)$$

$$= X_{LF} - \frac{m_T}{1+m}\Delta T \text{ (unit square wave)}$$

The complementary solution is found by setting the right side of Eq. (6-4) equal to zero. Its solution may be expressed as:

$$\overline{X}_L = e^{V_c z/2\mathfrak{D}_c}\left\{A\sinh\left[\sqrt{1+4\frac{\mathfrak{D}_c p}{V_c^2}}\left(\frac{V_c z}{2\mathfrak{D}_c}\right)\right] + B\cosh\left[\sqrt{1+4\frac{\mathfrak{D}_c p}{V_c^2}}\left(\frac{V_c p}{2\mathfrak{D}_c}\right)\right]\right\} \tag{6-5b}$$

The constants A and B may be evaluated from the two boundary conditions:

$$A_n = -\left(\frac{m_T \Delta T}{1+m}\right)\left[\frac{\sqrt{1+4\frac{\mathcal{D}_c p}{V_c^2}}\ \sinh+\cosh}{\left(1+2\frac{\mathcal{D}_c p}{V_c^2}\right)\sinh+\sqrt{1+4\frac{\mathcal{D}_c p}{V_c^2}}\ \cosh}\right]\left[\frac{\left(\frac{n\pi}{\Delta t}\right) p}{\left(\frac{n\pi}{\Delta t}\right)^2+p^2}\right]\frac{[1-(-1)^n]}{n\pi}$$

$$B_n = +\left(\frac{m_T \Delta T}{1+m}\right)\left[\frac{\sinh+\sqrt{1+4\frac{\mathcal{D}_c p}{V_c^2}}\ \cosh}{\left(1+2\frac{\mathcal{D}_c p}{V_c^2}\right)\sinh+\sqrt{1+4\frac{\mathcal{D}_c p}{V_c^2}}\ \cosh}\right]\left[\frac{\left(\frac{n\pi}{\Delta t}\right) p}{\left(\frac{n\pi}{\Delta t}\right)^2+p^2}\right]\frac{[1-(-1)^n]}{n\pi}$$

where

$$\sinh = \sinh\left[\sqrt{1+4\frac{\mathcal{D}_c p}{V_c^2}}\left(\frac{V_c Z}{2\mathcal{D}_c}\right)\right]$$

$$\cosh = \cosh\left[\sqrt{1+4\frac{\mathcal{D}_c p}{V_c^2}}\left(\frac{V_c Z}{2\mathcal{D}_c}\right)\right]$$

Since there is only interest in $\overline{X}_L(z,p)$ at $z = Z$, the arguments of the hyperbolic functions may be expressed as:

$$\sqrt{1+4\frac{\mathcal{D}_c p}{V_c^2}}\left(\frac{V_c Z}{2\mathcal{D}_c}\right) = \sqrt{1+4\frac{\mathcal{D}_c p}{V_c^2}}\ \zeta.$$

The final form of the transform is found by substitution of the constants A_n and B_n back into Eq. (6-5b) and combining Eqs. (6-5a) and (6-5b) evaluated at $z = Z$:

$$\overline{X}_L(Z,p) = X_{LF} - \left(\frac{m_T \Delta T}{1+m}\right)\left(\frac{1}{\pi}\right)\sum_{n=1}^{\infty}\frac{[1-(-1)^n]}{n}\frac{\left(\frac{n\pi}{\Delta t}\right)p}{\left(\frac{n\pi}{\Delta t}\right)^2+p^2}\left\{1 - e^{\zeta}\frac{\sqrt{1+4(\mathcal{D}_c p/V_c^2)}}{\left(1+2p\frac{\mathcal{D}_c}{V_c^2}\right)\sinh+\sqrt{1+4\frac{\mathcal{D}_c p}{V_c^2}}\cosh}\right\} \qquad (6\text{-}6)$$

Equation (6-6) must now be inverted to obtain the concentration profile at the exit of a single zone. The first term in the summation may simply be inverted to give a square-wave function of $(t/\Delta t)$:

$$\mathscr{L}^{-1} \sum_{n=1}^{\infty} \left\{ \frac{[1-(-1)^n]}{n} \frac{\left(\frac{n\pi}{\Delta t}\right)p}{\left(\frac{n\pi}{\Delta t}\right)^2 + p^2}(1) \right\} = \sum_{n=1}^{\infty} \frac{[1-(-1)^n]}{n} \sin\left(\frac{n\pi}{\Delta t}\, t\right) \tag{6-6a}$$

The second term is more difficult to invert. Let Eq. (6-6) be rewritten in the following form:

$$\overline{X}_L(Z,p) = X_{LF} - \left(\frac{m_T \Delta T}{1+m}\right)\left(\frac{1}{\pi}\right) \sum_{n=1}^{\infty} \frac{[1-(-1)^n]}{n} \frac{\left(\frac{n\pi}{\Delta t}\right)p}{\left(\frac{n\pi}{\Delta t}\right)^2 + p^2} \left\{ 1 - \frac{N(p)}{D(p)} \right\}$$

where

$$N(p) = \sqrt{1 + 4p(\mathfrak{D}_c/V_c^2)}\; e^{\zeta}$$

$$D(p) = \left[1 + 2p(\mathfrak{D}_c/V_c^2)\right]\sinh + \sqrt{1 + 4p(\mathfrak{D}_c/V_c^2)}\cosh$$

There are poles at $p = \pm i(n\pi/\Delta t)$ because of the function $(n\pi/\Delta t)^2 + p^2$. There is also the possibility of poles because of the function $D(p)$, however, these are all negative, leading to negative, real values of p. These correspond to the transient solution, which is not of interest. The poles at $p = \pm i(n\pi/\Delta t)$ are those of interest, resulting in the steady-state solution.

The second term in the summation of Eq. (6-6) may now be inverted by evaluation of the residues at the two pole values. Residue at $p = +i(n\pi/\Delta t)$:

$$= \lim_{p \to i\left(\frac{n\pi}{\Delta t}\right)} \left\{ \left[\frac{\left(\frac{n\pi}{\Delta t}\right) p}{\left(\frac{n\pi}{\Delta t}\right)^2 + p^2} \right] \left[\frac{N(p)}{D(p)p} \right] \left(p - i\frac{n\pi}{\Delta t}\right) \right\} e^{+i\left(\frac{n\pi}{\Delta t}\right)t}$$

$$= \frac{1}{2} \frac{N\left(+i\,\frac{n\pi}{\Delta t}\right)}{iD\left(+i\,\frac{n\pi}{\Delta t}\right)} \; e^{+i\left(\frac{n\pi}{\Delta t}\right)t}$$

Residue at $p = -i(n\pi/\Delta t)$:

$$= \lim_{p \to -i\left(\frac{n\pi}{\Delta t}\right)} \left\{ \left[\frac{\left(\frac{n\pi}{\Delta t}\right) p}{\left(\frac{n\pi}{\Delta t}\right)^2 + p^2} \right] \left[\frac{N(p)}{D(p)p} \right] \left(p + i\frac{n\pi}{\Delta t}\right) \right\} e^{-i\left(\frac{n\pi}{\Delta t}\right)t}$$

$$= -\frac{1}{2} \frac{N\left(-i\,\frac{n\pi}{\Delta t}\right)}{D\left(-i\frac{n\pi}{\Delta t}\right)} \; e^{-i\left(\frac{n\pi}{\Delta t}\right)t}$$

Therefore,

$$\mathscr{L}^{-1}\left[\frac{\left(\frac{n\pi}{\Delta t}\right) p}{\left(\frac{n\pi}{\Delta t}\right)^2 + p^2} \; \frac{N(p)}{D(p)} \right] = \text{sum of residues}$$

$$= \frac{1}{2}\left[\frac{N\left(+i\,\frac{n\pi}{\Delta t}\right)}{iD\left(+1\,\frac{n\pi}{\Delta t}\right)} \; e^{+i\left(\frac{n\pi}{\Delta t}\right)t} - \frac{N\left(-i\,\frac{n\pi}{\Delta t}\right)}{iD\left(-i\,\frac{n\pi}{\Delta t}\right)} \; e^{-i\left(\frac{n\pi}{\Delta t}\right)t} \right] \tag{6-6b}$$

All terms of Eq. (6-6) have now been inverted. However, it remains to determine how the function $N(p)/D(p)$ acts along the imaginary axis. Consider the function,

$$\sqrt{1 + 4p\,\frac{\mathcal{D}_c}{V_c^2}} = \sqrt{1 \pm 4i\,\frac{\mathcal{D}_c}{V_c^2}\,\frac{n\pi}{\Delta t}} = \sqrt{1 \pm 4\pi nqi} \tag{6-7}$$

where $q = \mathcal{D}_c/V_c^2\Delta t$

Let the square root in Eq. (6-7) be set equal to $\alpha \pm i\beta$, and now solve for α and β, considering only the real root:

$$\alpha = \sqrt{\frac{1 + \sqrt{1 + 16\pi^2 n^2 q^2}}{2}}$$

$$\beta = \frac{2\pi nq}{\alpha}$$

N(p) and D(p) may now be evaluated:

$$N(p) = \alpha \pm i\beta$$

$$D(p) = (1 \pm i2n\pi q)\sinh[(\alpha \pm i\beta)\zeta] + (\alpha \pm i\beta)\cosh[(\alpha \pm i\beta)\zeta]$$
$$= R \pm iS$$

where

$$R = \sinh\alpha\zeta \cos\beta\zeta - 2n\pi q \cosh\alpha\zeta \sin\beta\zeta + \alpha\cos\alpha\zeta \cos\beta\zeta - \beta\sinh\alpha\zeta \sin\beta\zeta$$

$$S = 2\pi nq \sinh\alpha\zeta \cos\beta\zeta + \cosh\alpha\zeta \sin\beta\zeta + \alpha\sinh\alpha\zeta \sin\beta\zeta + \beta\cosh\alpha\zeta \cos\beta\zeta$$

Eq. (6-6b) may now be evaluated as follows:

$$\mathscr{L}^{-1}\left[\frac{\left(\frac{n\pi}{\Delta t}\right)p}{\left(\frac{n\pi}{\Delta t}\right)^2 + p^2}\,\frac{N(p)}{D(p)}\right] = \frac{(\alpha+i\beta)}{2i(R+iS)}e^{i\left(\frac{n\pi}{\Delta t}\right)t} - \frac{(\alpha-i\beta)}{2i(R-iS)}e^{-i\left(\frac{n\pi}{\Delta t}\right)t}$$

$$= \frac{(\alpha+i\beta)(R-iS)}{2i(R^2+S^2)}e^{i\left(\frac{n\pi}{\Delta t}\right)t} - \frac{(\alpha-i\beta)(R+iS)}{2i(R^2+S^2)}e^{-i\left(\frac{n\pi}{\Delta t}\right)t} \qquad (6\text{-}8)$$

Through Eqs. (6-6a) and (6-6b), the inverse of Eq. (6-6) may finally be obtained:

$$\mathscr{L}^{-1}\{\text{Eq.}(6\text{-}6)\} = X_L(Z,t) = X_{LF} - \left(\frac{m_T\Delta T}{1+m}\right)\frac{1}{\pi}\sum_{n=1}^{\infty}\frac{[1-(-1)^n]}{n}\left[\sin\left(\frac{n\pi}{\Delta t}\right)t\right.$$

$$\left. - e^{\zeta}\,\frac{(\alpha+i\beta)(R-iS)}{2i(R^2+S^2)}e^{i\left(\frac{n\pi}{\Delta t}\right)t} + e^{\zeta}\,\frac{(\alpha-i\beta)(R+iS)}{2i(R^2+S^2)}e^{-i\left(\frac{n\pi}{\Delta t}\right)t}\right]$$

Rearrangement gives the final form of the equation for the effluent concentration profile for a single zone with constant, continuous feed, experiencing a square-wave temperature response:

$$X_L(Z,t) = X_{LF} - \left(\frac{m_T\Delta T}{1+m}\right)\left(\frac{1}{\pi}\right)\sum_{n=1}^{\infty}\frac{[1-(-1)^n]}{n}\left[\sin\left(\frac{n\pi}{\Delta t}\,t\right)\right.$$

$$\left. - e^{\zeta}\left(\frac{\alpha R+\beta S}{R^2+S^2}\right)\sin\left(\frac{n\pi}{\Delta t}\,t\right) + e^{\zeta}\left(\frac{\alpha S-\beta R}{R^2+S^2}\right)\cos\left(\frac{n\pi}{\Delta t}\,t\right)\right] \quad (6\text{-}9)$$

It is seen from Eq. (6-9) that the effluent concentration profile consists of two parts: (1) a standing wave given by the term $\{[1-(-1)^n]/n\}\sin(\frac{n\pi}{\Delta t}\,t)$ which is in equilibrium with the solid; and (2) a traveling wave which is shifted in phase and attenuated by diffusion. This is given by the last two terms in Eq. (6-9).

<u>Continuous Flow, Constant-Feed Concentration, Single-Zone Operation (Analytic Solution, Zero Diffusion)</u>

Equation (6-9) may be reduced to give the extreme case of a square-wave effluent concentration response by letting the diffusion coefficient be zero. In this case $q = 0$, $\beta = 0$, $\alpha = 1$, and $\zeta = \infty$. However, it is seen that

$(q\zeta) = (1+m)Z/(2V\Delta t)$, and $(\beta\zeta) = 2\pi nq\zeta/\alpha = n\pi(1+m)Z/(V\Delta t)$, which have finite values. From these values it can be shown that $R = e^{\alpha\zeta}\cos(\beta\zeta)$, $S = e^{\alpha\zeta}\sin(\beta\zeta)$, $R^2+S^2 = e^{2\alpha\zeta}$, $\alpha R+\beta S = e^{\alpha\zeta}\cos(\beta\zeta)$, and $\alpha S-\beta R = e^{\alpha\zeta}\sin(\beta\zeta)$. The final form of Eq. (6-9) for a zero diffusion coefficient is:

$$X_L(Z,t) = X_{LF}-\left(\frac{m_T\Delta T}{1+m}\right)\left(\frac{1}{\pi}\right)\sum_{n=1}^{\infty}\frac{[1-(-1)^n]}{n}\left[\sin\left(n\pi\frac{t}{\Delta t}\right)-\sin\left(n\pi\frac{t}{\Delta t}-\beta\zeta\right)\right] \tag{6-10}$$

This result shows that, in the absence of diffusion, the traveling concentration wave is not attenuated. For values of

$$\beta\zeta = n\pi(1+m)/V\Delta t = n\pi$$

the standing and traveling square waves will reinforce. Then the exit fluid amplitude will be $2m_T\Delta T/(1+m)$, as shown by Pigford, Baker, and Blum (36).

Continuous-Flow, Constant-Feed Concentration, Single-Zone Operation (Analytic Solution, Infinite Diffusion)

The opposite extreme case occurs then the diffusion coefficient becomes infinite. This case is analogous to a perfectly mixed tank with input of constant contration and output concentration varying with time. Consideration of a cycling zone adsorption column as a perfectly mixed zone is made in the following calculations to develop the effluent concentration profile for infinite diffusion, for

constant, continuous feed, and for a square-wave temperature response of the column. Material balance:

$$\alpha V[X_F - X_L(t)] = \frac{d}{dt}\left[Z\alpha X_L(t) + Z\frac{(1-\alpha)\epsilon}{\alpha}X_s(t)\right] \qquad (6\text{-}11)$$

Use of Eq. (6-2) and the isotherm equation results in the following form of Eq. (6-11):

$$\frac{V}{Z}[X_F - X_L(t)] = (1+m)\frac{dX_L(t)}{dt} + m_T\frac{dT}{dt} \qquad (6\text{-}12)$$

The temperature is again written as a Fourier series as indicated by Eq. (6-3a) and its time derivative by Eq. (6-3b). Substitution into Eq. (6-12) gives,

$$\frac{dX_L(t)}{dt} + \left[\frac{V}{Z(1+m)}\right]X_L(t) = \left[\frac{V}{Z(1+m)}\right]X_F - \left(\frac{m_T}{1+m}\right)\frac{\Delta T}{\Delta t}\sum_{n=1}^{\infty}[1-(-1)^n]\cos\left(n\pi\frac{t}{\Delta t}\right) \qquad (6\text{-}13)$$

Assume the following solution for Eq. (6-13):

$$X_L(t) = X_F + C\exp\{[-Vt/Z(1+m)]\} + Q(t)$$

where the exponential part of the solution represents the transient behavior, which is not of interest. The solution then takes the form

$$X_L(t) = X_F + Q(t) \qquad (6\text{-}14)$$

Let $Q_n(t) = A_n\sin(n\pi t/\Delta t) + B_n\cos(n\pi t/\Delta t)$. The coefficients A_n and B_n may be solved by substitution of Eq. (6-14), with

the assumed form of Q(t), back into Eq. (6-13). The following forms of A_n and B_n are then derived:

$$A_n = -\left(\frac{m_T \Delta T}{1+m}\right) n\pi \frac{\left[\frac{Z(1+m)}{V\Delta t}\right]^2}{n^2\pi^2\left[\frac{Z(1+m)}{V\Delta t}\right]^2 + 1} [1-(-1)^n] \qquad (6\text{-}15)$$

$$B_n = -\left(\frac{m_T \Delta T}{1+m}\right) \frac{\left[\frac{Z(1+m)}{V\Delta t}\right]}{n^2\pi^2\left[\frac{Z(1+m)}{V\Delta t}\right]^2 + 1} [1-(-1)^n] \qquad (6\text{-}16)$$

The coefficients of Eqs. (6-15) and (6-16) may now be substituted back into Eq. (6-14) to give the final form of the effluent concentration as a function of time:

$$X_L(t) = X_F - \frac{m_T \Delta T Z}{V\Delta t} \sum_{n=1}^{\infty} \frac{[1-(-1)^n]}{n^2\pi^2\left[\frac{Z(1+m)}{V\Delta t}\right]^2 + 1} \left[\frac{n\pi Z(1+m)}{V\Delta t} \sin\left(n\pi \frac{t}{\Delta t}\right) + \cos\left(n\pi \frac{t}{\Delta t}\right)\right] \qquad (6\text{-}17)$$

Through the use of Eqs. (6-9), (6-10), and (6-17), it is now possible to investigate the effect of longitudinal diffusion upon the effluent concentration profile for a single-zone operating with a continuous, constant-feed composition and experiencing a square-wave temperature change. Effluent concentration profiles given by these three equations were obtained by use of the College of Chemistry computer, an XDS 910. The following operating conditions were used in the calculations:

$V = 0.0466$ cm/sec

$\Delta t = 1160$ seconds

$\Delta T = 59°C$

$T_{avg} = 29.5°C$

$Z = 38$ cm

$m = 0.5098$ (m and m_T from the equilibrium isotherms at the average temperature and feed composition)

$m_T = -0.0006823/°C$

$X_F = 0.247$ volume fraction toluene

$d_p = 0.05$ cm (20-to 60-mesh particles)

The diffusion coefficients were determined from five selected values of the Peclet Number, $Vd_p/\mathcal{D}$:

N_{Pe}	D (cm^2/sec)
0.000	∞ (perfect mixing)
0.002	1.165
0.020	1.165×10^{-1}
0.200	1.165×10^{-2}
∞	0.000 (no diffusion)

Figure 6-1 compares Eq. (6-9) for the five Peclet Numbers with an experimentally obtained effluent concentration profile. The experimental concentration profile was obtained through the SGM of operation to insure a square-wave temperature response of the column. The figure reveals the attenuation effect and the peak phase-shift effect of the diffusion coefficient upon the concentration profile. For a Peclet Number of 0.002 ($\mathcal{D}$ = 1.165 cm^2/sec), the peak product concentrations are approximately 73% of the change predicted by the simplified mathematical analysis of Chapter 3. The simplified theory predicts a

Figure 6-1

Dimensionless Plot of Eq. (6-9) for Five Values of the Peclet Number

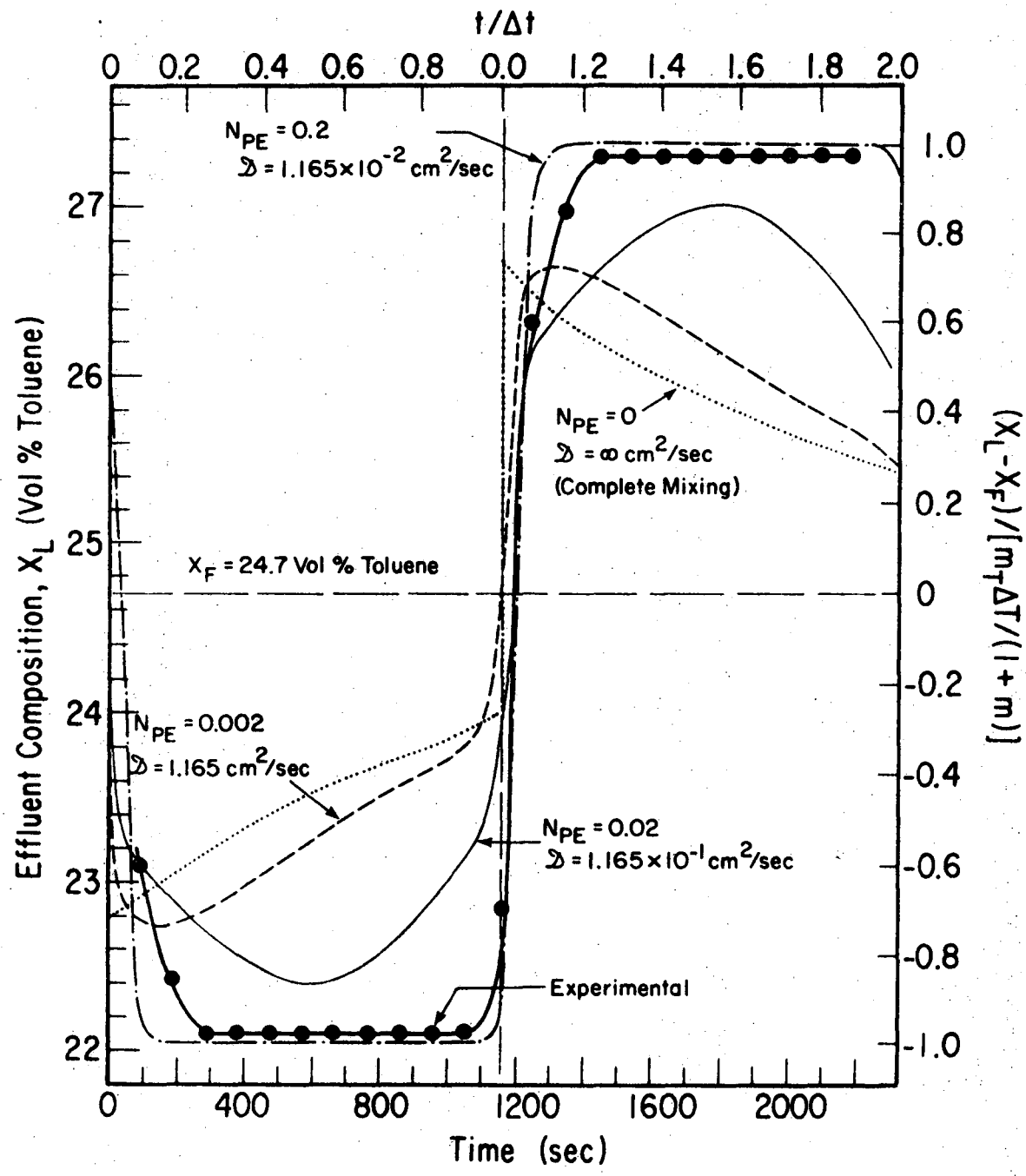
t/Δt
0
0.2
0.4
0.6
0.8
0.0
1.2
1.4
1.6
1.8
2.0
N_{PE} = 0.2
$\mathcal{D}$ = 1.165×10^{-2} cm^2/sec
N_{PE} = 0
$\mathcal{D}$ = ∞ cm^2/sec
(Complete Mixing)
X_F = 24.7 Vol % Toluene
N_{PE} = 0.002
$\mathcal{D}$ = 1.165 cm^2/sec
N_{PE} = 0.02
$\mathcal{D}$ = 1.165×10^{-1} cm^2/sec
Experimental
Effluent Composition, X_L (Vol % Toluene)
27
26
25
24
23
22
$(X_L - X_F)/[m_T \Delta T/(1+m)]$
1.0
0.8
0.6
0.4
0.2
0
-0.2
-0.4
-0.6
-0.8
-1.0
0
400
800
1200
1600
2000
Time (sec)

change of ±2.666 vol % from the feed composition following a temperature switch, whereas operation with a Peclet Number of 0.002 only gives a change of ±1.95 vol %. Peak product durations are approximately zero, occurring only as points during a full period of operation. For such large diffusivities longitudinal diffusion (driven by the concentration change due to the temperature switch) virtually destroys the large separations and large durations of peak product flows. Diffusion is so great that the initial step change in concentration is spread throughout the length of the column. Rapid diffusion results in the initial appearance of an attenuated product peak in the effluent stream, followed by a long steady approach of the effluent concentration to that of the initial feed concentration.

Consider the two following extreme cases of Peclet Number being zero ($\mathfrak{P}$ = infinity) and Peclet Number = infinite ($\mathfrak{P}$ = 0). Equation (6-10) may be used to develop the effluent concentration profile for the case of zero diffusion. The result is the expected square-wave effluent concentration profile. This compares with the result predicted by the simplified mathematical analysis if the simple wave and concentration shock-wave phenomena are excluded. Were a system found that had a diffusion coefficient that was approximately zero, the simplified mathematical analysis, using the method of characteristics, would be a more favorable tool than Eq. (6-10).

Equation (6-17) may be used to determine the effluent concentration profile for a Peclet Number = 0, the diffusion coefficient being infinite. The result is that expected for the effluent concentration profile of a perfectly mixed tank with constant composition feed input. The obvious difference is the step change in effluent concentration due to the step change in column temperature.

Figure 6-1 also contains an experimentally derived effluent concentration profile, obtained under the same operating conditions as those used for the analytic profiles of Fig. 6-1. A diffusion coefficient of about 10^{-2} cm^2/sec yield an analytic effluent concentration profile that can be superimposed upon the experimental profile.

It has been found experimentally that effluent concentration profiles are nearly linear over the range of experimental feed concentrations (10 vol % toluene to 80 vol % toluene). It is therefore possible to calculate a dimensionless analytic effluent concentration profile. Such a profile, through the use of experimentally derived breakthrough times, discussed in Chapter 4, can then be used to describe the effluent behavior of actual columns operating with a constant-feed concentration input and experiencing a square-wave temperature change. Besides allowing the investigation of diffusional effects, Eq. (6-9) may be used to design an appropriately staged cascade permitting large separations <u>via</u> cycling zone adsorption.

Continuous-Flow, Variable-Feed Input, Single-Zone Operation (Analytic Solution)

It is possible, through a change of boundary conditions, also to develop an analytic expression for the effluent concentration profile that accounts not only for a square-wave temperature response, but also for a square-wave feed input to the column. The new inlet boundary condition may be expressed as follows:

$$X_{LF} = X_{FAVG} + \left(\frac{\Delta F}{\pi}\right) \sum_{n=1}^{\infty} \frac{[1-(-1)^n]}{n} \sin\left(\frac{n\pi t}{\Delta t} - F\pi\right)$$

therefore,

$$X_{FAVG} + \left(\frac{\Delta F}{\pi}\right) \sum_{n=1}^{\infty} \frac{[1-(-1)^n]}{n} \sin\left(\frac{n\pi t}{\pi t} - F\pi\right)$$

$$= X_L(0,t) - \frac{\Phi_c}{V_c} \frac{\partial X_L}{\partial z} (0,t) \qquad (6\text{-}18)$$

where ΔF is the step change in feed concentration and $F\pi$ is a phase shift between the time at which the temperature step change occurs and the time at which the feed step change occurs.

Equation (6-4) must now be solved. This equation is altered in that X_{LF} is replaced by X_{FAVG}. The new boundary conditions, operated upon by the LaPlace transform, are as follows:

$$1.\quad \overline{X}_L(0,p) - \frac{\vartheta_c}{V_c}\frac{d\overline{X}_L}{dz}(0,p) = X_{FAVG}$$

$$+ \frac{\Delta F}{\pi}\sum_{n=1}^{\infty}\frac{[1-(-1)^n]}{n}\left\{\frac{\left(\frac{n\pi}{\Delta t}\right)p}{\left(\frac{n\pi}{\Delta t}\right)^2+p^2}\left[\cos F\pi - \frac{\Delta t}{n\pi}\,p\,\sin F\pi\right]\right\}$$

$$2.\quad 0 = \frac{d\overline{X}_L}{dz}(Z,p)$$

Equation (6-4) is now solved in the previous manner using the two above boundary conditions. The final form of the equation to be inverted is as follows:

$$\overline{X}_L(Z,p) = X_{FAVG} - \left(\frac{m_T}{1+m}\right)\left(\frac{\Delta T}{\pi}\right)\sum_{n=1}^{\infty}\frac{[1-(-1)^n]}{n}\,\frac{\left(\frac{n\pi}{\Delta t}\right)p}{\left(\frac{n\pi}{\Delta t}\right)^2+p^2}\left\{1\right.$$

$$\left. - \frac{e^{\zeta}\sqrt{1+4\vartheta_c/V_c^2}}{\left(1+2\frac{\vartheta_c p}{V_c^2}\right)\sinh+\sqrt{1+4\frac{\vartheta_c p}{V_c^2}}}\left[1+\left(\frac{1+m}{m_T}\right)\frac{\Delta F}{\Delta T}\left(\cos F\pi-\frac{\Delta t}{n\pi}p\sin F\pi\right)\right]\right\} \qquad (6\text{-}19)$$

Inversion of Eq. (6-19) follows the same procedure as for the inversion of Eq. (6-6). The final result is the same as Eq. (6-9), except for the addition of terms due to the introduction of the step change in feed concentration. The final result takes the following form:

$$X_L(Z,t) = X_{FAVG} - \left(\frac{m_T}{1+m}\right)\frac{\Delta T}{\pi}\sum_{n=1}^{\infty}\frac{[1-(-1)^n]}{n}\left\{\sin\left(\frac{n\pi}{\Delta t}t\right)\right.$$

$$- e^{\zeta}\left(\frac{\alpha R+\beta S}{R^2+S^2}\right)\sin\left(\frac{n\pi}{\Delta t}t\right) + e^{\zeta}\left(\frac{\alpha S-\beta R}{R^2+S^2}\right)\cos\left(\frac{n\pi}{\Delta t}t\right)$$

$$+ e^{\zeta}\left(\frac{1+m}{m_T}\right)\left(\frac{\Delta F}{\Delta T}\right)\left[\left(\frac{\alpha R+\beta S}{R^2+S^2}\right)\cos\left(\frac{n\pi}{\Delta t}t\right) + \left(\frac{\alpha S-\beta R}{R^2+S^2}\right)\sin\left(\frac{n\pi}{\Delta t}t\right)\right]\sin(F\pi)$$

$$\left. - e^{\zeta}\left(\frac{1+m}{m_T}\right)\left(\frac{\Delta F}{\Delta T}\right)\left[\left(\frac{\alpha R+\beta S}{R^2+S^2}\right)\sin\left(\frac{n\pi}{\Delta t}t\right) - \left(\frac{\alpha S-\beta R}{R^2+S^2}\right)\cos\left(\frac{n\pi}{\Delta t}t\right)\right]\cos(F\pi)\right\}$$

(6-20)

From Eq. (6-20), the effluent concentration profile due only to the step change in feed concentration may be developed. It takes the following form:

$$X_L(Z,t) = X_{FAVG} - e^{\zeta}\frac{\Delta F}{\pi}\sum_{n=1}^{\infty}\frac{[1-(-1)^n]}{n}\left\{\sin\left(\frac{n\pi}{\Delta t}t\right)\left[\left(\frac{\alpha S-\beta R}{R^2+S^2}\right)\sin(F\pi)\right.\right.$$

$$\left. - \left(\frac{\alpha R+\beta S}{R^2+S^2}\right)\cos(F\pi)\right] + \cos\left(\frac{n\pi}{\Delta t}t\right)\left[\left(\frac{\alpha R+\beta S}{R^2+S^2}\right)\sin(F\pi)\right.$$

$$\left.\left. + \left(\frac{\alpha S-\beta R}{R^2+S^2}\right)\cos(F\pi)\right]\right\} \qquad (6\text{-}21)$$

Equation (6-20) is therefore composed of a function, Eq. (6-9), that accounts for the effect of the square-wave temperature change of the zone, and a function, Eq. (6-21), that accounts for the effect of a square-wave feed input into the zone.

Equation (6-20) may be used to determine analytically the proper switching sequence of temperature and variable-feed input into a single zone of a cycling zone adsorber. Computer solutions are developed under the following conditions,

$$V = 0.466 \text{ cm}^2/\text{sec}$$

$$\Delta t = 1800 \text{ seconds}$$

$$\Delta T = 59°C$$

$$T_{avg} = 29.5°C$$

$$Z = 38 \text{ cm}$$

$$m = 0.81878$$

$$m_T = -0.00109865$$

$$X_{FAVG} = 0.130 \text{ volume fraction toluene}$$

$$\Delta F = 0.05 \text{ volume fraction toluene}$$

$$d_p = 0.05 \text{ cm (20- to 60-mesh size particles)}$$

$$\mathfrak{D}_c = 4.0 \times 10^{-2} \text{cm}^2/\text{sec (from Figure 5-8)}$$

Figure 6-2 is a plot of effluent concentration profiles, for a half-cycle, using Eq. (6-20), for variations of the phase shift factor $F\pi$ (F varies by 0.2 from 0.0 to 2.0). As expected, the analytic profiles of Figure 6-2 indicate that maximum separation occurs when F = 1.00. This physically means that when the temperature is switched to the high value, the feed into the column is switched to the low feed-concentration value. Low-concentration feed is therefore displacing high-concentration product. At a value of F = 0.00, a high temperature switch occurs when

Figure 6-2

Dimensionless Plot of Eq. (6-20) for Variations in the Phase Shift Factor F

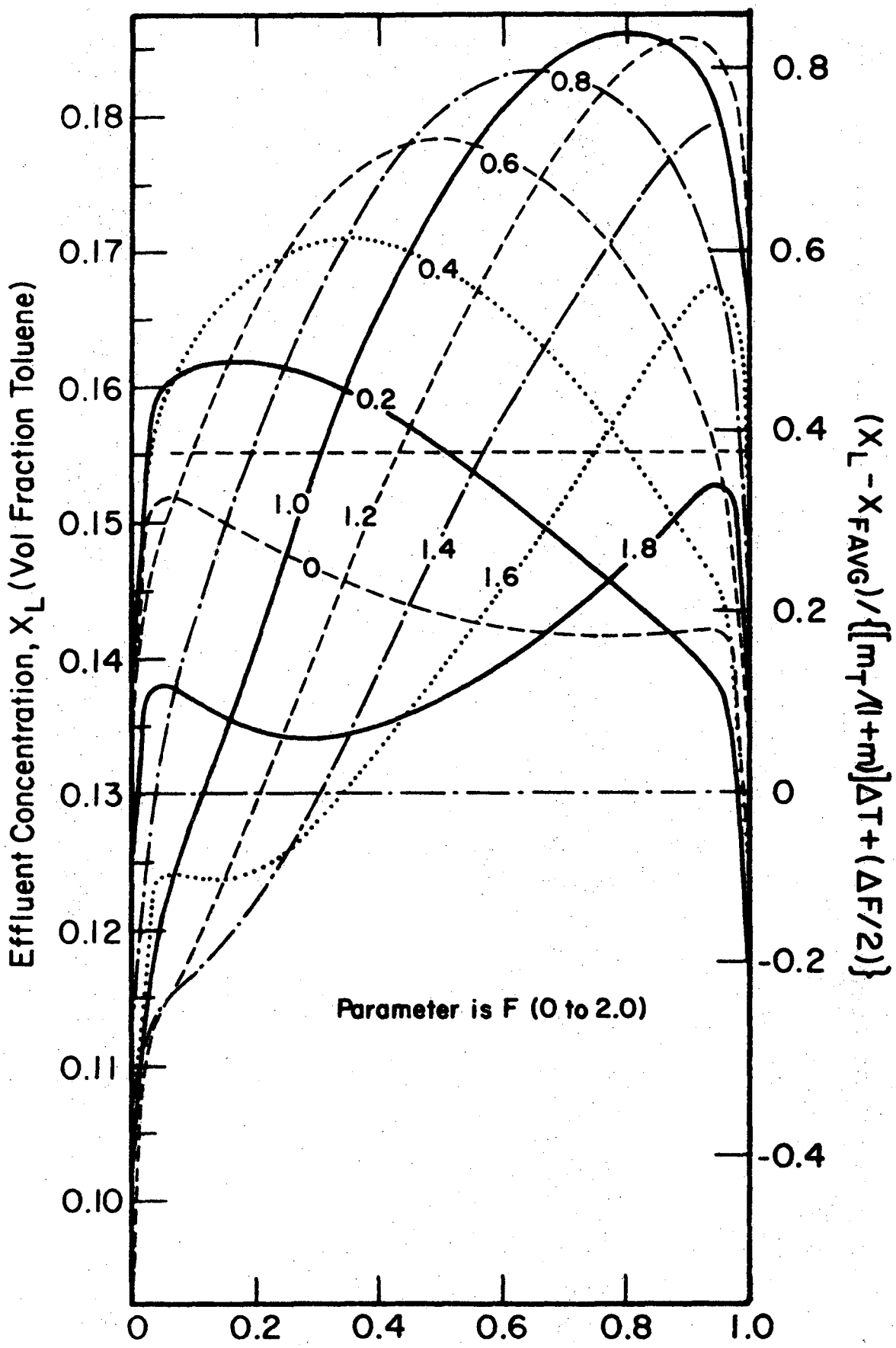
Effluent Concentration, X_L (Vol Fraction Toluene)
$(X_L - X_{FAVG})/\{[m_T/(1+m)]\Delta T + (\Delta F/2)\}$
Parameter is F (0 to 2.0)
0.18
0.17
0.16
0.15
0.14
0.13
0.12
0.11
0.10
0.8
0.6
0.4
0.2
0
-0.2
-0.4
0
0.2
0.4
0.6
0.8
1.0
0.8
0.6
0.4
0.2
1.0
1.2
1.4
1.6
1.8
0

the feed is switched to its high-concentration value; in this case high-concentration feed is displacing. Here the switches are 180° out of phase. In this case an enrichment of low-concentration feed column liquid is caused by the switch to the high temperature value. The result is a low peak value of the product. As the value of F increases to the optimum at 1.00, the peak values increase to the maximum given at F = 1.00. As F increases from 1.00 to 2.00 there is a decrease from the maximum back to the minimum given at F = 2.00 or 0.00. Because of the symmetry of the profiles, only the first half-cycle, from $t/\Delta t$ = 0.00 to 1.0, need be considered. This is apparent from Figure 6-1.

The analytic results of Eq. (6-20), Figure 6-2, may be more clearly elucidated by separately accounting for the contributions due to the step change in temperature and the step change in the feed-concentration input. Equation (6-9) may be used to develop the analytic effluent concentration profile caused by the square-wave temperature response of the column. This is plotted in Figure 6-3. Equation (6-21) may be used to develop the analytic effluent concentration profile caused by the square-wave feed concentration input to the zone. This is plotted in Figure 6-4 with the parameter F varying between 0.00 and 2.00. Combination of Figures 6-3 and 6-4 results in effluent concentration profiles given by Eq. (6-20), Figure 6-2. It is seen that from Figures 6-2 and 6-4, the maximum product concentration occurs at the value of F = 1.00. This again

Figure 6-3

Dimensionless Plot of Eq. (6-9): Temperature Switch Effect Upon Effluent Concentration Profile

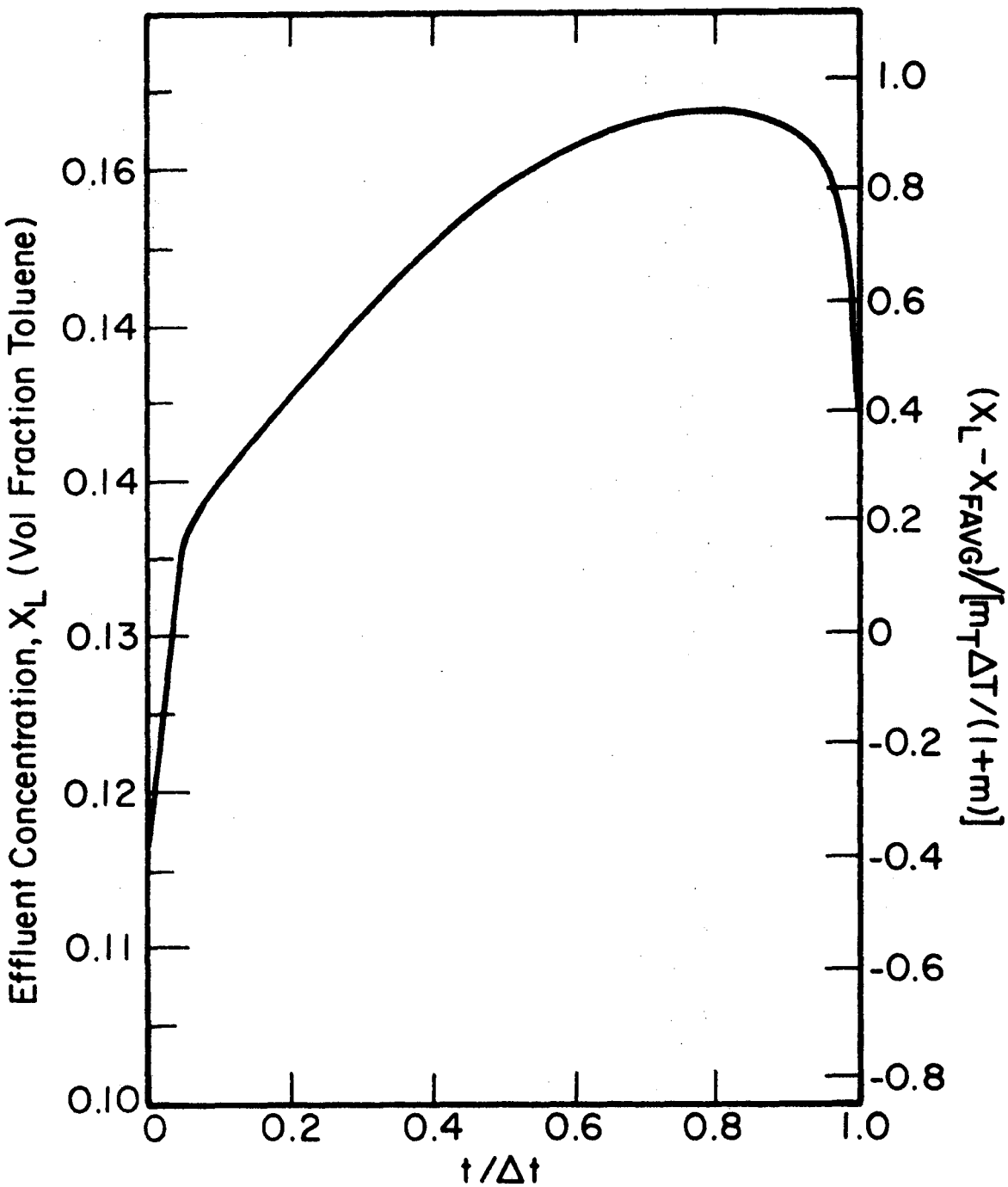
Effluent Concentration, X_L (Vol Fraction Toluene)
0.16
0.14
0.14
0.13
0.12
0.11
0.10
0
0.2
0.4
0.6
0.8
1.0
$t/\Delta t$
1.0
0.8
0.6
0.4
0.2
0
-0.2
-0.4
-0.6
-0.8
$(X_L - X_{FAVG})/[m_T \Delta T/(1+m)]$

0 0 0 0 3 8 0 . . . 3 2

Figure 6-4

Dimensionless Plot of Eq. (6-21): Effect of Feed Amplitude Upon Effluent Concentration Profile for Variation of Phase Shift Factor F

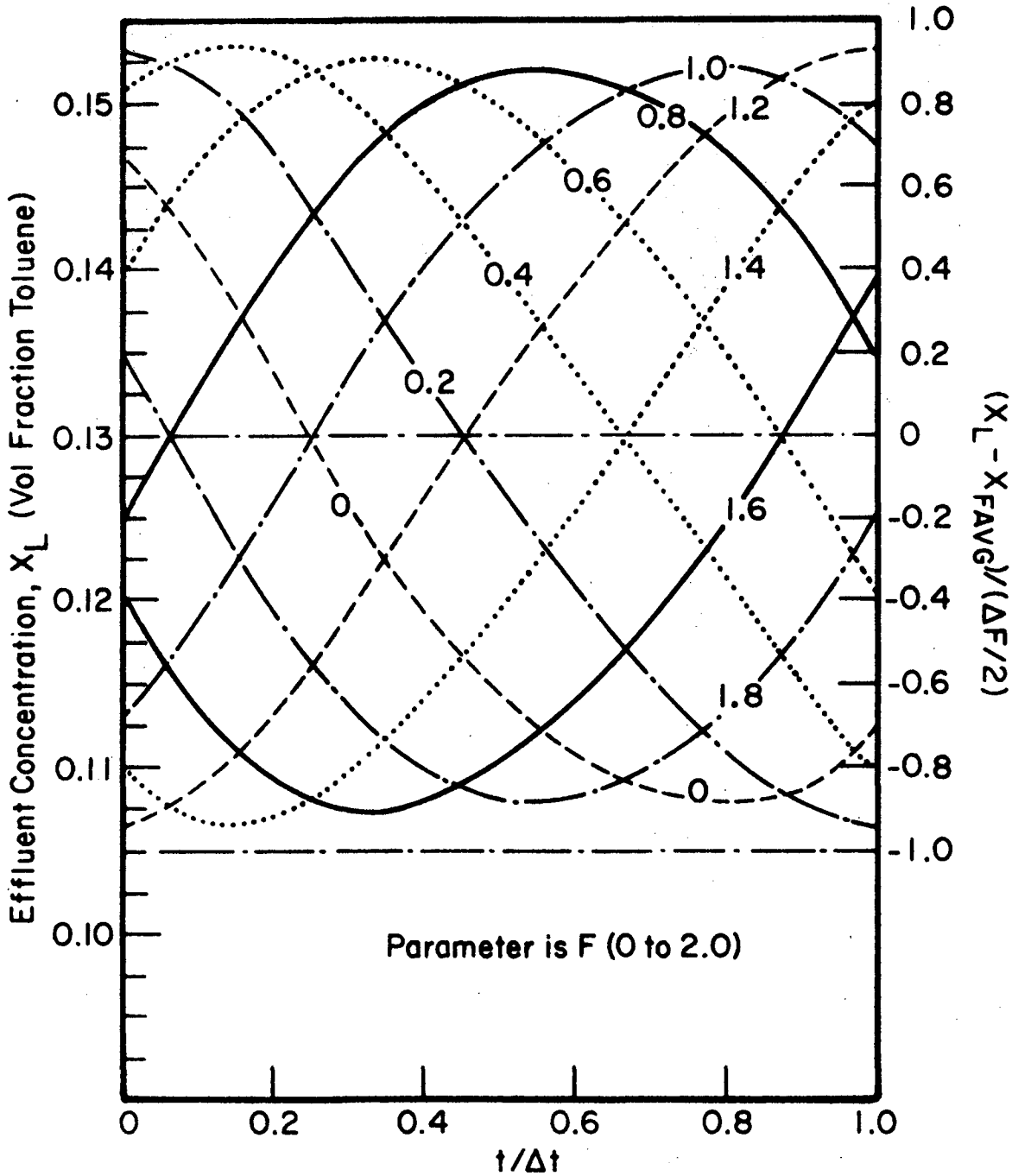
Effluent Concentration, X_L (Vol Fraction Toluene)
0.15
0.14
0.13
0.12
0.11
0.10
$(X_L - X_{FAVG})/(\Delta F/2)$
1.0
0.8
0.6
0.4
0.2
0
-0.2
-0.4
-0.6
-0.8
-1.0
0
0.2
0.4
0.6
0.8
1.0
$t/\Delta t$
1.0
0.8
1.2
0.6
0.4
1.4
0.2
0
1.6
1.8
0
Parameter is F (0 to 2.0)

establishes F = 1.00 as the optimum switching sequence (high temperature and low-feed concentration, or low temperature and high-feed concentration). It is important to note that diffusional effects in the column change the input square concentration wave considerably. As shown by Figure 6-4, the effluent concentration profile was rounded off and became more like a sine wave than the initial square wave input. But more importantly, the amplitude of the wave has been reduced from its initial input value. If an enriched or depleted product stream is to be produced, the effect of the temperature swing, as shown in Figure 6-3, must overcome the losses due to diffusion shown in Figure 6-4. It is obvious that longitudinal diffusion limits the amplitude of the input concentration wave, obtained by recycle. Enrichment or depletion due to temperature changes then compete with amplitude reduction due to diffusion.

The value of Eq. (6-20) is two-fold: It determines the optimum temperature-feed switching sequence for a dual-feed operation, and it allows the development of a dimensionless profile for a given step change in temperature and feed input. The dimensionless profile may be used to calculate the actual effluent concentration profile for a given step change in feed concentration and for any desired average feed concentration. Such a curve then greatly simplifies calculations necessary to design a

cycling zone adsorption, dual-feed cascade. Such calculations appear in the Chapter 7.

Computer Programs for Effluent Concentration Profiles

As previously stated, Eqs. (6-10), (6-17), and (6-20) have been programmed for computer to solve for the effluent concentration profiles from a single zone. The following FORTRAN variables are used in the programs and are defined below:

B = $m_T \Delta T/(1+m)$
D = $\sin(\pi nt/\Delta t)$
DELF = incremental change in the phase shift factor F
DELT = Δt = temperature switching time
DT = incremental change in time for which each data point is calculated
E = $\sin(\pi nt/\Delta t - SIG\pi n)$
F = phase shift factor between step change in feed concentration and temperature.
FMAX = maximum value of phase shift factor
PI = π = 3.14159265
Q = $q = \mathcal{D}(1+m)/V^2\Delta t$
R = $\sinh\alpha\zeta\cos\beta\zeta - 2\pi nq\cosh\alpha\zeta\sin\beta\zeta + \alpha\cosh\alpha\zeta\cos\beta\zeta - \beta\sinh\alpha\zeta\sin\beta\zeta$
S = $\cosh\alpha\zeta\sin\beta\zeta + 2\pi nq\sinh\alpha\zeta\cos\beta\zeta + \alpha\sinh\alpha\zeta\sin\beta\zeta + \beta\cosh\alpha\zeta\cos\beta\zeta$
SQI = $\zeta = VZ/2\mathcal{D}$
T = t = time in seconds
TMAX = $2\Delta t$ = one period of operation (two switching times)
U = $(\alpha R+\beta S)/(R^2+S^2)$
V = $(\alpha S+\beta R)/(R^2+S^2)$
W = ΔF = feed-concentration input amplitude

XN = n = 1,2,3,4,5,6.....XNMAX
XNMAX = total number of summations taken
Y = effluent concentration
YF = X_{feed} = feed concentration input
YFAVG = average feed concentration input (average concentration of high and low feeds used in a variable-feed operation)
YSWF = effluent concentration due only to square-wave feed concentration input
YSWT = effluent concentration due only to square-wave temperature change

$$ALFA = \sqrt{\frac{1 + \sqrt{1 + 16\pi^2 n^2 q^2}}{2}}$$

$$ALFA1 = m_T \Delta TZ/V\Delta t$$
$$BETA = 2\pi nq/\alpha$$
$$BETA1 = Z(1+m)n\pi/V\Delta t = \beta\zeta$$
$$GAMMA = \beta\sin(\pi n\ t/\Delta t) + \cos(\pi n\ t/\Delta t)$$
$$SIG = (1+m)Z/V\Delta t$$

Equation (6-10) describes the effluent concentration profile for a single zone operating under a square-wave temperature change, with constant feed concentration, and with zero diffusion. It takes the following form used in the computer program:

$$Y = YF - (B/PI) \sum_{n=1}^{100} \left[\frac{1-(-1)^n}{n}\right](D-E)$$

$$= YF - (B/PI)SUM$$

Equation (6-17) describes the effluent concentration profile for a single zone operating under a square-wave

temperature change, with continuous flow, constant feed concentration, and with infinite diffusion (perfectly mixed zone):

$$Y = YF - (ALFA1) \sum_{n=1}^{150} \left[\frac{1-(-1)^n}{BETA1^2+1} \right] GAMMA$$

$$Y = YF - (ALFA1)SUM$$

Equation (6-20) describes the effluent concentration profile for a single zone operating under a square-wave temperature change, with continuous flow, variable-feed input, and an intermediate diffusion coefficient. The program calculates the total effluent concentration profile, Y, due to both the step change in temperature and the step change in feed input. It also calculates the effluent concentration profiles due only to the step change of temperature, YSWT, and due only to the step change in the feed concentration, YSWF. The three effluent profiles take the following forms:

$$YSWT = YFAVG - (B/PI)SUMA$$

$$YSWF = YFAVG - (W/PI)SUMB$$

$$Y = YFAVG - [(B/PI)SUMA + (W/PI)SUMB]$$

The complete computer programs for Eqs. (6-10), (6-17), and (6-20) are as follows, respectively.

```
C     COMPUTING EFFLUENT CONCENTRATION PROFILE, ZERO DIFFUSION
      XNMAX=FILL IN
      TMAX=FILL IN
      DT=FILL IN
      DELT=FILL IN
      YF=FILL IN
      B=FILL IN
      PI=3.14159265
      SIG=FILL IN
      T=0.0
    7 SUM=0.0
      XN=1.0
    1 D=SIN(XN*PI*(T/DELT))
      E=SIN((XN*PI*(T/DELT))-SIG*XN*PI)
      SUM=SUM+(((1.0-(-1.0)**XN)/XN)*(D-E))
      IF(XNMAX-XN)3,3,2
    2 XN=XN+1.0
      GO TO 1
    3 Y=YF-((B/PI)*SUM)
      PRINT 4,T,Y
    4 FORMAT($TIME=$,E13.6,1X,$SECONDS$,6X,$Y=$,E13.6)
      IF(T-TMAX)5,5,6
    5 T=T+DT
      GO TO 7
    6 STOP
      END
```

```
C     COMPUTING EFFLUENT CONCENTRATION PROFILE FOR PECLET NUMBER
C     =0, DIFFUSIVITY=INFINITY.  CASE ANALOGOUS TO A PERFECTLY
C     MIXED COLUMN.
      XNMAX=FILL IN
      TMAX=FILL IN
      DT=FILL IN
      PI=3.14159265
      DELT=FILL IN
      YF=FILL IN
      ALFA1=FILL IN
      T=0.0
    7 SUM=0.0
      XN=1.0
    1 BETA1=FILL IN
      GAMMA=BETA1*SIN(XN*PI*(T/DELT))+COS(XN*PI*(T/DELT))
      SUM=SUM+((1.0-(-1.0)**XN)/(BETA1**2.0+1.0))*GAMMA
      IF(XNMAX-XN)3,3,2
    2 XN=XN+1.0
      GO TO 1
    3 Y=YF-ALFA1*SUM
      PRINT 4,T,Y
    4 FORMAT($TIME=$,E13.6,1X,$SECONDS$,6X,$Y=$,E13.6)
      IF(T-TMAX)5,5,6
    5 T=T+DT
      GO TO 7
    6 STOP
      END
```

```
C     COMPUTING EFFLUENT CONCENTRATION PROFILE FOR SQUARE WAVE
C     FEED INPUT AND SQUARE WAVE TEMPERATURE CHANGE OF THE COLUMN.
C     THE PROGRAM ALLOWS FOR A PHASE SHIFT BETWEEN THE STEP CHANGE
C     IN THE FEED CONCENTRATION AND THE TEMPERATURE SWITCH.
      W=FILL IN
      XNMAX=FILL IN
      TMAX=FILL IN
      DT=FILL IN
      DELT=FILL IN
      Q=FILL IN
      YFAVG=FILL IN
      SQI=FILL IN
      B=FILL IN
      PI=3.14159265
      FMAX=2.0
      DELF=0.20
      F=0.00
   14 PRINT 11,F
   11 FORMAT($F=$,E13.6)
      T=0.0
    7 SUM=0.0
      SUMA=0.0
      SUMB=0.0
      XN=1.0
    1 ALFA=SQRT((1.0+SQRT(1.0+XN**2*(157.90*Q**2)))/2.0)
      BETA=(XN/ALFA)*(2.0*PI*Q)
      R=0.5*(COS(BETA*SQI)-BETA*SIN(BETA*SQI))*((1.0-EXP(-2.0*
     1ALFA*SQI))/(EXP(-ALFA*SQI)))+0.5*(ALFA*COS(BETA*SQI)-2.0
     1*XN*PI*Q*SIN(BETA*SQI))*((1.0+EXP(-2.0*ALFA*SQI))/(EXP
     1(-ALFA*SQI)))
      S=0.5*(SIN(BETA*SQI)+BETA*COS(BETA*SQI))*((1.0+EXP(-2.0
     1*ALFA*SQI))/(EXP(-ALFA*SQI)))+0.5*(ALFA*SIN(BETA*SQI)+2.0
     1*XN*PI*Q*COS(BETA*SQI))*((1.0-EXP(-2.0*ALFA*SQI))/(EXP(
     1-ALFA*SQI)))
```

```
      U=(ALFA*R+BETA*S)/(R**2+S**2)
      V=(ALFA*S-BETA*R)/(R**2+S**2)
      SUMA=SUMA+((1.0-(-1.0)**XN)/XN)*(SIN(XN*PI*(T/DELT))*(1.0-EXP(
     1SQI)*U)+COS(XN*PI*(T/DELT))*EXP(SQI)*V)
      SUMB=SUMB+(EXP(SQI))*((1.0-(-1.0)**XN)/XN)*(SIN(F*PI)*(U*COS(XN*PI
     1*(T/DELT))+V*SIN(XN*PI*(T/DELT)))-COS(F*PI)*(U*SIN(XN*PI*
     1(T/DELT))-V*COS(XN*PI*(T/DELT))))
      SUM=SUM+(B/PI)*SUMA+(W/PI)*SUMB
      IF(XNMAX-XN)3,3,2
    2 XN=XN+2.0
      GO TO 1
    3 YSWT=YFAVG-(B/PI)*SUMA
      YSWF=YFAVG-(W/PI)*SUMB
      Y=YFAVG-((B/PI)*SUMA+(W/PI)*SUMB)
      PRINT4,T,Y,YSWT,YSWF
    4 FORMAT($TIME=$,E13.6,1X,$SECONDS$,6X,$Y=$,E13.6,6X,$YSWT=
     1$,E13.6,6X,$YSWF=$,E13.6)
      IF(T-TMAX)5,5,6
    5 T=T+DT
      GO TO 7
    6 CONTINUE
      IF(FMAX-F)12,13,13
   13 F=F+DELF
      GO TO 14
   12 STOP
      END
```

0 0 0 0 3 8 0 7 3 6 7

CHAPTER 7

SINGLE-ZONE STAGING IN THE DEVELOPMENT OF A CYCLING ZONE ADSORPTION CASCADE

Introduction..... 208

Continuous-Flow Operation With Constant-Feed Concentration Input to Each Zone..... 208

Effect of Recycle Stream Mixing Location... 221

Zone-to-Zone Calculations in the Development of a Cascade..... 229

Use of Finite-Difference Equations..... 234

A Graphical Solution Technique..... 239

Continuous-Flow Operation With Square-Wave Feed Concentration Input to Each Zone (Variable-Feed Operation)..... 243

Use of Finite-Difference Equations..... 252

Graphical Solution Technique..... 255

Noncontinuous-Flow Operation of a Single, Variable-Feed Zone..... 255

CHAPTER 7

SINGLE-ZONE STAGING IN THE DEVELOPMENT OF A CYCLING ZONE ADSORPTION CASCADE

Introduction

Development to this point has been concerned with the operation of *single* zone. As pointed out, operation under continuous-flow conditions allows only small separations, the maximum being approximately 3 vol % above or below the feed concentration to a zone. It can be concluded that as a single-zone operation, cycling-zone adsorption is not a promising method for obtaining large separations for this particular system. However, advantage may be taken of the small separations of a single zone by the appropriate staging of zones into a multi-zone cascade. Such an arrangement of optimally designed single zones should then allow very large separations. It is the purpose of this chapter to investigate a number of staged cascades operating with single feeds and with variable feeds. Finally, a noncontinuous-flow system will also be discussed.

Continuous-Flow Operation With Constant-Feed Concentration into Each Zone

Figure 7-1 is a dimensionaless effluent concentration profile for each single zone that will appear in a cascade. The portion, designated "A", of the effluent profile has a

Figure 7-1

Dimensionless Plot of Eq. (6-9) Used in Cascade Design

A = low-concentration product cut

B = high-concentration product cut

C = $C_1 + C_2 + C_3$ = intermediate cut (equal to feed concentration)

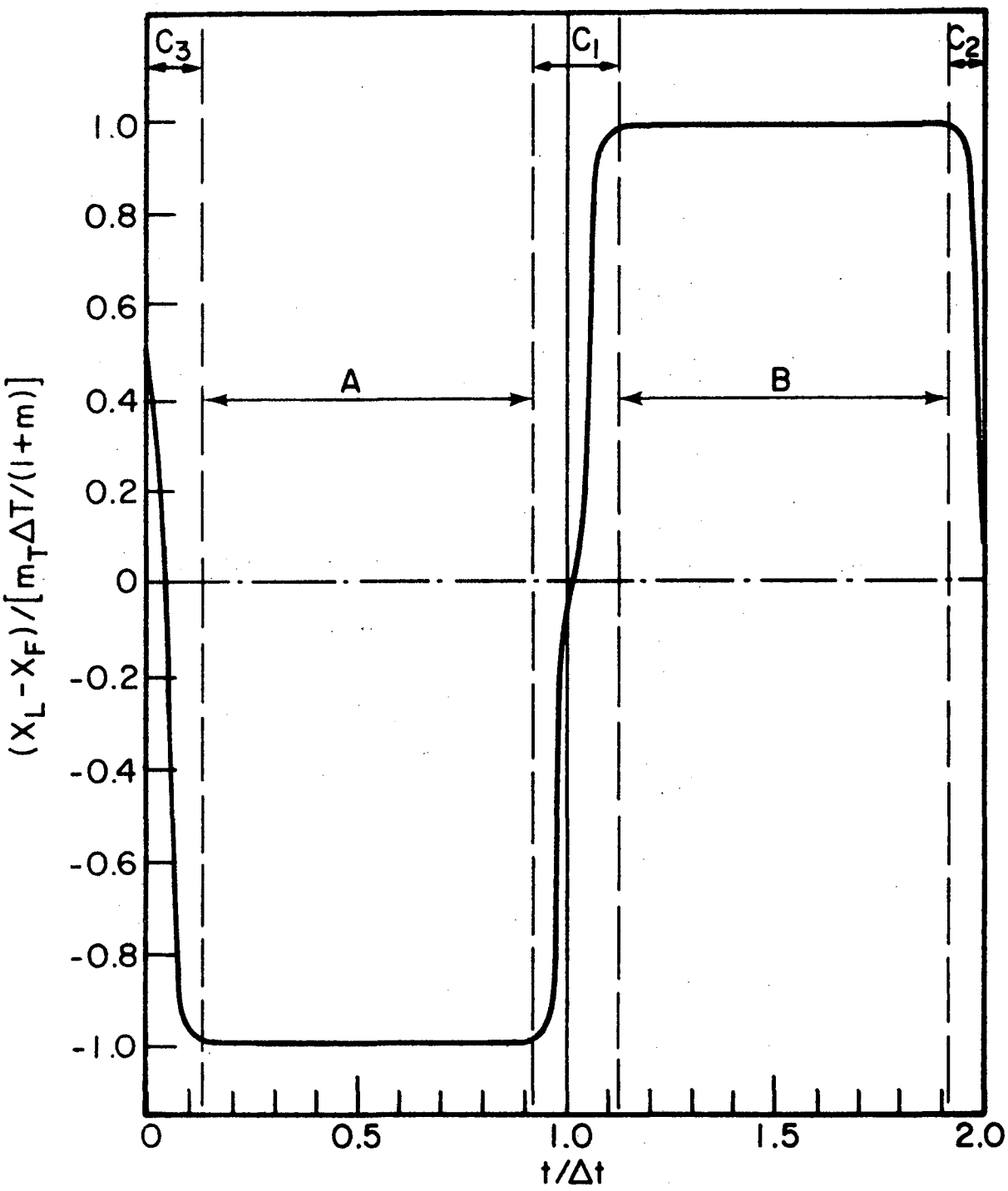
C3
C1
C2
A
B
1.0
0.8
0.6
0.4
0.2
0
-0.2
-0.4
-0.6
-0.8
-1.0
(XL-XF)/[mTΔT/(1+m)]
0
0.5
1.0
1.5
2.0
t/Δt

dimensionless concentration of -1.0 = $(X_L - X_{LF})/[m_T \Delta t/(1+m)]$, and a dimensionless duration of flow of 0.7833 = $t/\Delta t$. The portion, designated "B", has a dimensionless concentration of +1.0, with a dimensionless duration of flow of 0.7833 = $t/\Delta t$. The remainder of the profile, $(C_1 + C_2 + C_3)$ has a dimensionless concentration of zero--the feed concentration--and a duration of flow equal to 0.4334 = $t/\Delta t$.

Figure 7-2 is a plot of the term $P = m_T \Delta t/(1+m)$ and m versus the feed concentration, X_{LF}, into each single zone. This figure allows the calculation of the concentration change following a temperature switch. Use of Figure 7-2 also allows the determination of the nondimensionless effluent concentration profile for any feed concentration in conjunction with the dimensionless profile in Figure 7-1.

As previously discussed, for the same switching time for all the zones in a cascade, the length of each individual zone must be different because of the difference in concentration wave velocities experienced in each zone. It has been pointed out that a zone whose feed concentration is low in toluene requires a zone length somewhat shorter than a zone whose feed concentration is high. The following dimensionless ratio may be used to calculate the length of a zone for any chosen switching time, Δt, interstitial fluid velocity V, and the feed-concentration-dependent factor $m = [(1-\alpha)/\alpha]\epsilon(\partial X_S/\partial X_L)T_{avg}$:

$$\frac{2(1+m)Z}{V\Delta t} = \pi \qquad (7\text{-}1)$$

Figure 7-2

The Factors $P = m_T \Delta T/(1+m)$ and m Versus Volume Fraction Toluene in Feed, X_{LF}

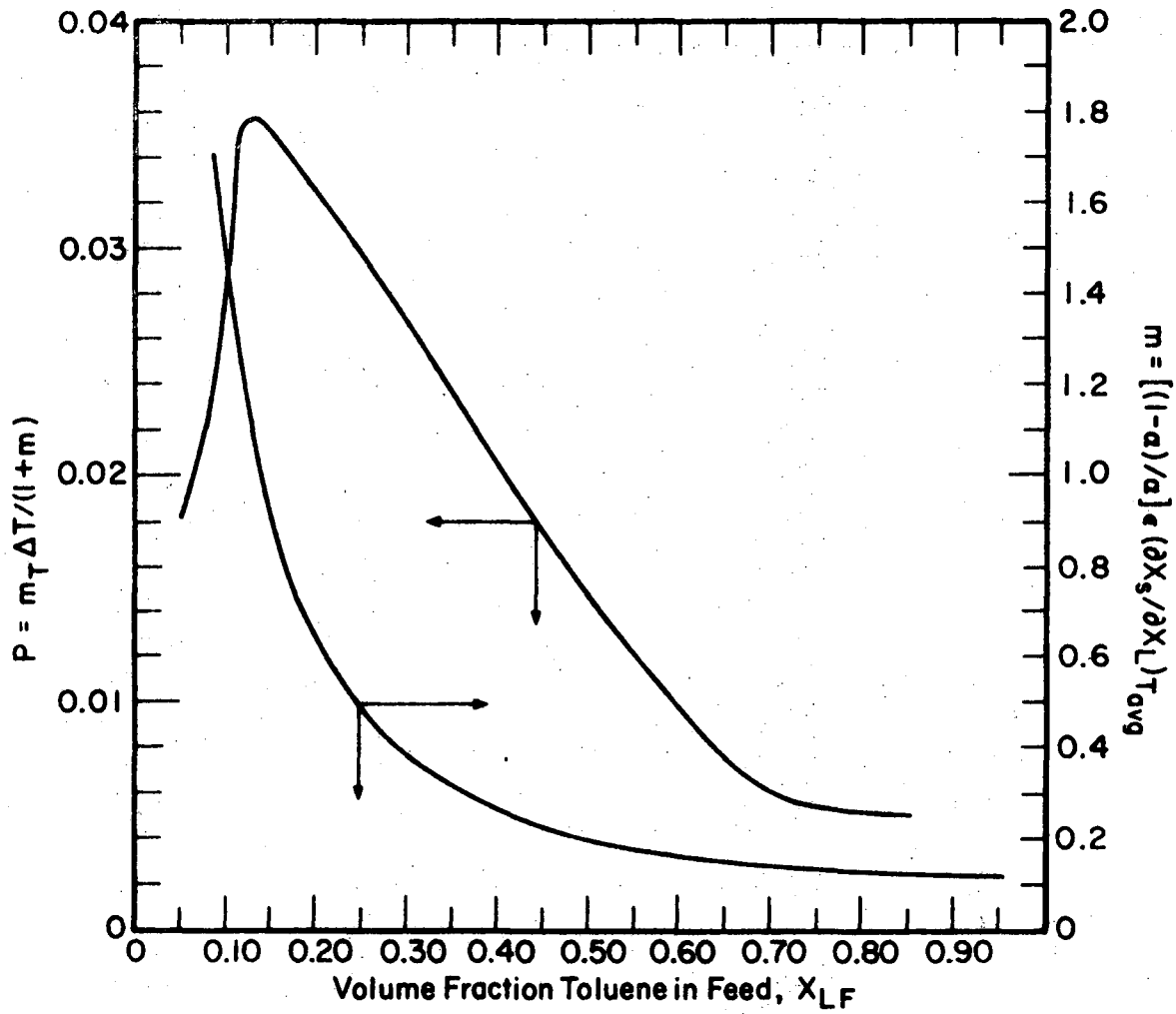
0.04
0.03
0.02
0.01
0
2.0
1.8
1.6
1.4
1.2
1.0
0.8
0.6
0.4
0.2
0
0.10
0.20
0.30
0.40
0.50
0.60
0.70
0.80
0.90
Volume Fraction Toluene in Feed, X_{LF}
$P = m_T \Delta T/(1+m)$
$m = [(1-a)/a] * (\partial X_s/\partial X_L)_{T_{avg}}$

Through the use of Figures 7-1 and 7-2 and Eq. (7-1), a continuous-flow cascade (with constant-feed concentration into each individual zone) may now be designed.

The cascade will consist of a repetitive unit combination of two single zones in series. Each zone will receive recycle streams from the following zone. Such a repeating linkage of two zones is pictured in Figure 7-3. Here the low-concentration product from a previous stage is passed on to each successive stage for further separation. The constant-feed concentration stream for stage N is made up from the low-concentration product from the stage N+1 (designated portion "A" of the dimensionless effluent concentration profile, Figure 7-1), from the feed-concentration recycle stream (designated $C_1 + C_2 + C_3$) of stage N, and from the high-concentration recycle stream from stage N-1 (designated portion "B" of the dimensionless effluent concentration profile, Figure 7-1). To produce a high-concentration product, the portions "A" and "B" are simply reversed, portion "A" becoming a recycle stream while portion "B" is now passed directly from one zone to the next.

From such a recycle scheme, it is obvious that the cross-sectional areas of successive stages cannot be the same. This is because each successive stage from the feed stage only receives a volumetric flow rate of liquid that is proportional to the amount of low- or high-concentration

0 0 0 0 3 8 0 7 3 7 1

Figure 7-3

Repetitive Combination of Two Single Zones

in Series With Recycle

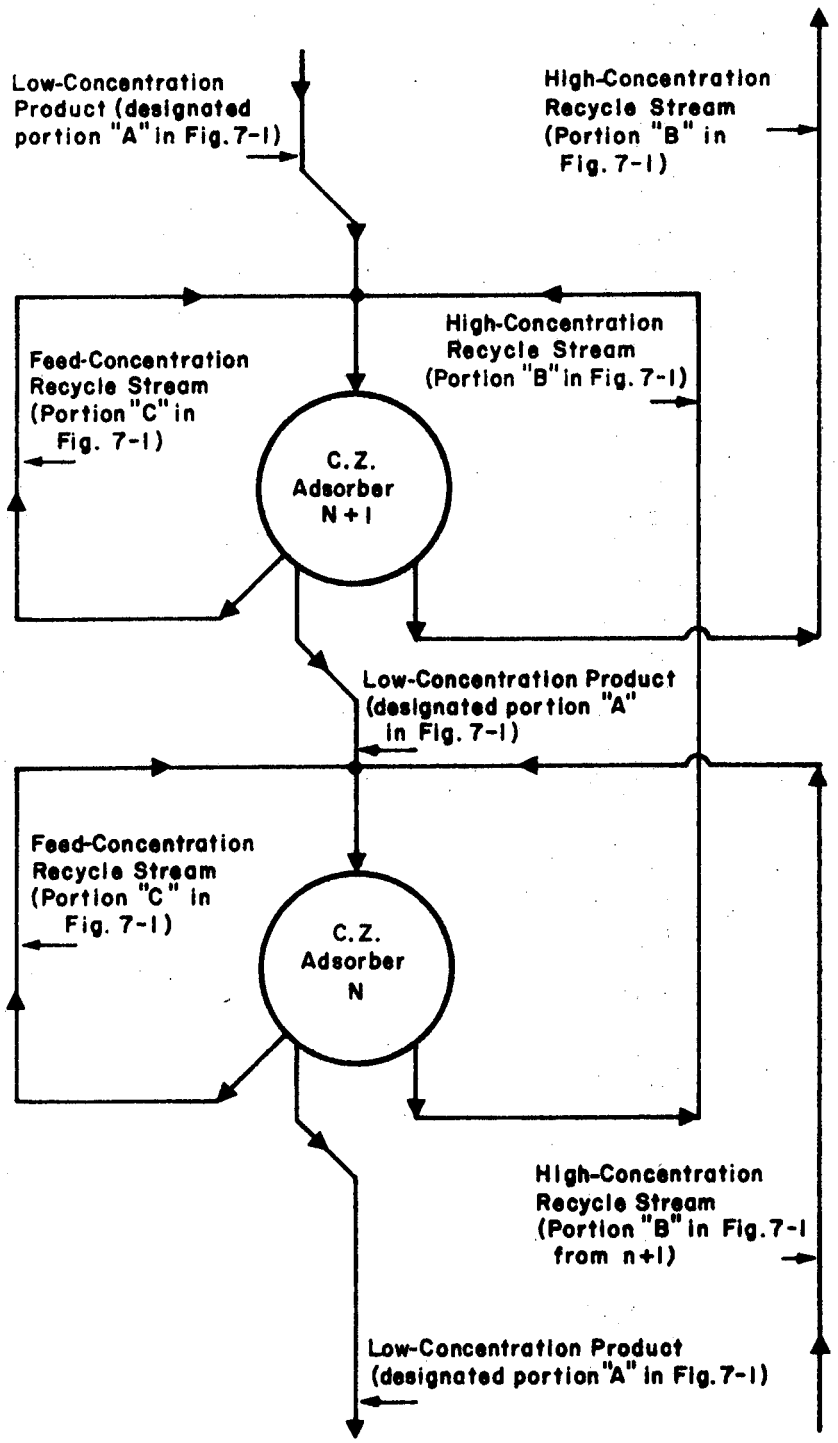
Low-Concentration Product (designated portion "A" in Fig. 7-1)
High-Concentration Recycle Stream (Portion "B" in Fig. 7-1)
High-Concentration Recycle Stream (Portion "B" in Fig. 7-1)
Feed-Concentration Recycle Stream (Portion "C" in Fig. 7-1)
C.Z. Adsorber N+1
Low-Concentration Product (designated portion "A" in Fig. 7-1)
Feed-Concentration Recycle Stream (Portion "C" in Fig. 7-1)
C.Z. Adsorber N
High-Concentration Recycle Stream (Portion "B" in Fig. 7-1 from n+1)
Low-Concentration Product (designated portion "A" in Fig. 7-1)

product produced by the previous stage. If the switching time for each zone remains the same--a necessary condition--and the interstitial velocity remains constant, the cross-sectional areal of successive zones from the feed stage must decrease. For example, if the dimensionless effluent concentration profile were a perfect square-wave (high-concentration product for a duration of $t/\Delta t = 1.0$ and low-concentration product for a duration of $t/\Delta t = 1.0$), then each successive stage would have a cross-section area equal to one half that of the previous stage. The final result is a cascade that tapers in cross section from the feed stage. This is an inherent characteristic of a staged, series operation of cycling zone adsorption separation.

Figure 7-4 is a schematic diagram of an illustrative, continuously operating cycling zone adsorption cascade, using the repetitive two-zone recycle unit of stages shown in Figure 7-3. The cascade consists of a feed zone, designated "F", with two legs, one finally producing low-concentration product (10 vol %), and one producing high-concentration product (50 vol%). Table 7-1 summarizes the volumetric flow rate and concentration of each stream appearing in the diagram. The material balance equations appear in the following section entitled "Zone-to-Zone Calculations in the Development of a Cascade."

In each case above, the volumetric flow rates are expressed as functions of the interstitial fluid velocity

Figure 7-4

Continuously Operating Cycling Zone Adsorption Cascade

(Repetitive core shown in Figure 7-3)

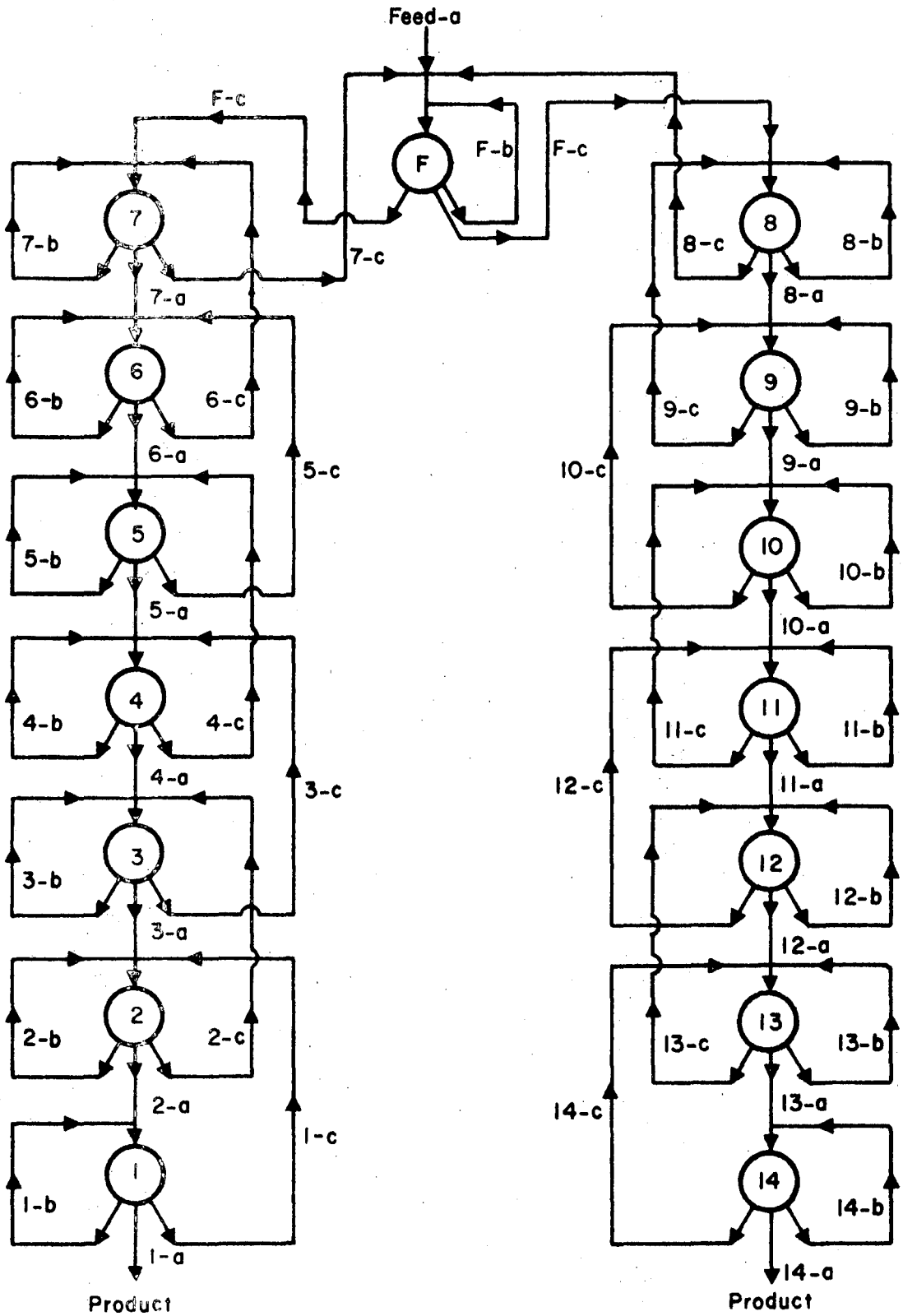
Feed-a
F
F-b
F-c
F-c
7
7-b
7-c
7-a
6
6-b
6-c
6-a
5-c
5
5-b
5-a
4
4-b
4-c
4-a
3-c
3
3-b
3-a
2
2-b
2-c
2-a
1-c
1
1-b
1-a
Product
8
8-c
8-b
8-a
9
9-c
9-b
9-a
10-c
10
10-b
10-a
11
11-c
11-b
11-a
12-c
12
12-b
12-a
13
13-c
13-b
13-a
14-c
14
14-b
14-a
Product

Table 7-1. Concentration and Flow Rate Data:

Continuous-Flow, Two-Zone Recycle Cascade

Zone (N)	X_{N-a} (Prod. From Stage N+1) (%)	Volume Flow Rate For X_{N-a}	X_{N-b} (%)	Volume Flow Rate For X_{N-b}	X_{N-c} (%)	Volume Flow Rate For X_{N-c}
1	10.000	0.391650VA	13.600	0.216700VA	17.200	0.3916500VA
2	13.600	0.783300VA	17.200	0.433400VA	20.800	0.783300VA
3	17.200	1.174950VA	20.500	0.650100VA	23.800	1.1749500VA
4	20.350	1.566600VA	23.450	0.866800VA	26.550	1.5666000VA
5	23.240	1.958250VA	26.200	1.083500VA	29.200	1.9582500VA
6	26.000	2.349900VA	28.800	1.300200VA	31.600	2.3499000VA
7	28.515	2.741550VA	31.150	1.516400VA	33.800	2.7415500VA
F	30.000	0.783300VA	33.325	1.733600VA	30.825 35.825	3.1332000VA
8	38.260	2.741550VA	36.00	1.516900VA	33.800	2.7415500VA
9	40.500	2.349900VA	38.400	1.300200VA	36.300	2.3499000VA
10	43.040	1.958250VA	41.100	1.083500VA	39.100	1.9582500VA
11	45.080	1.566600VA	43.200	0.866800VA	41.300	1.5666000VA
12	46.860	1.174950VA	45.100	0.650100VA	43.440	1.1749500VA
13	48.400	0.783300VA	46.700	0.433400VA	45.000	0.7833000VA
14	50.000	0.391650VA	48.400	0.216700VA	46.800	0.3916500VA

V, and the interstitial cross sectional area, A, of the final product zone. Also note that streams designated by N-a are feed streams before the mixing point to each zone. Table 7-2 summarizes the mixed feed concentration and volumetric flow rate into each zone and also the interstitial cross-sectional area for flow for each zone in the cascade.

The length of each zone in the cascade may be calculated from the use of Eq. (7-1) and Figure 7-2.

Effect of Recycle Stream Mixing Location

Recycle, in the design of a complete cascade, plays two important roles. The effect of recycling a stream of the same composition as the feed stream back to the same zone tends to reduce the required flow rate from the previous zone. This results in a minimizing of the cross-sectional areas of zones in a series cascade. This can be seen in the cascade of Figure 7-4. As the recycle streams are fed to zones farther away in the cascade, the reduction of the cross-sectional areas of successive zones decreases. On this basis only, it would then be best to recycle as close to the original zone producing the recycle stream. However, compositional effects now come into consideration. For instance, recycle of a low-concentration stream to a zone many stages away in the series has the effect of requiring a high-concentration product stream to be produced from the zone to which the low-concentration recycle stream

Table 7-2

Feed Concentration, Flow Rate, and Cross-Sectional Area Data: Continuous-Flow, Two-Zone Recycle Cascade

Zone (N)	Mixed Feed Concentration	Volume Flow Rate	Int. C.S.A.
1	13.600%	1.00VA	1.00A
2	17.200%	2.00VA	2.00A
3	20.500%	3.00VA	3.00A
4	23.450%	4.00VA	4.00A
5	26.200%	5.00VA	5.00A
6	28.800%	6.00VA	6.00A
7	31.150%	7.00VA	7.00A
F	33.325%	8.00VA	8.00A
8	36.000%	7.00VA	7.00A
9	38.400%	6.00VA	6.00A
10	41.100%	5.00VA	5.00A
11	43.200%	4.00VA	4.00A
12	45.100%	3.00VA	3.00A
13	46.700%	2.00VA	2.00A
14	48.400%	1.00VA	1.00A

is fed. In this manner the concentration changes from zone to zone become larger due to mixing at the feed point, and the number of zones in the series is then reduced. However, the cross-sectional area of each zone in the series becomes larger. Thus both effects of recycling tend to minimize the total volume of the cascade. For example, recycling many stages away in the series results in fewer stages but in a large increase in the cross-sectional areas of each stage; recycling to adjacent stages reduces the cross-sectional areas of stages, but increases the number of stages in the cascade. Design of a large number of example recycle cascades has allowed the conclusion that the total volume of the cascade will remain roughly the same. However, in the final design it seems best to reduce the number of stages as much as possible, thus reducing control and heat-transfer equipment costs.

To elucidate this point further, Figure 7-5 is a schematic diagram of the left-hand two-zone recycle leg of the cascade in Figure 7-4 and a three-zone recycle leg. The core of this series scheme consists of three zones with major recycle stream being mixed three zones away. This arrangement is compared with the two-zone recycle scheme. The length, and consequently the volume, of each zone is calculated from Eq. (7-1), with $V = 1.0$ cm/sec and $\Delta t =$ 1000 seconds. Table 7-3, under the conditions prescribed by Eq. (7-1), summarizes a leg of the two-zone recycle

Figure 7-5

Comparison of a Two-Zone Recycle Leg and a Three-Zone Recycle Leg Producing the Same Separation

Type of Recycle	Total Interstitial Volume	No. of Stages	Separation (vol % toluene)
Two-zone	40,000A	8	22
Three-zone	49,000A	6	22

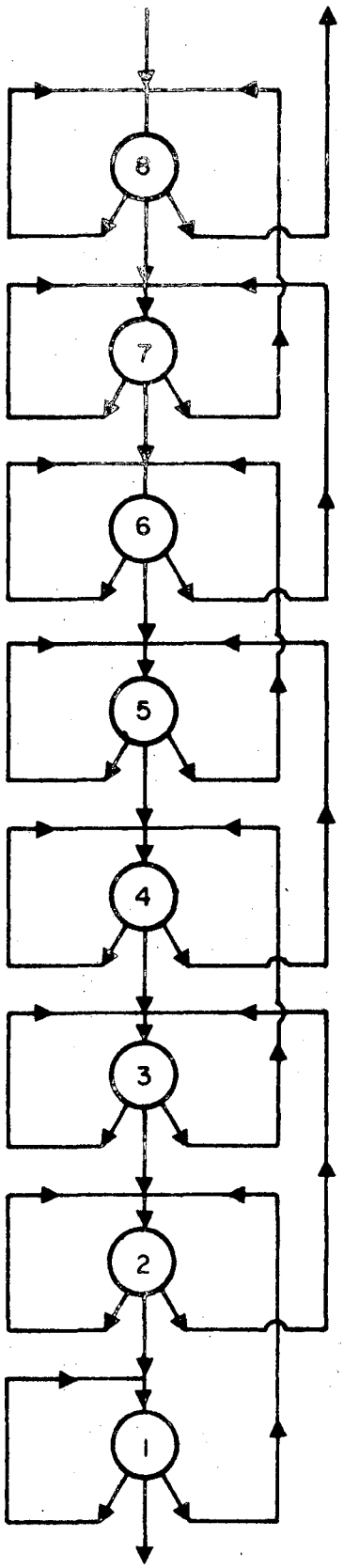

Final Product
(Two-Zone Recycle Leg)

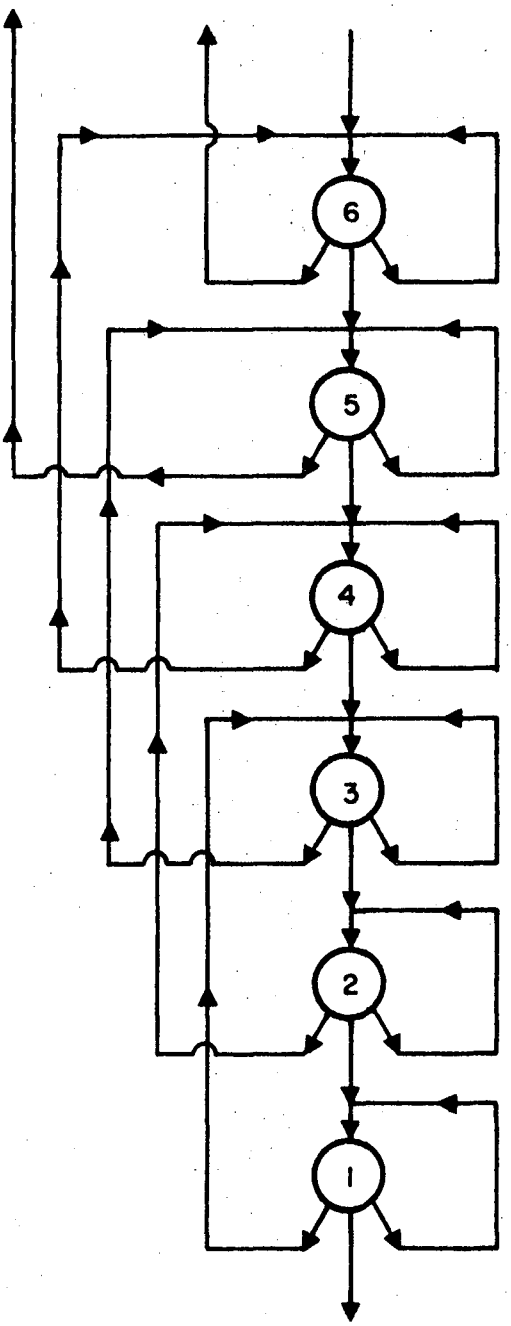

Final Product
(Three-Zone Recycle Leg)

Table 7-3

Low-Product Leg Characteristics of Continuous-Flow, Two-Zone Recycle Cascade

Zone (N)	Feed Concentration (%)	Intermediate Feed (Product From Zone N+1) (%)	Length (cm)	C.S.A.	Interstitial Volume
1	13.600	13.600	781.59	1.0A	781.59A
2	17.200	17.200	887.50	2.0A	1775.00A
3	20.500	20.350	969.75	3.0A	3879.00A
4	23.450	23.340	1026.80	4.0A	4107.20A
5	26.200	26.000	1072.35	5.0A	5361.77A
6	28.800	28.515	1118.15	6.0A	6708.90A
7	31.150	30.825	1150.92	7.0A	8056.40A
8	33.300	32.046	1176.78	8.0A	9414.23A

cascade. The total interstitial volume of the two-zone recycle led of the cascade is 40.000 A for a total concentration change of 32.046 - 10.00 = 22.046 vol = toluene. This may be expressed as 1,800 A units of volume for each percent increase in the volume percent of toluene.

Table 7-4, under the conditions prescribed by Eq. (7-1), summarizes a leg of a three-zone recycle cascade. The total interstitial volume of the three-zone recycle leg of the cascade is 49,800 A for a total concentration change of 32.015 - 10.000 = 22.015 vol % toluene. This may be expressed as 2,260.0 A unite of volume for each percent increase in volume percent of toluene separated.

Comparison of the total interstitial volume of the two legs of the cascade indicates that the two-zone and three-zone recycle schemes require roughly the same volume of solid particles. (The three-zone recycle scheme requires roughly 15% more solids than the two-zone recycle scheme.) However, the three-zone recycle scheme provides the same separation with only six total zones, while the two-zone scheme requires eight total zones. Although the difference in volume requirements is small, the final design of a cycling zone adsorption cascade operating under constant feed to each zone would favor the three-zone recycle scheme because of the fewer stages required. It may therefore be concluded that recycling a number of zones

Table 7-4

Low-Product Leg Characteristics of Continuous-Flow, Three-Zone Recycle Cascade

Zone (N)	Feed Concentration (%)	Intermediate Feed (Product From Zone N+1) (%)	Length (cm)	C.S.A.	Interstitial Volume
1	13.6	13.60	781.5	1.0A	781.5A
2	17.2	17.20	887.5	2.0A	1775.0A
3	20.5	21.34	969.7	4.0A	3879.0A
4	24.3	24.94	1040.4	7.0A	7282.8A
5	27.8	28.60	1098.6	12.0A	13183.2A
6	31.2	32.01	1150.9	20.0A	23018.3A

away is more beneficial than adjacent-zone recycle, which minimizes the total cascade volume.

Zone-to-Zone Calculations in the Development of a Cascade

Zone-to-zone calculations necessary in the design of a cycling zone adsorption cascade such as Figure 7-4 contain certain characteristics which lend themselves to simplified computer or graphical solution methods. The two-zone recycle cascade of Figure 7-4 reveals that the design calculations must begin at the product zone of each leg of the cascade, successive calculations preceding towards feed zone. The production of each following zone is therefore dependent upon that in the previous zone due to the recycle stream. Such a cascade is then designed by calculations from the two end zones, upward to the feed zone. Such a procedure requires trial and error, since it is desired (but not required) that the feed zone produce two product streams that become the feed streams to the two respective legs of the cascade. Such calculations are then analogous to stagewise calculations for a multicomponent distillation column. It would therefore be advantageous to write a set of equations that would allow such a calculation to be made systematically.

Consider Figure 7-6, which is the low-concentration-product leg of a two-zone recycle cascade. Let the following variables be defined:

Figure 7-6

A Generalized Two-Zone Recycle Leg of a Cascade

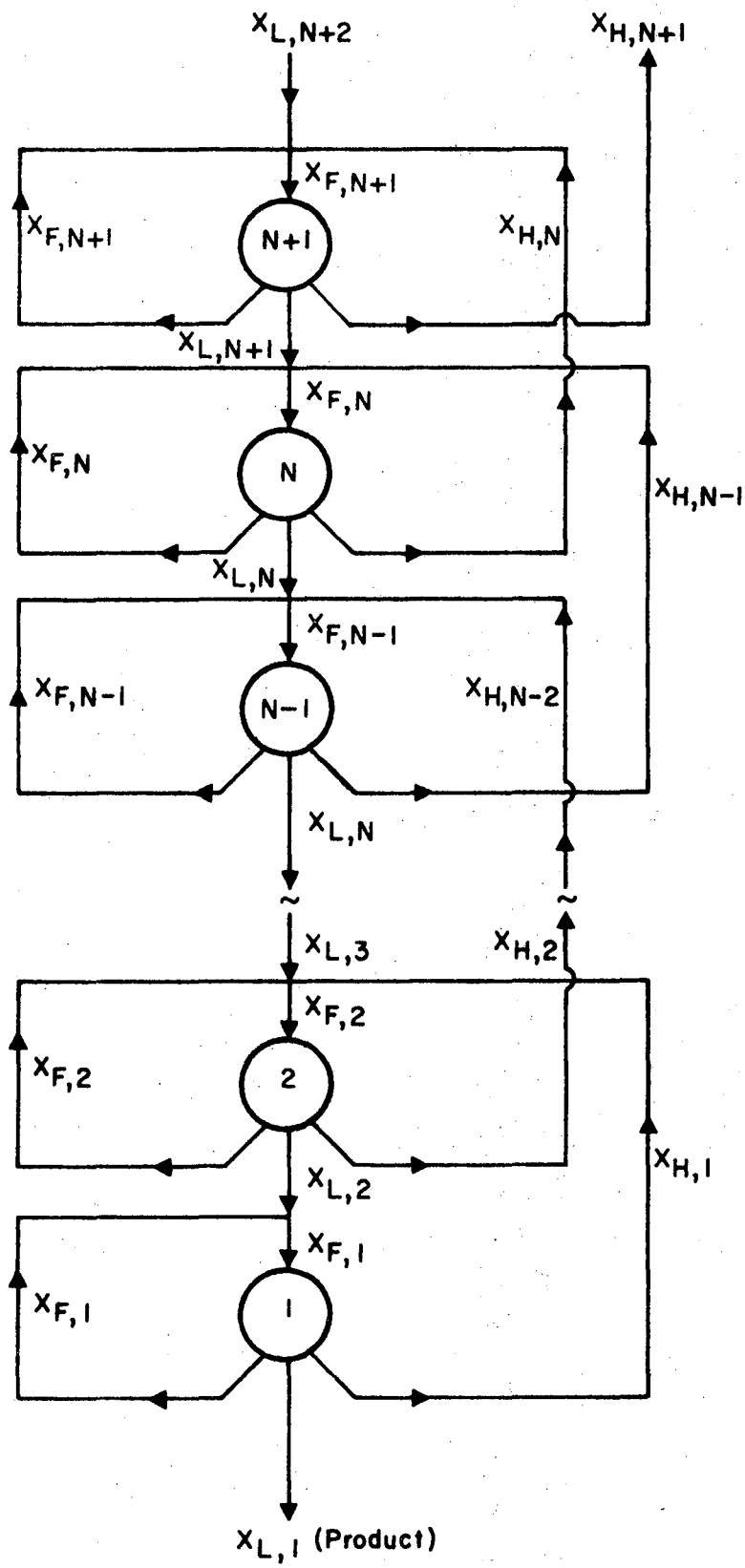
$X_{L,N+2}$
$X_{H,N+1}$
$X_{F,N+1}$
$X_{F,N+1}$
N+1
$X_{H,N}$
$X_{L,N+1}$
$X_{F,N}$
$X_{F,N}$
N
$X_{H,N-1}$
$X_{L,N}$
$X_{F,N-1}$
$X_{F,N-1}$
N−1
$X_{H,N-2}$
$X_{L,N}$
$X_{L,3}$
$X_{H,2}$
$X_{F,2}$
$X_{F,2}$
2
$X_{H,1}$
$X_{L,2}$
$X_{F,1}$
$X_{F,1}$
1
$X_{L,1}$ (Product)

f = the fraction of the total period ($2\Delta t$) for which the high-concentration cut (designated "B") flows and for which the low-concentration cut (designated "A") flows.

$1-2f$ = the fraction of the total period ($2\Delta t$) for which the one-zone intermediate recycle cut flows (designated C). The average concentration of this cut is equal to the feed concentration.

V = interstitial fluid velocity (the same for every zone in the cascade).

A = cross-sectional area for interstitial flow in a zone. The total cross-sectional area of a zone is equal to A/α.

$X_{F,L,H}$ = volume fraction toluene in the feed, the low-cut, and the high-cut fraction, respectively.

N = zone number.

P = $(m_T\Delta t)/(1+m)$, the concentration change due to the step change in temperature. From Figure 7-2, which relates P to the feed concentration, X_F, it is possible to derive a relationship of P to X_L.

By material balance, the following equations may be developed to describe each successive zone in the leg of the cascade.

$$X_{L,N} = \frac{NX_{L,1} + 2\sum_{i=1}^{N-1} iP_i}{N} \qquad (7\text{-}2)$$

$$X_{F,N} = \frac{NX_{L,1} + 2\sum_{i=1}^{N-1} iP_i + NP_N}{N} = X_{L,N} + P_N \qquad (7\text{-}3)$$

$$X_{H,N} = \frac{NX_{L,1} + 2\sum_{i=1}^{N} iP_i}{N} = X_{L,N} + 2P_N \qquad (7\text{-}4)$$

$$A_N = NA_1 \qquad (7\text{-}5)$$

$$\left.\begin{array}{l} \text{Volumetric flow rate for } X_{H,N} = fVA_N \\ \text{Volumetric flow rate for } X_{L,N} = fVA_N \\ \text{Volumetric flow rate for } X_{F,N} = VA_N \\ \text{Volumetric flow rate for the feed} \\ \text{concentration recycle} = (1-2f)VA_N \end{array}\right\}^{*} \qquad (7\text{-}6)$$

*All flow rates expressed for a time duration of a period of $(2\Delta t)$.

Starting with a given value of $X_{L,1}$, V, F, and A_1, Eqs. (7-3) through (7-5) may be used to design the low-concentration, two-zone recycle led of the cascade. To calculate the high-concentration product leg of the cascade, following similar equations may be used:

$$X_{H,N} = \frac{NX_{H,1} - 2\sum_{i=1}^{N-1} iP_i}{N} \qquad (7\text{-}7)$$

$$X_{F,N} = \frac{NX_{H,1} - 2\sum_{i=1}^{N-1} iP_i - NP_N}{N} = X_{H,N} - P_N \qquad (7\text{-}8)$$

$$X_{L,N} = \frac{NX_{H,1} - 2\sum_{i=1}^{N} iP_i}{N} = X_{H,N} - 2P_N \qquad (7\text{-}9)$$

The cross-sectional area relationship is the same as Eq. (7-5) and the volumetric flow rate relationships are the same as Eq. (7-6). For given values of $X_{H,1}$, V, f, and A_1, Eqs. (7-5) through (7-9) may be used to design the high-concentration leg of the cascade. The final feed stage of the cascade may be calculated from the following equations:

$X_{L,F} = X_{F,N}$, from the low-concentration product leg of the cascade, Eq. (7-2)

$X_{H,F} = X_{F,N}$, from the high-concentration product leg of the cascade, Eq. (7-7)

$$X_{F,F} = X_{L,F} + P_F = X_{H,F} - P_F$$

The calculation involves trial and error such that the correct single value of P_F will tie the feed zone to the last zone of each leg of the cascade. Such a calculation is simplified for use of a computer by establishing either the high- or low-concentration product desired, and then varying one or the other until a match occurs at the feed zone.

Use of Finite-Difference Equations

It is seen from the previous equations that zone-to-zone calculations involve discrete step-wise changes in concentrations. Such abrupt finite changes then allow the use of finite difference calculus to obtain the concentrations of a stage N without knowing all the concentrations of the N-1 following stages.

Again consider the low-concentration leg of a two-zone recycle cascade as in Figure 7-6. The product zone is numbered 1, the following zone is 2, and so on up to the feed zone F. The following calculations develop an expression for $X_{L,N}$:

From Eq. (7-2), for zone N,

$$NX_{L,N} = NH_{L,1} + 2 \sum_{i=1}^{N-1} iP_i \tag{7-10}$$

For zone N+1,

$$(N+1)X_{L,N+1} = (N+1)X_{L,1} + 2 \sum_{i=1}^{N} iP_i \tag{7-11}$$

Subtracting Eq. (7-10) from (7-11) gives,

$$(N+1)X_{L,N+1} - NX_{L,N} - \frac{1}{2}X_{L,1} = NP_N \tag{7-12}$$

Figure 7-2 reveals that P versus X_F is a linear relationship for $15.0\% \leq X_F \leq 50.0\%$. Therefore, P_N may be expressed as a linear function of either $X_{H,N}$, $X_{F,N}$, or $X_{L,N}$. Figure 7-7 is a plot of P_N versus these three concentrations. P_N as a function of $X_{L,N}$ takes the following form:

$$P_N = a + bX_{L,N} = 4.2 - 0.057\ X_{L,N} \tag{7-13}$$

Substitution of Eq. (7-13) into Eq. (7-12) gives the final form of the finite-difference equation describing the low-concentration leg of the two-zone recycle cascade:

$$(N+1)X_{L,N+1} = (1+2b)NX_{L,N} + X_{L,1} + 2aN \tag{7-14}$$

Figure 7-7

P_N Versus $X_{L,N}$, $X_{H,N}$, and $X_{F,N}$ (Constant-Feed Operation)

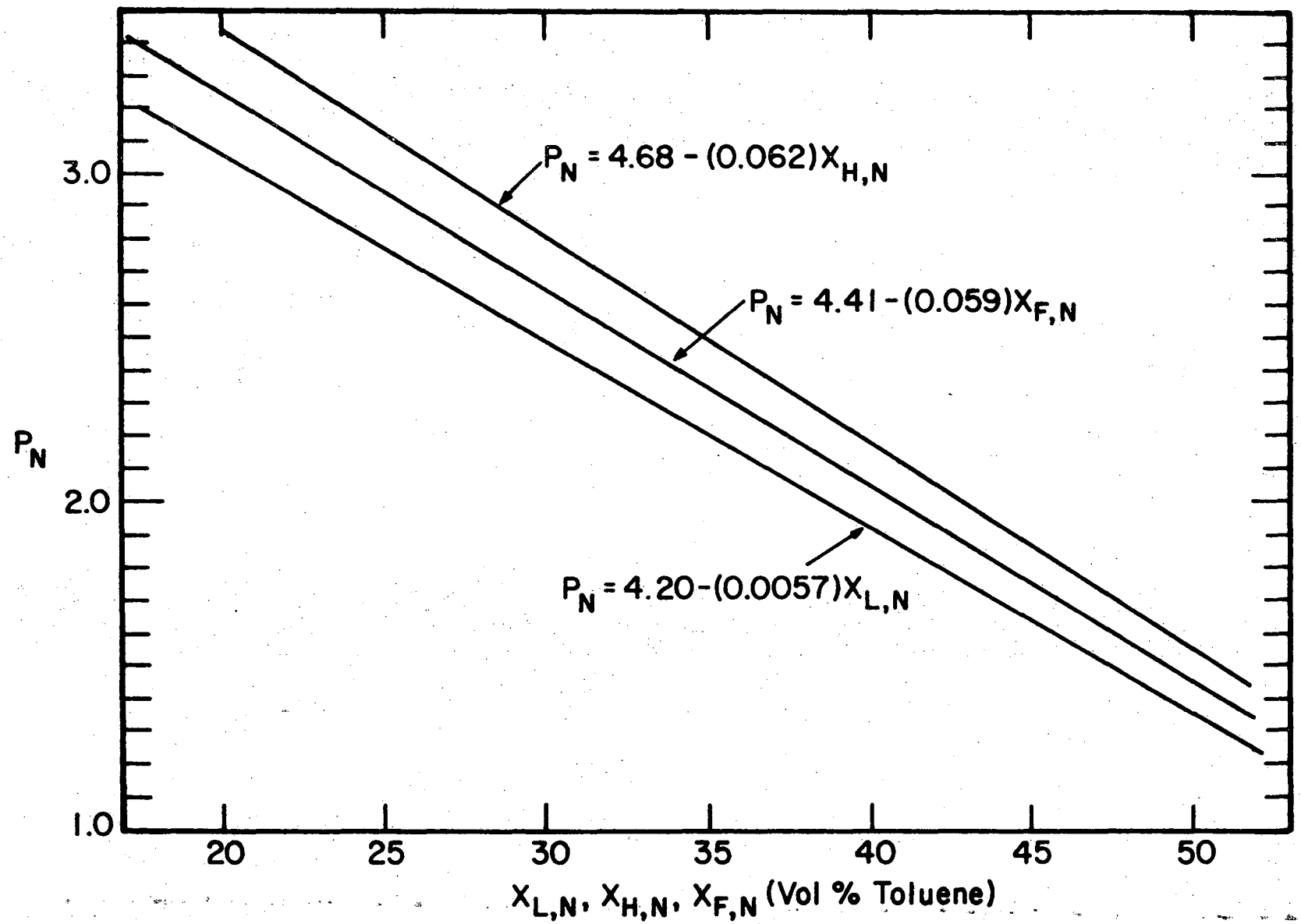
$P_N = 4.68 - (0.062)X_{H,N}$
$P_N = 4.41 - (0.059)X_{F,N}$
$P_N = 4.20 - (0.0057)X_{L,N}$
P_N
3.0
2.0
1.0
20
25
30
35
40
45
50
$X_{L,N}$, $X_{H,N}$, $X_{F,N}$ (Vol % Toluene)

Equation (7-14) is a first-order, linear, finite-difference equation with variable coefficients. Its solution may be obtained by analytic methods or by inductive method which takes advantage of the repetitive appearance of terms for successive zone calculations. By induction, the solution of Eq. (7-14) is

$$X_{L,N+1} = \frac{\sum_{i=0}^{N} (1+2b)^{i} X_{L,1} + 2a \sum_{i=0}^{N-1} (N-1)(1+2b)^{i}}{N+1} \tag{7-15}$$

For a given value of the low-concentration product, $X_{L,1}$, and the values of the constants a and b, from Eq. (7-13), the low-concentration leg of the two-zone recycle cascade may be developed. The cross-sectional area to flow for each zone is calculated from Eq. (7-5).

In the manner just described, the high-concentration leg of the two-zone recycle cascade may be calculated. Again, the high-concentration product zone is numbered 1, the following zone 2, up to the common feed zone F. The finite-difference equation describing the high-concentration product leg of the cascade takes the following form:

$$(N+1)X_{H,N+1} = (1-2b')NX_{H,N} + X_{H,1} - 2Na' \tag{7-16}$$

where, from Figure 7-7, $P_N = a' + b'X_{H,N} = 4.68 - 0.062 X_{H,N}$, valid for $15.0\% \leq X_F \leq 50.0\%$.

By induction, the solution of Eq. (7-16) is:

$$X_{H,N+1} = \frac{\sum_{i=0}^{N} (1-2b')^{i} X_{H,1} - 2a' \sum_{i=0}^{N+1} (N-1)(1-2b')^{i}}{N+1} \tag{7-17}$$

For given values of the high-concentration product, $X_{H,1}$, and the constants a' and b', the high-concentration product leg of the two-zone recycle cascade may be developed.

It is of importance to remember that Eqs. (7-15) and (7-17) are valid only for a linear relationship between P and X. A curved relationship, which in this study occurs at the high- and low-concentration regions, would require a number of linear relationships to describe the curve, each with its own set of constants for the particular concentration range.

Graphical Solution Technique

The solutions of the finite-difference equations, as given by Eqs. (7-15) and (7-17), provide the easiest method of cascade design calculations to this point. However, a graphical method, comparable to those used in distillation, would provide a considerable savings of time. Such a graphical method is restricted to the concentration range where P_N is a linear function of the concentrations involved.

Figure 7-8 depicts the graphical technique developed to calculate the low-concentration leg of a two-zone

Figure 7-8

Generalized Graphical Solution for Design of a Two-Zone Recycle Cascade

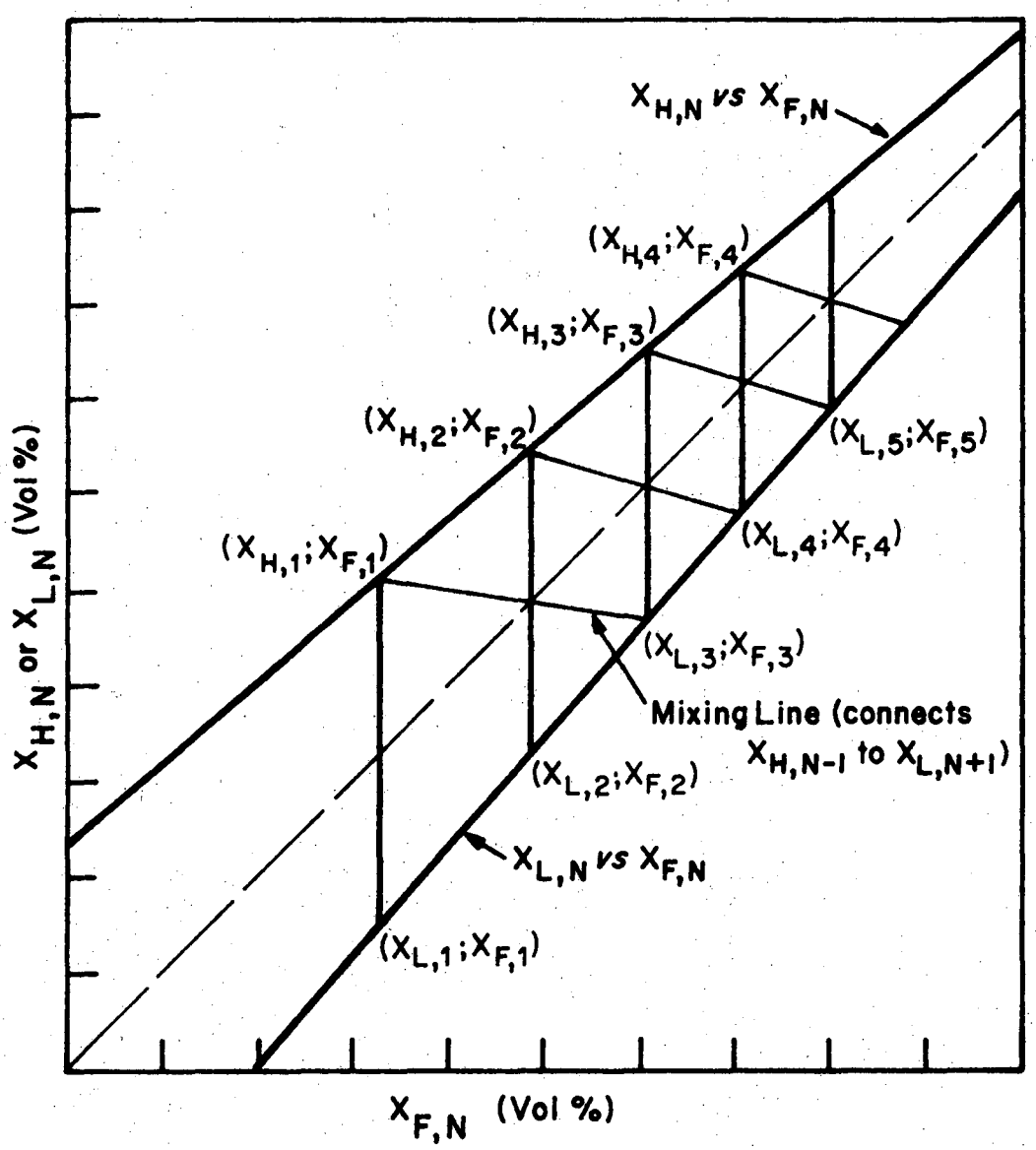
$X_{H,N}$ vs $X_{F,N}$
$(X_{H,4};X_{F,4})$
$(X_{H,3};X_{F,3})$
$(X_{H,2};X_{F,2})$
$(X_{H,1};X_{F,1})$
$(X_{L,5};X_{F,5})$
$(X_{L,4};X_{F,4})$
$(X_{L,3};X_{F,3})$
Mixing Line (connects $X_{H,N-1}$ to $X_{L,N+1}$)
$(X_{L,2};X_{F,2})$
$X_{L,N}$ vs $X_{F,N}$
$(X_{L,1};X_{F,1})$
$X_{H,N}$ or $X_{L,N}$ (Vol %)
$X_{F,N}$ (Vol %)

recycle cascade. The value of the desired low-concentration product is given as $X_{L,1}$. From this value, the feed concentration, $X_{F,1}$, and the high-concentration recycle stream, $X_{H,1}$, are established by a vertical line. Because there is no high-concentration recycle to the first zone in the leg, the feed concentration, $X_{F,1}$, is equal to the low-concentration stream from zone 2, $X_{L,2}$. A vertical line again establishes $X_{F,2}$ and $X_{H,2}$. Zone 2 now has the high-concentration recycle stream from the previous zone 1 entering at a mixing point above zone 2. This is characteristic of all following zones in the cascade. At the mixing point three streams of concentrations $X_{F,2}$, $X_{H,1}$, and $X_{H,1}$ are mixed to form a feed stream of concentration $X_{F,2}$. These three concentrations should therefore fall on the same line, according to the commonly used mixing rule. From this, the concentration $X_{L,3}$ may now be established, and the graphical technique may be carried out for the following zones up to the feed zone.

To graphically calculate the high-concentration product leg of the two-zone recycle cascade the same technique is used except for the following changes. $X_{H,1}$ is given and a mixing line connects $X_{L,N-1}$, $X_{F,N}$, and $X_{H,N+1}$.

Such a graphical solution of the design greatly reduces the time required by the calculations involved in Eqs. (7-15) and (7-17).

Continuous-Flow Operation With Square-Wave Feed Concentration Input to Each Zone (Variable-Feed Operation)

In the previous discussion of this chapter, each zone in the cascade experienced a constant-feed concentration input, the output concentrations depending upon the concentration change due to the step change in temperature. This section is concerned with the design of a single variable-feed zone that may be used in a cycling zone adsorption cascade.

Figure 7-9 is a plot of the dimensionless concentration profile for a variable-feed zone. In this case, the effluent concentration profile is affected by the temperature change and the magnitude of the step-change in feed input. The dimensionless profile is developed from the use of Eq. (6-20) where the step-change in feed concentration, ΔF, is 5 vol % toluene. This profile may be used for any average feed concentration, X_{FAVG}, and any value of ΔF, with the corresponding values of m_T and m.

A zone operating under variable-feed conditions must be able to maintain the actual high- and low-concentrations through product recycle back to the same zone. Because of the shape of the effluent concentration profile, the ability of the zone to maintain the two feed concentrations becomes less as the step-change in feed, ΔF, becomes larger. It is obvious that there is some maximum value of

Figure 7-9

Dimensionless Effluent Concentration Profile for Variable-Feed Operation in the Design of a Cascade [Eq. (6-20)]

A = average high-concentration cut
B = average low-concentration cut
C = $C_1 + C_2$ = intermediate cut (equal to feed concentration)

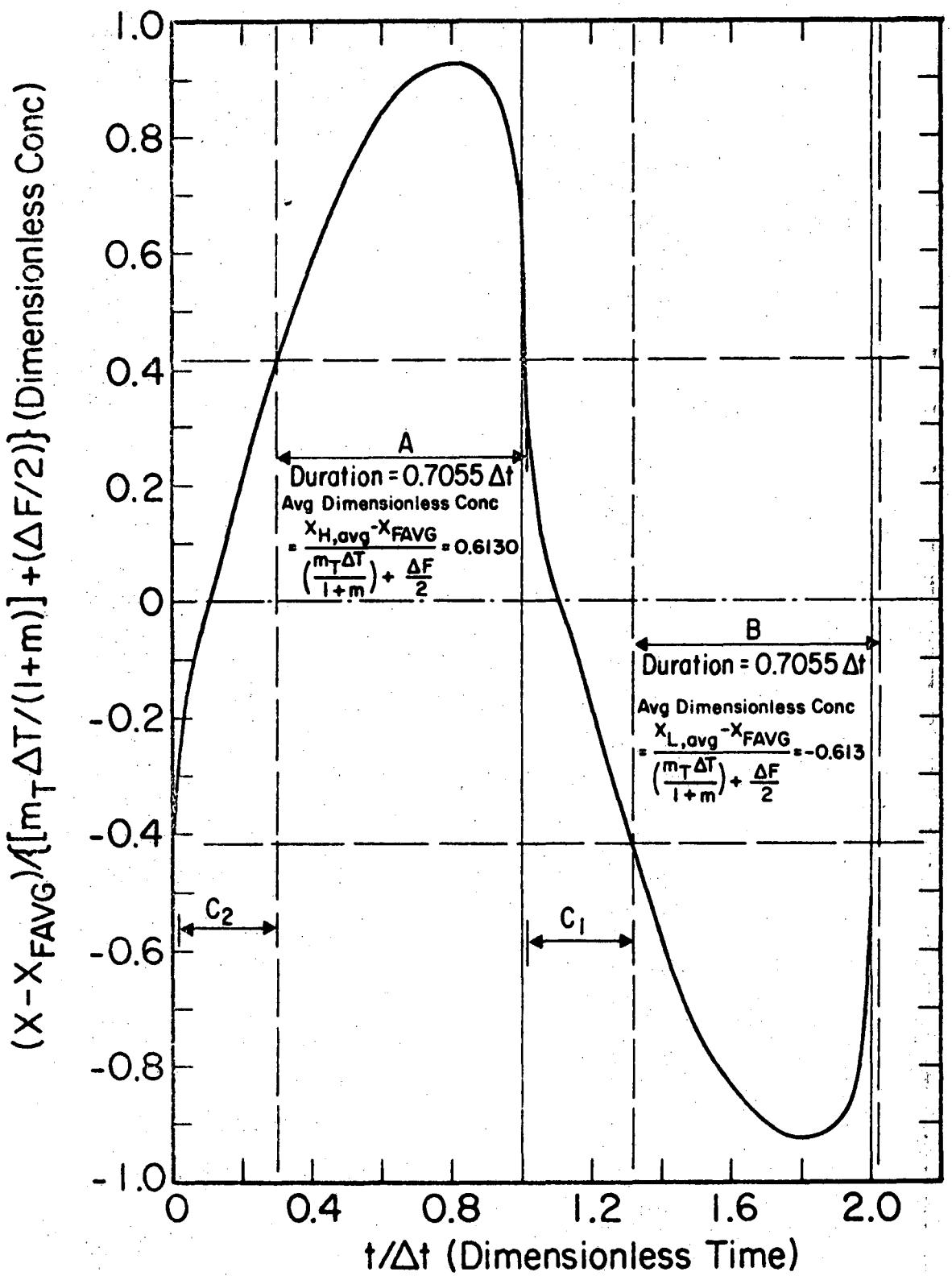
1.0
0.8
0.6
0.4
0.2
0
-0.2
-0.4
-0.6
-0.8
-1.0
0
0.4
0.8
1.2
1.6
2.0
t/Δt (Dimensionless Time)
(X-X_FAVG)/{[m_T ΔT/(1+m)] + (ΔF/2)} (Dimensionless Conc)
A
Duration = 0.7055 Δt
Avg Dimensionless Conc
= (X_H,avg - X_FAVG) / ((m_T ΔT/(1+m)) + ΔF/2) = 0.6130
B
Duration = 0.7055 Δt
Avg Dimensionless Conc
= (X_L,avg - X_FAVG) / ((m_T ΔT/(1+m)) + ΔF/2) = -0.613
C2
C1

ΔF for which recycling of the product streams will not maintain the two feed stream concentrations.

Consider the three following regions of the dimensionless effluent concentration profile, Figure 7-9. Region "A" has an average dimensionless high product concentration of +0.613, and a duration of flow of 0.705 Δt. Region "B" has an average dimensionless low product concentration of -0.613 and a duration of flow of 0.705 Δt. The remaining region, $C = C_1 + C_2$, has an average dimensionless concentration of 0.00 (equal to the feed concentration), and a duration of flow equal to 0.589 Δt. The average concentrations of each of these individual cuts of the effluent stream over a full period ($2\Delta t$) of operation is a function of the duration of flow desired for each cut. This then remains an option in the design of a single variable-feed zone. Trial-and-error calculation concerning cut durations would then be required to optimize the recycle design of the zone. This is not done here since the purpose of this section is to only show how a variable-feed zone may be incorporated into a cascade.

Figure 7-10 is a plot of $Q_N = (0.613)[m_T\Delta T/(1+m) + (\Delta F/2)]$ versus X_{FAVGN}, $X_{L,avgN}$, and $X_{H,avgN}$ for the concentration range where Q_N is a linear function of the concentrations X. This plot allows the calculation of streams in successive zones in a cascade involving the linkage of single, variable-feed zones. This plot is

Figure 7-10

Q_N Versus X_{FAVG}, $X_{H,avgN}$, $X_{L,avgN}$

(Variable-Feed Operation)

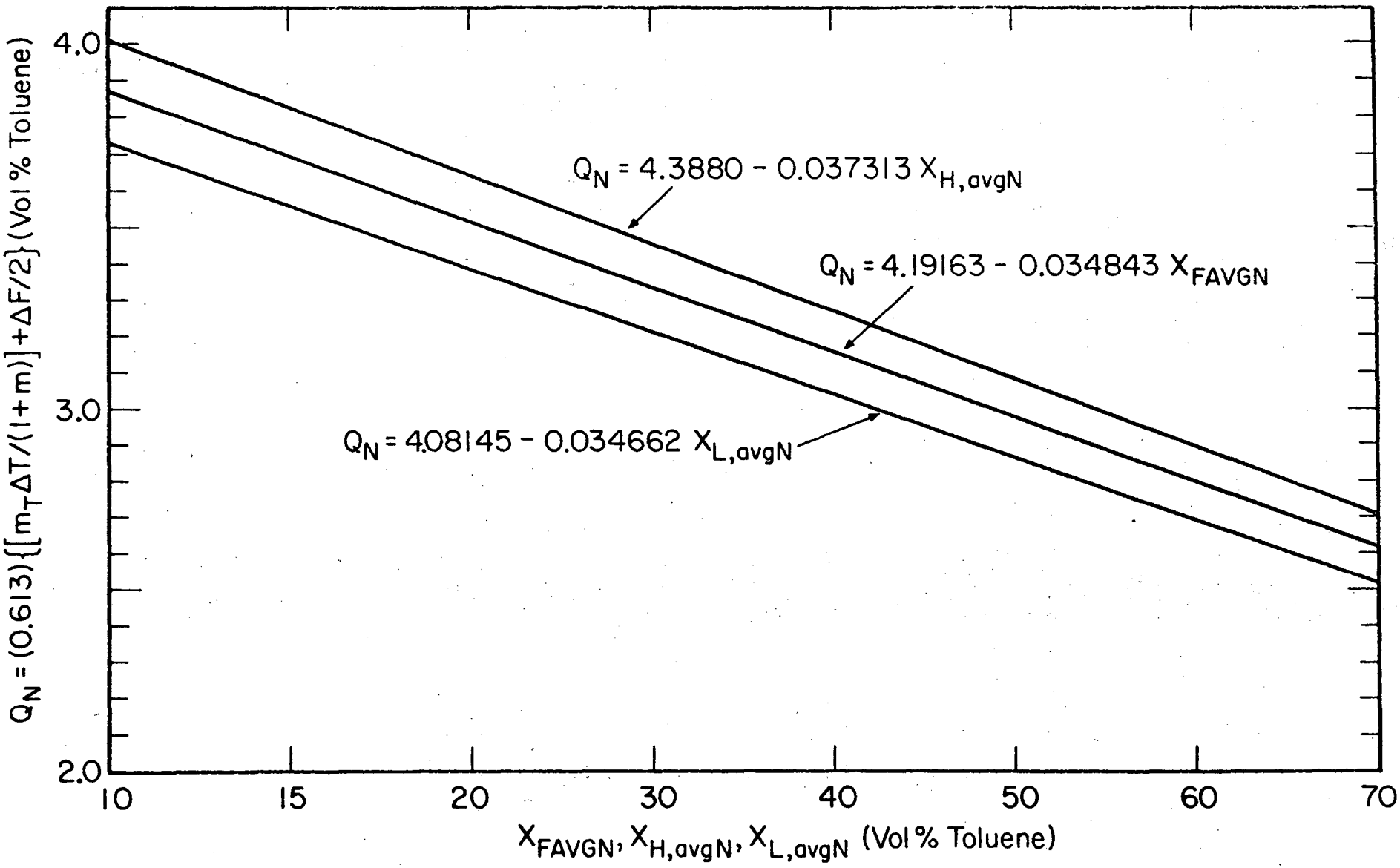
$Q_N = (0.613)\{[m_T \Delta T/(1+m)] + \Delta F/2\}$ (Vol % Toluene)
4.0
3.0
2.0
$Q_N = 4.3880 - 0.037313\ X_{H,avgN}$
$Q_N = 4.19163 - 0.034843\ X_{FAVGN}$
$Q_N = 4.08145 - 0.034662\ X_{L,avgN}$
10
15
20
30
40
50
60
70
$X_{FAVGN}, X_{H,avgN}, X_{L,avgN}$ (Vol % Toluene)

similar to Figure 7-7, P_N versus $X_{L,N}$, $X_{H,N}$, and $X_{F,N}$ except for the addition of the term $\Delta F/2$ to account for the step-change in feed concentration at the inlet, and the term 0.613 accounted for in Figure 7-9, the dimensionless effluent concentration profile.

Figure 7-11 is a schematic drawing of a typical single, variable-feed recycle zone that may be incorporated into the leg of a variable-feed recycle cascade. From Figure 7-10, the dimensionless effluent profile, it is seen that for $X_{FAVG} = 13.0\%$, $X_{F,low} = 10.5\%$, and $X_{F,high} = 15.5\%$. The average high- and low-concentration products, $X_{H,avg}$ and $X_{L,avg}$, are determined from

$$X_{FAVG} \pm (0.613)\left(\frac{m_T \Delta T}{1+m} + \frac{\Delta F}{2}\right) = 16.678\% \text{ and } 9.322\%$$

respectively. The flow rates, for an interstitial cross-sectional area to flow of 1.0A are determined from the time duration of the cuts designated by Figure 7-10. The flow rates for the high- and low-average concentration cuts, designated "A" and "B", are both equal to 0.7055VA for a duration of Δt (actual flow rate is equal to 1.0VA for a duration of 0.7055 ΔT, however these streams must be recycled for a duration of a half-period, Δt), while the average feed concentration cut has a flow rate of 0.2945A for a duration of $2\Delta T$ (a whole period of operation).

Such a variable-feed recycle scheme produces a product amplitude which is considerably larger than that produced by the previously discussed single zone with constant-feed

Figure 7-11

Variable-Feed, Single-Zone Recycle Core of Cascade

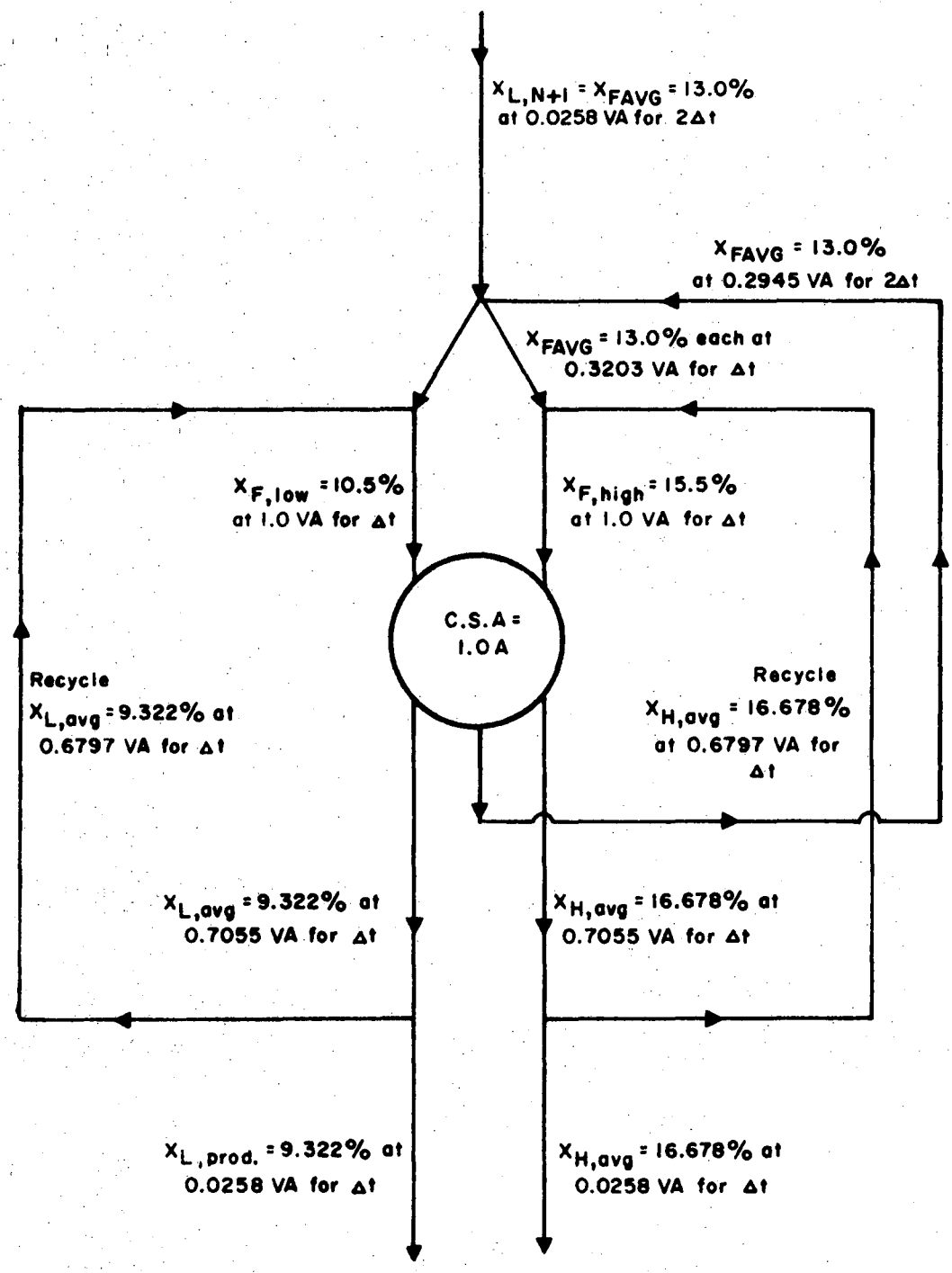
$X_{L,N+1} = X_{FAVG} = 13.0\%$
at 0.0258 VA for $2\Delta t$
$X_{FAVG} = 13.0\%$
at 0.2945 VA for $2\Delta t$
$X_{FAVG} = 13.0\%$ each at
0.3203 VA for Δt
$X_{F,low} = 10.5\%$
at 1.0 VA for Δt
$X_{F,high} = 15.5\%$
at 1.0 VA for Δt
C.S.A =
1.0 A
Recycle
$X_{L,avg} = 9.322\%$ at
0.6797 VA for Δt
Recycle
$X_{H,avg} = 16.678\%$
at 0.6797 VA for
Δt
$X_{L,avg} = 9.322\%$ at
0.7055 VA for Δt
$X_{H,avg} = 16.678\%$ at
0.7055 VA for Δt
$X_{L,prod.} = 9.322\%$ at
0.0258 VA for Δt
$X_{H,avg} = 16.678\%$ at
0.0258 VA for Δt

concentration. This variable-feed, single-zone recycle stage shall now be combined into a variable-feed cascade.

Use of Finite-Difference Equations

Consider the two-zone, variable-feed recycle scheme of Figure 7-12, consisting of a low- and high-average concentration leg and a common feed zone. The design of each individual zone is shown in Figure 7-11. This recycle cascade is the same as the simple two-zone recycle cascade, pictured in Figure 7-4, except that each zone is now variable-feed instead of constant feed, and there is single-zone recycle of the high- and low-average concentration streams. It is therefore possible to use Eqs. (7-15) and (7-17) with a change in the value of the constants a, b, a', and b'. For the variable-feed recycle scheme, the value of the constants may be determined from the plot of Q_N versus $X_{L,avgN}$, and $X_{H,avgN}$, Figure 7-10:

$$Q_N = 4.081 - 0.0346\ X_{L,avgN} = a + b\ X_{L,avgN} \quad (7\text{-}18)$$

$$Q_N = 4.388 - 0.0373\ X_{H,avgN} = a' + b'\ X_{H,avgN} \quad (7\text{-}19)$$

From the value of the constants in Eqs. (7-18) and (7-19) it is possible to use Eqs. (7-15) and (7-17) to calculate the concentrations for any zone N in the variable-feed recycle cascade.

Figure 7-12

Generalized Variable-Feed Cycling Zone Adsorption Cascade With Recycle

(Single Zones Described in Figure 7-11)

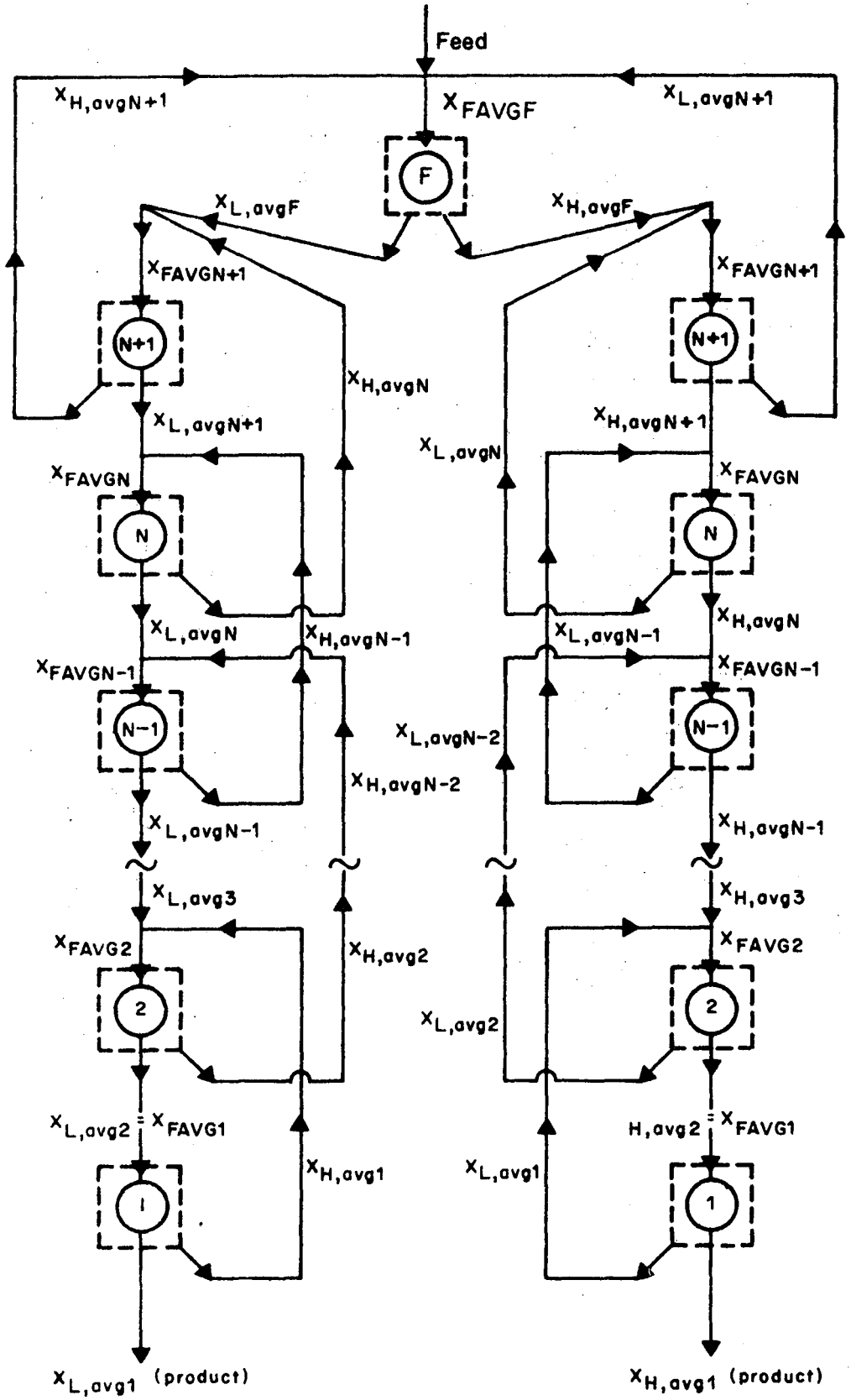
Feed
$X_{H,avgN+1}$
X_{FAVGF}
$X_{L,avgN+1}$
F
$X_{L,avgF}$
$X_{H,avgF}$
$X_{FAVGN+1}$
$X_{FAVGN+1}$
N+1
N+1
$X_{H,avgN}$
$X_{L,avgN+1}$
$X_{H,avgN+1}$
$X_{L,avgN}$
X_{FAVGN}
X_{FAVGN}
N
N
$X_{L,avgN}$
$X_{H,avgN-1}$
$X_{L,avgN-1}$
$X_{H,avgN}$
$X_{FAVGN-1}$
$X_{FAVGN-1}$
N−1
N−1
$X_{L,avgN-2}$
$X_{H,avgN-2}$
$X_{L,avgN-1}$
$X_{H,avgN-1}$
$X_{L,avg3}$
$X_{H,avg3}$
X_{FAVG2}
$X_{H,avg2}$
X_{FAVG2}
2
2
$X_{L,avg2}$
$X_{L,avg2}$
X_{FAVG1}
H,avg2
X_{FAVG1}
$X_{H,avg1}$
$X_{L,avg1}$
1
1
$X_{L,avg1}$ (product)
$X_{H,avg1}$ (product)

Graphical Solution Technique

The two-zone variable-feed recycle cascade may also be represented graphically as was done for the constant feed case. Figure 7-13 presents a graphical technique for stepping off zones in the cascade for the low average concentration leg of such a cascade. The technique is exactly the same as that shown in Figure 7-8 since both cascades have a mixing point preceding each zone except the final zone of each leg of the cascade. The same graphical solution may be used to calculate the high-average concentration leg of the cascade. Such a calculation starts with given values of the high- and low-average product concentrations and zones are stepped off to the feed zone. If there isn't a stringent product concentration requirement, it is simplier to take a given feed zone concentration and step off the zones graphically to any desired product concentrations.

NonContinuous-Flow Operation of a Single Variable-Feed Zone

Consider the following operation of a single variable-feed zone. During the cold-phase operation the zone is filled with the high-concentration feed. Flow stops once the zone is completely filled with the high feed. The zone is now switched to the high temperature, displacing toluene from the solid silica gel. The zone is now *totally* filled with the high concentration product, X_{high}. The

Figure 7-13

Generalized Graphical Solution of a

Variable-Feed Recycle Cascade

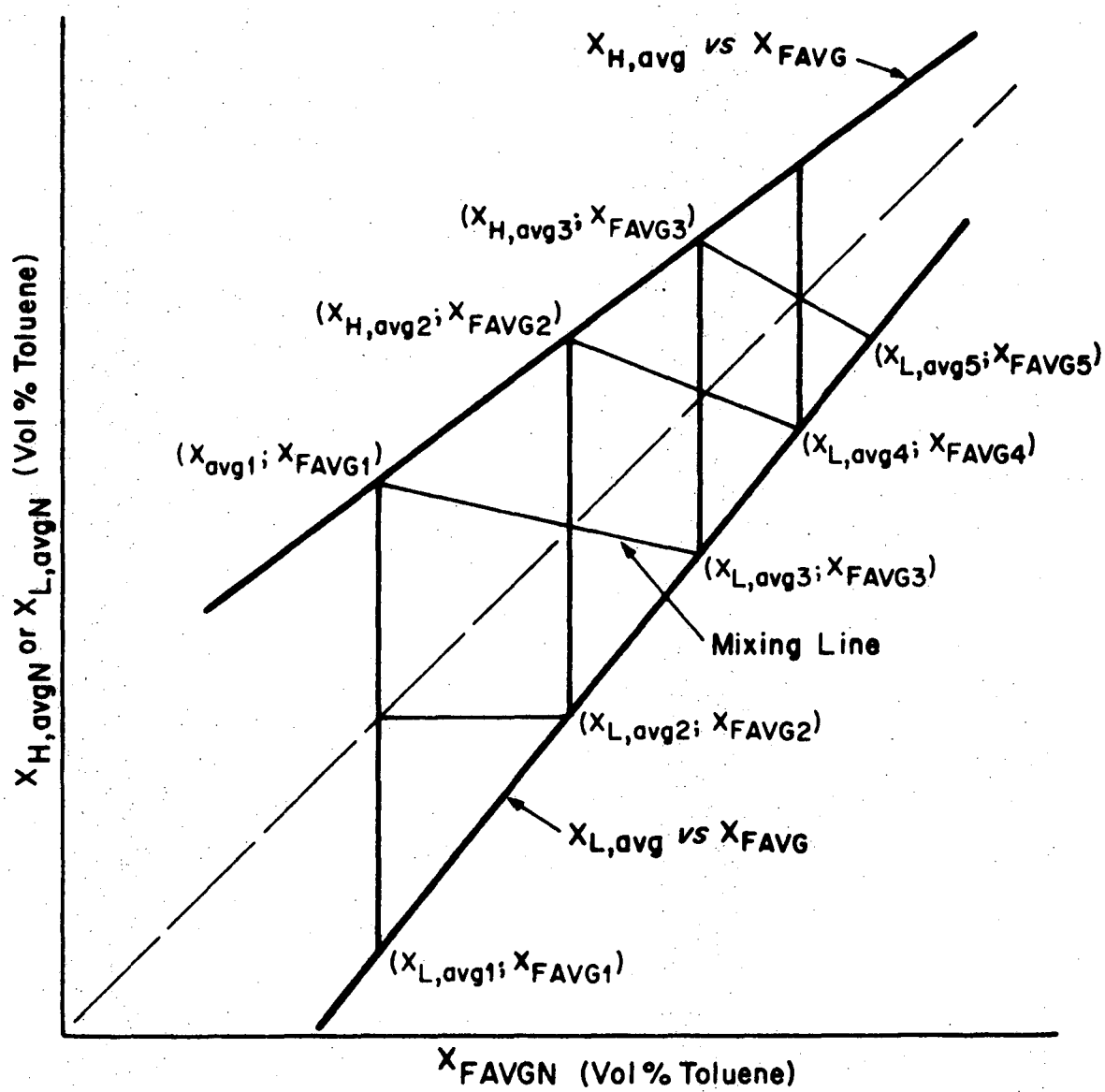
$X_{H,avg}$ vs X_{FAVG}
$(X_{H,avg3}; X_{FAVG3})$
$(X_{H,avg2}; X_{FAVG2})$
$(X_{avg1}; X_{FAVG1})$
$(X_{L,avg5}; X_{FAVG5})$
$(X_{L,avg4}; X_{FAVG4})$
$(X_{L,avg3}; X_{FAVG3})$
Mixing Line
$(X_{L,avg2}; X_{FAVG2})$
$X_{L,avg}$ vs X_{FAVG}
$(X_{L,avg1}; X_{FAVG1})$
$X_{H,avgN}$ or $X_{L,avgN}$ (Vol % Toluene)
X_{FAVGN} (Vol % Toluene)

flow now starts and the high product is *very rapidly* displaced by the low-concentration feed. The zone is now filled with low-concentration feed, and the flow stops. The temperature is now switched to the low value, and the fluid within the zone now becomes low-concentration product due to the adsorption of toluene by the silica gel. Flow starts again, and the low-concentration product is *very rapidly* displaced by high-concentration feed. The zone then continues to operate in this intermittent fashion.

The advantage of this mode of operation is the use of the very rapid displacement velocity of the feed concentration fluid. As pointed out in Chapter 5, the higher the experimental interstitial fluid velocity, the less the spread of the breakthrough curve attributed to longitudinal diffusion. Extrapolation indicates that at a high enough interstitial velocity the initial step change in concentration at the entrance to the zone should be preserved. Figure 5-12, of Chapter 5, indicates that an interstitial velocity of approximately 7.0 cm/sec should be high enough to minimize the distortion of the concentration square-wave for $\Delta F \cong 20\%$.

A second advantage of this mode of operation is that there is no restriction upon the amplitude of the feed concentration. Because of longitudinal diffusion, the feed amplitude is severely reduced at low interstitial velocities. However, at high displacement velocities it is now possible to use much higher feed amplitudes. One

zone should therefore be able to produce a very large separation.

Figure 7-14 describes the operation of a single, variable-feed zone with recycle under the assumption that the effluent concentration profile is preserved as a square-wave, due to a high displacement velocity.

For this particular case, the average feed concentration is 30.0 vol % toluene. By recycle of low- and high-concentration product, a feed stream alternating between 13.0% and 47.0% is maintained. The final product stream varies between 10.0% and 50.0% toluene. A material balance requires that the concentration change upon a temperature switch must be the same for either direction of temperature change, here taken as 3.0 vol % toluene. The interstitial c.s.a. of the zone is taken as A, while its length is designated as L. The throughput is given in terms of the interstitial volume rather than as a flow rate.

The operation of a zone in this manner alleviates diffusional distortion of the concentration waves because of the noncontinuous flow and because of the very rapid displacement velocity.

A comparison of the three recycle schemes (continuous-flow, two-zone recycle cascade with constant feed concentration; continuous-flow, two-zone, variable-feed recycle cascade; and noncontinuous flow, single-zone, variable-feed

Figure 7-14

Noncontinuous-Flow Operation of a Single Cycling Zone Adsorber

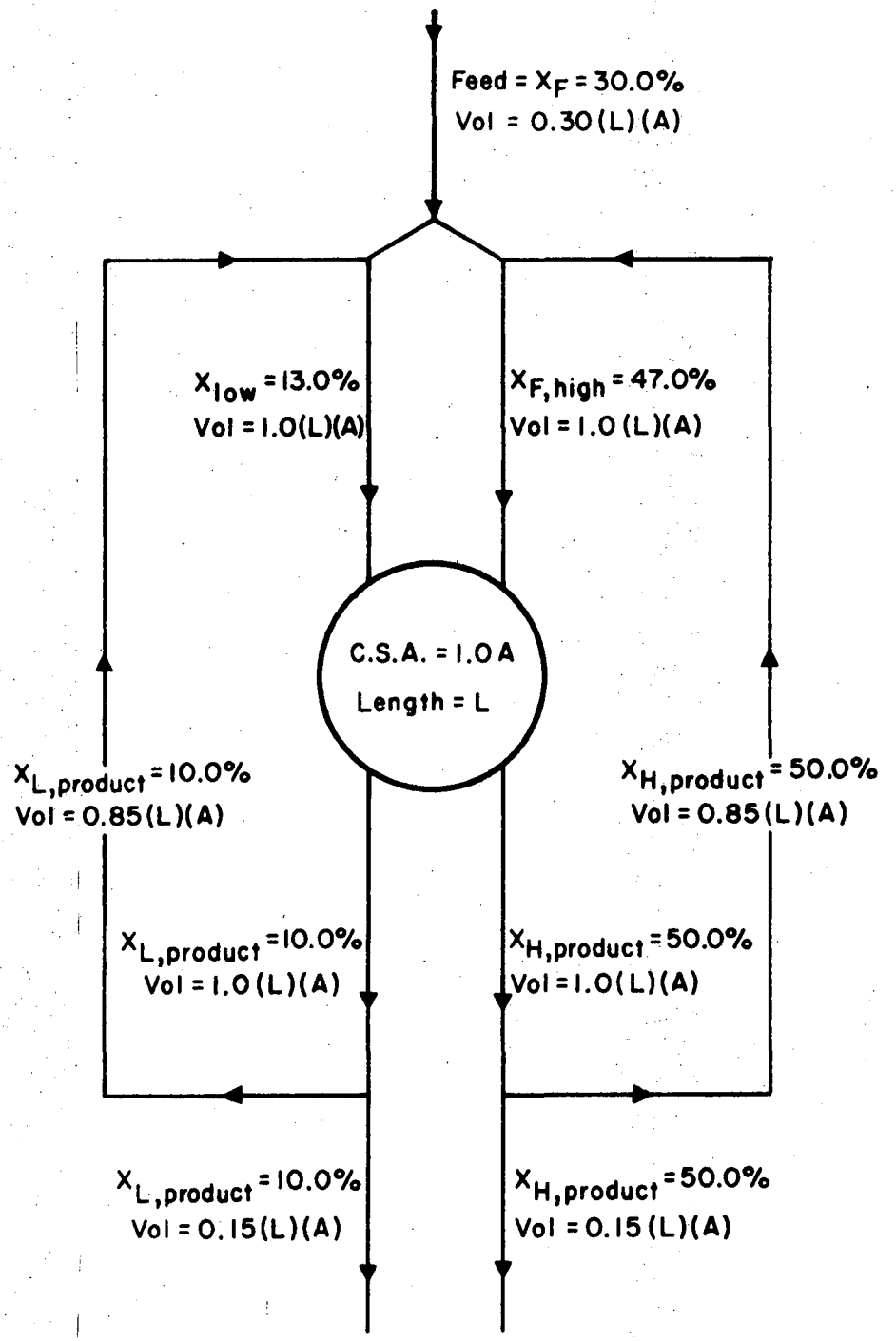
Feed = X_F = 30.0%
Vol = 0.30 (L) (A)
X_{low} = 13.0%
Vol = 1.0(L)(A)
$X_{F,high}$ = 47.0%
Vol = 1.0 (L)(A)
C.S.A. = 1.0 A
Length = L
$X_{L,product}$ = 10.0%
Vol = 0.85 (L)(A)
$X_{H,product}$ = 50.0%
Vol = 0.85 (L)(A)
$X_{L,product}$ = 10.0%
Vol = 1.0 (L)(A)
$X_{H,product}$ = 50.0%
Vol = 1.0 (L)(A)
$X_{L,product}$ = 10.0%
Vol = 0.15 (L)(A)
$X_{H,product}$ = 50.0%
Vol = 0.15 (L)(A)

recycle cascade) indicates that the last scheme is the most attractive since it involves the operation of only one zone rather than many zones linked in a cascade.

The following chapter (Chapter 8) is a comparison of a distillation separation versus the noncontinuous-flow, single-zone, variable-feed cycling zone adsorption operation. The simplified comparison will neglect initial investment costs and be concerned solely with heat consumption.

CHAPTER 8

HEAT LOAD REQUIREMENTS FOR DISTILLATION VERSUS CYCLING ZONE ADSORPTION

Introduction..... 264

Heat Load Requirements for Cycling Zone Adsorption..... 265

Heat Load Requirements for Distillation. 267

CHAPTER 8

HEAT LOAD REQUIREMENTS FOR DISTILLATION VERSUS CYCLING ZONE ADSORPTION

Introduction

Since cycling zone adsorption is an innovation concerning the well-known adsorption techniques, it would be of interest to compare cycling zone adsorption with one of the conventional separation techniques such as distillation. Because only bench-scale operations of cycling zone adsorbers have been carried out to date, it seems fair to base the comparison upon the heat consumption by both separation techniques. Fixed charges cannot be compared reliably until more development has occurred. The following comparison will therefore neglect initial equipments costs and all operating costs other than those proportional to the heat requirements. The following comparisons for C.Z.A. and distillation are developed on the basis of equal production rates of a low-concentration toluene product.

Heat Load Requirements for Cycling Zone Adsorption

Consider the noncontinuous-flow, single-zone, variable-feed recycle scheme in Figure 7-14 of Chapter 7. The production rate will be based upon one hour's operation. Within the one hour the temperature of the zone will be switched twice, from 59°C to 2.0°C and from 2.0°C back to

59.0°C. Therefore during the hour of operation, product streams of high and low toluene concentration will both be produced.

The following list summarizes the assumed operating characteristics of such a cycling zone adsorption separation of n-heptane-toluene using silica gel:

A = interstitial c.s.a. = 201.30 cm^2

A' = total zone c.s.a. = 500.0 cm^2

L = zone length = 331.2 cm

$Vol_{int.}$ = interstitial volume of zone
= 6.67×10^4 cm^3

$Vol_{tot.}$ = total volume of the zone
= 1.65×10^5 cm^3

V = interstitial fluid velocity = 10 cm/sec

Displacement time of one interstitial zone volume = L/V = 33.1 seconds

Time allowed for one complete temperature change = 30 min - $L/V \cong$ 29.5 min

Here there is allowed the option of varying the length, L, and the cross-sectional area of the zone to obtain adequate time for the temperature swing required by the process. By adjustment of the zone c.s.a. and length it is then possible to very the down-time required for the temperature swing, and consequently the displacement time. As previously pointed out, it is desired to make the displacement time as small as possible to preserve the square-wave effluent concentration profile.

$Wt_{solids} = (Vol_{tot})(\rho_{sb}) = 1.26\times10^5$ g of silica gel.

Vol_{liquid} = volume of liquid in and between the solids

$= Vol_{int.} + (\text{solids capacity})(Wt_{solids})$.

$= 1.04\times10^5$ cm^3 liquid.

Production rate = 10,000 cc/switch of 10.0 vol % toluene and 10,000 cc/switch of 50.0 vol % toluene.

Feed rate = 20,000 cc of 30.0 vol % toluene/period (two temperature switches).

Q_{solids} = solids heat load/switch

$= (0.122 \text{ cal/g °C})(126{,}000 \text{ g})(57°\text{C/switch})$

$= 8.79\times10^5$ cal/switch.

$Q_{liquid} = (0.45 \text{ cal/g °C})(0.745 \text{ g/cc})(104{,}000 \text{ cc})(57°\text{C/switch}) = 2.00\times10^6$.

$Q_{feed} = (0.45 \text{ cal/g °C})(0.745 \text{ g/cc})(20{,}000 \text{ cc})(57°\text{C/switch}) = 3.8\times10^5$ cal/period of operation (one hour).

$Q_{tot} = Q_{feed} + 2(Q_{solids} + Q_{liquid})$

$= 6{,}120{,}000$ cal/period of operation

$$Q_{tot} = 6.12\times10^6 \text{ cal/hr.}$$

Heat req./mole of 10.0 vol % product

$= 8.65\times10^4$ cal/g mole.

Heat req./mole of 30.0 vol % feed

$= 4.02\times10^4$ cal/g mole

Heat req./g mole of 50.0 vol % product

$= 7.54\times10^4$ cal/g mole.

Heat Load Requirements for Distillation

The binary system distillation calculations are made using the McCabe-Thiele graphical technique.

X_D = 86.7 mole % heptane = 10.0 vol % toluene

X_F = 62.7 mole % heptane = 30.0 vol % toluene

X_W = 42.0 mole % heptane = 50.0 vol % toluene

D = 70.8 mole/hr = 10,000 cc/hr

W = 82.3 mole/hr = 10,000 cc/hr

F = 153.14 g mole/hr = 20,000 cc/hr (saturated liquid

$(L/V)_{min}$ = 0.7760

L/V = 1.10 to 1.25 $(L/V)_{min}$ = 0.8536 to 0.9700

V = 483.8 to 2,361.0 g mole of vapor/hr

$Q_{cond.}$ = (7,433 cal/g mole)(483.8 to 2,361.0 g mole vapor/hr)
= 3,596,160.0 to 17,549,313.0 cal/hr

$Q_{reboiler}$ = (7,760 cal/g mole)(483.8 to 2,360.0 g mole vapor/hr)
= 3,754,365.0 to 18,321,360.0 cal/hr

Q_{feed} = (44.6525 cal/g mole °C)(153.14 mole/hr)(80.8°C)
= 552,517.0 cal/hr

$Q_{tot} = Q_{cond.} + Q_{reboiler} + Q_{feed}$

$= 7.90\times10^6$ to 3.64×10^7 cal/hr

Number of theoretical plates = 12.0 to 16.0 plates

Assumed overall efficiency = 50.0%

Actual number of plates = 24 to 32 plates

Plate spacing = 20.0 inches = 50.8 cm

Column height = 1.2×10^3 to 1.6×10^3 cm

Column cross-sectional area = 122.0 cm^2 to 163.0 cm^2

Column volume = 150,000 cm^3 to 265,000 cm^3

Heat req./g mole of feed = 51.60×10^3 to 238.8×10^3 cal/g mole feed

Heat req./g mole distillate = 111.5×10^3 to 514.2×10^3 cal/g mole distillate

Heat req./g mole bottoms = 96.0×10^3 to 442.5×10^3 cal/g mole bottoms

The following ratio of heat loads, distillation to C.Z.A., may now be made:

$$Q_{totDist}/Q_{totCZA} = 1.30 \text{ to } 6.000$$

It is obvious for the full operating range of a distillation column, as indicated by the liquid to vapor ratio, that a separation effected by cycling zone adsorption is at least as effective and possibly six times as effective is expected as the same separation obtained by distillation.

In the calculation of the heat load for the single cycling adsorption zone, the heat requirements for the two recycle streams have not been considered. Since the temperature of both streams are out of phase with the temperature required by the zone, and since they are both of opposite temperature, one being high while the other is low, these streams may be run through a counter-current heat exchanger to develop the required temperature of the zone. Theoretically, such a heat exchanger is all that is needed to produce the full temperature swing of each recycle stream.

Of prime interest in the design of a single zone, variable-feed recycle unit, as shown in Figure 7-14, is the pressure drop through the packed zone and consequently the pumping requirements. Were interstitial fluid velocities very low, as in the case of a continuous flow cascade, pumping consideration would be negligible, however, in the noncontinuous flow operation the displacement velocity needs to be very high to maintain the square-wave effluent concentration profile. Assuming spherical silica gel particles of diameter 0.05 cm, a viscosity of 0.45 cp, density of 0.745 g/cc, interstitial fluid velocity of 10.0 cm/sec, and a void fraction of 0.4026, the Ergun Equation (9) may be used to calculate the pressure drop through a packed zone of length L:

$$\Delta P = (L)(1.48 \times 10^{-2} \text{ atm/cm})$$

For a zone length of L = 331.2 cm, the pressure drop through the zone is calculated to be ΔP = 4.90 atmospheres.

It may therefore be concluded, based upon a simple heat load analysis, that cycling zone adsorption may be a process competitive with distillation.

CHAPTER 9

SUMMARY AND CONCLUSIONS

Chapter 3. A Simplified Mathematical Statement of Cycling Zone Adsorption (Exclusion of Diffusion Term)..... 271

Chapter 4. Experimental: Single-Zone, Continuous-Flow Separation of n-Heptane and Toluene on Silica Gel..... 273

Chapter 5. Experimental: Variable-Feed Operation of a Single Zone..... 275

Chapter 6. Mathematical Statement of Cycling Zone Adsorption Allowing for Longitudinal Diffusion. 276

Chapter 7. Single-Zone Staging in the Development of a Cycling Zone Adsorption Cascade..... 279

Chapter 8. Heat Load Requirements for Distillation Versus Cycling Zone Adsorption..... 280

0 0 0 0 3 8 0 / 0 9

CHAPTER 9

SUMMARY AND CONCLUSIONS

It has been theoretically and experimentally demonstrated that cycling zone adsorption is a feasible separation process. This has been illustrated by the separation of n-heptane-toluene by solid silica gel. The following summarizes the developments of each chapter, beginning with Chapter 3, and the conclusions that may be drawn from each chapter.

Chapter 3. A Simplified Mathematical Statement of Cycling Zone Adsorption (Exclusion of Diffusion Term)

By material balances about a differential element of packing in a zone, equations describing the behavior of a zone operating under a periodic temperature change have been developed. The primary assumptions are that local (instantaneous) equilibrium exists and that there is no diffusional resistance between phases. Longitudinal diffusion was assumed to be absent. A graphical solution of the effluent concentration profiles is obtained by the Method of Characteristics.

The equations in Chapter 3 reveal three important phenomena which occur in the operation of a cycling zone adsorber: (1) from the slope of the concentration characteristics, Eq. (3-9), it is found that concentration waves move through the zone at different velocities, depending

upon the concentration; and (2) there exist "concentration shock-waves" due to the difference in concentration wave velocities. This is shown by Eq. (3-14). This phenomenon occurs during the displacement of a low-concentration product by a high concentration feed at the low temperature; and (3) there exists a "simple-wave" emergence due to the difference of concentration wave velocities. This phenomenon occurs when a high-concentration product is being displaced by a low-concentration feed at the high temperature. This is shown by Figure 3-4.

Chapter 3 provides a sample calculation using the simplified equilibrium theory to obtain the operating characteristics of a single zone experiencing a constant concentration feed and a periodic square-wave temperature change.

From the mathematical development of Chapter 3, it may be concluded that,

1. The simplified mathematical analysis adequately predicts concentration changes due to the periodic temperature change of the zone.
2. The simplified mathematical analysis, through its prediction of concentration wave velocities, can be used to predict the temperature switching time and length of a single zone operating under constant feed concentration.

Since the simplified mathematical statement of cycling zone adsorption excludes any consideration of second-order diffusional terms, it is therefore limited in its ability to predict the experimental operation of a cycling zone adsorber. Its main utilization lies in the ability to predict maximum concentration changes due to periodic temperature changes of the zone (conclusion 1).

Chapter 4. Experimental: Single-Zone, Continuous-Flow Separation of n-Heptane-Toluene on Silica Gel

Chapter 4 investigates the operation of a single-zone, operating under constant feed concentration and experiencing a square-wave temperature change. The main purpose of this chapter has been to study parameters which optimize the performance of a single zone in respect to peak separations and peak flow durations. These parameters are as follows:

1. The establishment of optimum zone length and temperature switching time.

This effect has been investigated experimentally through the use of feed concentration breakthrough experiments. Such experiments, run with different feed concentrations, allow the determination of the optimum temperature switching frequency for a given zone length, or alternately, the optimum zone length for a given switching frequency.

2. The effect of solid particle size upon the peak separation and upon peak flow durations.

This effect has been investigated experimentally by operating a single zone using silica gel of particle size varying from 4 to 180 mesh. It was found that as the particle size decreased the effective capacity of the silica gel increased. This therefore allowed maximum separation. Because of the small particle's ability to reach equilibrium more rapidly, peak flow durations were found to increase with a decrease in particle size.

3. The effect of a perfect square-wave temperature response of the zone.

Because of the simple equipment design, it was experimentally impossible to develop a square-wave temperature response under continuous-flow conditions. A SGM of operation was employed to obtain a square-wave response. Using the SGM, it was possible to investigate the effect of a perfect square-wave temperature response upon the effluent concentration profile. The result was a very large increase in the peak product flow durations.

The effect of Chapter 4 is to show through a number of very simple experiments that optimization of single-zone performance can be achieved without complicated theoretical considerations. The main conclusions of Chapter 4 are:

1. The effect of operating a cycling zone adsorber at a temperature switching frequency other than the optimum tends to reduce the concentration

0 0 0 0 3 8 0 7 0 1

change developed by the temperature change of the zone.

2. Maximum separation and approach to local equilibrium is greatly enhanced by the use of small-sized silica gel particles. With a decrease in the particle size, the effective capacity of the particle approaches its true capacity.
3. The shape of the effluent concentration profile closely follows that of the temperature profile of the zone. It is therefore concluded that the development of a square-wave temperature response of the zone will provide the maximum peak product concentration flow durations in the operation of a single zone.

Chapter 5. Experimental: Variable-Feed Operation of a Single Zone

Chapter 5 investigates the operation of a single zone experiencing a variable-feed input and a square-wave zone temperature response. The chapter discusses the logic of a variable-feed operation and the diffusional difficulties caused by large feed amplitudes at the entrance to the zone. Overall diffusion coefficients for the transition between product concentration and displacing feed concentration have been calculated. The spread of the breakthrough curves, caused by logitudinal mixing, is explained through consideration of density and viscosity differences

between the product fluid and the displacing feed fluid. The effect of displacement velocity upon the shape of the breakthrough curve is also discussed. Experimental data are developed to determine the effect of the feed amplitude upon the duration of high peak concentration product flow.

The developments of Chapter 5 allow the following two major conclusions to be reached:

1. Variable-feed operation, through the use of product recycle streams, takes advantage of small separation, produced by the periodic temperature change, to develop very large separations of a feed stream.
2. Longitudinal mixing is the major effect causing distortion of the effluent concentration profile from a desired square-wave profile. Longitudinal mixing is the principal factor limiting the operation of a variable-feed, product-recycle zone.

Chapter 6. Mathematical Statement of Cycling Zone Adsorption Allowing for Longitudinal Diffusion

Chapter 6 is an extension of simplified mathematical analysis of Chapter 3. The analysis of Chapter 6 includes the diffusion term which was investigated experimentally in Chapter 5. Analytic solutions are developed for the following operating conditions of a cycling zone adsorber:

0 0 0 0 0 8 0 7 0 0 2

1. Continuous-flow, constant-concentration feed to a single zone experiencing a square-wave temperature variation. Any practical value of the overall diffusion coefficient may be used in this analysis.
2. A perfectly mixed zone (diffusion coefficient = ∞) operating under the conditions described in statement 1.
3. An unmixed zone (diffusion coefficient = 0) operating under the conditions described in statement 1.
4. Continuous-flow, variable-feed to a single zone experiencing a square-wave temperature variation. For a given feed amplitude, the diffusion coefficient is that prescribed by the experimental investigation of Chapter 5. This analysis investigates the contribution to the concentration change not only by the temperature change but also by the initial step change in the feed concentration at the entrance to the zone.

The phase relationship between the temperature switching and the switching of the feed to the zone is also investigated by the analysis. It is found that the optimum relationship prescribes that the temperature switch to be 180° out of phase with the switching of the feed concentration to the zone.

Since the analytic solutions of Chapter 6 are for linear differential equations, it is possible to obtain a dimensionless effluent concentration profile from the one dimensionless profile for any feed concentration and given feed amplitude. The mathematical analysis also allows the determination of the optimum length and temperature switching frequency.

From the extended mathematical developments of Chapter 6 the following may be concluded:

> If a system of interest may be separated by cycling zone adsorption and if the differential equations describing the system are linear (that is, if the nondimensionless effluent concentration profiles for the whole range of feed concentrations may be superimposed to a reasonable degree), then an analytic solution for the dimensionless effluent profile may be developed that will describe the system behavior over the whole range of feed concentrations for any given feed amplitude. Such a solution may simply be developed from a knowledge of the system isotherms and the value of the overall diffusion coefficient, obtained from breakthrough data.

0 0 0 0 0 8 0 7 0 0 3

Chapter 7. Single-Zone Staging in the Development of a Cycling Zone Adsorption Cascade

From the dimensionless effluent concentration profiles developed in Chapter 6 and from the solid-liquid equilibrium isotherms, Chapter 7 investigates the design of the following types of cascades employing single-cycling zone adsorbers:

1. Continuous-flow, constant-concentration feed, two-zone recycle cascade and three-zone recycle cascades.
2. Continuous-flow, variable-feed, two-zone recycle cascade.
3. Noncontinuous-flow, single-zone-recycle cycling zone adsorber.

The effect of recycle stream location is investigated with respect to the total volume of the cascade and the number of zones required by the cascade. Equations, requiring solution techniques similar to those used for distilling columns, are developed to allow the design calculations for a cycling zone adsorption cascade. Solution of finite-difference equations are also obtained for calculation of stream concentrations for each individual zone. An extension of the finite-difference equation solutions is made to develop a simple graphical technique to design a cascade of a series of single zones with two-zone

recycle streams. These calculation techniques are also applied to the variable-feed, two-zone recycle cascade. The following conclusions may be made from the cascade design techniques of Chapter 7:

> As recycle streams are returned at zones farther away from the zone producing the streams, the number of total zones in the cascade decreases; however, there is a slight increase in the total volume of the cascade. As recycle streams are returned to zones closer to the zone producing the streams, the number of zones in the cascade increase; however, the total volume of the cascade decreases slightly.

Chapter 8. Heat Load Requirements for Distillation Versus Cycling Zone Adsorption

Chapter 8 investigates the operating heat load requirements for the noncontinuous flow, variable-feed single-cycling zone adsorber versus that required by distillation for the same product concentration and product rate. The following conclusion may be made:

> On the basis of operating heat load requirements, it is concluded that for the separation of n-heptane-toluene cycling zone adsorption is at least equal to and possibly six times as efficient as distillation.

It has been shown theoretically and experimentally for the separation of a common binary liquid system, n-heptane-toluene, that cycling zone adsorption is a very promising and competitive separation technique.

Nomenclature

$A = (1-\alpha)\epsilon/\alpha$

A' = cross-sectional area

C_p = heat capacity

= diffusion coefficient

$\mathcal{D}_c = \mathcal{D}/(1+m)$

F = functional relationship between X_s, T, and X_L

ΔF = feed amplitude, vol % toluene

L = zone length

N = zone number

$P = m_T \Delta T/(1+m)$

Q = const. $[m_T \Delta T/(1+m) + (\Delta F/2)]$

R = defined above Eq. (6-8)

R.I. = refractive index

S = defined above Eq. (6-8)

T = temperature

U_{shock} = shock-wave velocity

V = interstitial fluid velocity

V_c = interstitial concentration wave velocity

X = volume fraction or vol % toluene

$Z = L$ = zone length

c = concentration

$\langle d^2 \rangle$ = mean square displacement

d_p = particle diameter

f = fraction of total period ($2\Delta t$) for which the high- or low-concentration product flows

Nomenclature (Continued)

k = thermal conductivity

$m = A(\partial X_s/\partial X_L)_{T_{avg}}$

$m_T = A(\partial X_s/\partial T)_{\check{X}_L}$

n = positive whole interger

p = LaPlace transform operator

$q = \mathfrak{D}_c/V_c^2\Delta t$

t = time

$t_{1/2}$ = defined by Figure 5-13

t = time required for a half-cycle of operation, *i.e.*, the temperature switching time

z = distance along the axial direction

α = interparticle void fraction

$\alpha = \sqrt{\frac{1+\sqrt{1+16\pi^2n^2q^2}}{2}}$, found only in Chapter 6

α_{RV} = defined by Eq. (2-1)

$\beta = 2\pi nq/\alpha$, α as defined in Chapter 6

ϵ = intraparticle void fraction

$\zeta = V_cZ/2$

θ = time t

λ = latent heat

$\xi = (z - V_ct)/2\mathfrak{D}_ct$

ρ = density

0 0 0 0 3 8 0 / 3 0 3

Nomenclature (Continued)

Subscripts

avg = average

C = cold temperature

¢ = centerline

F = feed concentration

FAVG = average feed concentration

F,high = high feed concentration

F,low = low feed concentration

H = high concentration or high temperature

High = high concentration

i = interface

L = liquid concentration or low concentration

Low = low concentration

L-low = low concentration liquid

L-high = high concentration liquid

s = solid

s-high = high solid concentration

s-low = low solid concentration

sb = dry packed state of solid particles

+ = leading edge

- = trailing edge

Bibliography

1. Acrivos, A., *I.& E.C.*, 48, 703 (1956).
2. Alexis, R. W., *Chem. Eng. Prog.*, No. 5, 63, 69-71 (May 1967).
3. Alexis, R. W., *Chem. Eng. Prog. Symp. Series*, No. 74, 63, 51 (1967).
4. Amundson, N. R., and R. Aris, *Proc. Roy. Soc. (London)*, A286, 129 (1965).
5. Aris, R., *I.& E.C. Fundamentals*, 8, 603 (1969).
6. Baddour, R. F., U.S. Patent No. 3,250,058 (1966).
7. Baker, B. III, and R. L. Pigford, *I.& E.C. Fundamentals*, No. 2, 10, 283-292 (May, 1971).
8. Berg, C., *Trans. A.I.Ch.E.*, 42, 665 (1946).
9. Bird, R. B., W. E. Stewart and E. N. Lightfoot, "Transport Phenomena," John Wiley and Son, New York, London, Sydney, 1965.
10. Bohrer, B. B., U.S. Patent No. 3,223,748 (1965).
11. Booij, H. L., *I.& E.C. Fundamentals*, No. 2, 8, 231-235 (May, 1969).
12. Cairns, E. J., and J. M. Prauznitz, *Chem. Eng. Science*, No. 1, 12, 20 (1960).
13. Cassidy, H. G., "Adsorption and Chromatography," Interscience, New York, 1951.
14. Carberry, S. S., and R. H. Bretton, *A.I.Ch.E. J.*, 4, 367 (1958).

0 0 0 0 3 8 0 7 0 0 0

Bibliography (Continued)

15. Deisler, P. F., and R. H. Wilhelm, *I.& E.C.*, No.6, 45, 1219 (1953).

16. DeVault, D., *J. Amer. Chem. Soc.*, 65, 532 (1943).

17. Dryden, C. E., and W. B. Kay, *I.& E.C.*, 46, 2294 (1954).

18. Edwards, M. F., and J. F. Richardson, *Chem. Eng. Science*, No. 2, 23, 109-123 (May, 1968).

19. *Ibid*, 24, 1741 (1969).

20. Findl, E., and K. Lui, *J. Gas Chromatography*, 6, 165-168 (March, 1968).

21. Fuller, E. N., P. D. Schettler and J. C. Giddings, *I.& E.C.*, 58, 19 (1966).

22. Glueckauf, E., *Trans. Faraday Soc.*, 51, 34 (1955).

23. *Ibid.*, 60, 729 (1964).

24. Grant, R. J., M. Manes and S. B. Smith, *A.I.Ch.E.J.*, 8, 403 (1962).

25. Gregory, R. A., and N. H. Sweed, *Chem. Eng. J.*, 1, 207 (1970).

26. Hall, K. R., L. C. Eagleton, A. Acrivos, and T. Vermeulen, *I.& E.C. Fundamentals*, 5, 212 (1966).

27. Helfferich, F., "Ion Exchange," McGraw-Hill, New York, (1962.

28. Holson, J. N., and M. R. Strunk, *I.& E.C. Fundamentals*, 2, 143 (1964).

Bibliography (Continued)

29. Hyun-Kee, R., and N. R. Amundson, *I.& E.C. Fundamentals*, 9, 303 (1970).

30. Jenczewski, T. J., and A. L. Myers, *A.I.Ch.E.J.*, No. 3, 14, 509 (1968).

31. Kehde, H., *Chem. Eng. Prog.*, 44, 575 (1948).

32. Kipling, J. J., "Adsorption From Solutions of Non-Electrolytes," Academic Press, New York, London, 1965.

33. Kraus, K. A., and R. S. Raridon, *J. Phys. Chem.*, 63, 1901 (1959).

34. Lawson, A. E., and Miller, J. M., *J. Gas Chromatography*, 4, 273 (1966).

35. Myers, A. L., *I.& E.C.*, 60, 45 (1968).

36. Pigford, R. L., B. Baker, III, and D. E. Blum, *I.& E.C. Fundamentals*, 8, 144 (1969).

37. *Ibid.*, 8, 604 (1969).

38. *Ibid.*, 8, 848 (1969).

39. Pigford, R. L., B. Baker, III, and D. E. Blum, U.S. Patent No. 3,542,525 (1970).

40. Rolke, R. W., and R. H. Wilhelm, *I.& E.C. Fundamentals*, No. 2, 8, 235-246 (May, 1969).

41. Ross, Sidney Oliver, "On Physical Adsorption," Interscience, New York, 1964.

42. Ryan, J. M., R. S. Timmins and J. F. O'Donnell, *Chem. Eng. Prog.*, 64, 53 (1968).

Bibliography (Continued)

43. Schettler, P. D., and J. C. Giddings, *Analytic Chemistry*, No. 4, 37, 835-840 (June, 1965).

44. Skarstrom, C. W., *Ann. N. Y. Acad. Sci.*, 72, 751 (1959).

45. Stack, R., and C. B. Rice, "Chromatographic Methods," Chapman and Hall, London, 1967.

46. Strang, D. A., and C. J. Geankoplis, *I.& E.C.*, No. 9, 50, 1305 (1958).

47. Sweed, N. H., and R. H. Wilhelm, *I.& E.C. Fundamentals*, No. 2, 8, 221 (1969).

48. Timmins, R. S., L. Mir and J. M. Ryan, *Chem. Eng.*, 170 (May 19, 1969).

49. Van Ness, H. C., *I.& E.C. Fundamentals*, 8, 464 (1969).

50. Wilhelm, R. H., *Pure and Applied Chemistry*, 5, 403 (1962).

51. Wilhelm, R. H., "Intracellular Transport," Academic Press, New York, 1966.

52. Wilhelm, R. H., A. W. Rice and A. R. Bendelius, *I.& E.C. Fundamentals*, No. 1, 5, 141 (Feb., 1966).

53. Wilhelm, R. H., A. W. Rice and N. H. Sweed, *I.& E.C. Fundamentals*, No. 3, 7, 337 (Aug., 1968).

54. Wilhelm, R. H., and N. H. Sweed, *Science*, 159, 522 (Feb., 1968).

Bibliography (Continued)

Dissertations

55. Baker, III, B., *Cycling Zone Adsorption: Separation by Thermal Wave Propagation*, University of California, Berkeley, 1969.

56. Blum, D. E., *Cycling Zone Adsorption: Separation of Gas Mixtures*, University of California, Berkeley, 1971.

57. Rolke, R. W., *Recuperative Parametric Pumping: Model Development, Evaluation, and Use for Study of Separation Capabilities*, Princeton University, 1967.

58. Sweed, N. H., *Parametric Pumping: Separation Via Direct Thermal Mode*, Princeton University, 1968.

Private Communications

59. Dr. Burke Baker, III (1969).

60. Dr. Dwain E. Blum (1969-1972).

61. Dr. Richard C. Forrester, III (1969-1972).

62. Dr. L. Louis Hegedus (1970-1972).

63. Professor Robert L. Pigford (1969-1972).

LEGAL NOTICE

This report was prepared as an account of work sponsored by the United States Government. Neither the United States nor the United States Atomic Energy Commission, nor any of their employees, nor any of their contractors, subcontractors, or their employees, makes any warranty, express or implied, or assumes any legal liability or responsibility for the accuracy, completeness or usefulness of any information, apparatus, product or process disclosed, or represents that its use would not infringe privately owned rights.

TECHNICAL INFORMATION DIVISION
LAWRENCE BERKELEY LABORATORY
UNIVERSITY OF CALIFORNIA
BERKELEY, CALIFORNIA 94720